THE UNIVERSITY
of EDINBURGH

This thesis has been submitted in fulfilment of the requirements for a postgraduate degree (e.g. PhD, MPhil, DClinPsychol) at the University of Edinburgh. Please note the following terms and conditions of use:

This work is protected by copyright and other intellectual property rights, which are retained by the thesis author, unless otherwise stated.
A copy can be downloaded for personal non-commercial research or study, without prior permission or charge.
This thesis cannot be reproduced or quoted extensively from without first obtaining permission in writing from the author.
The content must not be changed in any way or sold commercially in any format or medium without the formal permission of the author.
When referring to this work, full bibliographic details including the author, title, awarding institution and date of the thesis must be given.

Functional Consequences of Mutations in *GRIN2A* and *GRIN2B* associated with Mental Disorders

Katie F. M. Marwick
MA MB ChB MRCPsych

A thesis presented for the degree of
Doctor of Philosophy

Supervisors
Prof Giles E. Hardingham
Prof David J. A. Wyllie
Dr Paul Skehel

College of Medicine and Veterinary Medicine
University of Edinburgh
United Kingdom
2016

Declaration

I composed the work and analysis presented in this thesis, except where indicated in the text. This thesis has not been submitted for any other degree or professional qualification.

Acknowledgements

I am grateful for the help I have received from many people during the preparation of this PhD. I would firstly like to thank my supervisors Giles Hardingham, David Wyllie and Paul Skehel for their guidance, support and encouragement. I would also like to thank all the people in the lab who taught me techniques and advised on data analysis: Sean McKay, Matt Livesey, Nora Markus, Jing Qiu, Jamie McQueen, Marc-Andre Martel, Paul Baxter, Philip Hasel, Sam Booker, Adam Jackson, Daumante Suminaite, Emma Perkins. I am particularly grateful to Kasper Hansen, University of Montana, for allowing me to visit his lab and perform experiments using a technique he had recently developed. I am also grateful to his lab members Feng Yi and Gina Bullard who assisted and welcomed me. I thank Peter Kind for his contribution to the generation of the new animal models described within. I would also like to thank Steve Traynelis, University of Emory, for his helpful suggestions regarding the cause of an unexpected result. Pete Parker completed an undergraduate project with me and some of his data is included within (noted in the relevant figure legend). I am also indebted to John Iredale, Brian Walker and Andrew Jackson, the directors of the PhD scheme which funded this work, who provided me with mentorship and much constructive criticism. I also thank the Wellcome Trust for their financial support. Finally, I would like to thank my family for shaping me and inspiring me to pursue a PhD, and my fiancé Jon for helping me to learn LaTeX and bravely bearing the intrusions of his rival: the thesis.

Abstract

GRIN2A and *GRIN2B* encode the GluN2A and GluN2B subunits of the NMDA receptor, a subtype of ionotropic glutamate receptor that displays voltage-dependent block by Mg^{2+} and a high permeability to Ca^{2+}. These receptors play important roles in synaptogenesis, synaptic transmission and synaptic plasticity, as well as contributing to neuronal loss and dysfunction in several neurological disorders. Recently, individuals with a range of childhood onset epilepsies, intellectual disability and other neurodevelopmental abnormalities have been found to carry heterozygous gene-disrupting or protein-altering point mutations in *GRIN2A* and *GRIN2B*.

This thesis addresses the hypothesis that these point mutations cause key functional disturbances to NMDA receptor properties that contribute to neurodevelopmental disorders. To test this hypothesis, a group of related mutations were selected for functional assessment in heterologous systems: four missense mutations affecting residues in or near the subunit pore regions, all of which are associated with epilepsy and intellectual disability. To model the impact of gene disrupting mutations in *GRIN2A*, a preliminary analysis of the functional consequences of GluN2A haploinsufficiency in a genetically modified rat was also performed.

Three of the four missense mutations were found to be associated with profound alterations in fundamental NMDA receptor properties: compared to wild type, $GluN2A^{N615K}$ was found to reduce Mg^{2+} block, $GluN2B^{N615I}$ and $GluN2B^{V618G}$ to cause potentiation by Mg^{2+}, and $GluN2A^{N615K}$ and $GluN2B^{N615I}$ showed reduced conductance. $GluN2A^{R586K}$ was not found to influence the parameters assessed. When $GluN2A^{N615K}$ was expressed alongside wild type subunits in the same NMDA receptor, it was found to have a dominant negative effect. Finally, I established successful gene targeting in a new rat *Grin2A* knock-out model, and observed that heterozygous neurons had lower GluN2A protein expression and current density, making a good model to study human epilepsies associated with loss of a *GRIN2A* allele.

This thesis provides evidence that three missense mutations in *GRIN2A* and *GRIN2B* affect physiologically important properties of the NMDA receptor, and that GluN2A haploinsufficiency influences important neural properties *in vitro*. This is consistent with these mutations causing disease and highlights these and related mutations as potential therapeutic targets in the future.

Lay Summary

The N-methyl-D-aspartate receptor (NMDAR) is an important protein in the brain that helps to transmit chemical signals between brain cells. Some people with brain disorders like intellectual disability, autism and epilepsy, have mutations in their genetic code for these receptors. It is probable that these mutations are at least part of the cause of their disorder. However, it isn't known exactly how the change in the gene might lead to a change in brain function: the aim of this project was to investigate this.

This project found that three mutations in the NMDAR cause big changes to how the receptor functions, making it harder for brain cells to communicate with each other. In the case of one of these mutations, the receptor's functioning was altered even when normal versions of the NMDAR genes were present too. This shows that just one mutation is enough to affect the receptor's behaviour. The way the receptor's functioning was affected by these mutations suggests that it will be less able to participate in normal brain activities like learning and memory.

This project also designed an animal model which is missing one of its NMDAR genes. This is similar to what is found in some people with epilepsy, who are also missing a copy of this gene. Brain cells missing the gene showed some differences in function which will be interesting to follow up in the future.

In summary, this project found that mutations in NMDARs, or removing a copy of a NMDAR gene, cause changes in receptor and brain cell function consistent with these mutations having a role in causing brain disorders.

Contents

Declaration i

Acknowledgements iii

Abstract v

Lay Summary vii

Table of Contents vii

List of Figures xi

List of Tables xv

Abbreviations xvii

1 Introduction **1**

1.1 Chapter summary 2

1.2 Overview of pathogenesis of neurodevelopmental disorders 3

1.3 Identification and classification of ionotropic glutamate receptors 6

1.4 NMDAR structure and function 8

1.5 What non-genetic evidence links NMDARs to brain disorders? 19

1.6 What genetic evidence links NMDARs to mental disorder? 21

1.7 Description of phenotypes associated with mutations in *GRIN2A* and *GRIN2B* . 32

1.8 Thesis aims 37

2 Materials and methods **39**

2.1 Preparation of DNA constructs 40

2.2 Techniques used with oocytes 42

2.3 Techniques used with HEK293 and HEK293T cells 44

2.4 Techniques used with cultured primary mouse and rat cortical neurons 47

2.5 Generation and validation of genetically modified rat 52

2.6 Materials 54

2.7 Statistical analysis . . . 54
2.8 Ethics . . . 54

3 Three missense mutations alter important NMDAR properties 55

3.1 Chapter summary and key findings . . . 56
3.2 Introduction . . . 57
3.3 Expression of mutant diheteromers in oocytes . . . 60
3.4 Expression of mutant subunits in neurons . . . 67
3.5 Single channel properties of mutant diheteromers . . . 86
3.6 Discussion . . . 100

4 One missense mutation has a dominant negative effect in triheteromeric NMDARs 107

4.1 Chapter summary and key findings . . . 108
4.2 Introduction . . . 109
4.3 Glutamate deactivation rates . . . 112
4.4 Mg^{2+} block in diheteromeric and triheteromeric NMDARs containing $GluN2A^{N615K}$ subunits . . . 125
4.5 Mg^{2+} block in diheteromeric NMDARs containing $GluN2B^{N615I}$ or $GluN2B^{V618G}$ subunits . . . 136
4.6 Discussion . . . 141

5 Validation and initial functional assessment of two new rat models: constitutive and conditional knock-out of GluN2A 145

5.1 Chapter summary and key findings . . . 146
5.2 Introduction . . . 147
5.3 Confirmation of targeted genome modification by sequencing . . . 153
5.4 Validation of *Grin2a*$^{flox/flox}$ rat model . . . 155
5.5 Validation of *Grin2a*$^{-/+}$ rat model . . . 158
5.6 Functional assessment of *Grin2a*$^{-/+}$ rat model . . . 167
5.7 Discussion . . . 179

6 General discussion 185

Bibliography 209

List of Figures

Introduction **1**

1.1 Genetic architecture of complex disease 4

1.2 Some of the post-synaptic proteins mutated in intellectual disability 5

1.3 Influence of subunit identity on NMDAR properties 9

1.4 Function of NMDAR domains 11

1.5 Role of glutamate receptors in generation of gamma oscillations 14

1.6 NMDAR mediated synaptic plasticity 16

1.7 NMDARs facilitate dendritic arbor development and synaptogenesis 17

1.8 Influence of synaptic and extra-synaptic NMDAR activation on neuronal survival 18

1.9 Missense mutations identified in *GRIN2A* and *GRIN2B* 24

1.10 *De novo* missense mutations identified in *GRIN2A* and *GRIN2B* 26

1.11 Gene disrupting mutations identified in *GRIN2A* and *GRIN2B* 28

1.12 *De novo* gene disrupting mutations identified in *GRIN2A* and *GRIN2B* 29

1.13 Disorders included in the epilepsy-aphasia spectrum 33

Materials and methods **39**

2.1 Crispr/Cas9 strategy for generation of rat models 52

Three missense mutations alter important NMDAR properties **55**

3.1 The "N" site shown in GluN2B crystal structure 58

3.2 NMDARs containing GluN2A^{N615K} show reduced Mg^{2+} and memantine block 62

3.3 NMDARs containing GluN2A^{N615K} show reduced Mg^{2+} and amantadine block 63

3.4 NMDARs containing GluN2A^{N615K} show reduced block by ketamine 64

3.5 NMDARs containing GluN2A^{N615K} show increased block by dextromethorphan 65

3.6 NMDARs containing GluN2A^{R586K} have normal Mg^{2+} block 66

3.7 Representative traces from neurons transfected with wild type GluN2A or GluN2A^{N615K} 69

3.8 Ifenprodil inhibition is reduced in neurons transfected with wild type GluN2A or GluN2A^{N615K} 70

3.9 Mg^{2+} block is reduced in neurons transfected with GluN2A^{N615K} 71

3.10 Current density is reduced in neurons transfected with GluN2A^{N615K} 72

3.11 Representative traces from neurons transfected with wild type GluN2A or GluN2A^{R586K} 73

3.12 Ifenprodil inhibition is reduced in neurons transfected with wild type GluN2A or GluN2A^{R586K} 74

3.13 Mg^{2+} block is normal in neurons transfected with GluN2A^{R586K} 75

3.14 Current density is unaffected in neurons transfected with GluN2A^{R586K} 76

3.15 Representative traces from neurons transfected with wild type GluN2B or GluN2B^{N615I}, wild type and ifenprodil insensitive forms 78

3.16 Ifenprodil inhibition is reduced in neurons transfected with ifenprodil insensitive forms of wild type GluN2B and GluN2B^{N615I} 79

3.17 Mg^{2+} block is reduced in neurons transfected with ifenprodil insensitive GluN2B^{N615I} 80

3.18 Current density is reduced in neurons transfected with GluN2B^{N615I} and ifenprodil insensitive GluN2B^{N615I} 81

3.19 Representative traces from neurons transfected with wild type GluN2B or GluN2B^{V618G}, wild type and ifenprodil insensitive forms 82

3.20 Ifenprodil inhibition is reduced in neurons transfected with GluN2B^{V618G} but not with ifenprodil insensitive GluN2B^{V618G} 83

3.21 Mg^{2+} block is reduced in neurons transfected with GluN2B^{V618G} 84

3.22 Current density is reduced in neurons transfected with GluN2B^{V618G} and ifenprodil insensitive GluN2B^{V618G} 85

3.23 GluN2A^{N615K} reduces single channel conductance in oocytes 87

3.24 GluN2A^{N615K} does not influence NMDAR open times in oocytes 88

3.25 GluN2A^{R586K} does not influence single channel conductance in oocytes 90

3.26 GluN2A^{R586K} does not influence NMDAR open times in oocytes 91

3.27 GluN2A^{N615K} reduces single channel conductance in HEK293 cells 93

3.28 GluN2A^{N615K} increases NMDAR open times in HEK293 cells 95

3.29 GluN2B^{N615I} reduces single channel conductance in HEK293 cells 97

3.30 GluN2B^{N615I} does not influence NMDAR open times in HEK293 cells 99

3.31 Biochemical properties of amino acids 101

3.32 Sites important for binding of memantine 102

One missense mutation has a dominant negative effect in triheteromeric NMDARs 107

4.1 Generation of obligate triheteromeric NMDAR. 110

4.2 Glutamate deactivation rates following 5 ms exposure are unaffected by modification of C termini 114

4.3 Glutamate deactivation rates following 2 s exposure are unaffected by modification of C termini 115

4.4 GluN2A^{N615K} does not alter glutamate deactivation rates 117

4.5 GluN2A^{N615K} subunits can form triheteromers with wild type GluN2 subunits 120

4.6 GluN2B pore mutations do not alter glutamate deactivation rates 122

4.7 Glutamate deactivation rates in construct pairings designed to produce GluN2B^{N615I} and GluN2B^{V618G} containing triheteromers suggest GluN2A diheteromeric escape current 124

4.8 Representative traces showing Mg^{2+} block in wild type and GluN2A^{N615K} mutant diheteromers and triheteromers 126

4.9 Mg^{2+} block is not altered by modified C termini 127

4.10 Mg^{2+} block is reduced in GluN2A^{N615K} mutant diheteromers and triheteromers 128

4.11 Mg^{2+} block is reduced in GluN2A^{N615K} mutant diheteromers and triheteromers: current–voltage curves 130

4.12 Triheteromers containing GluN2A^{N615K} have slower Mg^{2+} on rates 133

4.13 Triheteromers containing GluN2A^{N615K} have slower Mg^{2+} off rates 135

4.14 Mg^{2+} potentiates current in 2B mutant diheteromers: representative traces . . . 136

4.15 Mg^{2+} potentiates current in 2B mutant diheteromers 137

4.16 Mg^{2+} potentiates current in 2B mutant diheteromers: current–voltage curves . 138

4.17 Potentiation of current by Mg^{2+} in 2B mutant diheteromers is unlikely to be due to increased Ca^{2+} conductance 138

4.18 Increasing Mg^{2+} concentration increases Mg^{2+} potentiation in GluN2B^{V618G} mutant diheteromers 139

4.19 Mg^{2+} block in GluN2B pore mutants: previous work 143

Validation and initial functional assessment of two new rat models: constitutive and conditional knock-out of GluN2A 145

5.1 Genome modification approach to generate *Grin2a*$^{T1845A(flox)/+}$ 148

5.2 Genome modification events that generated *Grin2a*$^{flox/+}$ and *Grin2a*$^{-/+}$ 149

5.3 NMDAR hypofunction impairs inhibitory circuits 151

5.4 Sequencing strategy and results for genetically modified rat lines 153

5.5 GluN2A protein levels are normal in *Grin2a*$^{flox/flox}$ rat 156

5.6 GluN2A is deleted following Cre recombination in *Grin2a*$^{flox/flox}$ rat 157

5.7 *Grin2a* mRNA levels are reduced in *Grin2a*$^{-/+}$ and *Grin2a*$^{-/-}$ rats 159

5.8 GluN2A protein levels are reduced in *Grin2a*$^{-/+}$ and *Grin2a*$^{-/-}$ rats 160

5.9 Representative spermine potentiation traces from neurons expressing wild type GluN2A and GluN2A^{N615K} NMDARs 162

5.10 Spermine potentiation is reduced in neurons transfected with wild type GluN2A or GluN2A^{N615K} 163

5.11 GluN2A expression is demonstrated by a reduction in spermine potentiation by three weeks *in vitro* in cultured neurons 164

5.12 Spermine potentiation is increased in *Grin2a*$^{-/+}$ and *Grin2a*$^{-/-}$ rats 165

5.13 Spermine potentiation is better than ifenprodil sensitivity for detecting *Grin2a*$^{-/+}$ haploinsufficiency 166

5.14 Current density is reduced in *Grin2a*$^{-/+}$ and *Grin2a*$^{-/-}$ rat neurons after two weeks in culture 168

5.15 Representative trace showing AMPAR mediated mEPSCs 169

5.16 mEPSC amplitudes and frequencies in cultured neurons are unaffected by *Grin2a* knock-out 170

5.17 Representative trace showing GABAR mediated mIPSCs 171

5.18 mIPSC amplitudes and frequencies in cultured neurons are unaffected by *Grin2a* knock-out 172

5.19 Ratio of mEPSC:mIPSC amplitudes and frequencies in cultured neurons are unaffected by *Grin2a* knock-out 173

5.20 Representative traces showing Ca^{2+} levels in response to bicuculline in neurons cultured from wild type, *Grin2a*$^{-/+}$ and *Grin2a*$^{-/-}$ rats 175

5.21 Basal Ca^{2+} levels and cell density in cultured neurons are unaffected by *Grin2a* knock-out 176

5.22 Bicuculline-evoked coordinated Ca^{2+} spikes are less frequent in neurons cultured from *Grin2a*$^{-/-}$ rats 177

5.23 Cell death in cultured neurons is unaffected by *Grin2a* knock-out 178

List of Tables

Introduction **1**

1.1 Ionotropic glutamate receptor subunits 7

1.2 Studies reporting protein altering and protein disrupting mutations in *GRIN2A* 22

1.3 Studies reporting protein altering and protein disrupting mutations in *GRIN2B* 25

1.4 Key features of disorders on the epilepsy-aphasia spectrum 34

Materials and methods **39**

2.1 Wild type and mutant constructs 40

2.2 Mutagenising primers used with In-Fusion method 41

2.3 Mutagenising primers used with QuikChange 41

2.4 Primers used for qPCR 48

2.5 Primers used for nested PCR 53

2.6 Genotyping primers and expected band sizes 53

Three missense mutations alter important NMDAR properties **55**

3.1 Mutations selected for study 59

3.2 Summary values for channel blockers in oocytes 61

3.3 Summary values for Mg^{2+} block, current density and ifenprodil inhibition associated with expression of GluN2A and GluN2B mutant subunits in neurons 70

3.4 Summary values for outside-out single channel recordings in oocytes 86

3.5 Summary values for cell-attached single channel recordings in HEK293 cells . . 92

One missense mutation has a dominant negative effect in triheteromeric NMDARs **107**

4.1 Comparison of two related methodologies for generating triheteromeric NMDARs 109

4.2 Nomenclature used to describe wild type and mutant triheteromeric constructs 112

4.3 Glutamate deactivation time constants (1 mM, 5 ms exposure) for wild type NMDARs . . . 113

4.4 Glutamate deactivation time constants (1 mM, 2 s exposure) for wild type NMDARs . . . 113

4.5 Glutamate deactivation time constants (1 mM, 5 ms exposure) for GluN2A^{N615K} containing NMDARs . . . 119

4.6 Glutamate deactivation time constants (1 mM, 2 s exposure) for GluN2A^{N615K} containing NMDARs . . . 119

4.7 Glutamate deactivation time constants (1 mM, 5 ms exposure) for GluN2B^{N615I} and GluN2B^{V618G} containing NMDARs . . . 121

4.8 Glutamate deactivation time constants (1 mM, 2 s exposure) for GluN2B^{N615I} and GluN2B^{V618G} containing NMDARs . . . 121

4.9 1 mM Mg^{2+} block in wild type and GluN2A^{N615K} containing diheteromers and triheteromers . . . 129

4.10 100 μM Mg^{2+} block in wild type and GluN2A^{N615K} containing diheteromers and triheteromers . . . 129

4.11 Mg^{2+} (1 mM) on rates in wild type and GluN2A^{N615K} containing diheteromers and triheteromers in the continuous presence of glutamate (1 mM) . . . 132

4.12 Mg^{2+} (1 mM) off rates in wild type and GluN2A^{N615K} containing diheteromers and triheteromers in the continuous presence of glutamate (1 mM) . . . 134

4.13 Kinetics of Mg^{2+} potentiation in GluN2B pore mutant diheteromers . . . 140

Validation and initial functional assessment of two new rat models: constitutive and conditional knock-out of GluN2A **145**

5.1 Phenotypes observed in *Grin2a*$^{-/-}$ mice . . . 180

General discussion **185**

6.1 Functional consequences of mutations identified in *GRIN2A* and *GRIN2B* . . . 188

Abbreviations

aCSF	Artificial cerebrospinal fluid
AMPA	α-Amino-3-hydroxy-5-methyl-4-isoxazolepropionic acid hydrobromide
ATP	Adenosine 5-triphosphate
BCA	Bicinchoninic acid
BES	N,N-Bis(2-hydroxyethyl)-2-aminoethanesulfonic acid, N,N-Bis(2-hydroxyethyl)taurine
bp	Base pair
Cas-9	CRISPR-associated protein-9 nuclease
CAMKII	Ca^{2+}/calmodulin-dependent protein kinase II
7-CKA	7–chlorokynurenic acid
CNQX	6-Cyano-7-nitroquinoxaline-2,3-dione
CRISPR	Clustered regularly interspaced short palindromic repeats
DAPI	4',6–diamidino–2–phenylindole
D-AP5	D-2-amino-5-phosphonovalerate
DIV	Day *in vitro*
DTT	Dithiothreitol
DTPA	Diethylenetriaminepentaacetic acid
EEG	Electroencephalogram
EGTA	Ethylene glycol-bis(2-aminoethylether)-*N,N,N',N'*-tetraacetic acid
EPSC	Excitatory post synaptic current
GABA	γ-Aminobutyric acid
GAD67	Glutamate decarboxylase
GDEE	L-glutamic acid diethylester
GTP	Guanosine triphosphate
GFP	Green fluorescent protein
HEK	Human embryonic kidney cells
HEPES	4-(2-Hydroxyethyl)piperazine-1-ethanesulfonic acid, N-(2-Hydroxyethyl)piperazine-N-(2-ethanesulfonic acid)
HRP	Horse radish peroxidase
IPSC	Inhibitory post synaptic current
mEPSC/mIPSC	Miniature EPSC/IPSC
MK-801	(5S,10R)-(+)-5-Methyl-10,11-dihydro-5H-dibenzo[a,d]cyclohepten-5,10-imine maleate
NMDA	N-Methyl-D-aspartic acid
NP-40	Nonyl phenoxypolyethoxylethanol
PCR	Polymerase chain reaction
PVDF	Polyvinylidene fluoride
REM	Rapid eye movement
SDS	Sodium dodecyl sulfate
sgRNA	Single guide RNA
TBS	Tris buffered saline
Tris	2-Amino-2-hydroxymethyl-propane-1,3-diol
TTX	Tetrodotoxin

CHAPTER 1

Introduction

1.1 Chapter summary

1. Neurodevelopmental disorders are increasingly viewed as representing a continuum of symptoms with shared disruptions in biological pathways and overlapping genetic and environmental risk factors.

2. Hundreds of genes have been implicated in the aetiology of neurodevelopmental disorders, including NMDAR subunits.

3. NMDARs are already known to participate in many crucial brain functions, including synaptogenesis, synaptic transmission, synaptic plasticity, and neuronal survival.

4. NMDAR dysfunction has already been linked to a range of brain disorders.

5. Recent genetic evidence strongly implicates mutations in NMDARs as contributing to risk for neurodevelopmental disorders.

6. Neurodevelopmental disorders associated with NMDARs influence cognition and excitability.

7. Investigating the functional consequences of mutations in NMDAR subunits may highlight key disruptions in biological pathways underlying neurodevelopmental disorders.

1.2 Overview of pathogenesis of neurodevelopmental disorders

Mental disorders contribute substantially and increasingly to the global burden of disease (Murray et al., 2015), however, therapeutic advance is limited by their largely unknown pathogenesis. Although much time and effort in the past has been devoted to demarcating subtypes of mental disorder, the emerging concept now is that many mental disorders with onset in childhood and adolescence can be grouped together as a continuum of neurodevelopmental disorder comprising intellectual disability, autism spectrum disorders, schizophrenia and epilepsy. This theory is based partly on overlapping symptomatology and substantial comorbidity but is mainly driven by evidence of shared genetic risk and increasingly by evidence of shared biological underpinnings, as described below.

The increasing availability of whole exome sequencing data is opening up a new way to investigate the pathogenenesis of mental disorders, along with other complex disease. Most genetic risk for complex disease arises from multiple, common, inherited variants of individual small effect, making it hard to identify potentially subtle pathogenic effects of a given variant (see Figure 1.1). However, the ability to economically sequence the coding DNA of large numbers of individuals has allowed many rare mutations to be identified in particular disorders. Further, the parents of carriers of rare mutations can also be affordably screened, allowing identification of mutations as *de novo* (arising during germline development, thus present somatically in neither parent). These rarer mutations, particularly *de novo* ones, are more likely than common inherited mutations to reduce reproductive fitness, hence contribute a larger degree of risk for disorder to their carriers (Veltman and Brunner, 2012). This makes investigating their functional consequences a potentially useful route into identifying key pathological alterations underlying disease. This is the approach taken in this thesis.

Over the last five years, rare mutations in hundreds of genes have been implicated in neurodevelopmental disorders: 700 genes and rising in intellectual disability (Vissers et al., 2016), 400-1000 (predicted) in autism (Geschwind and State, 2015), > 100 in schizophrenia (Ripke et al., 2014) and > 300 in epilepsy (Allen et al., 2013). Despite being individually rare, as a group these mutations are estimated to be causal in up to 60% of severe intellectual disability (Gilissen et al., 2014) and 25% of autism (Geschwind and State, 2015).

Identifying the key biological mechanisms affected by these multitudinous variations is challenging. A common approach is to perform pathway analysis, where the rate of mutation in a set of genes with related functions is compared to what would be expected by chance. This approach is limited by incomplete understanding of the function of many genes and the reliance on protein interactions identified in non-physiological contexts. Despite this, there has been a degree of consistency in the biological pathways identified as important in neurodevelopmental disorders, with chromatin remodelling, synapse development and synaptic function all identified as frequently mutated pathways in intellectual disability (van Bokhoven, 2011), autism (Geschwind and State, 2015), schizophrenia (O'Dushlaine et al., 2015) and epilepsy (Myers and Mefford, 2015). Figure 1.2 shows some of the relationships between proteins identified to carry mutations in intellectual disability, arranged to highlight the sort of synaptic functions disrupted.

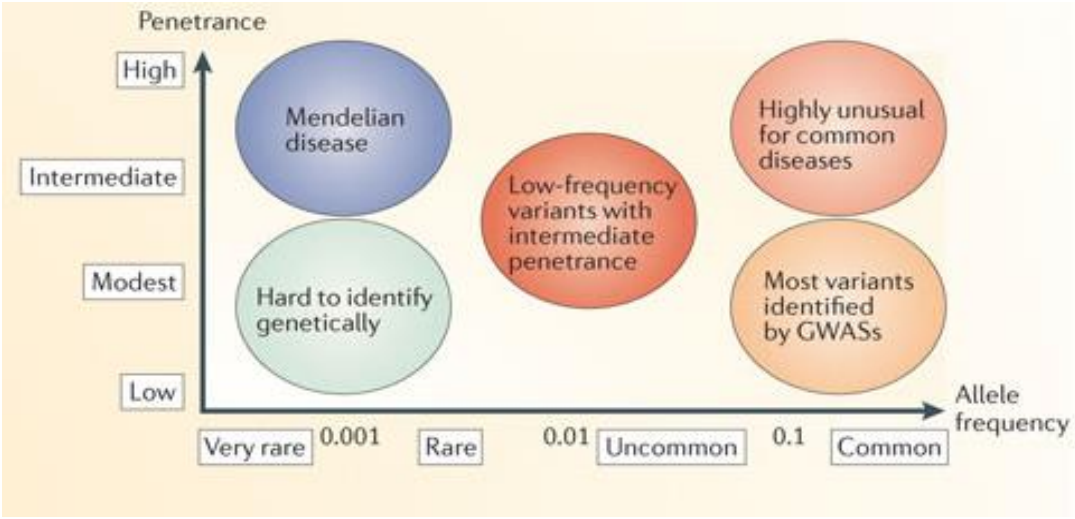

Figure 1.1: **Genetic architecture of complex disease**
The diagram shows a model for the genetic variants underlying mental disorder, and other complex disease. An individual's overall risk of disease will be influenced by multiple genetic variants with a range of penetrances, and their environmental experiences. Whole exome and whole genome sequencing is allowing the identification of a host of rare penetrant mutations of medium to high penetrance (represented on the diagram as "Mendelian disease" and "low frequency variants with intermediate penetrance"). Taken from Sullivan et al. (2012).

This array of dysfunctional genes and pathways identified in neurodevelopmental disorders offers a wonderful opportunity to explore the mechanisms underlying these disorders. However, it is also a daunting task - where to begin? Which genes matter and which are coincidental? What are the important, disease-relevant, outcomes that should be measured at the cellular, circuit and behavioural level? One way forward is to select a gene or genes which have strong genetic evidence linking them to neurodevelopmental disorder, and are also reasonably well characterised in terms of their products' normal function. This allows informed predictions to be made about the probable impact of mutations, facilitating targeted investigation. Further, if the gene selected is known to be important for normal brain function, this increases the biological plausibility of the hypothesis that mutations in it cause neurodevelopmental disorders.

One such pair of genes are the type 2A and 2B subunits of the NMDA receptor, the subject of the remainder of this thesis. In support of their importance, an overview of the discovery, structure and normal functions of NMDARs is given in the next two sections, followed by a brief overview of what is already known about NMDAR dysfunction in disease. The genetic evidence linking NMDAR mutations to neurodevelopmental disorders is then considered in detail, and a brief account provided of the clinical features of these putative "NMDAR synaptopathies". The introduction concludes with a statement of the aims of this thesis.

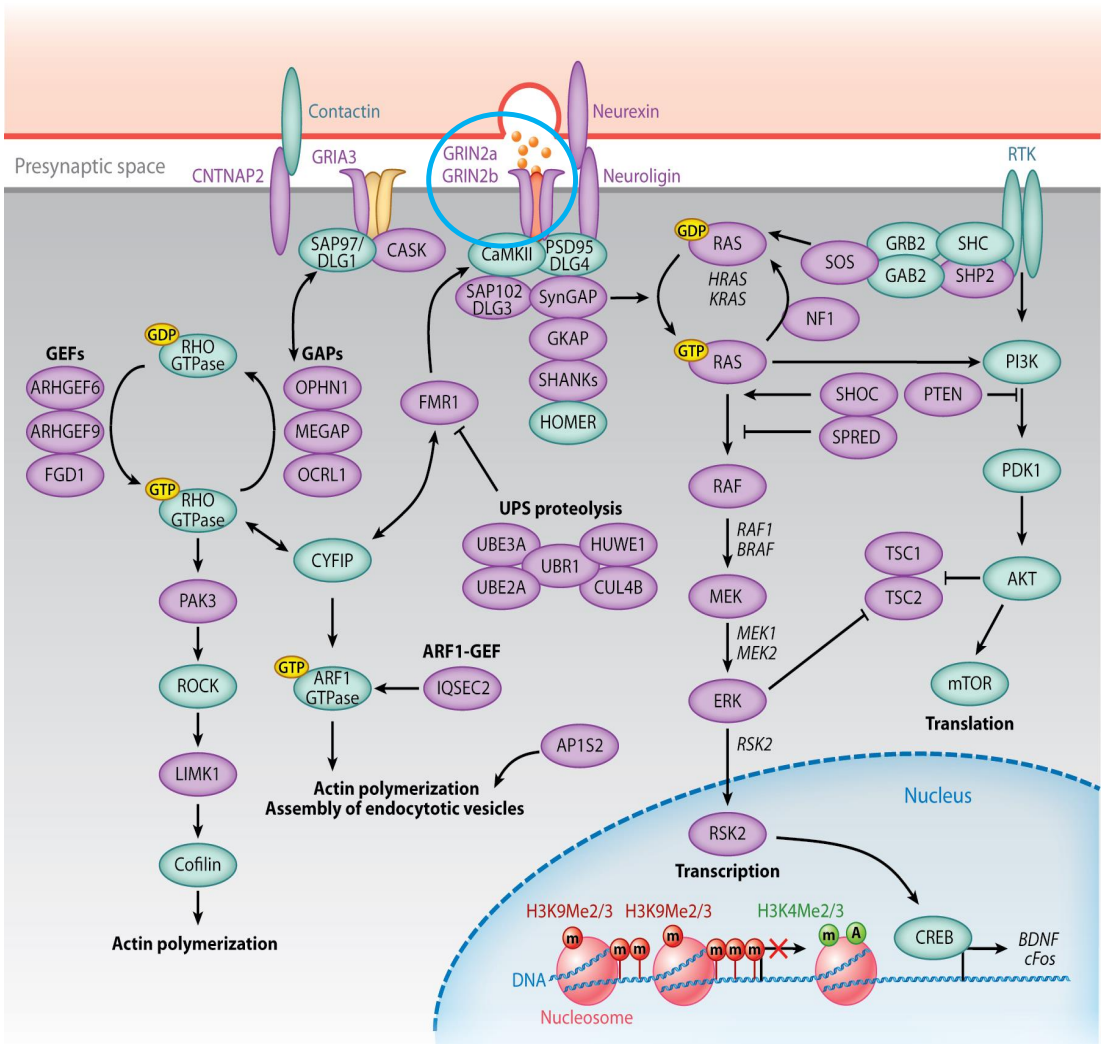

Figure 1.2: **Some of the post-synaptic proteins mutated in intellectual disability**
The diagram shows a post-synaptic region of a neuron highlighting pathways in which proteins have been found to be mutated in intellectual disability. Mutated proteins are shown in purple. The blue circle marks *GRIN2A* and *GRIN2B*, the subject of the remainder of this thesis. Taken from van Bokhoven (2011).

1.3 Identification and classification of ionotropic glutamate receptors

This section provides a brief historical background to the identification of NMDARs, placing them in context amongst related receptors.

The acidic amino acid L-glutamate was first considered as a neurotransmitter because of its high concentrations in brain (Berl and Waelsch, 1958), and its ability to induce convulsions (Hayashi, 1952), change electrical activity in rabbit cortex ("spreading depression" (van Harreveld, 1959), cause contraction of crustacean muscle (van Harreveld, 1959), and evoke action potentials in spinal neurons (Curtis et al., 1960).

Synthetic amino acids were used to demonstrate the existence of two populations of receptors responding to excitatory amino acids in the spinal cord, with some being "aspartate-preferring" (NMDA more potent) and some "glutamate-preferring" (kainate more potent) (McCulloch et al., 1974). Selective antagonists were used to subdivide the "glutamate-preferring" receptors further, with currents evoked by L-glutamate, or the partially selective agonist quisqualate, showing block by the antagonist GDEE, but those evoked by kainate showing insensitivity to GDEE (McLennan and Lodge, 1979). These three groups became known as NMDA, quisqualate and kainate receptors, with quisqualate replaced by AMPA once the latter was found to be more selective than quisqalate (which also activates metabotropic glutamate receptors (Sladeczek et al., 1985)). Initially it was thought that NMDA receptors were most likely to be activated by L-aspartate, and kainate and AMPA receptors by L-glutamate. However, binding studies with the NMDAR selective antagonist D-AP5 demonstrated that L-glutamate was far more potent than L-aspartate at displacing D-AP5 from NMDARs (Olverman et al., 1984), establishing L-glutamate as the key physiological activator of NMDARs.

The development of AMPA and kainate receptor-specific antagonists such as CNQX (Fletcher et al., 1988; Honore et al., 1988) allowed dissection of the contribution of different glutamate receptor subtypes to synaptic responses. Excitatory post synaptic potentials in *X. laevis* motoneurons were shown to be a summation of early, fast, non-NMDAR receptor currents, and later, slower, NMDAR currents (Dale and Roberts, 1985). This work demonstrated both that multiple types of glutamate receptor were present at the same synapse, and showed that NMDARs mediated longer lasting currents than other glutamate receptors.

A number of pharmacological differences between NMDARs extracted from different brain regions led to the suggestion that NMDARs may be comprised of different subtypes with different regional distributions (Reynolds and Palmer, 1991; Yoneda and Ogita, 1991). This was confirmed following cloning of glutamate receptor subunits in the late 1980s and early 1990s (reviewed in Lodge (2009)) and summarised in Table 1.1. The first glutamate receptor to be cloned was the AMPA receptor GluA1 subunit (initially thought to be a kainate receptor), identified by screening of cDNA libraries via mRNA injection in *X. laevis* oocytes followed by screening for glutamate-evoked currents (Hollmann et al., 1989). Sequence homology was used to clone three further AMPA receptor subunits, and five kainate receptor subunits were identified in this manner also. The first NMDAR subunit to be cloned, GluN1, again

required functional screening of cDNA libraries via oocytes (Moriyoshi et al., 1991). A further four genes encoding type 2 NMDAR subunits were identified within two years, but the two remaining NMDAR genes, encoding type 3 subunits, were not identified until 1995 and 2002. In addition, two "orphan" subunits were identified in the early 1990s, GluD1 and GluD2, which have substantial sequence homology with glutamate receptors yet are not known to assemble into any functional channels. Despite this, they have some physiological role, as the $\delta 2$ subunit is required for synaptic plasticity in the cerebellum and a gain of function mutation in it causes ataxia (Zuo et al., 1997).

Table 1.1: Ionotropic glutamate receptor subunits

AMPA	**Kainate**	**NMDA**	**Delta**
GluA1	GluK1	GluN1	GluD1
GluA2	GluK2	GluN2A	GluD2
GluA3	GluK3	GluN2B	
GluA4	GluK4	GluN2C	
	GluK5	GluN2D	
		GluN3A	
		GluN3B	

International Union of Basic and Clinical Pharmacology (IUPHAR) names.

Section summary

In summary, the NMDAR is one of a family of glutamate receptors, which together play an important role in excitatory synaptic transmission in the central nervous system. Early work found NMDARs to be distinguishable from other glutamate receptors by their pharmacology and kinetics of synaptic responses. The next section provides more detail on further unique properties of NMDARs, and how these contribute to their function.

1.4 NMDAR structure and function

This section gives a brief overview of NMDAR subunit composition, functional domains, regulation, and functional roles, highlighting key structural determinants where known. It focusses on the 2A and 2B subunit of the receptor, as these are the subunits in which most mutations have been found (see Section 1.6).

1.4.1 NMDAR overview

Ultimately the activity of NMDARs is thought to convert specific patterns of neural input into sustained alterations in synaptic location and strength, underpinning cognition (Bliss and Collingridge, 1993). They are well placed to do this because of an unusual set of properties. Firstly, they have high permeability to Ca^{2+} (MacDermott et al., 1986). This is important because Ca^{2+} is an important second messenger which is able to trigger signalling cascades leading to alterations in synaptic plasticity and gene expression (West et al., 2001). Secondly, they are "molecular coincidence detectors": voltage-dependent block of their pore by Mg^{2+} ions means their activation requires both the presence of glutamate and post-synaptic depolarisation, to expel the Mg^{2+} ion (Mayer et al., 1984; Nowak et al., 1984). Thirdly, they are made very sensitive to the extracellular environment by a range of modulatory sites for endogenous regulators, and by the requirement for a co-agonist (glycine or D-serine) (Johnson and Ascher, 1987; Mothet et al., 2000). Fourthly, they have slow deactivation rates, facilitating temporal integration of synaptic currents (Erreger et al., 2005). Finally, they have long cytoplasmic tails which contain sites for interaction with many other proteins in the post-synaptic density (Husi et al., 2000), allowing a high degree of regulation and potentially even non-ionotropic signal transduction (Gray et al., 2016).

1.4.2 NMDAR subunits

NMDARs are encoded by seven genes. NMDARs assemble as tetramers of two GluN1 subunits and two others, selected from four type two subunits (GluN2A-D) and two type three subunits (GluN3A, B) (Paoletti et al., 2013). The GluN1 subunit has eight functionally distinct splice variants (GluN1-1a-4a and GluN1-1b-4b). The GluN1-b isoforms contain an extra 21 amino acids in the N terminus which reduce proton sensitivity (Traynelis et al., 1995) and speed up deactivation rates (Rumbaugh et al., 2000). The GluN1-1-4 isoforms are distinguished by different combinations of three short casettes in the C terminus which influence trafficking (Horak and Wenthold, 2009). Glun1-1a and GluN1-2a are the commonest forms expressed in the rat forebrain, although GluN1-1b is also found in particular regions of cortex and hippocampus (Laurie and Seeburg, 1994). Although a number of splice variants exist in the other subunits they are not known to be functionally important (Cull-Candy et al., 2001). Recent X-ray crystallography structures showed the four subunits to arrange as a "dimer of dimers" with the subunit types alternating, rather than neighbouring an identical subunit (Karakas and Furukawa, 2014; Lee et al., 2014). If the two subunits partnering the

GluN1 subunit are the same, the receptors are termed diheteromers. If they are different, they are termed triheteromers.

Different subunit compositions lend different properties to NMDARs. NMDARs containing GluN2A and GluN2B subunits form one broad group, GluN2C/D subunits another, and GluN3A/B subunits a third. Figure 1.3 highlights the differences in subunit properties between GluN2 subunits: NMDAR diheteromers containing GluN2A/B show higher conductance, Ca^{2+} permeability, Mg^{2+} block, open probability and deactivation rate than GluN2C/D diheteromers (Wyllie et al., 2013). All of these properties are important in determining the integration of synaptic activity by NMDARs and thus the nature of any synaptic plasticity that arises in response to a given input.

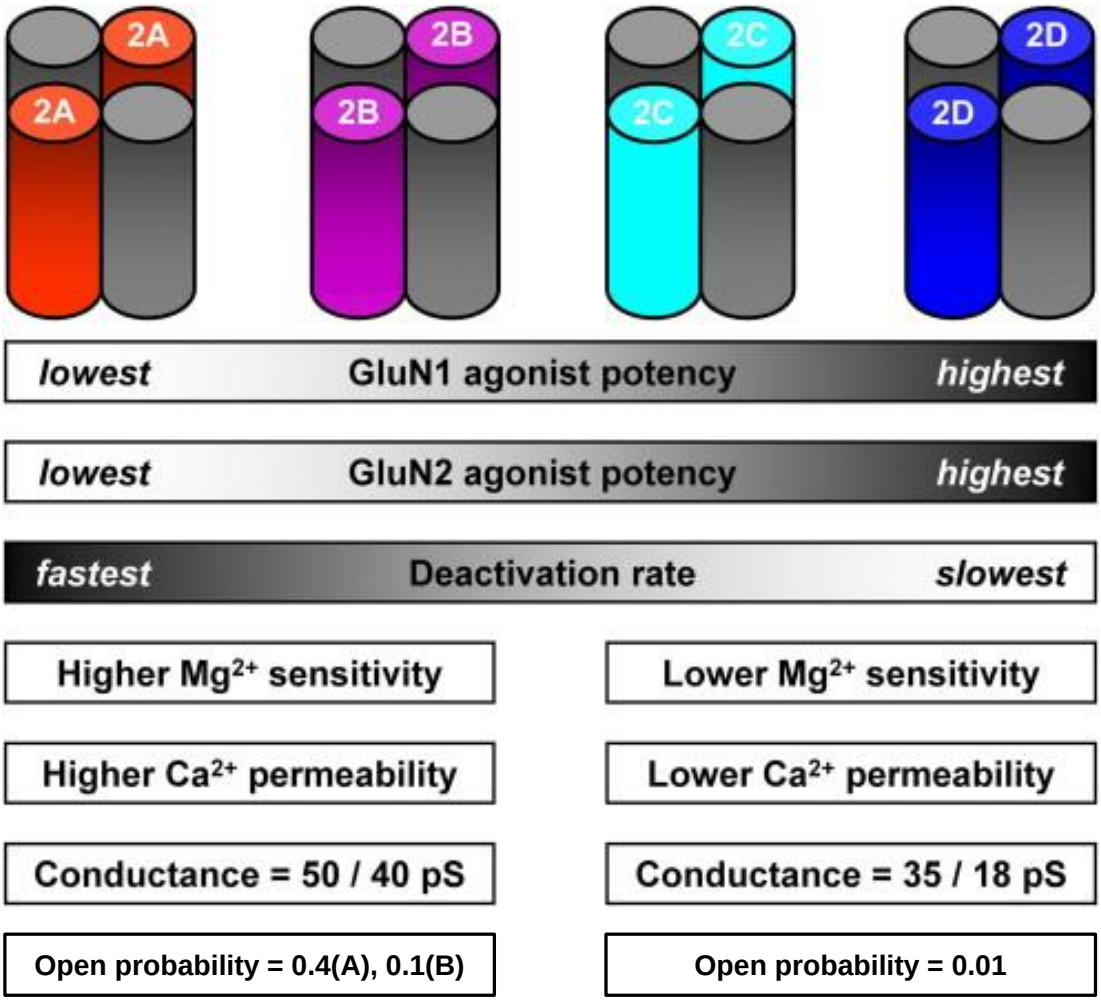

Figure 1.3: **Influence of subunit identity on NMDAR properties**
The schematic groups NMDAR subunits by influence on key biophysical properties, modified from Wyllie et al. (2013). The main and major sub-conductance level conductances are provided. Values for open probability taken from Traynelis et al. (2010) and Dravid et al. (2008).

GluN3 diheteromeric NMDARs are very different to other NMDARs: activated by glycine, not glutamate, with minimal Ca^{2+} conductance and no Mg^{2+} block, they are effectively excitatory glycine receptors (Chatterton et al., 2002). Recently, the existence of GluN3

diheteromers has been confirmed in optic nerve myelin (Pina-Crespo et al., 2010) and in hippocampal cultures (Rozeboom et al., 2015). However, GluN3 subunits are thought most likely to be expressed *in vivo* as triheteromers with GluN2 subunits. Such GluN2/3 triheteromers show reduced Ca^{2+} permeability, Mg^{2+} block, conductance and open probability compared to GluN2 diheteromers (reviewed in Pachernegg et al. (2012)). Overall, knowledge of the physiological roles of GluN3-containing NMDAR is considerably less advanced than for GluN2 subunits.

1.4.3 NMDAR subunit domains

NMDAR subunits have four main functional domains (reviewed in Paoletti et al. (2013) and Wyllie et al. (2013)), shown in Figure 1.4. The N terminus contains residues important in subunit assembly, allosteric modulation and gating. The agonist binding domain is comprised of two non-consecutive residue ranges termed S1 and S2, which interact to form a clam shell confirmation to bind glycine, in the case of GluN1 and GluN3, or glutamate, in the case of GluN2. The transmembrane domains form the pore, creating the ion selectivity filter and mediating Mg^{2+} block. The C terminus contains residues important for trafficking, anchoring and coupling of the receptor to myriad intracellular proteins.

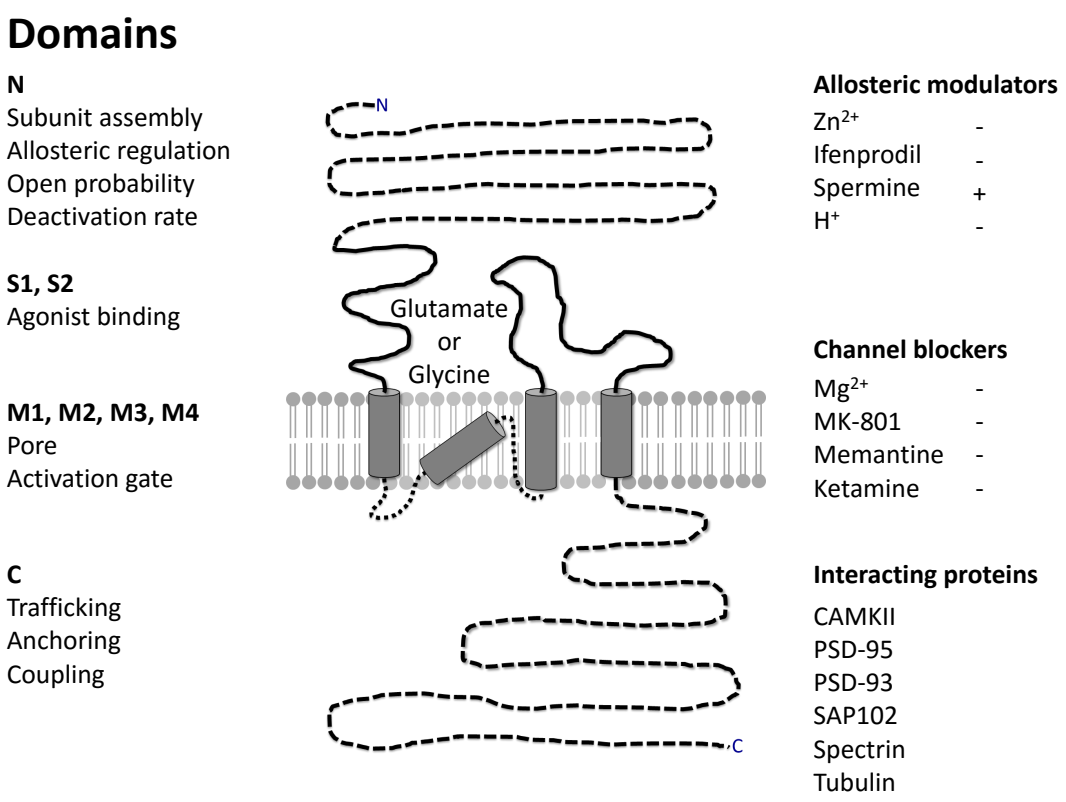

Figure 1.4: **Function of NMDAR domains**
The schematic shows principal NMDAR subunit domains: the dashed black lines represent the N and C termini, the solid black lines the ligand binding domain (S1 and S2), the cylinders the transmembrane domains (M1, M3, M4) and re-entrant loop (M2) and the dotted lines the M1-M2 and M2-M3 linker regions. The key functions of each domain are noted on the left. Glycine binds GluN1 and GluN3 subunits, and glutamate binds GluN2 subunits. Common regulatory ions and molecules are listed on the right, matched to approximate binding site. Whether they inhibit or potentiate is marked by + or -. The degree of their influence varies with subunit identity. Some key proteins which interact with the C terminus are listed on the bottom right. This list does not include many proteins shown to interact with NMDAR C termini.
Sources: Paoletti et al. (2013), Traynelis et al. (2010), Wenthold et al. (2003).

1.4.4 NMDAR subunit expression

NMDARs show substantial spatial and temporal regulation of expression, with marked differences between subunits. Detailed assessment of this has been performed using in situ hybridisation in mice (Watanabe et al., 1992) and rats (Monyer et al., 1994). Consistent with its obligatory role in all NMDARs, GluN1 is expressed ubiquitously from late gestation onwards, increasing into adulthood. GluN2B subunits are expressed in late gestation in all brain areas but gradually become confined to the forebrain by adulthood. In contrast, GluN2A expression commences after birth and gradually increases until GluN2A subunits are abundant throughout the brain. GluN2C is mainly expressed in the cerebellum and olfactory bulb and expression does not commence until postnatal day 10. Similarly to GluN2B, GluN2D expression commences prenatally, predominantly in the mid and hindbrain, but reduces throughout adolescence until by adulthood it is expressed mainly in the midbrain

at low levels. The expression of GluN3 subunits is also spatially and temporally restricted (reviewed in Pachernegg et al. (2012)). GluN3A is expressed at high levels in the few days after birth, particularly in layer V of the neocortex, before declining to very low levels in adulthood, whereas GluN3B slowly increases following birth until it is expressed at highest levels in the neocortex, hippocampus, cerebellum and motor neurons.

In humans, data are much scarcer due to the need for post-mortem tissue. However, the overall trends are the same as those found in rodents. In situ hybridisation of fetal tissue (8-20 weeks gestation) identified high levels of GluN1, GluN2B and GluN2D mRNA in most brain areas with detectable but low levels of GluN2A and GluN2C mRNA (Ritter et al., 2001). An in situ hybridisation study of the hippocampus only at older ages (5 weeks post-natally to adulthood) (Law et al., 2003) found GluN1 was expressed in neonates, with levels doubling over the age of 6-12 months. GluN2B was expressed at highest levels in neonates, declining over age 6-12 months to adult levels. GluN2A expression was stable from 1-3 months old into adulthood. The dorsolateral prefrontal cortex was also found to show a pattern of gradual increase in GluN1 mRNA and protein from gestation to adulthood (Henson et al., 2008) whereas GluN3A expression was found to peak in infancy and then decline (Henson et al., 2008). In contrast to these studies, immunoblotting of brains from 20 weeks gestation to adulthood found levels of all NMDAR subunits investigated (GluN1, GluN2A, GluN2B, GluN2C, GluN2D and GluN3A) to be highest prenatally (Jantzie et al., 2015). However, this sample contained relatively few adults and a large proportion of fetuses born prematurely or as stillbirths, which could conceivably influence NMDAR subunit expression. Taken together, it seems that human brains primarily express GluN1, GluN2B and GluN2D prenatally, with increases in GluN1 and GluN2A over childhood and adolescence, a decline in GluN2B over a similar time period, and a peak in GluN3A in the first year of life.

In addition to the gross regional expression patterns described above, NMDAR subunit expression varies between cell types and even by sub-cellular location. For example, within the same cell, layer 5 pyramidal cells have been found to show different NMDAR subunit compositions at synapses receiving input from local cortical circuits (mainly GluN2B) and synapses receiving input from the opposite hemisphere (mainly GluN2A) (Kumar and Huguenard, 2003). Further, there is a bias (not an absolute distinction) towards GluN2A being found synaptically and GluN2B both synaptically and extra-synaptically (reviewed in Parsons and Raymond (2014)).

1.4.5 NMDAR function: overview

What is the function of NMDARs in the central nervous system? They are clearly important as global knock-out of GluN1 in mice results in death within 24 hours of birth, with pups showing signs of respiratory difficulties and ataxia (Forrest et al., 1994; Li et al., 1994). The following sections give very brief overviews of the key areas of brain function in which NMDARs are known to be involved, highlighting the role of GluN2A and/or GluN2B subunits where applicable.

1.4.6 NMDAR function: synaptic transmission

NMDARs are cation permeable ion channels, allowing Na^+ and Ca^{2+} to enter the cell and K^+ to leave. Although their blockade by Mg^{2+} ions at resting membrane potentials makes them unable to initiate neuronal excitation, they are able to further enhance excitation at an already depolarised post-synaptic membrane (Collingridge et al., 1988). Their prolonged duration of activation relative to other glutamate receptor sub-types allows them to make a unique contribution to excitatory drive. The precise duration of depolarisation is very important for the cyclical circuit activity underlying the generation of neural oscillations, and there is evidence suggesting NMDARs are important in this process (see Figure 1.5). For example, NMDAR pharmacological blockade or genetic deletion in interneurons alters the generation of gamma oscillations in the cortex and hippocampus (reviewed in Gonzalez-Burgos and Lewis (2012)) and modelling studies suggest NMDARs temporally constrain visual cortex responses (Rangan et al., 2005) and thalamocortical responses to visual stimuli (Krukowski and Miller, 2001). A role in the generation of neural oscillations is important as coordinated neural activity is thought to underpin key cognitive processes such as perception, attention and working memory and be disrupted in subtle disorders of cognition such as autism and schizophrenia (Uhlhaas and Singer, 2012).

There is some evidence suggesting GluN2A may be particularly important in driving the inhibition required for coordinated neural activity, as parvalbumin positive interneurons in culture show a five-fold higher GluN2A:GluN2B ratio than neighbouring pyramidal cells (Kinney et al., 2006). Further, in *Grin2a* knock-out mice, NMDA evokes 50% less striatal GABA release than in wild type animals (Miyamoto et al., 2001).

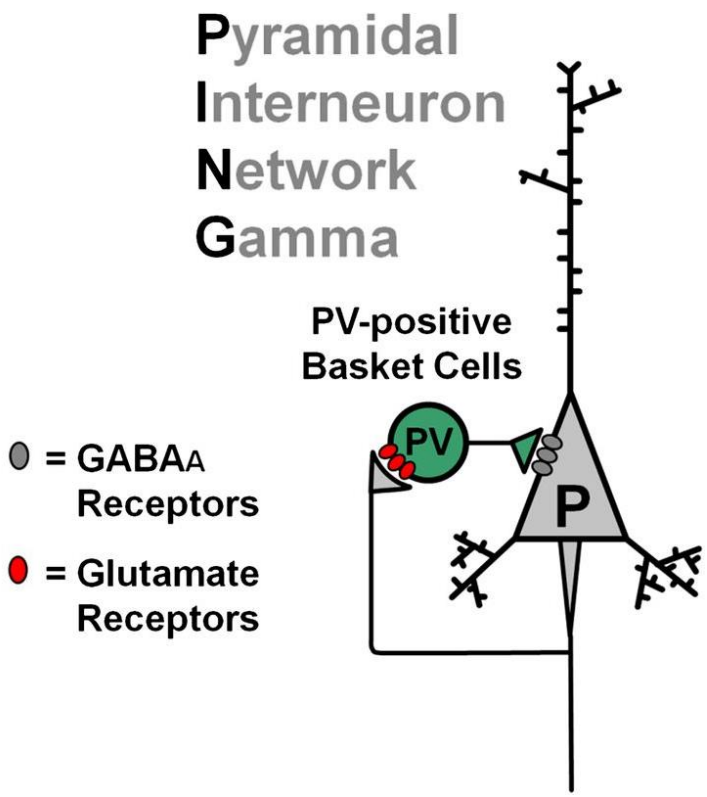

Figure 1.5: **Role of glutamate receptors in generation of gamma oscillations**
The diagram shows a popular model for how high frequency (gamma) oscillations are generated in neural networks. Pyramidal (P) cells stimulate excitatory glutamate receptors (AMPARs and NMDARs) on parvalbumin (PV) positive basket cell interneurons which in turn inhibit pyramidal cells via $GABA_A$ receptors. This negative feedback loop results in synchronised firing of groups of pyramidal cells, and thus generation of detectable oscillations. Taken from Gonzalez-Burgos and Lewis (2012).

1.4.7 NMDAR function: synaptic plasticity

In addition to NMDARs' important roles in neurotransmission, they are also able to integrate signals at synapses in a way that regulates synaptic abundance or strength. This is mediated by their ability to act as molecular coincidence detectors (see Figure 1.6). As alterations in synaptic strength are thought to underlie learning and memory (Kandel et al., 2014) the role of NMDARs in these processes has received a great deal of attention. This subsection provides a very brief account of this large and complex field.

The weakening or strengthening of synapses in response to activity is known as synaptic plasticity (Kandel et al., 2014). In the hippocampus, high frequency stimulation leads to an increase in subsequent response to stimulation (long term potentiation (LTP) (Bliss and Lomo, 1973)) whereas low frequency stimulation leads to a decrease in subsequent response (long term depression (LTD) (Dudek and Bear, 1992; Mulkey and Malenka, 1992). NMDARs were first identified as required for certain types of synaptic plasticity in the hippocampus, but are now known to be important in plasticity in multiple brain regions, including cortex (Sawtell

et al., 2003) and cerebellum (Rossi et al., 2002). However, not all forms of synaptic plasticity are NMDAR dependent, for example, mossy fibre LTP in the hippocampus (Harris and Cotman, 1986), Purkinje cell LTD in the cerebellum (Ito et al., 1982) and metabotropic glutamate receptor dependent LTD in the CA1 region of the hippocampus (Oliet et al., 1997).

The current paradigm for how NMDAR activity modulates synaptic strength has recently been reviewed (Huganir and Nicoll, 2013; Kandel et al., 2014) and is summarised here and in Figure 1.6. NMDARs are only activated when glutamate is released onto a synapse which has recently been activated and thus has a depolarised post-synaptic membrane. A strongly stimulated synapse results in a lot of NMDAR activation, and hence a lot of Ca^{2+} entry (leading to LTP), a weakly stimulated synapse results in modest levels of NMDAR activation and hence modest levels of Ca^{2+} entry (leading to LTD). The Ca^{2+} influx activates a range of intracellular proteins (CAMKII and protein kinases for LTP, calcineurin and protein phosphatases for LTD). These proteins then influence AMPAR trafficking to the membrane (increasing it in LTP, decreasing it in LTD) and alter gene expression in a way that maintains this altered AMPAR density. The alterations in gene expression can also lead to structural changes at the synapse, with enlargement or reduction in dendritic spine volume. Although this is the current working model for these processes, there are a number of challenges to various steps within it. In particular, duration and location of Ca^{2+} transients have been suggested to be at least as important as Ca^{2+} transient amplitude in controlling the direction of plasticity (reviewed in Evans and Blackwell (2015)). It has also recently been suggested that LTD may be initiated by metabotropic NMDAR signalling (reviewed in Gray et al. (2016)).

It seems paradoxical that the same receptor population could mediate synaptic plasticity in opposing directions. An appealing idea to explain this is that different NMDAR subunits underlie different types of plasticity (reviewed in Wyllie et al. (2013)). Pharmacological studies seeking to address this using subunit specific antagonists initially appeared to suggest that GluN2A was required for the initiation of LTP, and GluN2B for LTD. However, some studies were limited by the use of the so-called GluN2A selective antagonist NVP-AAM077 at doses which also block GluN2B containing receptors (Frizelle et al., 2006)). Further, the existence of triheteromeric receptors complicates the assessment of the role of the subunits comprising them, as antagonists which strongly inhibit receptors containing a given subunit diheteromerically may cause minimal inhibition of a receptor containing the same subunit triheteromerically. Genetic studies, knocking out GluN2A or GluN2B in forebrain neurons, show that loss of either subunit leads to deficits in LTP. The GluN2B C terminus appears to be particularly important, as demonstrated by experiments where the C termini of GluN2A and GluN2B subunits are swapped - GluN2B with a GluN2A C terminus is unable to support the same forms of LTP as GluN2B with its native terminus. These experiments de-emphasise the importance of receptor biophysical properties in mediating synaptic plasticity and instead highlight the role of interactions with proteins such as CAMKII (which can bind the GluN2B but not GluN2A C terminus). An emerging consensus is that the high Ca^{2+} flux offered by GluN2A's high open probability may work in concert with the CAMKII binding site in GluN2B's C terminus to mean the two subunits jointly facilitate synaptic plasticity (Paoletti et al., 2013).

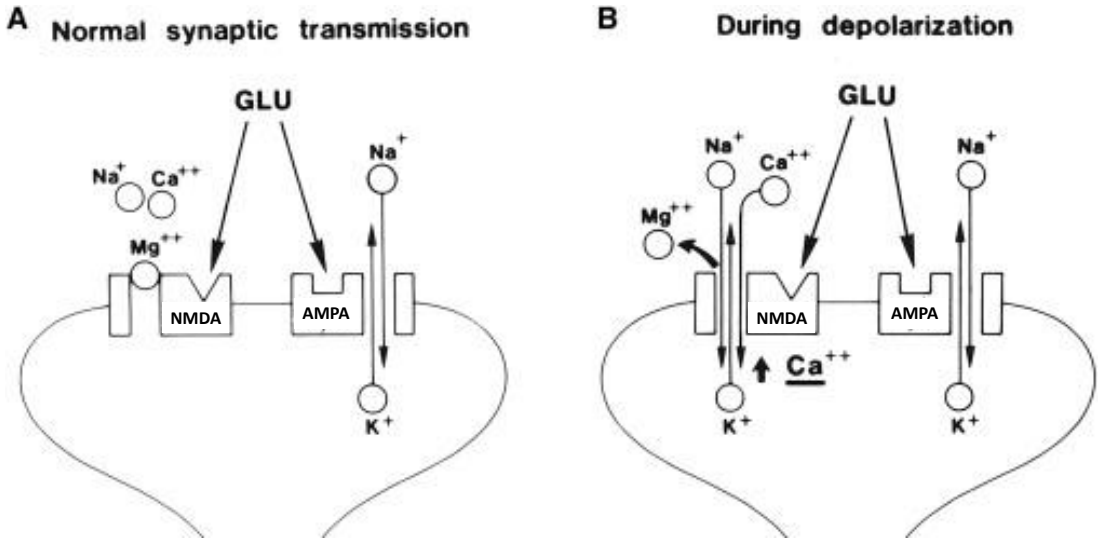

Figure 1.6: **NMDAR mediated synaptic plasticity**
The schematic shows a model first published in 1988 describing how NMDAR can initiate LTP in the hippocampus CA1 region (taken from Huganir and Nicoll (2013), with minor modifications). Although this model has become much more detailed, the basic principles are the same now as when it was first published. In **A**, glutamate release at a dendritic spine activates AMPARs but not NMDARs, due to Mg^{2+} block. In **B**, the synapse has been exposed to high frequency stimulation and the post-synaptic membrane is depolarised. This has expelled the positively charged Mg^{2+} ions from the NMDAR pore. Now, when glutamate is released, both AMPARs and NMDARs are activated, allowing Ca^{2+} to enter the spine and activate signalling proteins which lead to LTP.

1.4.8 NMDAR function: synaptogenesis and synaptic pruning

The ultimate way to alter synaptic strength is to create or remove synapses: synaptogenesis or synaptic pruning. NMDAR activity is also implicated in these processes. New synapses are thought to arise as follows (Cline and Haas, 2008): folllowing an initial contact between adhesion molecules on motile filopodia extending from two neurons' axons or dendrites, NMDARs are recruited to the post-synaptic membrane. These immature synapses are "silent" as the release of glutamate will not activate them at resting membrane potentials. However, when the post-synaptic neuron is depolarised, glutamate will activate NMDARs and allow the recruitment of AMPARs and additional proteins necessary for synaptic scaffolding and signalling (the post-synaptic density), via mechanisms similar to LTP. This is associated with morphological changes in the neuron, with dendritic arbor development and synapse formation/maturation thought to arise jointly (Cline and Haas, 2008). This process is illustrated in Figure 1.7.

Both GluN2A and GluN2B have been found to be important in this process, with possible opposing effects on the probability of functional synapse formation (Gambrill and Barria, 2011; Gray et al., 2011). More recent evidence has also suggested a role for NMDARs in synaptic pruning, particularly the GluN3A subunit (Kehoe et al., 2014; Zhang et al., 2013).

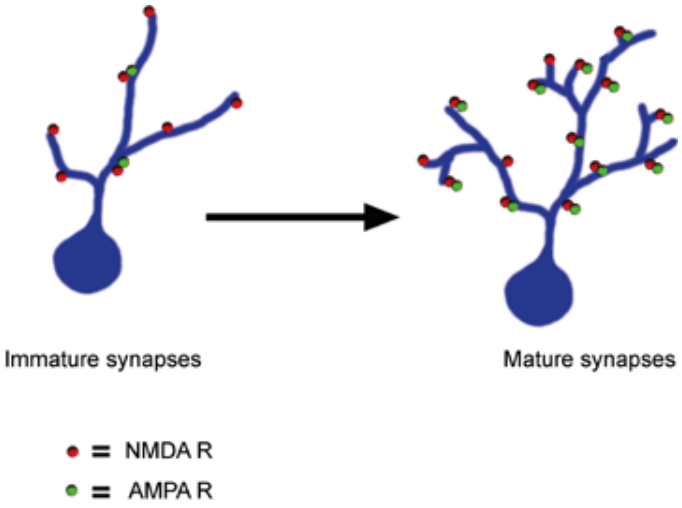

Figure 1.7: **NMDARs facilitate dendritic arbor development and synaptogenesis**
The diagram shows a neuron with a simple dendritic tree and several immature excitatory synapses where only NMDARs are present ("silent synapses"). After activation of NMDARs, AMPARs are recruited to the maturing synapses and the dendritic tree becomes more complex. Taken from Cline and Haas (2008).

1.4.9 NMDAR function: neuronal survival and death

The final function of NMDARs highlighted here is their role in neuronal survival and death. A range of evidence suggests that some NMDAR activation is required for neuronal survival, but too much results in cell death, with pro-survival signals arising mainly from synaptic NMDAR activation and pro-death signals arising mainly from extrasynaptic NMDARs (reviewed in Hardingham and Bading (2010), and see Figure 1.8).

The GluN2B subunit has a particularly important role in excitotoxicity as it is more likely to be present extra-synaptically (Parsons and Raymond, 2014) and its C terminus has been demonstrated to be more effective at transducing pro-death signals than that of GluN2A (Martel et al., 2012). GluN2B is also the more important subunit in determining survival, with GluN2B, but not GluN2A, required for survival of adult-born neurons (Kelsch et al., 2012).

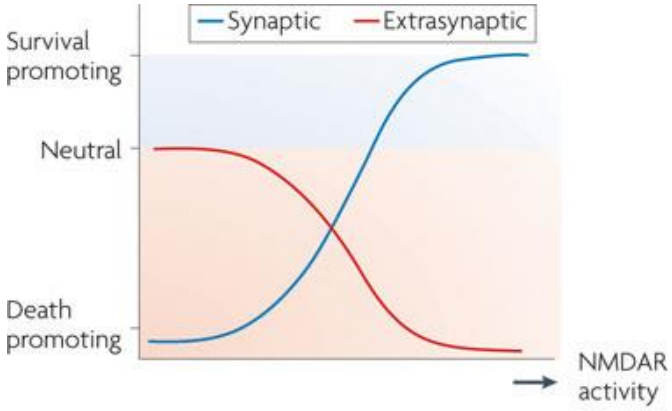

Figure 1.8: **Influence of synaptic and extra-synaptic NMDAR activation on neuronal survival**
The diagram shows how insufficient activity at synaptic NMDAR is death promoting, with higher activity levels promoting greater survival. In contrast, lack of activity at extrasynaptic NMDAR has no effect on survival, but higher levels promote cell death. Taken from Hardingham and Bading (2010).

Section summary

In summary, the NMDAR is an ionotropic glutamatergic neurotransmitter receptor with a number of unusual properties that make it well suited for its functions in contributing to coordinated neural activity, synaptic strength, synaptic abundance and neuronal survival. Different subunits confer different properties on the receptor, allowing it to diversify its effects. The GluN2A and GluN2B subunits are expressed in the forebrain and have important roles in key NMDAR functions, and alterations in their expression or properties would be anticipated to result in impairments in these brain functions.

1.5 What non-genetic evidence links NMDARs to brain disorders?

NMDAR dysfunction had been linked to brain disorders for several years prior to the emergence of genetic evidence. This section briefly considers what other lines of evidence link NMDAR dysfunction to brain disorders. The disorders are split into those associated with NMDAR overactivity and those associated with NMDAR underactivity.

The first group of disorders are those where NMDAR dysfunction may not trigger the condition, but is an important component of pathogenesis. They comprise neurodegenerative disorders (Alzheimer's disease, Parkinson's disease and Huntington's disease) and responses to tissue damage (stroke, traumatic brain injury, white matter injury and chronic pain). The overall pattern is that there is a damaging degree of overexpression or overactivation of NMDARs, predominantly those containing GluN2B subunits, resulting in cellular dysfunction and often an increase in cell death (summarised in Paoletti et al. (2013)). Blockade of NMDAR activation can alleviate symptoms, for example, the use of the NMDAR channel blocker memantine for moderate-severe Alzheimer's disease. These conditions highlight the potential damage that activating mutations in NMDAR subunits could cause, although the effects may not be as severe in the absence of other disrupted pathways or tissue damage.

The second group of disorders are those in which NMDAR underexpression or underactivation may be one of the initial events triggering the disorder: schizophrenia, and NMDAR auto-immune encephalitis. These disorders are of more relevance to disorders arising from mutations in NMDARs, where NMDAR dysfunction would also be predicted to be an initiating event, and so are considered in more detail below.

The NMDAR hypofunction theory of schizophrenia states that underactivation of NMDARs contributes to the symptoms of schizophrenia. It was first mooted when it was observed that the NMDAR channel blockers phenylcyclidine and ketamine caused symptoms similar to schizophrenia (psychosis and cognitive deficits) in healthy controls and worsened symptoms in those with schizophrenia (reviewed in Moghaddam and Krystal (2012)). Brain imaging studies also demonstrate abnormalities in glutamate levels in schizophrenia, as summarised in a recent meta-analysis (Merritt et al., 2016). Further, potentiation of NMDAR function by increasing availability of its co-agonists has been found to be of benefit in treating schizophrenia (reviewed in Hashimoto et al. (2013)). The hypoglutamatergic theory has been refined to propose that loss of GluN2A subunits from parvalbumin positive interneurons in particular may be a key step in schizophrenia pathogenesis. This theory is supported by the finding that selective knock-out of NMDARs in hippocampal and cortical GABAergic interneurons in mice leads to schizophrenia-like symptoms (Belforte et al., 2010) and by the observation of reduced density of GluN2A-positive parvalbumin positive interneurons in the pre-frontal cortex in schizophrenia post-mortem brains (Bitanihirwe et al., 2009).

In the last decade, the syndrome of NMDAR auto-immune encephalitis was recognised, which presents initially with psychosis, memory deficits, seizures and language disintegration (Dalmau et al., 2007). In this condition, patients generate antibodies against their own NMDARs (with the epitope comprising residues 368 and 369 of GluN1), causing receptor internalisation with a reduction in receptor density and NMDAR-mediated currents (reviewed

in (Masdeu et al., 2016)). The majority of patients recover if the antibodies can be removed or suppressed (Titulaer et al., 2013). This condition demonstrates that acute loss of NMDARs can be associated with devastating but reversible changes in brain function.

Section summary

Alteration of NMDAR expression or function has been observed in a number of neuropsychiatric disorders, and reversing the dysfunction has been shown to improve symptoms. This supports the hypothesis that a genetic change resulting in altered NMDAR expression or dysfunction could also cause neuropsychiatric disease, and also be potentially modifiable.

1.6 What genetic evidence links NMDARs to mental disorder?

1.6.1 Common variants

This section will focus on recently identified rare mutations in *GRIN2A* and *GRIN2B*. However, common variants in *GRIN2A* and related genes have also been found to influence risk for neurodevelopmental disorder. Early genetic evidence was provided by a genome wide linkage study which found a significant association between autism and single nucleotide polymorphisms in *GRIN2A* (Barnby et al., 2005). More recently, a genome wide association study in schizophrenia also highlighted a locus near *GRIN2A*, and another near *SRR* (encoding serine racemase, the enzyme that converts L-serine to the NMDAR co-agonist D-serine) as influencing risk for schizophrenia (Ripke et al., 2014). The convergence of common and rare variants in *GRIN2A* on risk for related neurodevelopmental disorders strengthens the evidence that *GRIN2A* is contributing to the pathogenesis of these disorders.

1.6.2 Rare variants

The first study to identify exonic mutations in NMDAR subunits was that of Endele et al. (2010) where a series of heterozygous point mutations and translocation break points in *GRIN2A* and *GRIN2B* were identified in people with comorbid epilepsy and intellectual disability. Over the next six years, this was followed by publication of over 100 other point mutations, microdeletions, copy number variants and translocations affecting these two genes and found heterozygously in people with a range of neurodevelopmental disorders. These findings are summarised in Table 1.2, Table 1.3 and Figures 1.9-1.12 and discussed further below. The majority of the mutations presented here have also been discussed in a review by Burnashev and Szepetowski (2015).

Mutations in other NMDAR subunits have also been idenfitied. *De novo* missense mutations in *GRIN1* have been found in five cases of epileptic encephalopathy (Allen et al., 2013; Ohba et al., 2015) and one of intellectual disability (Hamdan et al., 2011). Truncating mutations in *GRIN2C*, *GRIN3A* and *GRIN3B* have been found in people with autism and schizophrenia but are also found in controls so their relationship to disease is unclear (Myers et al., 2011; Tarabeux et al., 2011). As mutations in other NMDAR subunits so far appear to be much less common than those in *GRIN2A* and *GRIN2B* they are not considered further here.

Tables 1.2 and 1.3 show studies reporting *GRIN2A* and *GRIN2B* mutations. They highlight two things: the range of disorders in which mutations in *GRIN2A* and *GRIN2B* have been found, and the low prevalence of mutation within a given disorder. Mutations in *GRIN2A* have so far been found mainly in epilepsy-aphasia syndromes, and in *GRIN2B* mainly in autism, schizophrenia and intellectual disability. The highest prevalence of mutation are found with *GRIN2A* in the more severe form of epilepsy-aphasia syndomes, where one study found *GRIN2A* mutations in 100% of those with a family history of the disorder (Lesca et al., 2013) and another in 18% of those with the most severe form of the disorder, with or without a family history (Lemke et al., 2013). *GRIN2B* mutations so far have not been identified to be a

major contributor to any one disorder: prevalences of mutation are at most 1 in 50 for people with autism, schizophrenia or intellectual disability (considering studies assessing *GRIN2B* mutations in > 100 cases). The true mutation frequency is likely to be lower, as the tables give a falsely high impression of prevalence by not including studies which did not find any *GRIN2A* or *GRIN2B* mutations.

Table 1.2: Studies reporting protein altering and protein disrupting mutations in *GRIN2A*

Study	**Disorder**	**Mutation frequency**
	Epilepsy syndromes	
Dyment et al. (2015)	Refractory childhood epilepsy	22.2% (2/9)
Lesca et al. (2013)	Epilepsy-aphasia syndromes	14.9% (17/114)
Lemke et al. (2013)	Epilepsy-aphasia syndromes	8.6% (31/359)
Conroy et al. (2014)	Landau Kleffner syndrome	7.7% (1/13)
Reutlinger et al. (2010)	Epilepsy-aphasia syndromes	4.5% (3/66)
von Spiczak et al. (2011)	Photosensitive generalised epilepsy	2.1% (1/48)
Dimassi et al. (2014)	Rolandic epilepsy	2.1% (1/47)
Lesca et al. (2012)	Epilepsy-aphasia syndromes (LKS and CSWS only)	1.6% (1/61)
Carvill et al. (2013)	Epileptic encephalopathies	0.8% (4/519)
DeVries and Patel (2013)	Epilepsy and intellectual disability	Case series, n = 2
Yuan et al. (2014)	Epileptic encephalopathy	Case report
Singh et al. (2015)	Epileptic encephalopathy	Case report
Fainberg et al. (2016)	Landau Kleffner syndrome	Case report
	Other disorders	
Bramswig et al. (2015)	Coffin-Siris and Nicolaides-Baraitser syndromes	10.0% (1/10)
Endele et al. (2010)	Intellectual disability and epilepsy/abnormal EEG	3.1% (4/127) and 1 initial case
de Ligt et al. (2012)	Intellectual disability	2.0% (2/100)
Tarabeux et al. (2011)	Autism	1.4% (2/142)
	Schizophrenia	2.1% (9/429)

Studies which have identified heterozygous mutations in *GRIN2A* in association with mental disorder, ordered by frequency of mutation. Synonymous mutations or those found in controls not included. LKS = Landau Kleffner syndrome, CSWS = continuous spikes and waves during slow wave sleep. Coffin-Siris and Nicolaides-Baraitser syndromes are rare, closely related syndromes where severe intellectual disability is associated with particular congenital abnormalities.

Figure 1.9 shows all heterozygous missense mutations identified in *GRIN2A* and *GRIN2B*, however inherited. It is designed to highlight possible genotype:phenotype relationships. Comparing across subunits, it would appear that overall there are fewer mutations identified in *GRIN2B*. This may reflect its crucial role early in development, with mutations more likely to result in death *in utero*. Alternatively, *GRIN2B* mutations may result in a phenotype which has not yet been screened for *GRIN2B* variants. Mutations in *GRIN2A* are more often associated with epilepsy than those in *GRIN2B* and *GRIN2B* mutations are more often associated with intellectual disability than those in *GRIN2A*. However, there is substantial phenotypic overlap (at least at the level of diagnoses) between mutations in either gene.

Comparing across protein domains, the epilepsy-associated mutations are predominantly but not exclusively in the ligand binding and pore forming regions of the subunits, suggesting an influence on ion entry, whereas the schizophrenia or autism associated mutations are predominantly but not exclusively in the C or N terminals, suggesting an influence on interactions with signalling or regulatory proteins.

There are some caveats regarding the tentative genotype:phenotype conclusions drawn above. It is likely that at least some mutations found in patients are coincidental to their disorder. Comparison between subunits is difficult as the number of people sequenced for a given subunit varies (the mutations are derived from a mixture of whole exome and candidate gene studies). Comparison between disorders is difficult as the number of people with a given disorder sequenced varies (e.g. more people with epilepsy have been screened than people with intellectual disability). Finally, the phenotypic categories used overlap to some extent, and are sometimes based on incomplete information. For example, some people with *GRIN2B* mutations associated with autism also have mild intellectual disability, and some with intellectual disability have "autistic features". In others with autism, the presence or absence of intellectual disability is not reported. The approach used here has been to categorise phenotypes in line with the authors who reported the mutations e.g. if the cohort sequenced was selected for autism, the mutation is coded as this, regardless of intellectual disability.

Figure 1.10 shows only those missense mutations which were definitely inherited *de novo*. With one exception, these all influence the ligand binding or pore forming domain of either subunit. Of the nine missense mutations identified in the pore region, eight arose *de novo* and one was of unknown inheritance. This is consistent with mutations arising in these areas having more deleterious consequences than elsewhere, and thus being less likely to be passed on via reproduction.

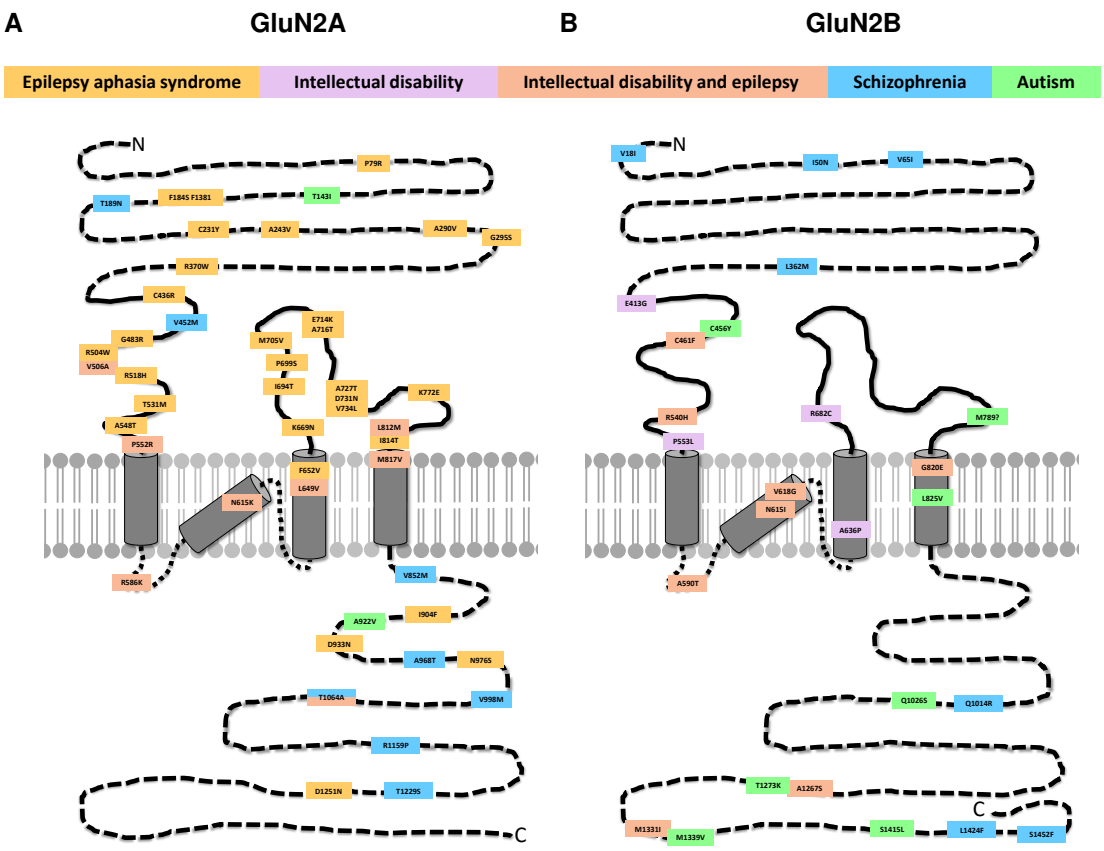

Figure 1.9: **Missense mutations identified in *GRIN2A* and *GRIN2B***
(A) This schematic shows the approximate location of heterozygous missense mutations within functional domains of the NMDAR, coloured by neurodevelopmental phenotype. NMDAR domains: the dashed black lines represent the N and C termini, the solid black lines the ligand binding domain (S1 and S2), the cylinders the transmembrane domains (M1, M3, M4) and re-entrant loop (M2) and the dotted lines the M2-M3 and M3-M4 linker regions (see Figure 1.4 for more information on functional domains). Synonymous mutations and those found in databases of single nucleotide polymorphisms are not included. Some mutations have been found multiple times in unrelated cases: R518H, A716T, D731N and N976S have all been found twice in unrelated families with epilepsy-aphasia syndromes, V452M has been found in a person with schizophrenia and a person with epileptic encephalopathy (who also carried a *de novo* sodium channel mutation) and the T1064A mutation has been found in three individuals (one with schizophrenia, one with epilepsy and one with intellectual disability with either EEG abnormalities or epilepsy).
(B) As **(A)** but for *GRIN2B*. V18I has been identified twice, in unrelated people with schizophrenia (inheritance unknown).
All mutations have been found heterozygously. The references for this figure are provided in Tables 1.2 and 1.3. A modified version of this figure has been published (Hardingham and Do, 2016).

Table 1.3: Studies reporting protein altering and protein disrupting mutations in *GRIN2B*

Study	Disorder	Mutation frequency
Autism and schizophrenia		
O'Roak et al. (2011)	Autism	5.0% (1/20)
Myers et al. (2011)	Autism; Schizophrenia;	2.0% (2/102) 2.2% (3/138)
Tarabeux et al. (2011)	Autism; Schizophrenia	0.7% (3/428); 1.6% (7/429)
Pan et al. (2015)	Autism	0.7% (2/275)
Kenny et al. (2014)	Autism; Schizophrenia;	0.7% (1/147); 0/273
Williams et al. (2012)	Schizophrenia	0.3% (2/690)
O'Roak et al. (2012b)	Autism	0.3% (3/1,073)
O'Roak et al. (2012a)	Autism	0.2% (4/2,446)
Talkowski et al. (2012)	Autism and neurodevelopmental disorder	0.03% (5/19,956) and 1 initial case
Intellectual disability		
Hamdan et al. (2014)	Intellectual disability	2.4% (1/41)
Endele et al. (2010)	Intellectual disability	1.5% (7/468) and 2 initial cases
Freunscht et al. (2013)	Intellectual disability	1.1% (1/93)
de Ligt et al. (2012)	Intellectual disability	1.0% (1/100)
Dimassi et al. (2013)	Intellectual disability with language delay	Case series, n=3
Adams et al. (2014)	Intellectual disability	Case report
Epilepsy syndromes		
Lemke et al. (2014)	Epilepsy	1.0% (4/404)
Allen et al. (2013)	Epileptic encephalopathies	0.4% (1/264)

Studies which have identified heterozygous mutations in *GRIN2B* in association with mental disorder, ordered by frequency of mutation. Synonymous mutations or those found in controls not included.

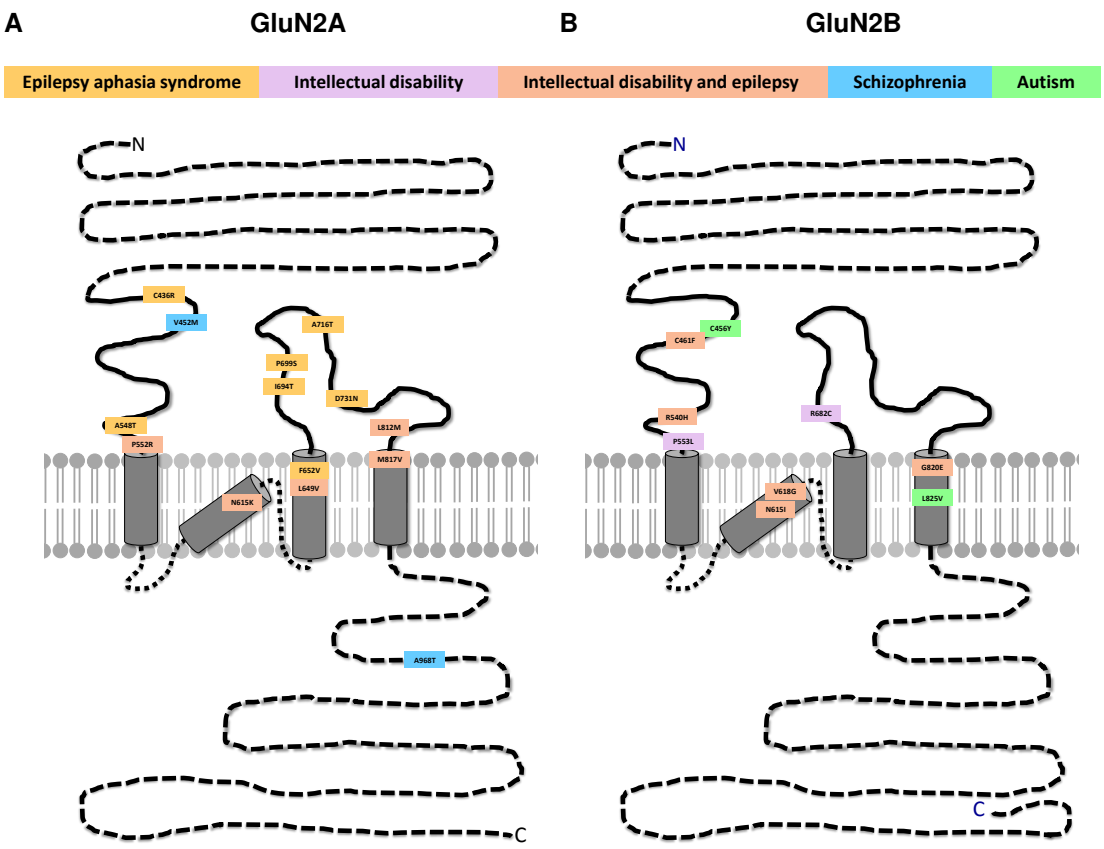

Figure 1.10: ***De novo* missense mutations identified in *GRIN2A* and *GRIN2B***
(A) This schematic shows the approximate location of *de novo* heterozygous missense mutations within functional domains of the NMDAR, coloured by neurodevelopmental phenotype. NMDAR domains are depicted as in Figure 1.9. Synonymous mutations and those found in databases of single nucleotide polymorphisms are not included.
(B) As **(A)** but for *GRIN2B*
All mutations have been found heterozygously. The references for this figure are provided in Tables 1.2 and 1.3.

Figure 1.11 shows heterozygous mutations which are predicted to result in absent or truncated protein products: absent start codons, premature stop codons, deleted codons, frameshifts, splice site mutations, microdeletions and copy number variants (deletions).

Although these mutations have been grouped together as "gene disrupting", their consequences may potentially be quite different - all can potentially prevent the protein from being expressed, but some could alternatively result in proteins with altered function and some could even result in normal proteins. For example, splice site mutations may not prevent normal protein expression if an alternative splice site is available. Premature stop codons may result in transcript degradation via nonsense-mediated decay (if the transcript terminates more than 50 bp to 5′ of the final exon), but this is not certain to occur (Holbrook et al., 2004). Thus any of the truncating mutations arising within the final exon, and potentially those before, could conceivably be expressed and generate an almost complete protein, terminating in novel residues in the case of frameshifts. The impact of the deletion of a single codon is also hard to predict, with outcome likely to depend on the structural context.

When the impact of these potential gene disrupting mutations has been assessed, they have mainly been found to reduce expression, as predicted. Two *GRIN2B* splice variants and a *GRIN2A* premature stop codon were not shown to result in alternatively spliced products, but a *GRIN2B* frameshift mutation was detected at the mRNA level (Endele et al., 2010). In summary, the majority of the mutations shown in Figure 1.11 probably result in monoallelic expression of the wild type allele but this is not definite for any of the mutations except those that completely delete the gene or the small number which have been experimentally assessed.

Making the assumption that the majority of these potentially gene disrupting mutations do indeed result in monoallelic expression, what can be inferred about the consequences of only one functional *GRIN2A* or *GRIN2B* allele? Firstly, the presence of neurodevelopmental disorders in their carriers suggests that this results in haploinsufficiency - one copy of a subunit is not enough (in contrast to the majority of genes). Secondly, all the *GRIN2A* disrupting mutations are associated with epilepsy, with the vast majority (23/29) of that being in the form of epilepsy-aphasia syndromes. In the case of *GRIN2B*, gene disuption is associated with a fairly even split of either autism or intellectual disability (or a combination). These phenotypic associations are less diverse than what was seen with missense mutations, reflecting the simpler proposed mechanism - an absence of protein, rather than a range of proteins with altered functions.

The final mutation diagram shows probable gene disrupting events which are known to have arisen *de novo* (Figure 1.12). Interestingly, very few of the *GRIN2A* disrupting events arose *de novo* whereas the majority of the *GRIN2B* disrupting events did. This suggests that the consequences of *GRIN2B* disruption may be more deleterious than that of *GRIN2A*, with disrupting mutations not passed on through reproduction.

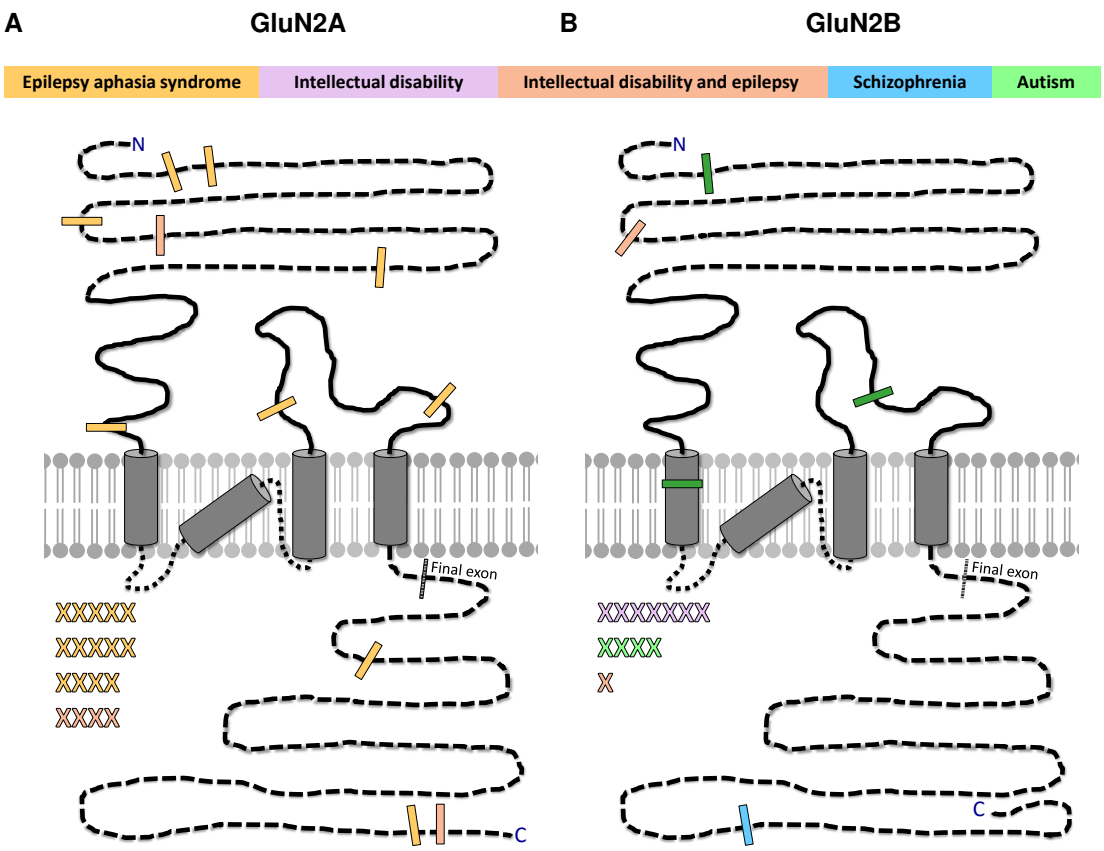

Figure 1.11: **Gene disrupting mutations identified in *GRIN2A* and *GRIN2B***
(A) This schematic shows mutations in *GRIN2A* likely to result in an absent or truncated protein, coloured by neurodevelopmental phenotype. NMDAR domains are depicted as in Figure 1.9. Bars mark premature stop codons, frameshifts, and a deleted codon, marked at their approximate locations. Those prior to the start of the final exon encode mRNA transcripts at risk of nonsense-mediated decay and hence no protein product. Crosses indicate more severe gene disruption (loss of start codon, splice site mutation, microdeletions partially or completely deleting the gene, copy number deletions, and a translocation disruption).
(B) As **(A)** but for *GRIN2B*. In addition, a *GRIN2B* copy number deletion has been identified in a person with an unspecified neurodevelopmental disorder (Talkowski et al., 2012) but has not been marked on the figure (because of the uncertain phenotype).
All mutations have been found heterozygously. The references for this figure are provided in Tables 1.2 and 1.3.

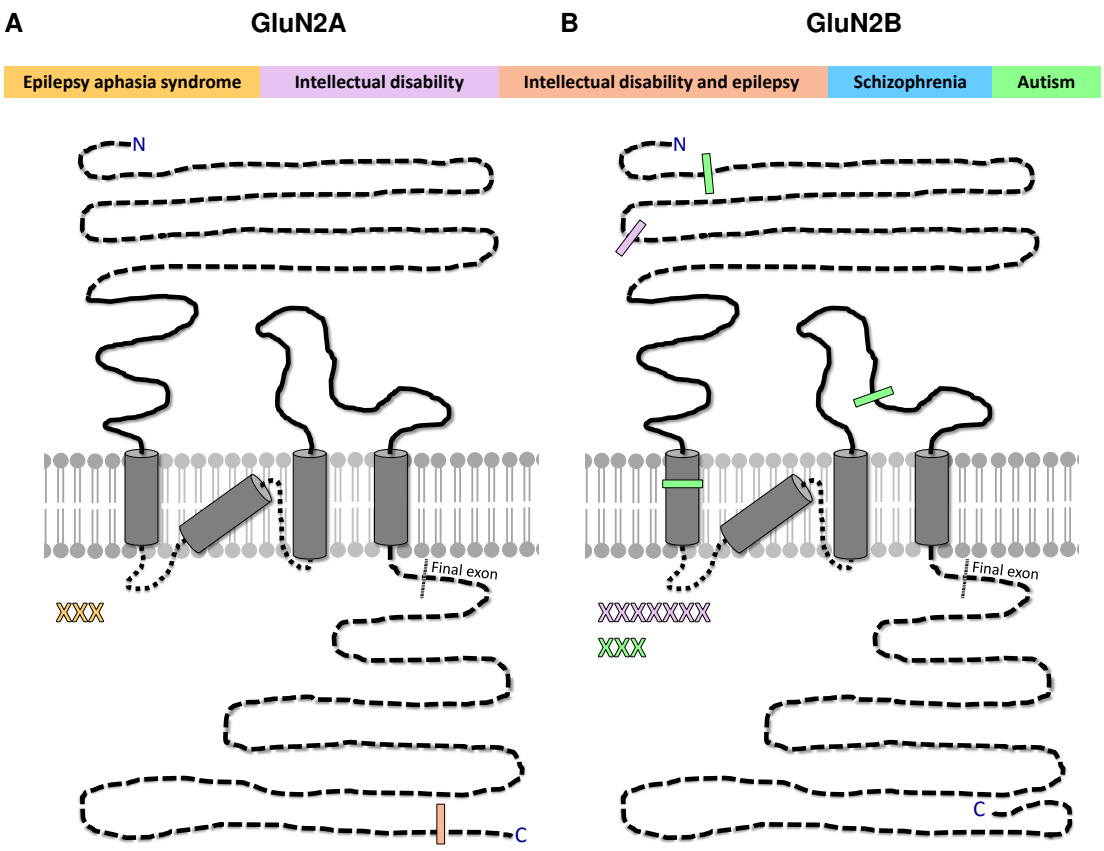

Figure 1.12: ***De novo* gene disrupting mutations identified in *GRIN2A* and *GRIN2B***
(A) This schematic shows *de novo* mutations in *GRIN2A* likely to result in an absent or truncated protein, coloured by neurodevelopmental phenotype. NMDAR domains are depicted as in Figure 1.9. The bar marks a frameshift mutation associated with severe intellectual disability and epilepsy. Crosses indicate three microdeletions, all associated with epilepsy-aphasia syndrome. **(B)** As **(A)** but for *GRIN2B*. The bars mark two frameshifts and two premature stop codons, marked at their approximate locations. They are all prior to the start of the final exon and so encode mRNA transcripts at risk of nonsense-mediated decay and hence no protein product. Crosses indicate more severe gene disruption (splice site mutations, and three microdeletions partially or completely deleting *GRIN2B*).
All mutations have been found heterozygously. The references for this figure are provided in Tables 1.2 and 1.3.

Too much *GRIN2B* may also be problematic. Several partial or complete chromosomal arm (12p) duplications including *GRIN2B* have been identified. All duplications also involve multiple other contiguous genes. In partial arm duplications involving *GRIN2B*, all carriers had intellectual disability but only one out of 20 cases were reported to have seizures (Poirsier et al., 2014; Talkowski et al., 2012). Thus, it is possible that GluN2B function is sensitive to gene dosage, and too much causes intellectual disability. This has implications for therapeutic strategies which might seek to increase the activity of wild type NMDARs: too much activity may also be a problem. However, the possibility that other genes in the duplicated regions cause the phenotype is a real one.

In summary, almost 100 mutations have been identified in *GRIN2A* in people with neurodevelopmental disorder (15 *de novo*), and almost 50 in *GRIN2B* (23 *de novo*), all likely to result in either a protein of altered function or an absent protein. But is this to be expected? Mutations do arise spontaneously - is the association with neurodevelopmental disorders just a chance finding?

There are two ways to approach this. In the case of inherited mutations, the cosegregation of disorder with mutation can be assessed. If a mutation is always associated with a phenotype in its carriers (cosegregation), this strengthens the evidence that it (or a locus nearby) is causing the phenotype. Conversely, if a mutation does not cause a phenotype in all its carriers, it is either not relevant to disease, or of low penetrance. Inherited mutations in *GRIN2A* and *GRIN2B* show both patterns, suggesting that in some cases at least the association with neurodevelopmental disorder is not a chance finding. Inherited mutations also highlight the variation in phenotype of carriers of identical mutations, suggesting that the consequences of a mutation are modified by stochastic developmental events, other gene variants, and/or environmental factors.

The second approach is statistical: assessing the probability of seeing the observed number of mutations in a group vs an expected number. In the case of *GRIN2A*, Lemke et al. (2014) compared the proportion of people with idiopathic focal epilepsy and heterozygous *GRIN2A* mutations (7.5%) with the proportion of people without epilepsy but with heterozygous *GRIN2A* mutations (0.6%) and found the rate of mutation in *GRIN2A* to be significantly higher than expected by chance. In the case of *de novo* mutations in *GRIN2B* O'Roak et al. (2012a) compared the rate of *de novo* mutation in *GRIN2B* against that simulated to occur by chance based on gene specific mutation rates and sequence information (the low rate of *de novo* mutation makes using control groups impractical), and found *de novo* mutations in *GRIN2B* to arise in autism at rates significantly above chance.

Section summary

This section has reviewed genetic evidence for the association of NMDAR GluN2A and GluN2B subunits with mental disorder. A large and statistically above chance number of mutations in individuals with neurodevelopmental disorder have been identified in the last six years, with mutations in *GRIN2A* predominantly associated with epilepsy-aphasia syndrome and mutations in *GRIN2B* with intellectual disability and autism. Further, a genome wide association study identified a locus near *GRIN2A* as impacting on risk for schizophrenia. There is therefore strong genetic evidence that alterations in GluN2A and GluN2B expression or properties are associated with mental disorder.

1.7 Description of phenotypes associated with mutations in *GRIN2A* and *GRIN2B*

The previous section introduced a lot of diagnostic terms, including some which refer to rare disorders, and some where the terminology is used variably by different authors. This section therefore gives an account of the key features of each class of disorder associated with mutations in *GRIN2A* or *GRIN2B*.

1.7.1 Epilepsy-aphasia syndromes

Epilepsy is the recurrent experience of seizures: defined by the International League Against Epilepsy (ILAE) as "a transient occurrence of signs and/or symptoms due to abnormal excessive or synchronous neuronal activity in the brain" (Fisher et al., 2014). It has a prevalence of around 0.6% (Forsgren et al., 2005).

Epilepsy-aphasia syndromes comprise a broad spectrum of disorders which all include childhood onset language difficulties associated with an abnormal EEG or epilepsy during sleep. The key features are (Loddenkemper et al., 2011):

1. Age specific presentation, with onset around age 4-5 years old and stabilisation, improvement or even resolution around the age of puberty

2. EEG discharges that increase and generalise during sleep (classically prolonged spike and wave activity during non-REM sleep)

3. Neuropsychological deficits or regression, in milder forms involving language regression only and in more severe forms global intellectual impairment

Epilepsy-aphasia syndromes form a spectrum, with some authors treating either extreme as independent of the intermediate disorders. This is not supported by the genetic evidence presented in the previous section. In this thesis, the spectrum of epilepsy-aphasia syndrome used is that suggested by Tsai et al. (2013): continuous spikes and waves during slow wave sleep, Landau Kleffner syndrome, intermediate epilepsy-aphasia disorder and benign childhood epilepsy with centrotemporal spikes, also known as rolandic epilepsy. Figure 1.13 is a Venn diagram showing the relationship between disorders. Table 1.4 describes key features of the two disorders at the mildest and at the most severe end of the spectrum (where the majority of *GRIN2A* mutations are found). The table highlights the difference in severity of cognitive deficits, EEG abnormalities and outcomes across the spectrum.

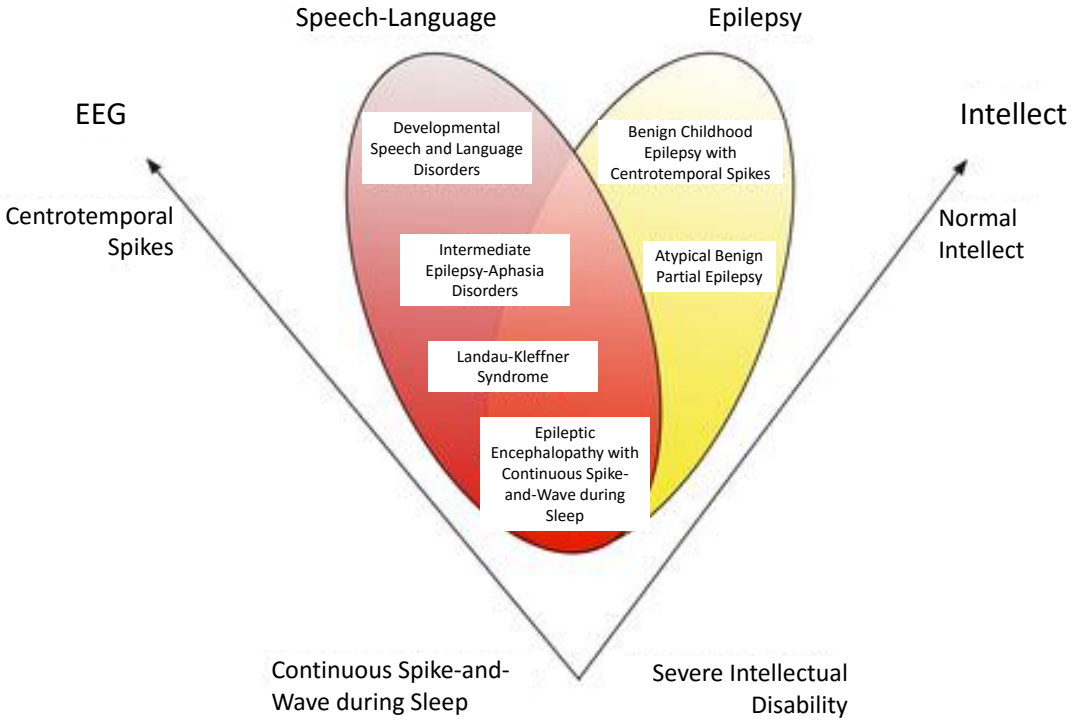

Figure 1.13: **Disorders included in the epilepsy-aphasia spectrum**
This figure shows the relationship of disorders on the epilepsy-aphasia spectrum, taken from Tsai et al. (2013) (text modified to increase legibility). The disorders vary along axes of cognition and EEG features/associated epilepsy. The mildest disorder is benign epilepsy with centrotemporal spikes (BECTS). which has mild epilepsy and mild defects in language dysfunction. The most severe end is continuous spike and wave during sleep (CSWS), where patients have a marked global cognitive impairment and frequent seizures.

Table 1.4: Key features of disorders on the epilepsy-aphasia spectrum

Disorder	CSWS	LKS	BECTS
Other names	ECSWS, CSWSS, EAS	EAS	BCE, Rolandic epilepsy
Prevalence	Rare	Rare (0.2% childhood epilepsy)	Common (10-15% childhood epilepsy)
Family history	10%	3%	18-36%
Sex	63% male	68% male	Slight male preponderance
Age of onset	5-7 years, 20% >9 years	5-7 years, 5% >9 years	7-9 years peak, range 1-14 years
Age of improvement	Puberty	Puberty	Puberty
Prognosis	**Poor.** 50% can live independently.	**Quite poor.** 50% "normal life". If aphasic for >1-2 years, lifelong language dysfunction.	**Good.** Either normal or very mild ongoing impairments.
Language	Reduction in or complete loss of speech Auditory agnosia (to non-verbal stimuli also)	As CSWS	Normal or mild difficulties (e.g. poor spelling, reading aloud) or listening comprehension)
Other cognition	**Severe and global impairment** Severe decline IQ Inattention and hyperactivity Aggression, compulsive behaviour Poor interpersonal contact Disinhibition, rarely psychosis	**Moderate** Inattention and hyperactivity Rarely, disinhibition and psychosis	**Normal or mild** difficulties in attention, visuospatial skills, picture naming
Seizure prevalence	100%	70%	100%
Commonest seizure type	Unilateral motor, generalised tonic-clonic	Simple partial motor (e.g. eye blinking, head drops, minor automatisms)	Simple partial motor (e.g. twitches, anarthria).
EEG while awake	Focal or bilateral anterior spikes	Bilateral temporal spikes	Centrotemporal spikes
EEG while asleep	>85% of non-REM sleep continuous spike and wave	Commonly (<85%) continuous spike and wave	Commonly (<85%) continuous spike and wave
Structural brain abnormalities	30-60% (perinatal vascular lesions, cortical malformations, atrophy, abnormal myelination)	13%	Up to 30% (atrophy, cortical dysplasias, white matter abnormalities)

Abbreviations: (E)CSW(S)S = (Epileptic encephalopathy with) continuous spikes and waves during slow wave sleep, LKS = Landau Kleffner syndrome, BECTS = benign epilepsy with centrotemporal spikes, EAS = Epilepsy aphasia spectrum disorders, BCE = Benign childhood epilepsy.

Sources: Smith and Hoeppner (2003), Loddenkemper et al. (2011), Tsai et al. (2013), Fejerman and Caraballo (2007), Kramer et al. (1998), Larsson and Eeg-Olofsson (2006), Shinnar et al. (1999).

1.7.2 Epileptic encephalopathies

The more severe forms of epilepsy-aphasia syndromes are often referred to as epileptic encephalopathies. Epileptic encephalopathies are defined by the ILAE as epileptic disorders where "the epileptic activity itself may contribute to severe cognitive and behavioral impairments above and beyond what might be expected from the underlying pathology alone" (Berg et al., 2010). Of course, without knowing the underlying pathology, this is a difficult definition to apply in practice. It is often used more broadly to apply to any disorder in which epilepsy is associated with severe intellectual disability, although some authors regard this as a misuse of the term (Shao and Stafstrom, 2016).

Epileptic encephalopathies are an even more diverse group of disorders than epilepsy-aphasia syndromes. They include a number of eponymous syndromes with characteristic seizure types, such as infantile spasms in West syndrome and febrile seizures in Dravet syndrome (Galanopoulou and Moshe, 2015). The disorders are individually rare; the commonest (West syndrome) affects 0.02% of children under 10 years old (Cowan, 2002). Some improvement may be seen in adolescence (Panayiotopoulos, 2005), but the outcome for epileptic encephalopathies is generally poor with high support needs (Cowan, 2002). Although an increasing number of genetic causes are being identified (McTague et al., 2016), hypoxia or infection around the time of birth, and congenital brain malformations are also frequent causes (Panayiotopoulos, 2005).

1.7.3 Intellectual disability

Intellectual disability, formerly known as learning disability or mental retardation, is defined as an intelligence quotient < 70 associated with impairments in adaptive functioning, and with onset before age 18 (WHO, 1992). The prevalence is around 1% (Maulik et al., 2011). It is associated with an increased risk of other psychiatric disorders, such as schizophrenia (Deb et al., 2001), and also an increased risk of epilepsy (Lhatoo and Sander, 2001). As with the other disorders discussed so far, intellectual disability refers to a spectrum of severity, with the mildest forms causing mild impairment in day to day living and the most severe forms requiring 24 hour care. The causes are also highly diverse, with both genetic (e.g. Down's syndrome) and environmental factors (e.g. birth complications) contributing (van Bokhoven, 2011).

1.7.4 Schizophrenia

Schizophrenia is a psychotic disorder characterised by hallucinations, delusions or disordered thought processes (WHO, 1992). Symptoms typically first manifest in late adolescence, or the early 20s. The prevalence is around 0.7% (McGrath et al., 2008). It is associated with an increased risk of epilepsy (Hyde and Weinberger, 1997) and lower premorbid IQ (Woodberry et al., 2008). Although some patients have a good functional outcome, the majority show a gradually declining course (Hegarty et al., 1994) with a 16 year reduction in life expectancy

(Laursen, 2011). Heritability is around 80% (Sullivan et al., 2003), with environmental risk factors including cannabis (Large et al., 2011) and early life adversity (Varese et al., 2012).

1.7.5 Autism

Autism is a syndrome of social impairment, communication impairment and repetitive or stereotyped behaviours with onset before 3 years old (WHO, 1992). The prevalence is around 0.6% (Elsabbagh et al., 2012). Comorbid epilepsy and intellectual disability is common (Kielinen et al., 2004). Heritability is around 80%, with environmental risk factors including birth complications (Ronald and Hoekstra, 2011). There is a wide range of severities and outcomes, with lower IQ predicting poorer outcome (Farley et al., 2009).

Section summary

Mutations in NMDAR GluN2A and GluN2B subunits are found in people with a range of frequently comorbid neurodevelopmental disorders, mainly of childhood onset, often influencing electrical activity in the brain and always influencing cognition, particularly language and social cognition. The symptoms caused by an acute reduction in NMDAR function (as seen with the use of channel blockers or in NMDAR encephalitis) partially mirror those found in carriers of NMDAR mutations. The fact that both putative and confirmed mechanisms of altered NMDAR function show converging consequences supports the hypothesis that the mutations are indeed influencing NMDAR function in a way that increases risk for mental disorder.

The functional outcomes for these NMDAR-associated neurodevelopmental disorders are variable, but a large proportion of people will require assistance with day to day living and experience a reduction in life expectancy. Although NMDAR mutations are rare, and not the predominant cause for any of the disorders with which they are associated, the disorders overall are common and represent a large burden of disability in society. This increases the value of any general pathophysiological insights which can be achieved through investigating the NMDAR related forms of the disorders.

1.8 Thesis aims

This introduction has summarised evidence that neurodevelopmental disorders arise from a genetically heterogenous set of disruptions in shared biological pathways. NMDAR subunits are amongst the hundreds of genes mutated. However, unlike many of the genes implicated, NMDAR subunits are already known to have a range of important brain functions, and to be dysfunctional in neuropsychiatric conditions. NMDAR subunits therefore represent biologically plausible, experimentally tractable genes with which to investigate the nature of neural changes which may contribute to neurodevelopmental disorder.

The overall aim of this thesis is thus to better understand the aetiology of mental disorders through investigating the functional consequences of disease-associated mutations in the NMDAR subunits GluN2A and GluN2B. This thesis hypothesises that mutations in NMDAR subunits alter their function in a way that contributes to their carriers' risk of neurodevelopmental disorder.

To address this hypothesis fully, it is necessary to assess the impact of NMDAR mutations at a range of levels of functional organisation: subunit, receptor, cell, circuit, and eventually, whole organism. The aims of each chapter of this thesis are therefore as follows:

The first results chapter aims to assess the impact of four NMDAR mutations at the subunit level by expressing mutant NMDAR subunits in heterologous systems.

The second results chapter aims to assess the impact of three NMDAR mutations at the receptor level, by expressing mutant NMDAR subunits in heterologous systems, with control over receptor subunit composition.

The third results chapter aims to assess the impact of gene disrupting mutations in NMDAR GluN2A subunits on cell and circuit function using two new transgenic rat models.

CHAPTER 2

Materials and methods

2.1 Preparation of DNA constructs

Table 2.1 lists the NMDAR constructs used in this study, and their origin. Details of the techniques used to modify the cDNA sequences follow the table.

Table 2.1: Wild type and mutant constructs

cDNA	Vector	Origin
Chapter 3		
hGluN1-1a (NP_015566)	pCI-neo	Gift from Dr Kasper Hansen
hGluN2A^{WT}(NP_000824)	pCI-neo	Gift from Dr Kasper Hansen and Dr Hongjie Yuan
hGluN2A^{R586K}	pCI-neo	Gift from Dr Kasper Hansen and Dr Hongjie Yua
hGluN2A^{N615K}	pCI-neo	Site-directed mutagenesis (In-Fusion)
hGluN2B^{WT}	pRK5	Gift from Prof Robert Harvey
hGluN2B^{N615I}	pRK5	Gift from Prof Robert Harvey
hGluN2B^{V618G}	pRK5	Gift from Prof Robert Harvey
hGluN2B^{D101A}	pRK5	Site-directed mutagenesis (In-Fusion)
hGluN2B$^{D101A,\ N615I}$	pRK5	Site-directed mutagenesis (In-Fusion)
hGluN2B$^{D101A,\ V618G}$	pRK5	Site-directed mutagenesis (In-Fusion)
Chapter 4		
rGluN1-1a eGFP (U08261)	pCI-neo	Gift from Dr Kasper Hansen
rGluN2A^{WT}(D13211)	pCI-neo	Gift from Dr Kasper Hansen
rGluN2A^{N615K}	pCI-neo	Ligation
rGluN2A$_{C1}$	pCI-neo	Gift from Dr Kasper Hansen
rGluN2A$_{C2}$	pCI-neo	Gift from Dr Kasper Hansen
rGluN2A$_{C1}{}^{N615K}$	pCI-neo	Site-directed mutagenesis (In-Fusion)
rGluN2A$_{C2}{}^{N615K}$	pCI-neo	Ligation
rGluN2B^{WT}(U11419)	pCI-neo	Gift from Dr Kasper Hansen
rGluN2B^{N615I}	pCI-neo	Site-directed mutagenesis (Quikchange)
rGluN2B^{V618G}	pCI-neo	Site-directed mutagenesis (Quikchange)
rGluN2B$_{AC1}$	pCI-neo	Gift from Dr Kasper Hansen
rGluN2B$_{AC2}$	pCI-neo	Gift from Dr Kasper Hansen
rGluN2B$_{AC1}{}^{N615I}$	pCI-neo	Site-directed mutagenesis (In-Fusion)
rGluN2B$_{AC2}{}^{N615I}$	pCI-neo	Site-directed mutagenesis (In-Fusion)
rGluN2B$_{AC1}{}^{V618G}$	pCI-neo	Site-directed mutagenesis (In-Fusion)
rGluN2B$_{AC2}{}^{V618G}$	pCI-neo	Site-directed mutagenesis (In-Fusion)

Genbank accession code given in brackets (where deposited). Dr Kasper Hansen is based at the University of Montana, Dr Hongjie Yuan at the University of Emory and Prof Robert Harvey at University College London.

2.1.1 Site-directed mutagenesis techniques

2.1.1.1 In-Fusion Method

Site-directed mutagenesis was performed via PCR with overlapping mutagenizing oligonucleotides (see Table 2.2) using a thermostable *Pfu* high fidelity DNA polymerase (New

England Biolabs, Ipswich, MA, USA). The PCR product was recircularised into a viable plasmid using an InFusion HD kit (Clontech, Mountain View, CA, USA). The double-stranded mutant DNA was transformed into TOP10 Competent Cells (Life Tech, Grand Island, NY, USA). Clones were amplified before DNA was extracted using QIAPrep Spin MiniPrep Kit (Qiagen, Venlo, Netherlands) as per the manufacturer's instructions. The mutations were verified by Sanger sequencing through the entire cDNA.

Table 2.2: Mutagenising primers used with In-Fusion method

Protein product	Forward primer (5′-3′)	Reverse primer (5′-3′)
hGluN2A^{cC1845A} (pN615K)	TTCAATAAA**A**TCCGTGCCTGTCCAGAAT	GCACGGA**T**TTATTGAACACCAGGCCC
rGluN2A^{cT1845A} (pN615K)	CTTCAACAAA**A**TCTGTGCCTGTCCAGAAT	GCACAGA**T**TTGTTGAAGACCAGGCCCCA
hGluN2B^{cA304C} (pD101A)	TTTGCTG**C**TGACACAGACCAGGAA	TGTGTCA**G**CAGCAAACACCACC
rGluN2B ^{cA1834T} (pN615I)	GGTGTTTA**T**CAACTCCGTACCTGTGCAG	CGGAGTTG**A**TAAACACCAGACCCCAGAG
rGluN2B^{cT1852G} (pV618G)	CAACTCCG**G**ACCTGTGCAGAACCCAAAG	GCACAGGT**C**CGGAGTTGTTAAACACCAG

Substituted nucleotides are marked in bold.

2.1.1.2 QuikChange Method

Site-directed mutagenesis was performed using the QuikChange Site-Directed Mutagenesis Kit method (Agilent Technologies, Santa Clara, CA, USA). Firstly, PCR was performed with overlapping mutagenizing oligonucleotides using a thermostable *PfuTurbo* DNA polymerase (see Table 2.3). The PCR product was then treated with the endonuclease *Dpn I*, which digests methylated parental DNA but leaves intact newly synthesized mutated DNA. The remaining mutant DNA was transformed into chemically competent cells by heat shock. Clones were amplified before DNA was extracted using GenElute MiniPrep (Sigma-Aldrich, St Louis, MO, USA) as per the manufacturer's instructions. The mutations were verified by sequencing across the point mutation and a region of the modified C terminus.

Table 2.3: Mutagenising primers used with QuikChange

Protein product	Forward primer (5′-3′)	Reverse primer (5′-3′)
rGluN2B^{N615I}	GGTCTGGTGTTTA**T**CAACTCCGTACCTG	CAGGTACGGAGTTG**A**TAAACACCAGACC
rGluN2B^{V618G}	GTGTTTAACAACTCCG**G**ACCTGTGCAGAACCC	GGGTTCTGCACAGGT**C**CGGAGTTGTTAAACAC

Substituted nucleotides are marked in bold.

2.1.1.3 DNA ligation

rGluN2A, rGluN2A$_{C2}$ and rGluN2A$_{C1}{}^{N615K}$ were digested with restriction enzymes Bsp120I and Sal1 for 1 hour at 37 °C. The relevant bands were then extracted using the illustra GFX PCR DNA and Gel Band Purification Kit (GE Healthcare, Buckinghamshire, UK) as per manufacturer's instructions before being ligated overnight at 16 °C with T4 DNA ligase and buffer (New England Biolabs). The product was used to transform chemically competent cells by heat shock. Resulting clones were amplified before DNA was extracted using GenElute MiniPrep (Sigma-Aldrich) as per the manufacturer's instructions. The mutations were verified by sequencing across the point mutation and a region of the modified C terminus.

2.2 Techniques used with oocytes

2.2.1 cRNA synthesis and receptor expression

cRNA for wild type and mutants was synthesized from linearized plasmid DNA as runoff transcripts using the T7 polymerase mMessage machine RNA synthesis kit (Life Technologies Ltd, Paisley, UK). Each oocyte was injected with 3.7-9 ng of cRNA, comprising a 1:1 molar ratio of GluN1 and GluN2A cRNAs diluted in RNAse free water.

Stage VVI *Xenopus laevis* oocytes were obtained from the UK Xenopus centre (Portsmouth, UK) and from Diaclean (CastropRauxel, Germany), collagenased (200 units/ml for 60 minutes), then manually defolliculated prior to injection. After injection oocytes were placed in separate wells of 24-well plates containing a modified Barth's solution with composition (in mM): 88 NaCl, 1 KCl, 2.4 $NaHCO_3$, 0.82 $MgCl_2$, 0.44 $CaCl_2$, 0.33 $Ca(NO_3)_2$, 15 Tris-HCl, adjusted to pH 7.35 with NaOH. This solution was supplemented with 50 IU/ml penicillin, 50 mg/ml streptomycin and 50mg/ml tetracycline. Oocytes were placed in an incubator (16-21°C) for 24-48 hours to encourage receptor expression and subsequently stored at 4 °C. Recordings were made 48-96 hours post injection.

2.2.2 Two-electrode voltage-clamp recordings

Two-electrode voltage-clamp (TEVC) recordings were made at room temperature (18-21°C) from oocytes that were placed in a solution that contained (in mM): 115 NaCl, 2.5 KCl, 10 HEPES, 1.8 $BaCl_2$, 0.01 EDTA; pH 7.35 with NaOH. Recordings were made using a GeneClamp 500B amplifier (Molecular Devices, Union City, CA, USA). Current and voltage electrodes were made from thin-walled borosilicate glass (GC150TF-7.5, Harvard Apparatus, Kent, UK) using a PP-830 electrode puller (Narashige Instruments, Japan). Filling with 3 M KCl gave resistances of between 0.2 and 1.5 MΩ. Application of solutions was determined manually. Data were filtered at 10 Hz and digitized at 100 Hz via a 1401 plus analogue-digital interface (Cambridge Electronic Design, Cambridge, UK) using WinEDR software (Strathclyde Electrophysiology Software, Strathclyde University, UK). Oocytes were voltage-clamped at –40, –60 or –80 mV. Recordings were rejected if the holding current (in nA) was greater than three times the holding potential (in mV) or if the holding current drifted by more than 10% of the agonist response across the course of the experiment.

The liquid-liquid junction potential for two-electrode voltage-clamp recordings was calculated to be +1 mV (using the open access software provided by (Marino et al., 2014)). All other internal/external pairings in this thesis were calculated to be between +16 to +17 mV (using Clampex software (Molecular Devices)).

2.2.3 Single-channel voltage-clamp recordings

Single-channel voltage-clamp recordings were made at room temperature (18-21°C) from outside-out patches pulled from oocytes that were placed in a solution that contained (in mM): 125 NaCl, 3 KCl, 1.25 NaH_2PO_4, 20 HEPES, 0.85 $CaCl_2$, 0.01 EDTA; pH 7.35 with NaOH. Steady state recordings were made in the presence of 30 μM glutamate and 30 μM glycine. Recording durations varied from 30 seconds to 5 minutes. Prior to recording vitelline membranes were removed from oocytes placed in a hypertonic solution that contained (in mM): 200 sodium methyl sulphate, 20 KCl, 10 HEPES, 1 $MgCl_2$, pH 7.4 with NaOH. Recordings were made using an AxoPatch 1D amplifier (Molecular Devices). Electrodes were made using thick walled borosilicate glass (GC150F-7.5, Harvard Apparatus) using a P-87 electrode puller (Sutter Instrument, Novato, CA, USA) and their tips fire polished to give resistances of 7 to 12 MΩ when filled with internal solution containing (in mM): 2.5 NaCl, 141 K-gluconate, 10 HEPES, 11 EGTA; pH 7.4 with KOH. Electrodes tips were coated in silicone elastomer ("sylgard 184", Dow Corning, Wiesbaden, Germany) to reduce capacitance. Application of solutions was controlled manually. Data were prefiltered at 2 kHz (–3 dB, 8th order Bessel filter) and digitized at 20 kHz via a Micro 1401 analogue-digital interface (Cambridge Electronic Design) using WinEDR software (Strathclyde Electrophysiology Software). Patches were voltage-clamped at -60 or –100 mV.

WinEDR v3.3.7 was used to idealise the traces (using a transition threshold of 50% of the unitary conductance level and a 100 μs open and shut resolution), to fit Gaussian curves to amplitude histograms and to fit multiple exponential curves to dwell time durations (all curves fitted using iterative maximum likelihoods). Any openings where more than one channel was open simultaneously were discarded. Conductance was calculated by dividing the current amplitude by the holding potential.

2.3 Techniques used with HEK293 and HEK293T cells

2.3.1 Culture

For single channel recordings (Chapter 3), human embryonic kidney 293 cells (HEK293) cells were cultured in Dulbeccos Modified Eagle Medium with GlutaMax-I supplemented with 10% foetal calf serum, and 1% antibiotic/antimycotic. Cells were passaged twice weekly and plated onto cover slips precoated in poly-D-lysine (0.05 mg/ml) to give a density of 10-30% on the day of recording.

For triheteromer experiments (Chapter 4), HEK293 cells containing the SV40 large T–antigen (HEK293T cells) were cultured in Dulbeccos Modified Eagle Medium with GlutaMax-I (Invitrogen, Carlsbad, CA, USA) supplemented with 10% dialyzed fetal bovine serum (Invitrogen, Waltham, MA, USA), 10 U/ml penicillin, and 10 μg/ml). HEK293T cells were chosen for their propensity to grow singly rather than in clumps, facilitating electrophysiological experiments involving rapid solution application. Cells were passaged twice weekly and plated onto cover slips precoated in poly-D-lysine (0.1 mg/ml) to give a density of 10-30% on the day of recording.

2.3.2 Transient transfection

For single channel recordings (Chapter 3), HEK293 cells were transfected using Lipofectamine 2000 (hereafter referred to as lipofectamine). For one well of a 24-well plate, plasmids containing hGluN1-1a, the hGluN2 subunits of interest and eGFP were mixed in a 1:2:1 mass ratio to give 500 ng total DNA in 25 μl opti-MEM and added to 2 μl lipofectamine in 25 μl opti-MEM. After 20 minutes at room temperature, 50 μl of transfection mix was added dropwise to each well. After 2-5 hours the media was replaced with fresh media containing NMDAR antagonists (10 μM D-AP5 and 1 μM 5,7-dichlorokynurenic acid) to avoid NMDAR mediated excitotoxicity. Recordings were made approximately 24-48 hours post transfection.

For triheteromer experiments (Chapter 4), HEK293T cells were transfected using the calcium phosphate precipitation method. Plasmids containing rGluN1-1a eGFP and the rGluN2 subunits of interest were mixed in a 1:1 mass ratio and diluted to 200 ng/μl with water. To transfect 4 wells of a 24-well plate, 10 μl of cDNA was mixed with 25 μl of 1 M $CaCl_2$ and 100 μl of 2xBES (50 mM BES, 280 mM NaCl, 1.5 mM Na_2HPO_4, pH 6.95), then mixed by pipetting. After 10-15 minutes, 50 μl of this mixture was added dropwise to each well. After 4-6 hours the media was replaced with fresh media supplemented with NMDA receptor antagonists (1 mM D-AP5 and 1 mM 7-CKA to avoid NMDAR excitotoxicity. Recordings were made approximately 24 hours post transfection.

2.3.3 Whole-cell voltage-clamp recordings

Transfected cells were identified by eGFP expression (excitation at 470 nm, coolLED pE-100 (coolLED Ltd, Andover, UK)). Whole-cell patch-clamp recordings were performed using an Axopatch 200B amplifer (Molecular Devices) at room temperature (21°C), with low-pass filter set to 100 kHz. The signal was then filtered using an 8 kHz 8–pole low-pass filter (–3 dB Bessel; Frequency Devices, Ottawa, IL, USA), and digitized at 20 kHz using a Digidata 1440A analogue-digital interface (Axon Instruments, Union City, CA) using Clampex software (Molecular Devices). Patch-pipettes were made from thin-walled borosilicate glass (TW150F-4, World Precision Instruments (Sarasota, FL, USA)) using a P-1000 puller (Sutter Instruments) to give a resistance of 4-5 MΩ when filled with an internal solution containing (in mM): 141 K-gluconate, 2.5 NaCl, 10 HEPES, 11 EGTA; pH 7.3 with KOH (300 mOsm). The extracellular solution was composed of (in mM) 150 NaCl, 10 HEPES, 3 KCl, 0.5 $CaCl_2$, 0.01 EDTA, 20 D-mannitol (pH 7.4 with NaOH). Rapid solution exchange (open tip solution exchange had 10-90% rise times of 0.7-0.9 ms) was achieved using a two-barrel theta-glass pipette controlled by a piezoelectric translator (Siskiyou Corporation, Grants Pass, OR).

Cells with glutamate evoked responses of less than 100 pA or greater than 1000 pA were rejected, to reduce error from noise and to avoid leak of undesired subunit pairings (see Chapter 4).

Amplitudes of whole-cell currents were analysed using Clampfit (Molecular Devices). To calculate glutamate deactivation rates and Mg^{2+} on and off rates, multi-component exponential decay curves were fitted to macroscopic response time courses in ChanneLab software (www.synaptosoft.com; Synaptosoft, Decatur, GA).
$\tau_{weighted}$ was calculated as: % $amplitude_{fast}$ * τ_{fast} + % $amplitude_{slow}$ * τ_{slow}.

2.3.4 Single-channel voltage-clamp recordings

Single-channel voltage-clamp recordings were made at room temperature (18-21°C) from cell attached patches formed on HEK293 cells placed in a solution that contained (in mM): 150 NaCl, 2.8 KCl, 10 HEPES, 2 $CaCl_2$, 10 glucose, 0.1 glycine; pH 7.35 using NaOH (300-330 mOsm). Patches were recorded from at a range of holding potentials. Transfected cells were identified by eGFP expression (excitation at 470 nm, coolLED pE-100 (coolLED Ltd)). Patch-pipettes were made from thick-walled borosilicate glass (GC150F-7.5, Harvard Apparatus) using a P-87 puller (Sutter Instruments) to give a resistance of 6-12 MΩ when filled with the external solution plus agonist (NMDA (33-500 μM)). Currents were recorded using an Axopatch 200B amplifier (Molecular Devices). Data were filtered at 2 kHz and digitized at 20 kHz via a National Instruments BNC-2090A analogue-digital interface (National Instruments, Newbury, UK) using WinEDR software (Strathclyde Electrophysiology Software).

WinEDR v3 was used to idealise the traces (using a transition threshold of 50% of the unitary conductance level and a 100 μs open and shut resolution), to fit Gaussian curves to amplitude histograms and to fit multiple exponential curves to dwell time durations (all curves fitted using iterative maximum likelihoods). Any openings where more than one

channel was open simultaneously were discarded from dwell time and amplitude analyses. To improve accuracy of amplitude estimates, a 1 ms minimum open time duration was applied. Because the membrane potential was not known, the patch potential was unknown. Therefore recordings were made at a range of holding potentials and the current plotted: the slope gave the conductance.

2.4 Techniques used with cultured primary mouse and rat cortical neurons

2.4.1 Culture

Culturing was a modified version of Furshpan and Potter (1989). Brains from E17.5 CD1 mice or E20.5 Long-Evans Hooded rats (sex not determined) were microdissected in medium containing (in mM): 8.8 Na_2SO_4, 27 K_2SO_4, 5.3 $MgCl_2$, 0.23 $CaCl_2$, 0.9 HEPES, 0.001% Phenol Red, 18 D-glucose, 0.0005 kynurenic acid, adjusted to pH 7.35 with NaOH. Cortices were incubated at 37°C for 40 minutes in papain enzyme (36,000 USP units/ml) (Worthington Biochemical Corporation, Lakewood, NJ, USA) then washed and triturated in NeuroBasal A medium (supplemented with 1% rat serum (Harlan laboratories, Indianapolis, IN, USA), 1 x B-27 supplement, 1% antibacterial/antimycotic and 1 mM glutamine). The cell suspension was diluted in opti-MEM (supplemented with 20 mM glucose and 1% antibacterial/antimycotic) to give an end concentration of 1 hemisphere per 7 ml, and 0.5 ml/coverslip plated onto 13 mm diameter coverslips precoated with poly-D-lysine (1.33% w/v in H_20) and laminin (0.5% w/v) (Roche, Basel, Switzerland) in 24-well plates. Plates were kept at 37°C in a humidified 5% CO_2 incubator for 2.5 hours before replacement of the cell suspension with supplemented NeuroBasal A. On DIV 4, 1 ml/well of supplemented NeuroBasal A containing 9.6 μM cytosine β-D-arabinofuranoside hydrochloride was added to the cells.

2.4.2 Quantitative PCR

RNA was isolated from cultured neurons using the Roche High Pure RNA Isolation Kit (including DNase treatment), according to manufacturer's instructions (Roche, Hertfordshire, UK). 3 wells from a 24-well plate were pooled for each animal. cDNA was synthesized from 13 μg RNA using a Transcriptor First Strand cDNA Synthesis Kit (Roche), according to manufacturer's instructions, then stored at –20°C. For real time PCR (RT-PCR), cDNA was diluted to the equivalent of 6 ng of initial RNA per 15 μl qPCR reaction, per gene of interest. Real-time PCR was performed in a Stratagene Mx3000P QPCR System (Agilent Technologies, Waldbronn, Germany), using the FS universal SYBR Green MasterRox mix (Roche), according to manufacturer's instructions. The required amount of template was mixed with water, SYBR Green MasterRox mix and forward and reverse primers (200 nM each final concentration, see Table 2.4 for sequences) to the required reaction volume. Technical replicates as well as no template and no RT negative controls were included. The qRT-PCR cycling programme was 10 min at 95°C, then 40 cycles of 30 sec at 95°C, 40 sec at 60°C with detection of fluorescence and 1 min at 72°C, followed by 1 cycle (for dissociation curve) of 1 min at 95°C and 30 sec at 55°C with a ramp up to 30 sec at 95°C (ramp rate: 0.2°C/sec) with continuous detection of fluorescence on the 55-95°C ramp. Data were normalised to GADPH expression.

Table 2.4: Primers used for qPCR

	Forward primer (5′-3′)	Reverse primer (5′-3′)
rGrin2A (exon 1-2)	AGCCAGAGACCCCGCTAC	TGGGGTGCACCTGGTAAC
rGADPH	AGAAGGCTGGGGCTCACC	AGTTGGTGGTGCAGGATGC

2.4.3 Immunoblotting

Neurons were lysed in 1.5x LDS sample buffer and sample reducing agent (NuPage, Life Technologies) and boiled at 100°C for 10 min. Approximately 20 μg of protein was loaded onto a precast gradient gel (4-12% Bis-Tris gel, Nupage, Life Technologies) and subjected to electrophoresis. Western blotting onto a PVDF membrane was then performed using the Xcell Surelock system (Invitrogen) according to the manufacturer's instructions. Following the protein transfer, the PVDF membranes were blocked for 1 hour at room temperature with 5% (w/v) non-fat dried milk in TBS with 0.1% Tween 20. The membranes were incubated at 4°C overnight with the primary antibodies diluted in blocking solution: Anti GluN2A N-terminus (Invitrogen 480031, 1 in 2000, rabbit) and anti β actin (Abcam 8227, 1 in 50,000, rabbit). For visualisation of immunoblots, HRP-based secondary antibodies were used followed by chemiluminescent detection on Kodak X-Omat film. A range of exposures were taken to ensure bands were not saturated. Loading was normalized using β actin as a loading control (run on the same blot). Immunoblots were digitally scanned and densitometric analysis was performed using Image J (Schneider et al., 2012). In some cases, lanes from non-adjacent lanes are spliced together, but the lanes are always from the same blot, processed in the same way, and the splicing point is clearly marked.

2.4.4 Transient transfection

Neurons were transfected on DIV 7 or 8 with plasmids containing cDNA for wild type and mutant GluN2A or GluN2B, or the inert control β globin, using lipofectamine in serum free non-trophic transfection medium composed of 10% minimum essential media (MEM) (+Earles, -L-glutamine), 88% Salt-Glucose-Glycine (SGG) (comprising in mM 114 NaCl, 26 $NaHCO_3$, 5.3 KCl, 1 $MgCl_2$, 2 $CaCl_2$, 10 HEPES, 1 glycine, 30 D-glucose, 0.5 sodium pyruvate, with phenol red 0.001%) supplemented with 1% antibiotic/antimycotic and 1% insulin–transferrin–selenium supplement. For each cover slip 2.3 μl of lipofectamine was mixed with 575 ng plasmid DNA comprising a 2:1 mass ratio of GluN2A/GluN2B and eGFP cDNA. Cotransfection rate was 96% (data not shown). Electrophysiological recordings were made 48 hours post transfection.

2.4.5 Viral transduction

Neurons were transfected on DIV 3 with 1.1e8 viral transduction units (1 μl/well of a 24-well plate) of an adeno-associated virus (serotype 2) expressing a Cre-eGFP fusion protein driven by the CMV promoter. Transduction efficiency was approximately 80%, determined at

DIV18 by assessing the proportion of cells expressing eGFP. The virus was purchased from the University of North Carolina Gene Therapy Center Vector Core.

2.4.6 Whole-cell voltage-clamp recordings

2.4.6.1 Assessing Mg^{2+} block and ifenprodil sensitivity

Recordings were made at room temperature (18–21°C) with neurons superfused (at a flow rate of 2 mL/min) with external recording solution as used in Section 2.3.4 except with the addition of 300 nM TTX to prevent action potentials by blocking voltage-gated sodium channels. Transfected cells were identified by eGFP expression as in Section 2.3.4. 150 μM NMDA was applied briefly twice to elicit desensitisation then until steady state (around 10 seconds) at which point 1 mM $MgCl_2$ was co-applied until steady state. Experiments were then repeated after perfusion with 3 μM ifenprodil for one minute. Application of solutions was controlled manually. Patch-pipettes were made from thick-walled borosilicate glass (GC150F-7.5, Harvard Apparatus) using a P-87 puller (Sutter Instruments) to give a resistance of 2-4 MΩ when filled with the same internal solution as Section 2.3.3. Currents were recorded using an Axopatch 200B amplifier (Molecular Devices). Data were filtered at 2 kHz and digitized at $\geq$ 20 kHz via a National Instruments BNC-2090A analogue-digital interface (National Instruments) using WinEDR software. Neurons were voltage-clamped at –65 mV, and recordings were rejected if the holding current was greater than 150 pA or if the series resistance was greater than 30 MΩ, or increased by greater than 20% during the course of the recording. Capacitance was calculated by calculating the area under the current response to a 5 mV test pulse plotted against time (giving the charge) and dividing by the voltage of the test pulse. Current density was then calculated as current / capacitance.

2.4.6.2 Assessing spermine potentiation

Neurons were initially voltage-clamped at –65mV using the internal solution and external described in Section 2.4.6.1. The neurons were then voltage-clamped at –30 mV and switched to a recording solution composed of (in mM): 70 NaCl, 60 choline chloride, 2.8 KCl, 20 HEPES, 10 glucose, 0.1 glycine, pH 6.5 with NaOH. 100 μM DTPA was also included otherwise rapid desensitization of the spermine potentiation was seen. The low external sodium concentration resulted in small currents, reducing the likelihood of large currents escaping voltage–clamp and biasing the potentiation seen. NMDA currents were evoked (as described in Section 2.4.6.1) then potentiated by 100 μM and 200 μM spermine consecutively. 200 μM spermine was originally included as an internal control: both 100 μM and 200 μM spermine are on the linear part of the dose-response and an approximate 2–fold increase in potentiation was expected jumping from 100 μM to 200 μM spermine. Only the % potentiation at 100 μM spermine was chosen for analysis. Only cells with NMDA-evoked currents greater than 40 pA (in low sodium external) were included. The equipment and settings used were as Section 2.4.6.1 except data were filtered at 5 kHz and digitised at 20 kHz.

2.4.6.3 Recording miniature excitatory post synaptic currents (mEPSCs)

Solutions, equipment and settings were as Section 2.4.6.1 except bicuculline 50 μM was added to the external solution (to block $GABA_A$ receptors) and data were filtered at 2 kHz and digitised at 20 kHz.

Additionally, to allow calculation of excitation:inhibition ratios, a subset of recordings were made using the same internal solution as for miniature inhibitory post synaptic potentials (see below).

Recordings were made for 10 minutes and analysed offline to obtain average data using Stimfit software (Guzman et al., 2014). Exemplar events were fitted with tri–exponential functions, then the fit parameters used as templates to extract all remaining events (using template scaling), with thresholds of 7.5 ms minimum between events, a T50 (time from peak to 50% of response) of 1 ms minimum and an amplitude at least three times the standard deviation of the neighbouring baseline.

2.4.6.4 Recording miniature inhibitory post synaptic currents (mIPSCs)

Recordings were made as for mEPSCs (Section 2.4.6.3) but with the AMPA receptor antagonist 20 μM CNQX present in the recording solution rather than bicuculline. To enhance the amplitude of mIPSCs, neurons were voltage-clamped at 0 mV, and a Cs-gluconate based internal used to block voltage-gated potassium channels (the internal used contained (in mM): 140 Cs-gluconate, 4 CsCl, 10 HEPES, 0.2 EGTA, 2 ATP magnesium salt, 2 ATP sodium salt, 0.3 GTP sodium salt, 0.1% Biocytin).

Recordings were analysed as for excitatory events, except that the minimum T50 threshold was increased to 3 ms, reflecting the slower time course of mIPSCs. For calculation of EPSC to IPSC ratios, average amplitude and frequency were calculated for each cell with paired recordings and expressed as a ratio.

2.4.7 Calcium imaging

DIV 17 neurons were transferred to a recording solution as used in Section 2.3.4 and loaded with 11 mM Fluo3 AM (from a stock solution of 2.2 mM Fluo3 dissolved in anhydrous dimethylsulfoxide containing 20% (w/v) Pluronic detergent) for 30 min at 37°C. Cells were washed with solution until a stable baseline was achieved, then drugs of interest applied. To calibrate images, Fluo-3 was saturated by adding 50 μM ionomycin to the perfusion chamber (to obtain F_{max}) and quenched with 20 μM $MnCl_2$ + 50 μM ionomycin to levels corresponding to 100 nM Ca^{2+} (Minta et al., 1989), which was in turn used to calculate F_{min}. Free Ca^{2+} concentrations were calculated from the fluorescence signal (F) according to the equation $[Ca^{2+}] = K_d(F - F_{min})/(F_{max} - F)$, and expressed as a multiple of the K_d of Fluo-3 (which is approximately 390 nM). Fluo3 fluorescence images (excitation 480 $\pm$ 20 nm, emission 527 $\pm$ 15 nm) were taken at one frame every second using a Leica DFC 360FX camera (Leica

Microsystems, Mannheim, Germany) through a x 10 dry objective (HC PL Fluotar 10x/0.3 Ph1, Leica) on an upright microscope (DMI 6000B, Leica) with a heated (37°C) stage. Fluorescence excitation was provided by a mercury lamp in combination with an excitation filter cube. Data were collected using Leica LAS AF v4.0.0 software.

Basal calcium levels were calculated by averaging $[Ca^{2+}]$ during the 50 s prior to bicuculline application. Bicuculline-evoked spike frequency was calculated as the number of spikes separated by a return to within 5% of baseline divided by the total period of bicuculline application. To account for baseline drift, baseline intensity was calculated as a moving median, considering the 20 s either side of a given point, except where a burst of very frequent spikes occurred, where baseline values neighbouring the spike cluster were used instead. 50 cells were analysed per cover slip.

Cell density was assessed by counting the number of cells visible in a field of view 480 μm by 640 μm (307 μm^2).

2.4.8 Induction of excitotoxicity

To apply an excitotoxic insult, neurons were first deprived of growth factors by being placed overnight into a medium containing 10% MEM, 89% SGG medium and 1% antibacterial/antimycotic (see Section 2.4.4 for SGG media composition). Neurons were then treated with NMDA at the indicated concentrations for 1 hour, after which medium was changed to NMDA-free. After a further 23 hours, neurons were fixed (in 3% paraformaldehyde and 4% sucrose in phosphate buffered saline) and stained with DAPI contained in Vectashield mounting medium (Vector Labs, Peterborough, UK). Cell death was quantified by counting (blind to genotype) the number of shrunken, pyknotic nuclei as a percentage of the total. Approximately 200–400 cells were analysed per condition, per replicate.

2.5 Generation and validation of genetically modified rat

2.5.1 Generation of rat models

Single cell Long Evans Hooded rat embryos underwent pronuclear microinjection of mRNA encoding the enzyme Cas9, single guide RNAs (sgRNA) binding to 5′ and 3′ of exon 8 of Grin2A, and a pUC57 plasmid containing 2142 bp of donor DNA (see Figure 2.1)) before being implanted into pseudopregnant mothers. The resulting live births were screened by PCR for either insertion of donor DNA via homology directed repair or genomic deletions due to repair by non-homologous end joining of double stranded breaks targeted to either side of exon 8. Separate founder mutants containing LoxP sites either side of exon 8, and a 1065 bp deletion spanning exon 8 (which encodes key pore forming domains of GluN2A) were identified using restriction digests, and confirmed by sequencing. The sgRNA design and generation of the founder animals was performed by Horizon Discovery Group plc (St Loius, MO, USA).

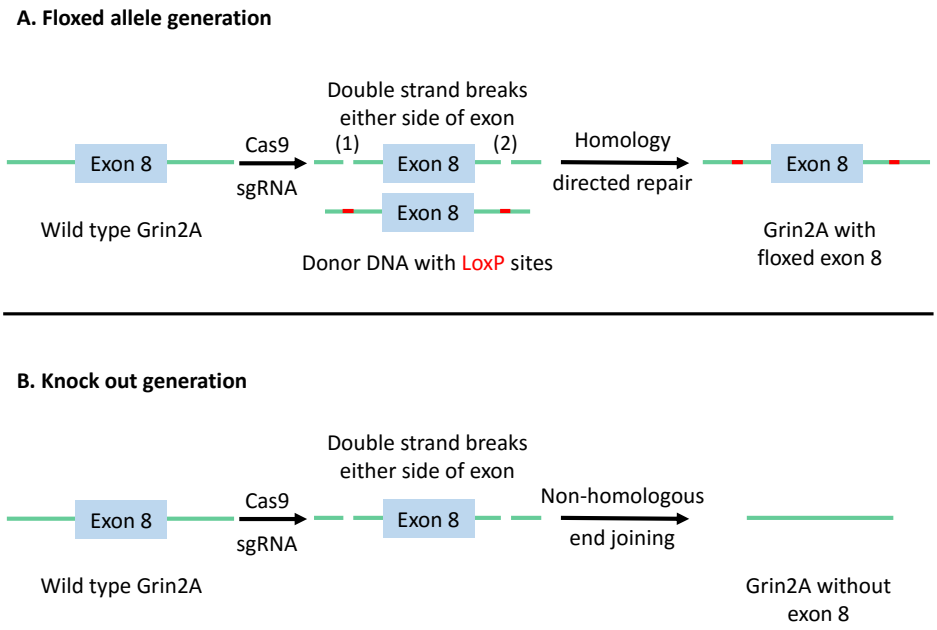

Figure 2.1: Crispr/Cas9 strategy for generation of rat models

2.5.2 Sequencing of rat models

Confirmation by Sanger sequencing was performed by PCR amplification of a genomic region spanning the donor DNA section and including endogenous DNA to 5′ and 3′. This was achieved using a high processivity enzyme (*Pfu* high fidelity DNA polymerase (New England Biolabs)) and a nested PCR approach (see Table 2.5). The region was initially amplified from genomic DNA with one pair of primers, then DNA oligomers and salts removed from the PCR product (using a PCR Clean-up kit (MaCherey-Nagel, Düren, Germany), used as per

manufacturer's instructions), then a second PCR run with primers internal to the first pair. Finally, the segment was sequenced with further internal primers. Settings for the first PCR were: 2 minutes at 96°C, then 35 cycles of 20 s at 96°C, 30 s at 65°C and 3 min at 72°C, then 10 min at 72°C. Settings for the second PCR were as for the first, but with only 25 cycles (to reduce amplification of non-specific products).

Table 2.5: Primers used for nested PCR

	Primer pair 1	Primer pair 2
Forward primer (5'-3')	TACTCAGGACATGGGGAGGG	AAGGCAGAGAGAGAGACAAAG
Reverse primer (5'-3')	CTTCCCCCGCCTAAAACG	TTACTTCTCCTGCTAAAAACTCG
WT band	2351 bp	2267 bp
Floxed exon band	2429 bp	2347 bp
Deleted exon band	1286 bp	1202 bp

2.5.3 Genotyping

Genomic DNA was extracted by heating a tissue sample (ear notch or pellet from 1.5 ml cell suspension) in 600 μl of 50 mM NaOH at 100°C for 30 minutes, with mixing by inversion after 15 minutes. 50 ul of 1 M Tris HCl (pH 6.8) was added before centrifuging at 13,000 rpm for 10 minutes at 4°C. 5 μl of supernatant was then amplified by PCR with *Taq* DNA polymerase (Qiagen). PCR settings were: 5 min at 95°C, then 35 cycles of 30 s at 95°C, 30 s at 58°C and 1 min at 68°C, then 5 min at 68°C. See Table 2.6 for primers and band sizes.

Table 2.6: Genotyping primers and expected band sizes

Rat model	Floxed exon 8	Deleted exon 8
Primer pair 1		
Forward primer (5'-3')	AGGGAAGAAGGGAACAGGAG	AGGGAAGAAGGGAACAGGAG
Reverse primer (5'-3')	ATGGCAGTTCCCAGTAGCAT	TCTCTGGGATTCAGTGCAGA
WT band	369 bp	1387 bp (not seen)
Mutant band	409 bp	322 bp
Primer pair 2		
Forward primer (5'-3')	–	AAGGCAGAGAGAGAGACAAAG
Reverse primer (5'-3')	–	ATGGCAGTTCCCAGTAGCAT
WT band		493 bp
Mutant band		No band

2.5.4 Immunoblotting

Rats were terminally anaesthetised by inhalation of isofluorane 100% w/w (Abbot Laboratories, Maidenhead, Berkshire, UK) before being decapitated. Brains were microdissected in ice cold cutting solution (comprised of, in mM: 86 NaCl, 1.2 NaH_2PO_4, 2.5 KCl, 25 $NaHCO_3$, 75 sucrose, 25 glucose, 0.5 $CaCl_2$, 7 $MgCl_2$) and regions of interest flash frozen and stored at –80°C. Samples were later manually homogenised in a RIPA buffer (comprised of: 150 mM NaCl, 1% NP–40, 0.5% sodium deoxycholate, 0.1% SDS, 50 mM Tris

(pH 8.0), protease inhibitors). Samples were centrifuged for 5 minutes at 13,000 rpm in a 4°C centrifuge and the supernatant used for experiments. A BCA assay was performed to allow equal masses of protein to be loaded. Samples were denatured by heating with 100 mM DTT and 2% SDS for ten minutes at 80°C. From the point of gel loading, samples were treated as described in Section 2.4.3.

2.6 Materials

Bicuculline, CNQX, 5,7-Dichlorokynurenic acid, D-AP5, EGTA, ifenprodil, ionomycin, NMDA, spermine and tetrodotoxin citrate were purchased from Tocris (Bristol, UK). Media, media supplements, lipofectamine 2000, foetal bovine serum, antibiotic/antimycotic, B-27 and Fluo-3 were purchased from Invitrogen (Paisley, UK). The remaining substances were purchased from Sigma-Aldrich (Dorset, UK) unless stated otherwise in the text.

2.7 Statistical analysis

Data in tables are presented as mean $\pm$ standard error of the mean (SEM). Bar graphs depict individual cells (circles), means (bars) and SEM (arrows).

R (v 3.1.2) (R Core Team, 2014) was used to perform statistical tests. Comparisons between multiple means are performed by ANOVA. Comparisons between two means are performed by independent, two-tailed, Welch t–tests (which do not assume equal variance between groups) unless otherwise stated. Correction for multiple comparisons is made using the Bonferroni method. The significance level used was $p < 0.05$. In tables and figures, * indicates $p < 0.05$, ** indicates $p < 0.01$ and *** indicates $p < 0.001$.

2.8 Ethics

Animal breeding, maintenance and procedures were performed in accordance with UK Animal Scientific Procedures Act (1986) under project license number 60/4290.

CHAPTER 3

Three missense mutations alter important NMDAR properties

3.1 Chapter summary and key findings

1. The GluN2A^{N615K} mutation significantly alter potency of a range of NMDAR channel blockers, including Mg^{2+}. It also reduces Mg^{2+} block and current density in cultured neurons, and reduces single channel conductance.

2. The GluN2A^{R586K} mutation has no effect on Mg^{2+} block, current density or single channel conductance.

3. The GluN2B^{N615I} mutation reduces Mg^{2+} block and current density in cultured neurons. It also reduces single channel conductance.

4. The GluN2B^{V618G} mutation reduces Mg^{2+} block and current density in cultured neurons.

5. The alteration of important physiological NMDAR properties seen with the mutations GluN2A^{N615K}, GluN2B^{N615I} and GluN2B^{V618G} supports their role in disease causation.

6. The absence of altered properties associated with GluN2A^{R586K} does not support a role in disease causation, but does not exclude it.

3.2 Introduction

Over 100 mutations have been identified in NMDAR subunits in people with a range of neurodevelopmental disorders (see Section 1.6). Although this thesis hypothesises that some of these mutations will contribute to their carriers' disorders, it is unlikely that they all do. Some missense mutations may cause no or minimal alteration to NMDAR properties, and some may cause alterations which are easily compensated for by existing homeostatic mechanisms. Screening mutations for functional consequences is a time consuming, resource intensive process. It is therefore necessary to select a subset of mutations which are a priority for investigation. As the overall aim of this thesis was to generate knowledge about key biological pathways underlying the pathophysiology of severe mental disorders, mutations which had large effects on receptor properties were desirable, rather than mutations with subtle or context-specific effects.

With the aim of identifying mutations likely to have a large influence on NMDAR properties, the first factor considered was the mode of genetic inheritance. *De novo* mutations are more likely to be associated with highly deleterious phenotypes than inherited mutations (Veltman and Brunner, 2012) and hence be the sole or major cause of disorders in their carriers, and hence have large effects on receptor properties. The second selection criterion was the nature of the phenotype. Neurodevelopmental disorders cover a broad spectrum of symptoms and severity. Disorders which are highly disabling and of early onset are more likely to be caused by mutations which cause a large change in receptor properties. The third criterion was existing knowledge about the mutated domain. Mutations in a domain already known to be important for receptor function are likely to have important consequences. Fourthly, mutations which resulted in substitution of an amino acid with one from a different class (e.g. hydrophilic versus hydrophobic) were prioritised, as being more likely to alter receptor properties. Finally, mutations which have had some functional investigation already and have been shown to impact on receptor properties are good candidates for further investigation.

With these factors in mind, four missense point mutations were selected for study in this chapter (see Table 3.1). Three of the four arose *de novo*, are associated with an early onset and severe phenotype of epileptic encephalopathy and affect the pore region of the NMDAR, with two of the mutations modifying residues previously identified as important for Mg^{2+} block (the "N" and "N+1" site asparagines (Burnashev et al., 1992; Mori et al., 1992; Sakurada et al., 1993; Wollmuth et al., 1998)). Figure 3.1 highlights the location of the "N" site. The fourth mutation (GluN2A^{R586K}) was chosen because of its proximity to the mutations above (affecting a residue in the intracellular loop linking the M1 and M2 pore regions), although less is known about the function of this receptor domain. Also, this mutation has weaker genetic evidence of causality in that it was inherited maternally (no information about the mother's phenotype was reported).

The two mutations affecting the pore of GluN2B were both found in individuals with a particular sub-type of epileptic encephalopathy: West syndrome. There are three cardinal features of West syndrome: seizures termed "infantile spasms" where the trunk flexes or extends, a characteristic EEG pattern between seizures called "hypsarrhythmia" where chaotic, multifocal high amplitude spikes are seen, and intellectual disability or other

neurodevelopmental difficulties (Galanopoulou and Moshe, 2015). The mutations were associated with all of these features in their carriers, and in addition, with "autistic like behaviour" in the case of GluN2B^{N615I} (Lemke et al., 2014). The mutation affecting the pore of GluN2A was found in a child with a similar phenotype of frequent myoclonies (muscle jerks) and severe intellectual disability, but an EEG different to West syndrome (generalised slowing with bilateral independent posterior spikes) (Endele et al., 2010). The GluN2A^{R586K} mutation was also identified by Endele et al. (2010) but was less well characterised. It was found in a person in a cohort selected to have an unspecified degree of intellectual disability and either epilepsy and/or an abnormal EEG.

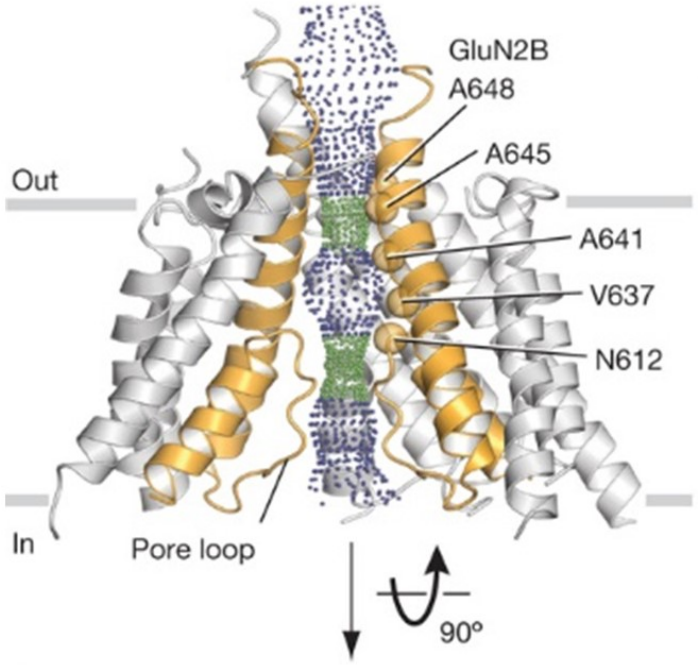

Figure 3.1: **The "N" site shown in GluN2B crystal structure**
This figure shows the crystal structure of the NMDAR GluN2B subunit transmembrane region, taken from Lee et al. (2014). The green and blue dots denote a solvent accessible pathway through the pore, with green dots indicating a pore radius less than 2.3 Ångströms. The "N" site asparagine is denoted here as a sphere labelled N612 (equivalent to N615 in the unmodified protein). The "N+1" site neighbours it. It can be seen that these residues are near the narrowest part of the pore. Although not shown here, the GluN2A pore structure is thought to be very similar.

Having identified a group of interesting mutations to investigate, it was necessary to prioritise properties to screen. This was done partly by making predictions from existing structure-function knowledge, partly by seeking to extend work done by other groups, and partly in response to results obtained during this study. Given that three of the four mutations influenced the pore, and had been found to affect Mg^{2+} block by others (Endele et al., 2010; Lemke et al., 2014), Mg^{2+} block and conductance were obvious properties to investigate (and whole cell current density, which is influenced by conductance amongst other things). Some work had already been done on the impact of GluN2A^{N615K} on channel blocker potency (Pierson et al., 2014) so this study sought to replicate and extend these findings by repeating

Table 3.1: Mutations selected for study

Mutation	GluN2A^{N615K}	GluN2B^{N615I}	GluN2B^{V618G}	GluN2A^{R586K}
Inheritance	*de novo*	*de novo*	*de novo*	Maternal (phenotype unknown)
Disorder	Epileptic encephalopathy	Epileptic encephalopathy (West syndrome)	Epileptic encephalopathy (West syndrome)	Intellectual disability and epilepsy*
Position in protein	Pore ("N+1") site	Pore ("N" site)	Pore	M1-M2 linker region
Existing functional work	Mg^{2+} block ↓; Ca^{2+} permeability ↓ [1] Memantine potency ↓; Amantadine potency ↓; Dextromethorphan potency ↑ [2]	Mg^{2+} block ↓; Ca^{2+} permeability ↑ [3]	Mg^{2+} block ↓; Ca^{2+} permeability ↑ [3]	None
First report	Endele et al. (2010)	Lemke et al. (2014)	Lemke et al. (2014)	Endele et al. (2010)

[1]: (Endele et al., 2010), [2]: (Pierson et al., 2014), [3]: (Lemke et al., 2014).
*GluN2A^{R586K} associated with abnormal EEG or epilepsy: detailed description of phenotype not reported (Endele et al., 2010).

the experiments at a range of holding potentials and including the additional channel blocker ketamine.

Uniquely, this study assessed the functional consequences of the mutations in cultured neurons. This is important as conceivably differences in trafficking, regulation or post-translational modifications could lead to differences in mutant subunit properties in neurons which would not be identified in systems which do not endogenously express NMDAR. However, endogenous expression of NMDAR is also a disadvantage, as it means that receptor populations will be a mixture of wild type and mutant receptors, complicating interpretation. To confirm expression of GluN2B mutant subunits, an additional mutation was introduced to artificially reduce their sensitivity to a GluN2B selective antagonist (discussed further in Section 3.4).

This chapter describes the assessment of Mg^{2+} block and current density for the mutant NMDAR subunits GluN2A^{N615K}, GluN2A^{R586K}, GluN2B^{N615I} and GluN2B^{V618G} expressed in cultured neurons. Conductance and channel state dwell times were assessed for GluN2A^{N615K}, GluN2A^{R586K} and GluN2B^{N615I} expressed in oocytes and HEK293 cells. The chapter begins with an assessment of the impact of GluN2A^{N615K} on channel blocker potency in oocytes.

The overall finding of this chapter is that the three mutations GluN2A^{N615K}, GluN2B^{N615I} and GluN2B^{V618G} all significantly impact important receptor properties, consistent with a role in causing the epileptic encephalopathies experienced by their carriers.

3.3 Expression of mutant diheteromers in oocytes

3.3.1 The GluN2A^{N615K} mutation reduces Mg^{2+} block and alters potency of NMDAR channel blockers

Previous work with the GluN2A^{N615K} mutation expressed in *X. laevis* oocytes identified a near absence of Mg^{2+} block at holding potentials of –70 mV (Endele et al., 2010). This study sought to extend these findings by comparing inhibition of glutamate-evoked currents by both Mg^{2+} and by small molecule channel blockers (memantine, amantadine, ketamine and dextromethorphan) in *X. laevis* oocytes expressing NMDAR containing wild type GluN2A and GluN2A^{N615K} using two-electrode voltage-clamp at holding potentials of –40 mV, –60 mV and –80 mV. In addition, experiments with memantine and amantadine were performed in the presence and absence of Mg^{2+} in order to identify any alterations in channel blocker potency associated with the presence of an approximately physiological concentration of Mg^{2+}.

The first finding was that Mg^{2+} block was reduced in NMDARs containing GluN2A^{N615K} compared to wild type GluN2A at all holding potentials (see Table 3.2 and Figures 3.2 and 3.3). Furthermore, block by memantine and amantadine was also reduced in NMDAR containing GluN2A^{N615K} compared to wild type GluN2A (Table 3.2, Figures 3.2 and 3.3). This reduction in blockade remained even in the presence of Mg^{2+}.

The GluN2A^{N615K} mutation also reduced block by ketamine at the majority of holding potentials tested (Table 3.2 and Figure 3.4) whereas block by dextromethorphan was increased at the majority of holding potentials tested (Table 3.2 and Figure 3.5).

Table 3.2: Summary values for channel blockers in oocytes

	GluN2A	GluN2A^{N615K}	GluN2A	GluN2A^{N615K}
	Memantine (10 μM)		Amantadine (100 μM)	
n	9	7	9	7
–40 mV	59 ± 2	11 ± 1	29 ± 4	9 ± 1
–60 mV	76 ± 2	27 ± 3	45 ± 4	17 ± 1
–80 mV	76 ± 2	28 ± 2	51 ± 5	17 ± 1
	Mg^{2+} (1 mM)			
n	9	7		
–40 mV	66 ± 4	0 ± 1		
–60 mV	89 ± 1	7 ± 2		
–80 mV	93 ± 2	2 ± 2		
	Memantine & Mg^{2+}		Amantadine & Mg^{2+}	
n	9	7	9	7
–40 mV	81 ± 2	10 ± 2	72 ± 3	6 ± 1
–60 mV	94 ± 1	29 ± 3	91 ± 1	20 ± 4
–80 mV	95 ± 3	27 ± 1	96 ± 1	18 ± 3
	Ketamine (10 μM)		Dextromethorphan (10 μM)	
n	9	6	7	8
–40 mV	65 ± 2	50 ± 3	24 ± 2	42 ± 8
–60 mV	79 ± 2	73 ± 1	45 ± 2	55 ± 3
–80 mV	85 ± 1	79 ± 1	57 ± 3	67 ± 3

Data are % inhibition, mean $\pm$ standard error of the mean

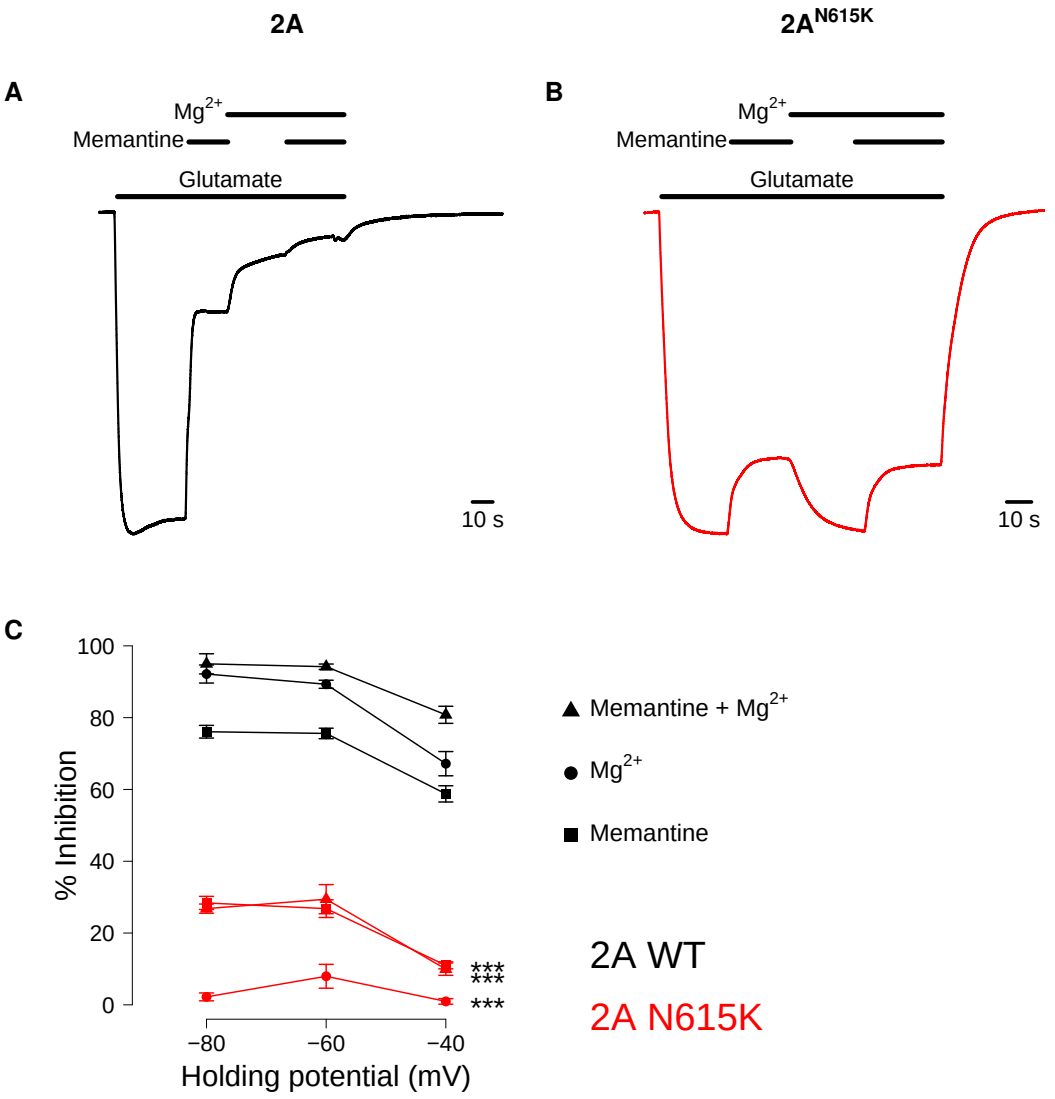

Figure 3.2: **NMDARs containing GluN2A^{N615K} show reduced Mg^{2+} and memantine block**
(A) Representative whole–cell voltage–clamp recordings from oocytes expressing 2A wild type NMDARs, showing inhibition by memantine (10 μM), Mg^{2+} (1 mM) and the two combined. Holding potential –60 mV. Responses are normalised to the peak amplitude.
(B) As for **(A)** but oocytes expressing 2A^{N615K} NMDARs.
(C) The line chart shows % inhibition by the channel blockers at three holding potentials (–40 mV, –60 mV, –80 mV). Stars indicate significance level of comparison of GluN2A^{N615K} means with wild type means for each combination of channel blockers (same significance at all holding potentials). A three-way repeated measures ANOVA showed main effects of subunit ($F(1,14) = 897$, $p < 4.3e{-}14$), channel blocker ($F(2, 28) = 301$, $p < 2e{-}16$), and holding potential ($F(2, 28) = 58$, $p < 1.2e{-}10$) with a significant three-way interaction ($F(4, 56) = 26$, $p < 3.3e{-}12$). Planned post-hoc t–tests (Bonferroni corrected) showed that at –40 mV, 2A^{N615K} subunits were associated with lower block than wild type for Mg^{2+} ($t(8.8) = 19.1$, $p_{corr} = 1.5e{-}7$), memantine ($t(10.7) = 19.4$, $p_{corr} < 9.5e{-}9$), and the two combined ($t(13.6) = 24.1$, $p_{corr} = 1.3e{-}11$). This pattern was also seen at –60 mV for Mg^{2+} ($t(7.4) = 23.2$, p_{corr} 3.2e-7), memantine ($t(10.1) = 17.0$, $p_{corr} = 8.8e{-}8$) and the two combined ($t(6.4) = 15.7$, $p_{corr} = 2.2e{-}5$), and at –80 mV for Mg^{2+} ($t(10.8) = 32.7$, $p_{corr} = 3.2e{-}11$), memantine ($t(13.6) = 18.7$, $p_{corr} = 3.9e{-}10$) and the two combined ($t(11.1) = 22.1$, $p_{corr} = 1.5e{-}9$).
See Table 3.2 for samples sizes and summary values.

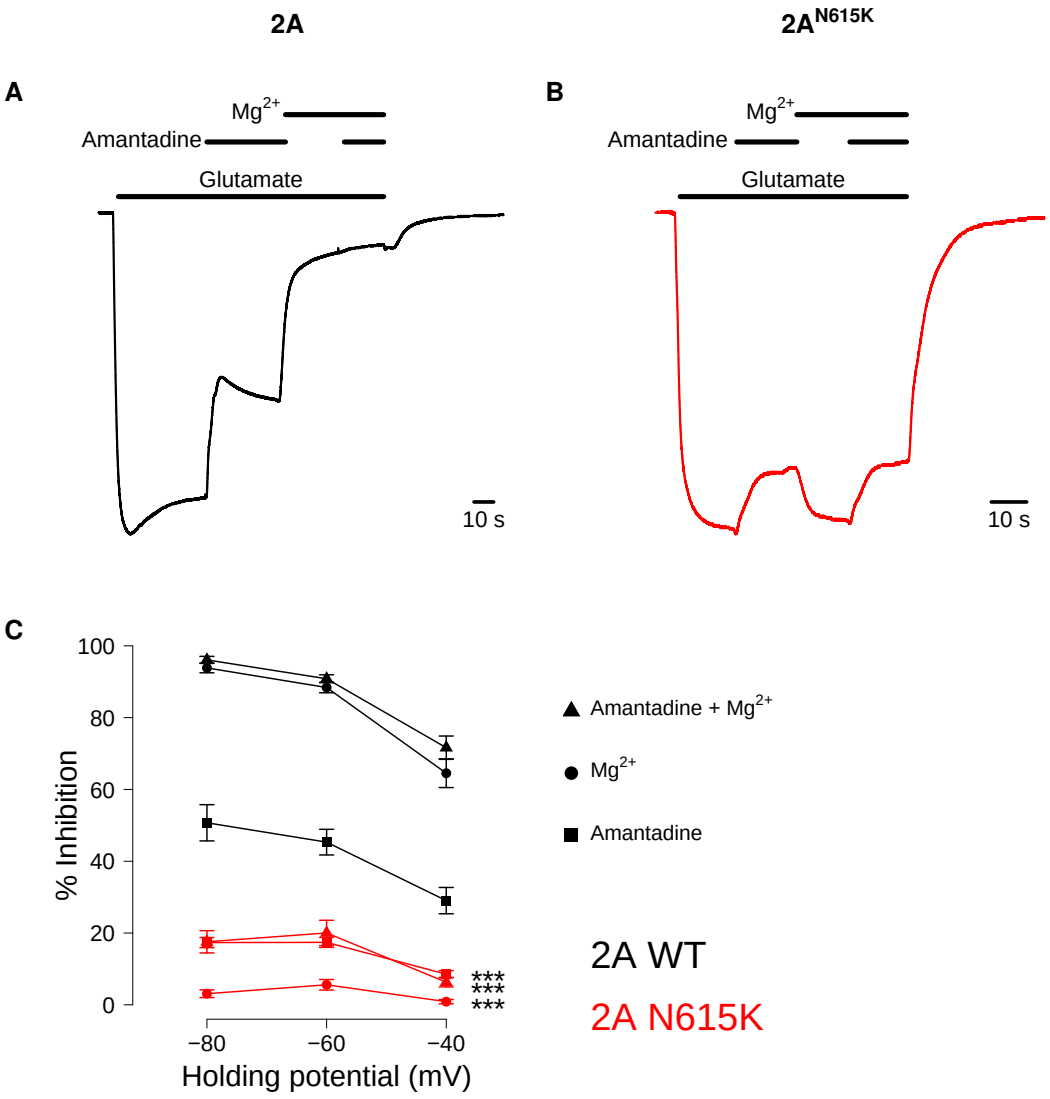

Figure 3.3: **NMDARs containing GluN2A^{N615K} show reduced Mg^{2+} and amantadine block**
(A) Representative whole–cell voltage–clamp recordings from oocytes expressing 2A wild type NMDARs, showing inhibition by amantadine (100 μM), Mg^{2+} (1 mM) and the two combined. Holding potential –60 mV. Responses are normalised to the peak amplitude.
(B) As for **(A)** but oocytes expressing 2A^{N615K} NMDARs.
(C) The line chart shows % inhibition by the channel blockers at three holding potentials (–40 mV, –60 mV, –80 mV). Stars indicate significance level of comparison of GluN2A^{N615K} means with wild type means for each combination of channel blockers. A three-way repeated measures ANOVA showed main effects of subunit ($F(1,14) = 509$, $p < 2.1e{-}12$), channel blocker ($F(2,28) = 170$, $p < 2.3e{-}16$), and holding potential ($F(2, 28) = 64$, $p < 3.3e{-}11$) with a significant three-way interaction ($F(4, 56) = 5.5$, $p < 0.0008$). Planned post-hoc t–tests (Bonferroni corrected) showed that at –40 mV, 2A^{N615K} subunits were associated with lower block than wild type for Mg^{2+} ($t(8.3) = 15.7$, $p_{corr} = 1.5e{-}6$), amantadine ($t(9.2) = 5.4$, $p_{corr} = 0.0036$), and the two combined ($t(10.5) = 18.6$, $p_{corr} = 2e{-}8$). This pattern was also seen at –60 mV for Mg^{2+} ($t(13.7) = 40.0$, p_{corr} 1.3e-14), amantadine ($t(10.3) = 7.3$, $p_{corr} = 0.0002$) and the two combined ($t(7.2) = 19.2$, $p_{corr} = 1.8e{-}6$), and at –80 mV for Mg^{2+} ($t(13.9) = 52.3$, $p_{corr} = 2e{-}15$), amantadine ($t(9.2) = 6.4$, $p_{corr} = 0.001$) and the two combined ($t(7.2) = 24.2$, $p_{corr} = 3.3e{-}7$).
See Table 3.2 for samples sizes and summary values.

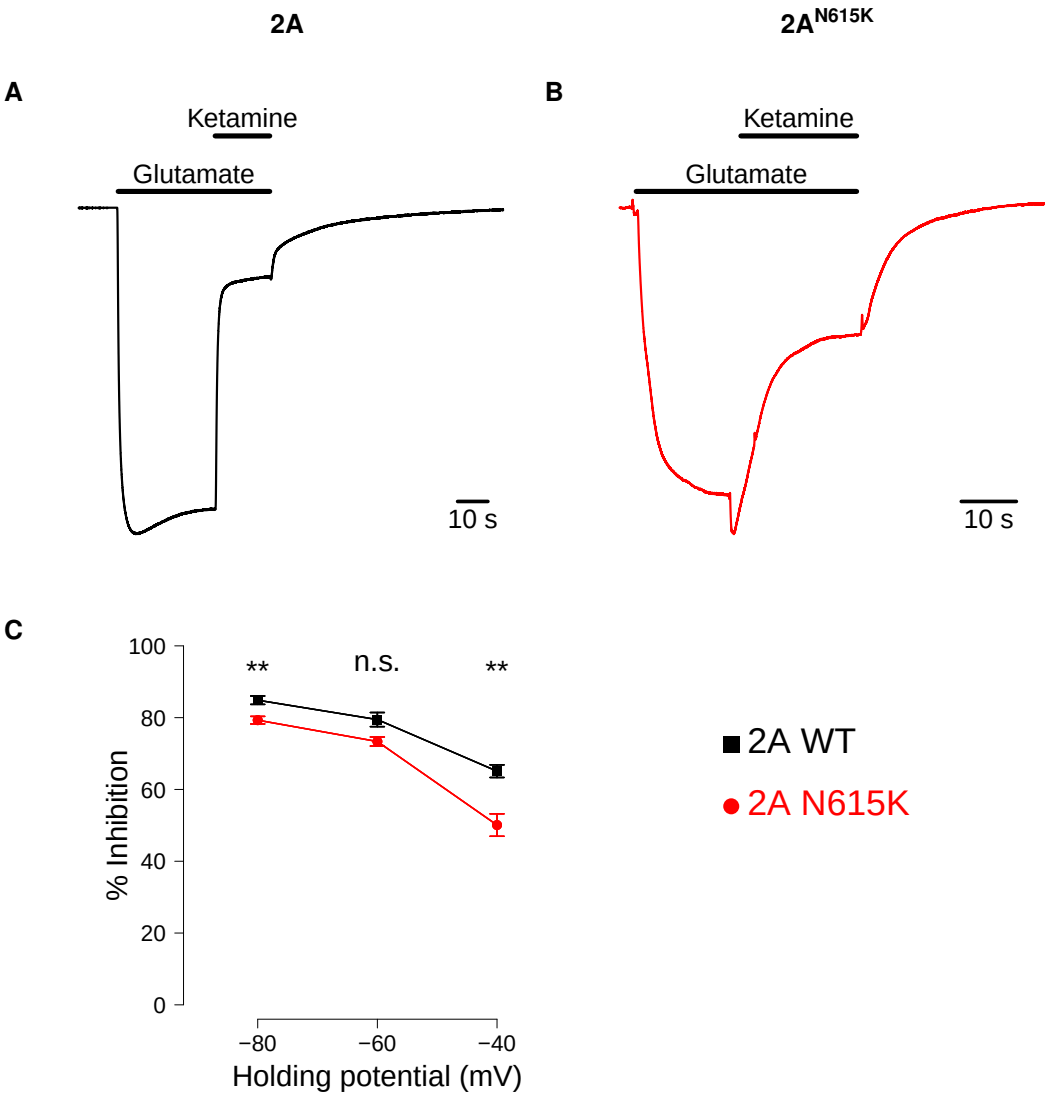

Figure 3.4: **NMDARs containing GluN2A^{N615K} show reduced block by ketamine**
(A) Representative whole–cell voltage–clamp recordings from oocytes expressing 2A wild type NMDARs, showing inhibition by ketamine (10 μM). Holding potential –60 mV. Responses are normalised to the peak amplitude.
(B) As for **(A)** but oocytes expressing 2A^{N615K} NMDARs.
(C) The line chart shows % inhibition by ketamine (10 μM) at three holding potentials (–40 mV, –60 mV, –80 mV). Stars indicate significance level of comparison of GluN2A^{N615K} means with wild type means at each holding potential. A two-way repeated measures ANOVA showed main effects of subunit ($F(1,15) = 19.8$, $p = 0.0005$) and holding potential ($F(2,30) = 125$, $p < 3e{-}15$) with a significant interaction ($F(2, 30) = 5.5$, $p = 0.009$). Planned post-hoc t–tests (Bonferroni corrected) showed that 2A^{N615K} subunits were associated with lower block by ketamine than seen in wild type at holding potentials of –40 mV ($t(8.3) = 4.2$, $p_{corr} = 0.0086$) and at –80 mV ($t(14.2) = 3.5$, $p_{corr} = 0.0097$) but not at –60 mV ($t(14.9) = 2.6$, $p_{corr} = 0.058$).
See Table 3.2 for samples sizes and summary values.

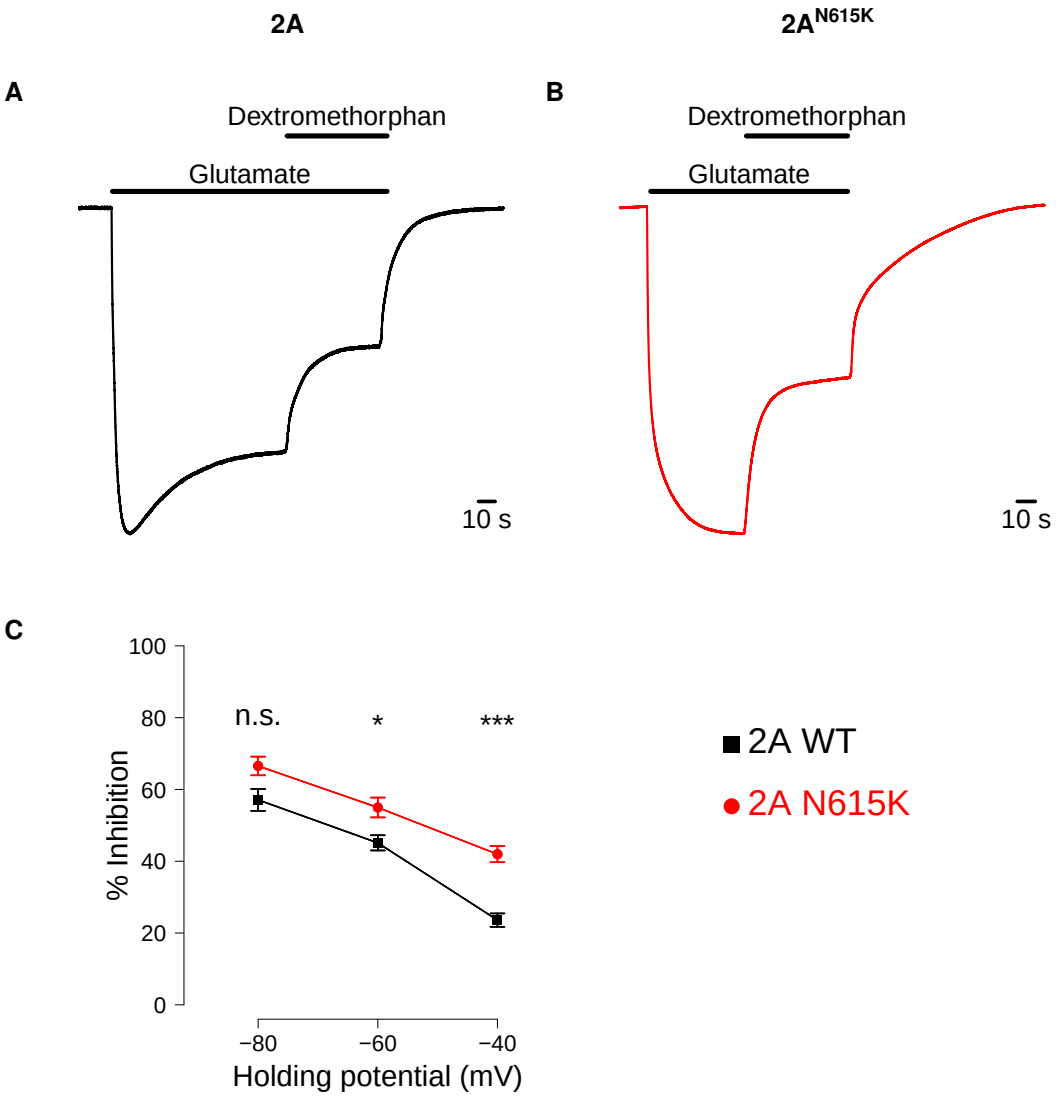

Figure 3.5: **NMDARs containing GluN2A^{N615K} show increased block by dextromethorphan** **(A)** Representative whole-cell voltage-clamp recordings from oocytes expressing 2A wild type NMDARs, showing inhibition by dextromethorphan (10 μM). Holding potential –60 mV. Responses are normalised to the peak amplitude.
(B) As for **(A)** but oocytes expressing 2A^{N615K} NMDARs.
(C) The bar chart shows % inhibition by dextromethorphan (10 μM) at three holding potentials (–40 mV, –60 mV, –80 mV). Stars indicate significance level of comparison of GluN2A^{N615K} means with wild type means at each holding potential. A two-way repeated measures ANOVA showed main effects of subunit ($F(1,13) = 15.5$, $p = 0.002$) and holding potential ($F(2,26) = 245$, $p < 2e{-}16$) with a significant interaction ($F(2, 26) = 7.4$, $p = 0.003$). Planned post-hoc t–tests (Bonferroni corrected) showed that 2A^{N615K} subunits were associated with higher block by dextromethorphan than seen in wild type at holding potentials of –40 mV ($t(12.8) = 6.3$, $p_{corr} = 9e{-}5$) and at –60 mV ($t(12.6) = 2.8$, $p_{corr} = 0.043$) but not at –80 mV ($t(12.3) = 2.4$, $p_{corr} = 0.109$). See Table 3.2 for samples sizes and summary values.

3.3.2 The GluN2A^{R586K} mutation does not affect Mg^{2+} block

The GluN2A^{R586K} mutation was investigated next. In contrast to the GluN2A^{N615K} mutation, this mutation showed no effect on Mg^{2+} block at –60 mV (Figure 3.6).

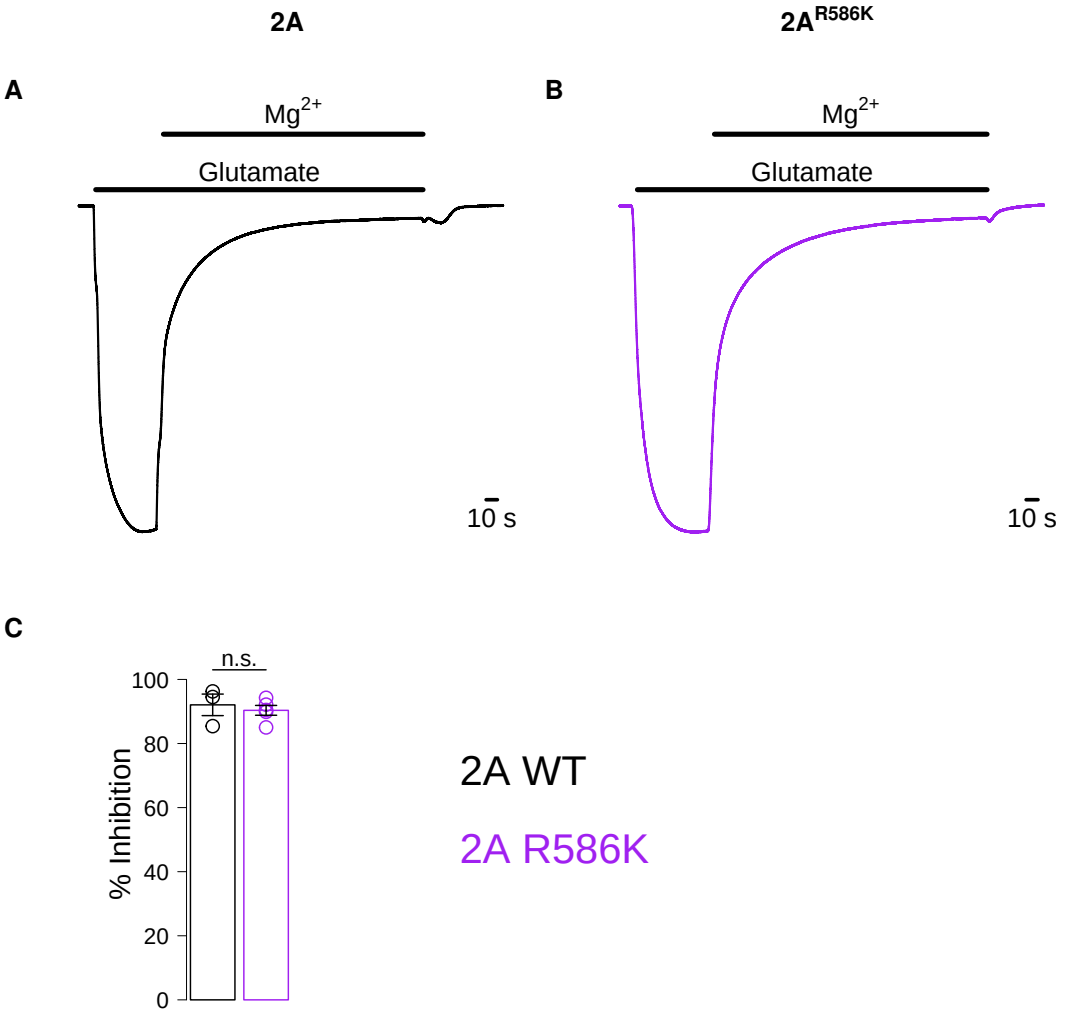

Figure 3.6: **NMDARs containing GluN2A^{R586K} have normal Mg^{2+} block**
(A) Representative whole–cell voltage–clamp recordings from oocytes expressing 2A wild type NMDARs, showing inhibition by Mg^{2+} (1 mM). Holding potential –60 mV. Responses are normalised to the peak amplitude.
(B) As for **(A)** but oocytes expressing 2A^{R586K} NMDARs.
(C) The bar charts show % inhibition by Mg^{2+} (1 mM) at a holding potential of –60 mV. A t–test showed no significant difference between Mg^{2+} block in NMDARs containing wild type (92 $\pm$ 3 %, n=3) or 2A^{R586K} (90 $\pm$ 2 %, n=5) subunits.
Some of the data in this figure was collected by Pete Parker, a medical undergraduate completing a summer project with me.

3.4 Expression of mutant subunits in neurons

Oocytes are extremely useful vehicles for expression of recombinant ion channels because they allow expression of a known population of receptors in a standardised fashion. However, to be relevant to disease, any alteration in NMDAR properties should also be observed in cells in which NMDARs are normally expressed: predominantly forebrain neurons (in the case of the GluN2A and GluN2B subunits). Conceivably, neuron-specific trafficking and regulation pathways could result in no expression of mutant subunits or some compensatory effect, such as increased expression of other subunits. This section therefore used cultured primary mouse cortical neurons as a highly relevant system in which to overexpress mutant subunits and assess their impact, if any, on NMDAR properties.

The interpretation of results in neurons is complicated by each cell giving a NMDA-evoked response which arises in part from endogenous NMDAR subunits and in part from transfected subunits. The age of culture used (DIV 9) was chosen so that virtually all the endogenous GluN2 subunits were GluN2B (McKay et al., 2012) (and see also Figure 5.12 in Chapter 5). The GluN2B selective antagonist ifenprodil could therefore be used to suppress the contribution of endogenous NMDARs and to confirm the transfection of the subunit of interest. In the case of mutations affecting GluN2A subunits, expression could be confirmed simply by ifenprodil sensitivity of less than around 80%, as GluN2B diheteromers show 80% block but GluN2A diheteromers minimal block at the concentration of ifenprodil used (3 μM) (Williams, 1993). To confirm expression of mutations affecting GluN2B subunits, however, an additional mutation was required to artificially reduce their ifenprodil sensitivity: the D101A point mutation. This mutation reduces ifenprodil sensitivity of GluN2B diheteromers to 9% (Perin-Dureau et al., 2002). Subunits carrying this mutation are denoted here as GluN2B$^{(ins)}$. In addition to confirming expression of transfected subunits, application of ifenprodil also allowed asessment of NMDAR properties from a population where an increased proportion contained the mutant subunit of interest. Therefore, where there are differences in parameters with and without ifenprodil, ifenprodil insensitive wild type and mutant subunits have been compared in the presence of ifenprodil, maximising the contribution of these subunits to the whole-cell currents.

The final general point about the methodological approach taken in this section is that the most relevant control for transfected cells are other transfected cells. This is both because the act of transfection has a detrimental impact on cells' health (Sandbichler et al., 2013), and because the characteristics of cells selected for patching may vary between transfected cells (where there is a limited number to choose from) and untransfected cells (where there are many cells to choose from). The data shown here therefore includes two controls, untransfected cells and cells transfected with an inert protein (β globin), but statistical comparisons for NMDAR subunit transfections are made only with β globin transfected cells.

3.4.1 The GluN2A^{N615K} mutation reduces Mg^{2+} block and current density in neurons

Cultured primary mouse cortical neurons were transiently transfected with GluN2A^{N615K}, wild type GluN2A and the inert control β globin. First, NMDA-evoked currents were assessed using whole-cell patch-clamping, and % inhibition by a physiological concentration of Mg^{2+} assessed. Next, cells were exposed to ifenprodil for a minimum of 1 minute (to allow full inhibition to develop) and NMDA-evoked currents and Mg^{2+} inhibition assessed again. Representative traces are shown in Figure 3.7.

Figure 3.8 and Table 3.3 show ifenprodil sensitivity. It can be seen that cells transfected with either GluN2A subunit type (wild type or mutant) show lower ifenprodil sensitivity than cells transfected with β globin. This confirms expression of the transfected GluN2A subunits.

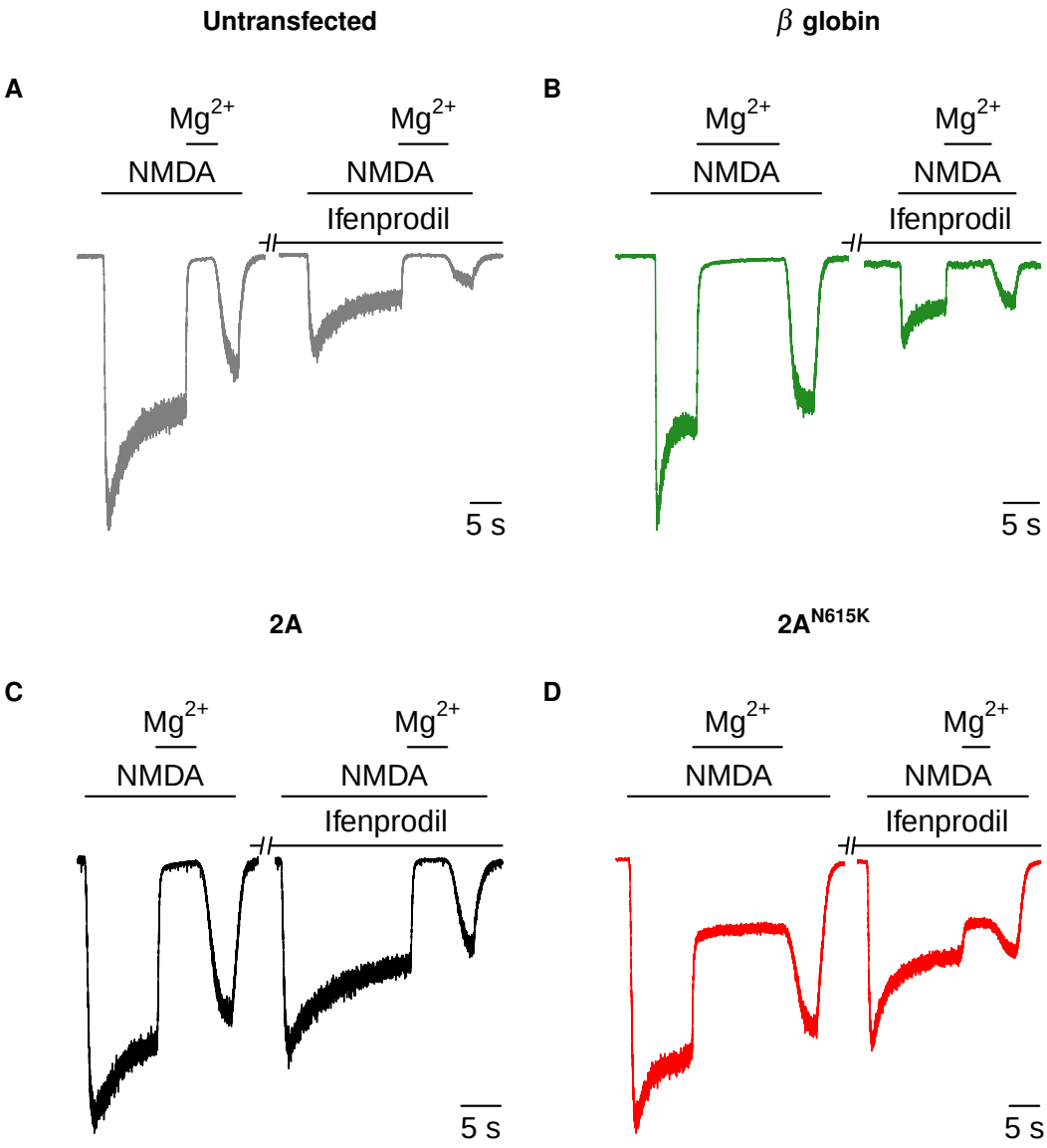

Figure 3.7: **Representative traces from neurons transfected with wild type GluN2A or GluN2A^{N615K}**

(A) Representative whole-cell voltage-clamp recording from untransfected DIV 9 neurons, showing inhibition of current evoked by saturating NMDA (150 μM) by Mg^{2+} (1 mM) before and after one minute of ifenprodil (3 μM) application. Holding potential –65 mV. Responses are normalised to the peak amplitude.

(B-D) As for **(A)** but neurons transfected with an inert control (β globin), 2A or 2A^{N615K} NMDAR subunits respectively.

Table 3.3: Summary values for Mg^{2+} block, current density and ifenprodil inhibition associated with expression of GluN2A and GluN2B mutant subunits in neurons

	Mg^{2+} block (%)	Mg^{2+} block (%) + Ifenprodil	Current density (pA/pF)	Current density (pA/pF) + Ifenprodil	Ifenprodil inhibition (%)	n
Untransfected*	94 ± 1	99 ± 1	52 ± 5	13 ± 2	76 ± 2	15
Globin*	97 ± 1	103 ± 2	45 ± 4	11 ± 1	75 ± 2	15
GluN2A	93 ± 1	95 ± 1	58 ± 5	38 ± 4	32 ± 3	15
$GluN2A^{N615K}$	52 ± 5	31 ± 5	40 ± 4	23 ± 3	43 ± 4	15
$GluN2A^{R586K}$	92 ± 2	93 ± 1	62 ± 6	47 ± 5	25 ± 3	12
GluN2B	94 ± 2	103 ± 1	56 ± 6	10 ± 1	84 ± 2	11
$GluN2B^{(ins)}$	95 ± 2	97 ± 2	40 ± 4	23 ± 3	45 ± 3	21
$GluN2B^{N615I}$	77 ± 6	92 ± 5	31 ± 4	8 ± 2	74 ± 3	11
$GluN2B^{N615I\ (ins)}$	86 ± 3	76 ± 3	33 ± 5	12 ± 1	60 ± 2	12
$GluN2B^{V618G}$	85 ± 3	91 ± 2	40 ± 3	7 ± 1	72 ± 2	11
$GluN2B^{V618G\ (ins)}$	90 ± 1	89 ± 3	36 ± 5	11 ± 2	67 ± 3	12

* Summary values represent cells from recording days shared with $GluN2A^{N615K}$ subunits. Other subsets of control cells matched by recording day used for statistical comparisons with other transfected NMDAR subunits.

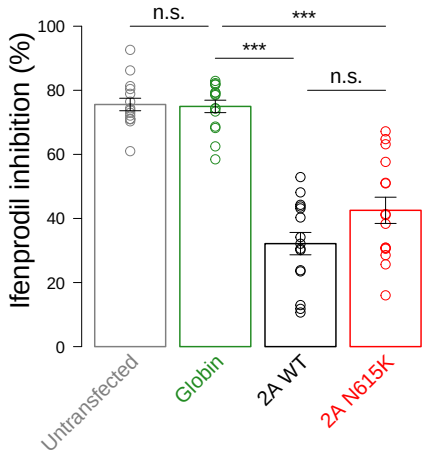

Figure 3.8: **Ifenprodil inhibition is reduced in neurons transfected with wild type GluN2A or $GluN2A^{N615K}$**

The bar chart shows % inhibition by ifenprodil (3 μM) for untransfected neurons, neurons transfected with an inert control (β globin), 2A and $2A^{N615K}$ NMDAR subunits. A one-way ANOVA showed a significant main effect of transfected subunit ($F(3,56) = 54.5$, $p < 2e{-}16$. Planned post-hoc independent t–tests showed no significant difference in ifenprodil sensitivity between untransfected neurons and neurons transfected with β globin. However, there was a highly significant reduction in ifenprodil sensitivity in neurons transfected with 2A ($t(21.9) = 10.7$, $p_{corr} = 1.4e{-}9$) and $2A^{N615K}$ ($t(20.0) = 7.2$, $p_{corr} = 2.5e{-}6$) when compared to a β globin transfection. Finally, there was no significant difference between neurons transfected with 2A and $2A^{N615K}$ subunits.

Figure 3.9 and Table 3.3 show Mg^{2+} block, in the presence and absence of ifenprodil. The key message of this figure is that there is no difference in Mg^{2+} block between untransfected cells, cells transfected with β globin or cells transfected with wild type GluN2A, but there was a marked reduction in Mg^{2+} block in cells transfected with $GluN2A^{N615K}$compared to

wild type GluN2A, in the presence or absence of ifenprodil. A two-way ANOVA identified a significant group by ifenprodil interaction (see figure legend) whereby Mg^{2+} block was greater in the presence of ifenprodil in the case of untransfected cells and lower in the presence of ifenprodil for cells transfected with GluN2A^{N615K}. This second finding is important as it shows that increasing the proportion of the response arising from mutant receptors increases the degree of alteration in receptor property observed. The finding in untransfected cells was not replicated with cells recorded on other days (Figures 3.17 and 3.21) and likely reflects incomplete wash out of NMDA from previous applications (this also allowed some cells to exhibit greater than 100% block by Mg^{2+}).

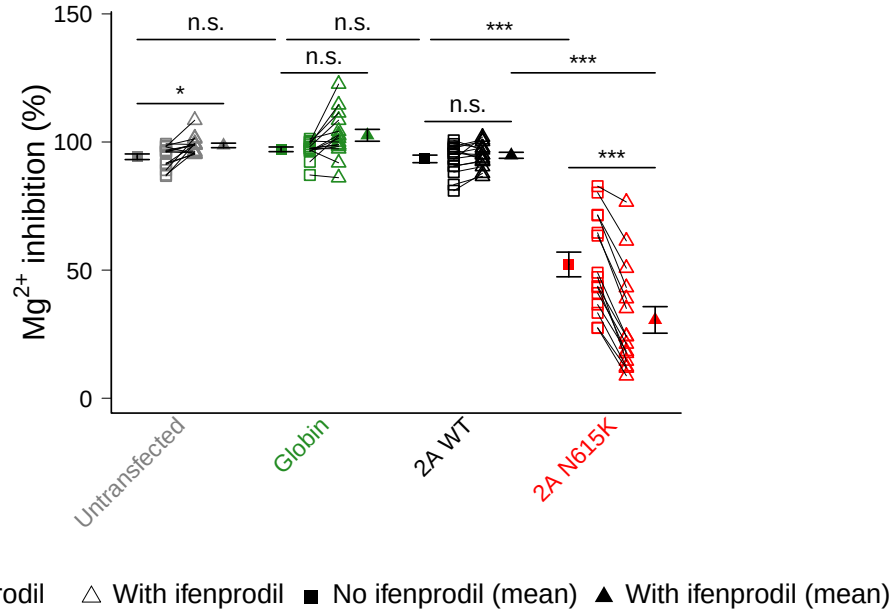

Figure 3.9: **Mg^{2+} block is reduced in neurons transfected with GluN2A^{N615K}**
The plot shows % inhibition by Mg^{2+} (1 mM) before and after ifenprodil (3 μM) application for untransfected neurons and neurons transfected with an inert control (β globin), 2A or 2A^{N615K} NMDAR subunits. A two-way repeated measures ANOVA showed main effects of transfected construct ($F(3,56) = 108$, $p < 2e{-}16$) and ifenprodill ($F(1,56) = 12.3$, $p = 0.0009$) with a significant interaction ($F(3,56) = 75$, $p < 2e{-}16$). Planned post-hoc paired t–tests (Bonferroni corrected) showed that ifenprodil was associated with a small but significant increase in Mg^{2+} block in untransfected neurons ($t(14) = 3.5$, $p_{corr} = 0.027$), no difference in Mg^{2+} block in neurons transfected with β globin or 2A , and a significant reduction in Mg^{2+} block in neurons transfected with 2A^{N615K} ($t(14) = 13.1$, $p_{corr} = 2.5e{-}8$). Further post-hoc independent t–tests were used to compare transfected constructs in the absence of ifenprodil; these showed no significant difference in Mg^{2+} block between untransfected neurons and neurons transfected with β globin or 2A , but a significant reduction in Mg^{2+} block in neurons transfected with 2A^{N615K} ($t(16.7) = 8.2$, $p_{corr} = 2.6e{-}6$). Finally, 2A and 2A^{N615K} were compared in the presence of ifenprodil, again demonstrating a significant reduction in Mg^{2+} block associated with 2A^{N615K} ($t(15.4) = 12.1$, $p_{corr} = 2.2e{-}8$).
See Table 3.3 for samples sizes and summary values.

Figure 3.10 and Table 3.3 show current density. The most prominent feature of these data is the substantial reduction in current density seen in all groups following application of ifenprodil. This reflects blockade of endogenous GluN2B-containing NMDARs. However, it is also evident that the cells transfected with GluN2A subunits show higher current density than the other groups (reflecting their lower ifenprodil sensitivity): there was no difference in current density post ifenprodil comparing untransfected and β globin transfected cells, but wild type GluN2A showed higher currents. Interestingly, cells transfected with GluN2A^{N615K} showed lower current density than cells transfected with wild type GluN2A in the presence of ifenprodil.

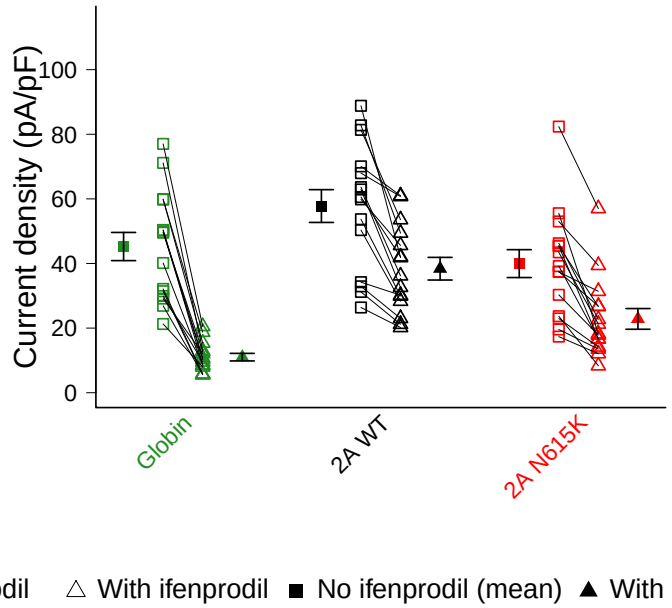

Figure 3.10: **Current density is reduced in neurons transfected with GluN2A^{N615K}**
The plot shows current density before and after ifenprodil (3 μM) application for untransfected neurons and neurons transfected with an inert control (β globin), 2A or 2A^{N615K} NMDAR subunits. A two-way repeated measures ANOVA showed main effects of transfected construct ($F(3,56) = 6.9$, $p = 0.0005$) and ifenprodill ($F(1,56) = 312$, $p < 2e{-}16$) with a significant interaction ($F(3, 56) = 12$, $p = 3.6e{-}6$). Planned post-hoc paired t–tests (Bonferroni corrected) showed that ifenprodil was associated with a significant reduction in current density with all groups: untransfected neurons ($t(14) = 12.1$, $p_{corr} = 9.8e{-}7$), β globin ($t(14) = 9.8$, $p_{corr} = 9.8e{-}7$), 2A ($t(14) = 6.1$, $p_{corr} = 0.0002$) and 2A^{N615K} ($t(14) = 7.0$, $p_{corr} = 4.7e{-}5$). Further post-hoc independent t–tests were used to compare transfected constructs in the presence of ifenprodil (as this is when the GluN2A subunits contributed the highest proportion to whole-cell currents); these showed no significant difference in current density between untransfected neurons and neurons transfected with β globin, but a significant increase in current density in neurons transfected with 2A ($t(17.1) = 7.4$, $p_{corr} = 8.0e{-}6$). Finally, 2A and 2A^{N615K} were compared in the presence of ifenprodil, demonstrating a significant reduction in current density associated with 2A^{N615K} ($t(27.8) = 3.3$, $p_{corr} = 0.023$).
See Table 3.3 for samples sizes and summary values.

3.4.2 The GluN2A^{R586K} mutation has no effect on Mg^{2+} block or current density

The next mutation to be investigated was the GluN2A^{R586K} mutation. The same experiments were performed as with the GluN2A^{N615K} mutation (Figure 3.11). As with the GluN2A^{N615K} mutation, expression of the mutant subunits was confirmed by reduced ifenprodil sensitivity (Figure 3.12). In contrast to GluN2A^{N615K}, there was no difference in Mg^{2+} block between wild type GluN2A and GluN2A^{R586K} transfected cells (Figure 3.13). The subset of β globin controls used for this series of experiments had an unusually high Mg^{2+} block, resulting in significant differences from untransfected and wild type GluN2A transfected cells. However, this pattern was not replicated with other data sets (Figures 3.9, 3.17, 3.21) and so is unlikely to be physiologically relevant.

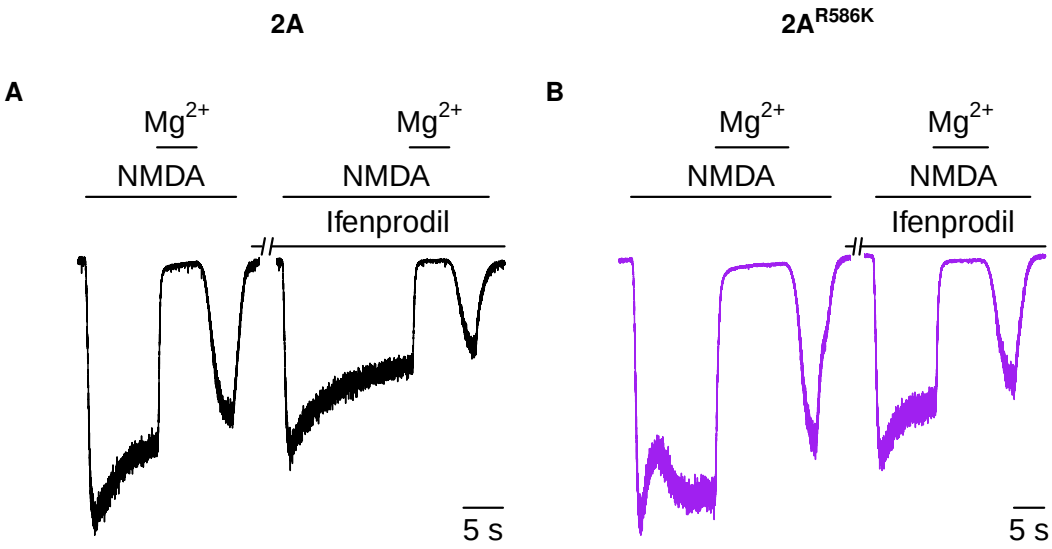

Figure 3.11: **Representative traces from neurons transfected with wild type GluN2A or GluN2A^{R586K}**
(A) Representative whole-cell voltage-clamp recording from DIV 9 neurons transfected with 2A, showing inhibition by Mg^{2+} (1 mM) before and after one minute of ifenprodil (3 μM) application. Holding potential –65 mV. Responses are normalised to the peak amplitude.
(B) As for **(A)** but neurons transfected with 2A^{R586K} NMDAR subunits.

Figure 3.14 shows current density. Again, all groups showed a marked reduction in current density in the presence of ifenprodil, with wild type GluN2A transfected cells showing higher current density than β globin transfected cells, in the presence of ifenprodil. However, there was no difference in current density between cells transfected with wild type GluN2A and GluN2A^{R586K} subunits.

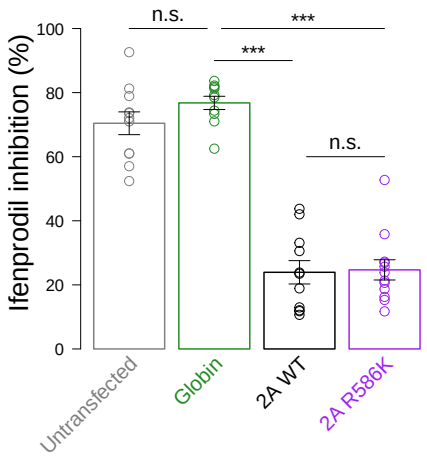

Figure 3.12: **Ifenprodil inhibition is reduced in neurons transfected with wild type GluN2A or GluN2A^{R586K}**

The bar chart shows % inhibition by ifenprodil (3 μM) for untransfected neurons, neurons transfected with an inert control (globin), 2A and 2A^{R586K} NMDAR subunits. A one-way repeated measures ANOVA showed a significant main effect of transfected subunit ($F(3,40) = 78.4$, $p <$ 2e–16). Planned post-hoc independent t-tests showed no significant difference in ifenprodil sensitivity between untransfected neurons and neurons transfected with β globin. However, there was a highly significant reduction in ifenprodil sensitivity in neurons transfected with 2A ($t(15.7) = 12.6$, $p_{corr} = 5.0e{-}9$) and 2A^{N615K} ($t(18.3) = 13.8$, $p_{corr} = 1.6e{-}10$) when compared to a β globin transfection. Finally, there was no significant difference between neurons transfected with 2A or 2A^{R586K} subunits.

See Table 3.3 for samples sizes and summary values.

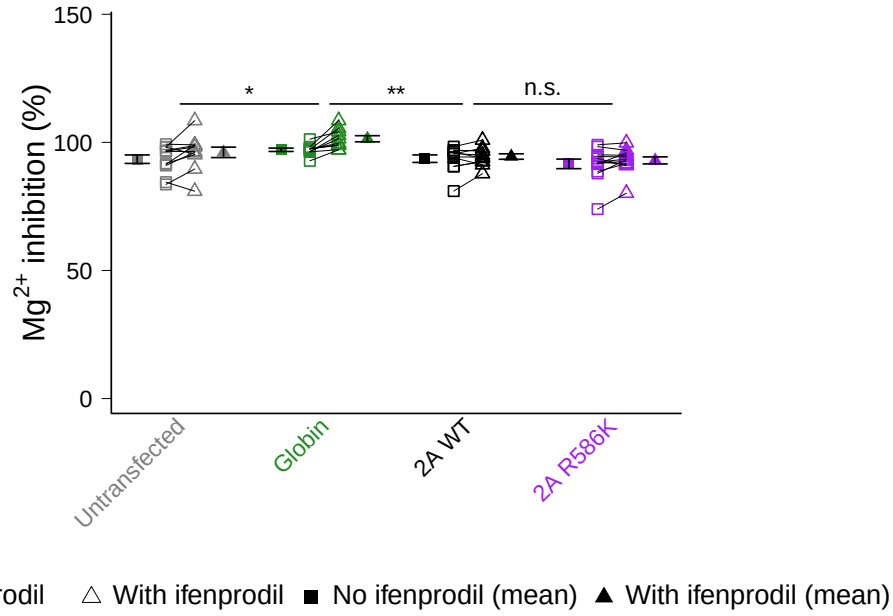

Figure 3.13: **Mg^{2+} block is normal in neurons transfected with GluN2A^{R586K}**
The plot shows % inhibition by Mg^{2+} (1 mM) before and after ifenprodil (3 μM) application for untransfected neurons and neurons transfected with an inert control (β globin), 2A or 2A^{R586K} NMDAR subunits. A two-way repeated measures ANOVA showed main effects of transfected construct ($F(3,40) = 4.2$, $p = 0.011$) and ifenprodil ($F(1,40) = 20.1$, $p = 6.1e{-5}$) with a non-significant interaction. Planned post-hoc independent t–tests were used to compare transfected constructs with results in the presence/absence of ifenprodil combined; these showed a small but significant increase in Mg^{2+} block in neurons transfected with β globin when compared to untransfected neurons ($t(40.0) = 4.3$, $p_{corr} = 0.026$) and neurons transfected with 2A ($t(40.0) = 4.3$, $p_{corr} = 0.00045$). There was no difference in Mg^{2+} block in cells transfected with 2A^{R586K} compared to 2A .
See Table 3.3 for samples sizes and summary values.

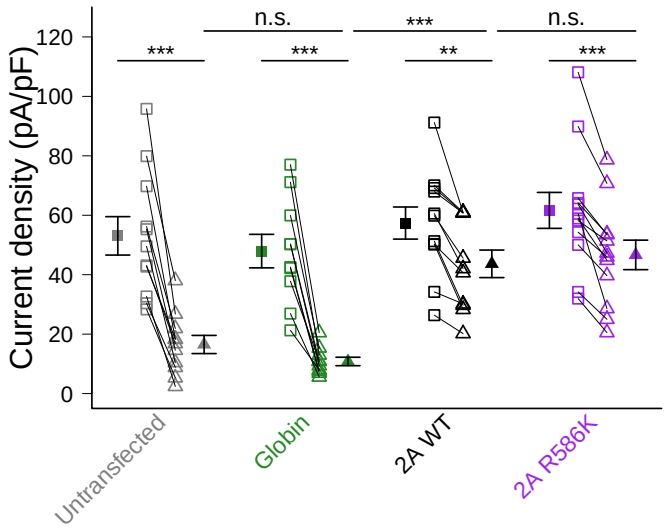

Figure 3.14: **Current density is unaffected in neurons transfected with GluN2A^{R586K}**
The plot shows current density before and after ifenprodil (3 μM) application for untransfected neurons and neurons transfected with an inert control (β globin), 2A or 2A^{R586K} NMDAR subunits. A 2 way repeated measures ANOVA showed main effects of transfected construct ($F(3,40) = 6.4$, $p = 0.0012$) and ifenprodill ($F(1,40) = 210$, $p < 2e{-}16$) with a significant interaction ($F(3, 40) = 14$, $p = 2.1e{-}6$). Planned post-hoc paired t–tests (Bonferroni corrected) showed that ifenprodil was associated with a significant reduction in current density with all groups: untransfected neurons ($t(10) = 8.5$, $p_{corr} = 4.9e{-}5$), β globin ($t(9) = 8.2$, $p_{corr} = 0.00012$, 2A ($t(10) = 5.5$, $p_{corr} = 0.0018$ and 2A^{R586K} ($t(11) = 6.4$, $p_{corr} = 0.00035$). Further post-hoc independent t–tests were used to compare transfected constructs in the presence of ifenprodil; these showed no significant difference in current density between untransfected neurons and neurons transfected with β globin, but a significant increase in current density in neurons transfected with 2A ($t(11.9) = 6.8$, $p_{corr} = 0.00015$). Finally, 2A and 2A^{R586K} were compared in the presence of ifenprodil, demonstrating no difference in current density.
See Table 3.3 for samples sizes and summary values.

3.4.3 The GluN2B^{N615I} mutation reduces Mg^{2+} block and current density

GluN2B mutations were examined next. Experiments comparing wild type GluN2B with GluN2B^{N615I} were peformed alongside ifenprodil insensitive versions of each subunit: GluN2B$^{(ins)}$ and GluN2B$^{N615I\,(ins)}$ (Figure 3.15). This was to allow confirmation of mutant expression, and to allow better assessment of the mutant subunit's impact on NMDAR properties by inhibition of endogenous, ifenprodil sensitive, NMDARs (for more details, see start of Section 3.4). As with GluN2A^{N615K}, ifenprodil sensitivity, Mg^{2+} block and current density were assessed.

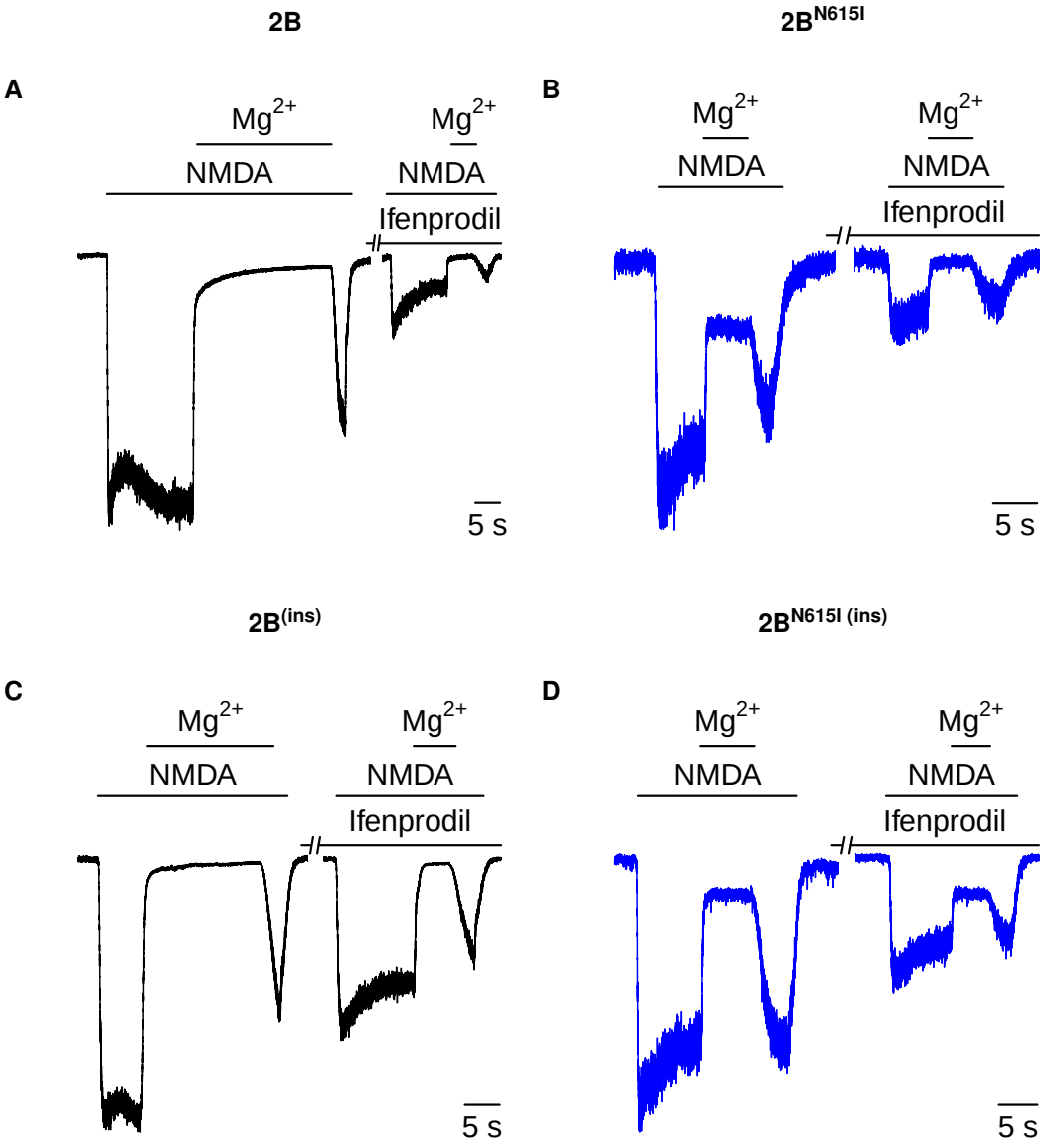

Figure 3.15: **Representative traces from neurons transfected with wild type GluN2B or GluN2B^{N615I}, wild type and ifenprodil insensitive forms**
(A) Representative whole-cell voltage-clamp recording from DIV 9 neuron transfected with 2B, showing inhibition by Mg^{2+} (1 mM) before and after one minute of ifenprodil (3 μM) application. Holding potential –65 mV. Responses are normalised to the peak amplitude.
(B-D) As for **(A)** but neurons transfected with 2B^{N615I}, 2B$^{(ins)}$ or 2B$^{N615I\ (ins)}$ NMDAR subunits respectively.

Figure 3.16 and Table 3.3 show ifenprodil sensitivity. The primary finding is that the ifenprodil insensitive forms show lower ifenprodil sensitivity than their standard sensitivity counterparts, confirming expression. Also of note is that the GluN2B$^{N615I\ (ins)}$ mutant shows greater ifenprodil sensitivity than cells transfected with GluN2B$^{(ins)}$ subunits. This may reflect lower expression, or it may reflect a reduction in current density in the mutant which gives a falsely high ifenprodil sensitivity when expressed alongside endogenous NMDARs.

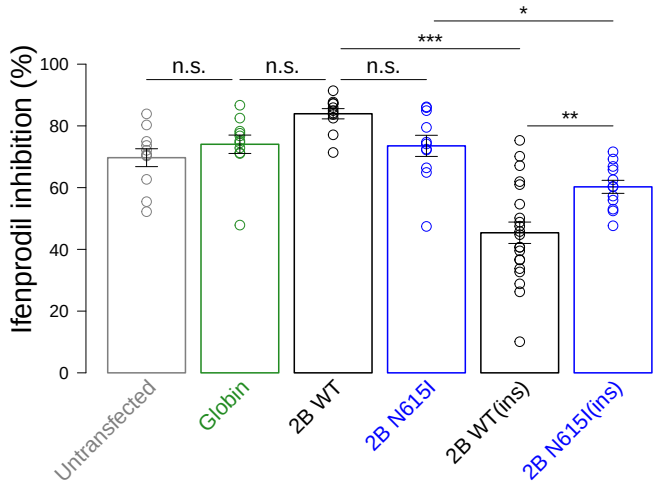

Figure 3.16: **Ifenprodil inhibition is reduced in neurons transfected with ifenprodil insensitive forms of wild type GluN2B and GluN2B^{N615I}**
The bar chart shows % inhibition by ifenprodil (3 μM) for untransfected neurons and neurons transfected with an inert control (β globin), 2B, 2B$^{(ins)}$, 2B^{N615I} or 2B$^{N615I\ (ins)}$ NMDAR subunits. A one-way ANOVA showed a significant main effect of transfected subunit ($F(5,71) = 22.2$, $p < 2.6e\text{-}13$). Planned post-hoc independent t-tests showed no significant difference in ifenprodil sensitivity between untransfected neurons and neurons transfected with β globin or 2B. However, there was a highly significant reduction in ifenprodil sensitivity in neurons transfected with 2B$^{(ins)}$ vs 2B ($t(21.9) = 10.7$, $p_{corr} = 8.0e\text{-}10$), and between 2B^{N615I} and 2B$^{N615I\ (ins)}$ ($t(16.8) = 3.3$, $p_{corr} = 0.030$). Neurons transfected with 2B$^{N615I\ (ins)}$ showed significantly higher ifenprodil sensitivity than those transfected with 2B$^{(ins)}$ ($t(30.1) = 3.7$, $p_{corr} = 0.0066$), but there was no significant difference comparing wild type and mutant forms without altered ifenprodil sensitivity.

Figure 3.17 and Table 3.3 show Mg^{2+} block. The key finding is that Mg^{2+} block is reduced in cells transfected with GluN2B$^{N615I\ (ins)}$ compared to GluN2B$^{(ins)}$, in the presence of ifenprodil. In contrast to this finding, Mg^{2+} block did not vary between wild type and mutant transfections without modified ifenprodil sensitivity. This may reflect the lower proportion of current contributed by mutant subunits in the absence of ifenprodil. A two-way ANOVA identified a significant group by ifenprodil interaction (see figure legend) whereby Mg^{2+} block was greater in the presence of ifenprodil in the case of cells transfected with 2B and 2B^{N615I} but lower in the presence of ifenprodil for cells transfected with GluN2B$^{N615I\ (ins)}$. The latter finding shows that increasing the proportion of the response arising from mutant receptors increases the degree of alteration in receptor property observed. The increase in Mg^{2+} block seen with ifenprodil for the unmodified subunits probably reflects the lack of complete NMDA wash out suggested previously.

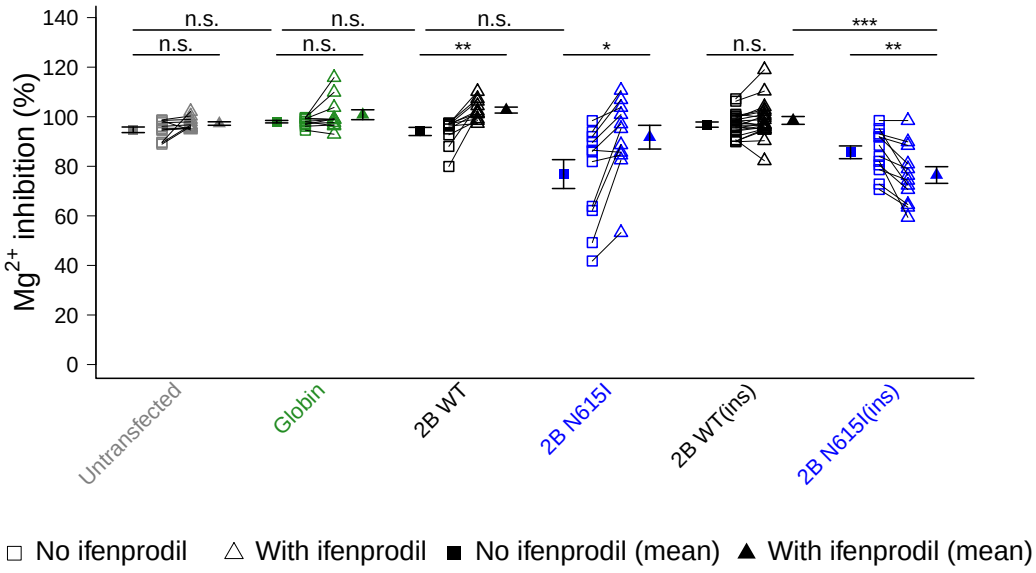

Figure 3.17: **Mg^{2+} block is reduced in neurons transfected with ifenprodil insensitive GluN2B^{N615I}**

The plot shows % inhibition by Mg^{2+} (1 mM) before and after ifenprodil (3 μM) application for untransfected neurons and neurons transfected with an inert control (β globin), 2B, 2B$^{(ins)}$, 2B^{N615I} or 2B$^{N615I\ (ins)}$ NMDAR subunits. A two-way repeated measures ANOVA showed main effects of transfected construct ($F(5,71) = 11.3$, $p < 5e{-}8$) and ifenprodill ($F(1,71) = 128.1$, $p = 6.3e{-}5$) with a significant interaction ($F(5, 71) = 17.6$, $p < 2.7e{-}11$). Planned post-hoc paired t–tests (Bonferroni corrected) showed that ifenprodil was associated with a small but significant increase in Mg^{2+} block in 2B neurons ($t(10) = 4.6$, $p_{corr} = 0.0097$), no difference in Mg^{2+} block in untransfected neurons or neurons transfected with β globin or 2B$^{(ins)}$, but a significant increase in Mg^{2+} block in neurons transfected with 2B^{N615I} ($t(10) = 4.4$, $p_{corr} = 0.014$) and a significant decrease in neurons transfected with 2B$^{N615I\ (ins)}$ ($t(11) = 4.6$, $p_{corr} = 0.0078$). Further post-hoc independent t–tests were used to compare transfected constructs in the absence of ifenprodil; these showed no significant difference in Mg^{2+} block between untransfected neurons and neurons transfected with β globin, 2B or 2B^{N615I} . Finally, 2B$^{(ins)}$ and 2B$^{N615I\ (ins)}$ were compared in the presence of ifenprodil, demonstrating a significant reduction in Mg^{2+} block associated with GluN2B$^{N615I\ (ins)}$($t(16.0) = 5.9$, $p_{corr} = 0.00022$).
See Table 3.3 for samples sizes and summary values.

Figure 3.18 and Table 3.3 show current density. All groups show lower currents in the presence of ifenprodil. The comparisons of interest are between wild type GluN2B and GluN2B^{N615I} in the absence of ifenprodil, highlighting a reduction in current density, and also between GluN2B$^{(ins)}$ and GluN2B$^{N615I\ (ins)}$ in the presence of ifenprodil, where there is also a reduction in current density.

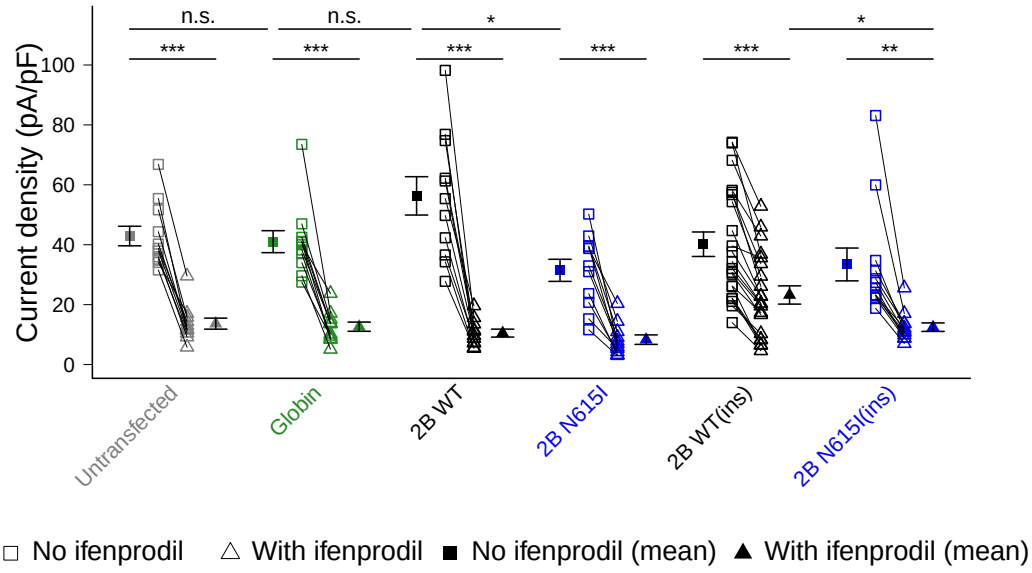

Figure 3.18: **Current density is reduced in neurons transfected with GluN2B^{N615I} and ifenprodil insensitive GluN2B^{N615I}**

The plot shows current density before and after ifenprodil (3 μM) application for untransfected neurons and neurons transfected with an inert control (β globin), 2B, 2B$^{(ins)}$, 2B^{N615I} or 2B$^{N615I\ (ins)}$ NMDAR subunits. A two-way repeated measures ANOVA showed main effects of transfected construct ($F(5,71) = 2.3$, $p = 0.0496$) and ifenprodil ($F(1,71) = 371$, $p < 2e{-}16$) with a significant interaction ($F(5, 71) = 9.5$, $p = 6.1e{-}7$). Planned post-hoc paired t–tests (Bonferroni corrected) showed that ifenprodil was associated with a significant reduction in current density in all groups: untransfected neurons ($t(10) = 13.0$, $p_{corr} = 1.4e{-}6$), β globin ($t(10) = 8.9$, $p_{corr} = 4.6e{-}5$), 2B ($t(10) = 7.9$, $p_{corr} = 0.00013$), 2B^{N615I} ($t(10) = 7.6$, $p_{corr} = 0.000019$), 2B$^{(ins)}$ ($t(20) = 9.8$, $p_{corr} = 4.6e{-}8$) and 2B$^{N615I\ (ins)}$ ($t(11) = 5.0$, $p_{corr} = 0.0038$). Further post-hoc independent t–tests were used to compare transfected constructs in the absence of ifenprodil; these showed no significant difference in current density between untransfected neurons and neurons transfected with β globin or 2B, but a significant reduction in current density in neurons transfected with 2B^{N615I} ($t(16.0) = 3.4$, $p_{corr} = 0.039$). Next, 2B$^{(ins)}$ and 2B$^{N615I\ (ins)}$ were compared in the presence of ifenprodil, demsontrating a significant reduction in current density associated with 2B$^{N615I\ (ins)}$ ($t(27.3) = 3.2$, $p_{corr} = 0.035$).

See Table 3.3 for samples sizes and summary values.

3.4.4 The GluN2B^{V618G} mutation reduces Mg^{2+} block and current density

The final mutation to be examined was GluN2B^{V618G}. The same experiments were performed as previously, with and without ifenprodil insensitive constructs (Figure 3.19).

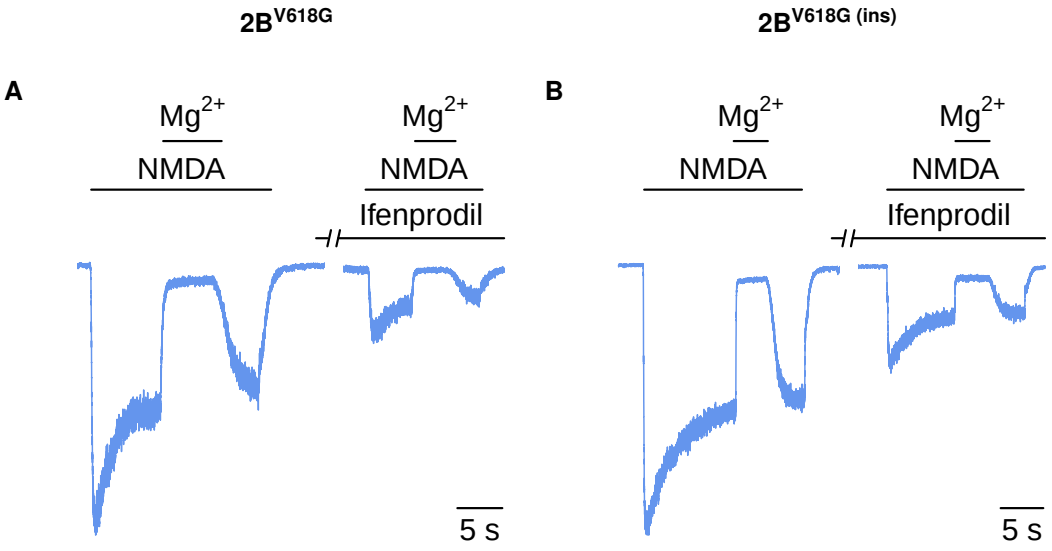

Figure 3.19: **Representative traces from neurons transfected with wild type GluN2B or GluN2B^{V618G}, wild type and ifenprodil insensitive forms**
(A) Representative whole-cell voltage-clamp recording from DIV 9 neuron transfected with 2B^{V618G}, showing inhibition by Mg^{2+} (1 mM) before and after one minute of ifenprodil (3 μM) application. Holding potential –65 mV. Responses are normalised to the peak amplitude.
(B) As for **(A)** but neurons transfected with 2B$^{V618G\ (ins)}$.

Figure 3.20 and Table 3.3 show ifenprodil sensitivity. As expected, ifenprodil sensitivity of GluN2B$^{(ins)}$ was lower than that of wild type GluN2B. However, unexpectedly the ifenprodil sensitivity of cells transfected with GluN2B$^{V618G\ (ins)}$ was not different to that of neurons transfected with GluN2B^{V618G}. Potentially this reflects poor transfection or expression of the GluN2B$^{V618G\ (ins)}$ subunits. The difference in ifenprodil sensitivity between GluN2B$^{(ins)}$ and GluN2B$^{V618G\ (ins)}$ is therefore of uncertain significance. Also unexpected is that the ifenprodil sensitivity of GluN2B^{V618G} subunits was lower than that of wild type GluN2B. This is hard to account for given that there is no theoretical reason the GluN2B^{V618G} mutation should affect ifenprodil sensitivity.

Figure 3.21 and Table 3.3 show Mg^{2+} block. The finding of most interest is the lower Mg^{2+} block in cells transfected with GluN2B^{V618G} versus wild type GluN2B, in the absence of ifenprodil. There was no difference between wild type and mutant ifenprodil insensitive forms, but this may reflect poor expression of the mutant subunit as suggested above. There was also an increase in Mg^{2+} block in wild type GluN2B in the presence of ifenprodil, which is again likely to reflect a technical issue with incomplete NMDA wash out.

Figure 3.22 and Table 3.3 show current density. As with all previous mutations, there is a striking reduction in current density in the presence of ifenprodil in all groups, reflecting blockade of endogenous receptors. The first comparison of note is between wild type GluN2B

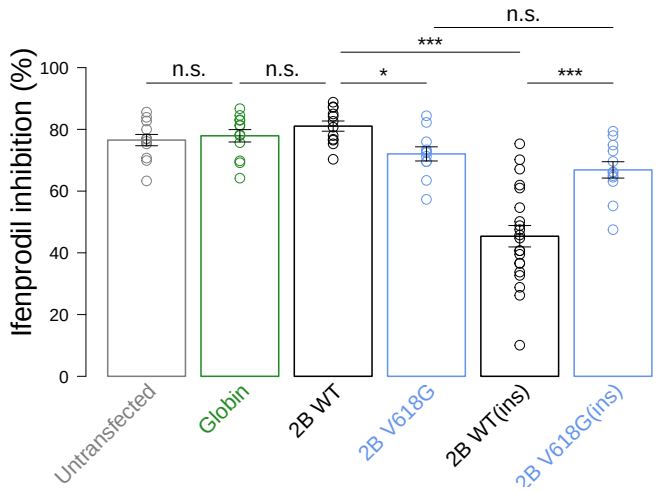

Figure 3.20: **Ifenprodil inhibition is reduced in neurons transfected with GluN2B^{V618G} but not with ifenprodil insensitive GluN2B^{V618G}**
The bar chart shows % inhibition by ifenprodil (3 μM) for untransfected neurons and neurons transfected with an inert control (β globin), 2B, 2B$^{(ins)}$, 2B^{V618G} or 2B$^{V618G\ (ins)}$ NMDAR subunits. A one-way ANOVA showed a significant main effect of transfected subunit ($F(5,74) = 28.2$, $p < 7.3e{-}16$). Planned post-hoc independent t–tests showed no significant difference in ifenprodil sensitivity between untransfected neurons and neurons transfected with β globin or 2B. There was a highly significant reduction in ifenprodil sensitivity in neurons transfected with 2B$^{(ins)}$ vs 2B ($t(27.6) = 9.3$, $p_{corr} = 3.3e{-}9$) although no significant difference between 2B^{V618G} and 2B$^{V618G\ (ins)}$. Interestingly, 2B^{V618G} showed lower sensitivity than 2B ($t(18.5) = 3.2$, $p_{corr} = 0.035$) and 2B$^{V618G\ (ins)}$ showed greater ifenprodil sensitivity than 2B$^{(ins)}$ ($t(31.0) = 4.9$, $p_{corr} = 0.00016$).

and GluN2B^{V618G}, where a reduction in current density is seen in the absence of ifenprodil. A similar pattern is seen with the ifenprodil insensitive forms in the presence of ifenprodil, although this finding is of uncertain significance as it may merely reflect the endogenous responses of cells poorly transfected with GluN2B$^{V618G\ (ins)}$.

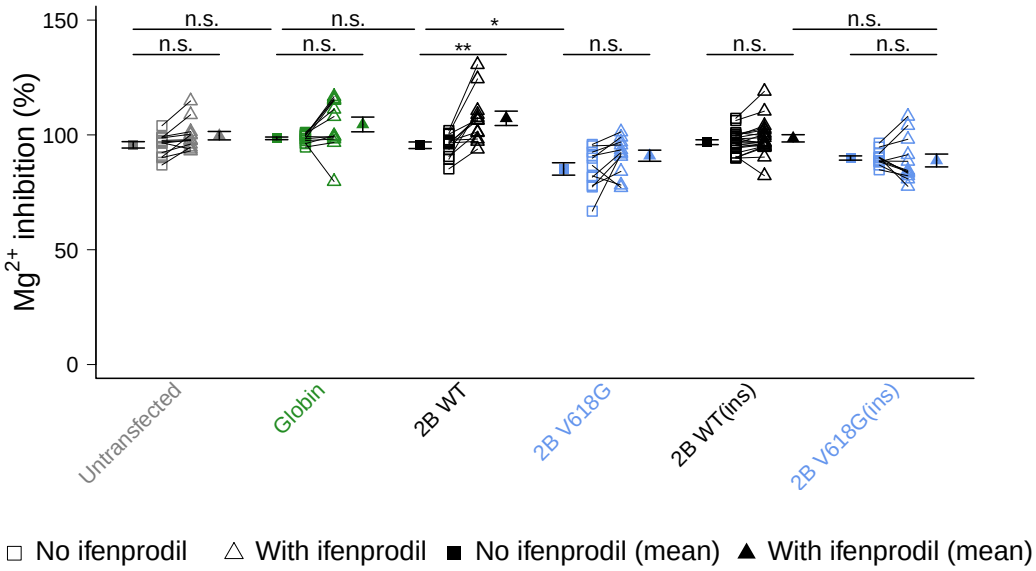

Figure 3.21: **Mg^{2+} block is reduced in neurons transfected with GluN2B^{V618G}**
The plot shows % inhibition by Mg^{2+} (1 mM) before and after ifenprodil (3 μM) application for untransfected neurons and neurons transfected with an inert control (β globin), 2B, 2B$^{(ins)}$, 2B^{V618G} or 2B$^{V618G\ (ins)}$ NMDAR subunits. A two-way repeated measures ANOVA showed main effects of transfected construct ($F(5,74) = 10.3$, $p = 1.6e{-}7$) and ifenprodil ($F(1,74) = 28.4$, $p = 1e{-}6$) with a significant interaction ($F(5, 74) = 4.6$, $p = 0.0011$). Planned post-hoc paired t–tests (Bonferroni corrected) showed that ifenprodil was associated with a small but significant increase in Mg^{2+} block in 2B neurons ($t(11) = 4.5$, $p_{corr} = 0.0086$), but no difference in Mg^{2+} block before and after ifenprodil application in any other groups. Further post-hoc independent t–tests were used to compare transfected constructs in the absence of ifenprodil; these showed no significant difference in Mg^{2+} block between untransfected neurons and neurons transfected with β globin or 2B, but a significant reduction in Mg^{2+} block in cells transfected with 2B^{V618G} compared with 2B ($t(15.4) = 3.4$, $p_{corr} = 0.040$). Finally, 2B$^{(ins)}$ and 2B$^{V618G\ (ins)}$ were compared in the presence of ifenprodil, with no significant difference in Mg^{2+} block seen after correction for multiple comparison.
See Table 3.3 for samples sizes and summary values.

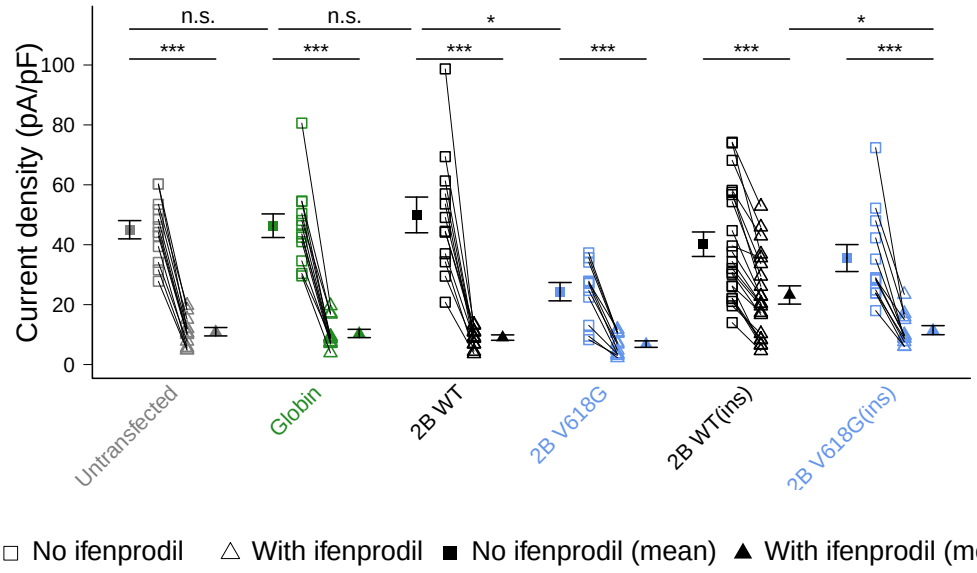

Figure 3.22: **Current density is reduced in neurons transfected with GluN2B^{V618G} and ifenprodil insensitive GluN2B^{V618G}**

The plot shows current density before and after ifenprodil (3 μM) application for untransfected neurons and neurons transfected with an inert control (β globin), 2B, 2B$^{(ins)}$, 2B^{V618G} or 2B$^{V618G\ (ins)}$ NMDAR subunits. A two-way repeated measures ANOVA showed main effects of transfected construct ($F(5,74) = 3.3$, $p = 0.0090$) and ifenprodil ($F(1,74) = 475$, $p < 2e{-}16$) with a significant interaction ($F(5, 74) = 11.5$, $p = 3.1e{-}8$). Planned post-hoc paired t–tests (Bonferroni corrected) showed that ifenprodil was associated with a significant reduction in current density in all groups: untransfected neurons ($t(11) = 17.2$, $p_{corr} = 2.8e{-}8$), β globin ($t(11) = 11.9$, $p_{corr} = 1.2e{-}6$), 2B ($t(11) = 7.5$, $p_{corr} = 0.00012$), 2B^{V618G} ($t(10) = 8.0$, $p_{corr} = 0.000012$), 2B$^{(ins)}$ ($t(20) = 9.8$, $p_{corr} = 4.6e{-}8$) and 2B$^{V618G\ (ins)}$ ($t(11) = 6.7$, $p_{corr} = 0.00039$). Further post-hoc independent t–tests were used to compare transfected constructs in the absence of ifenprodil; these showed no significant difference in current density between untransfected neurons and neurons transfected with β globin or 2B , but a significant reduction in current density in neurons transfected with 2B^{V618G} ($t(16.3) = 3.8$, $p_{corr} = 0.015$). Next, 2B$^{(ins)}$ and 2B$^{V618G\ (ins)}$ were compared in the presence of ifenprodil, demsontrating a significant reduction in current density associated with 2B$^{V618G\ (ins)}$ ($t(28.0) = 3.5$, $p_{corr} = 0.018$).

See Table 3.3 for samples sizes and summary values.

3.5 Single channel properties of mutant diheteromers

In the previous section, three of the four mutant subunits investigated were found to be associated with reduced current density when expressed in cultured neurons. This is an interesting finding which could be due to reduced membrane trafficking of receptors containing mutant subunits (suppressing endogenous subunits also) or to an alteration of NMDAR properties such that less current was able to flow when a receptor was activated. The location of the mutations inside the receptor pore suggested that ion conductance may well be altered. To test this possibility, single channel recordings were made and channel conductance directly measured.

An initial small data set was collected in outside-out patches pulled from oocytes expressing GluN2A^{N615K} and GluN2A^{R586K}-containing NMDARs. However, as oocytes are seasonally unavailable, HEK293 cells were used to generate a further, larger data set from GluN2A^{N615K} and GluN2B^{N615I} containing NMDARs. Unfortunately, low expression rates were achieved in HEK293 cells, with many silent patches. In order to maximise throughput, recordings were made from cell-attached patches rather than the gold standard of outside-out patches (which allow control of absolute holding potential, and offer more strategies to reduce noise).

3.5.1 The GluN2A^{N615K} mutation reduces conductance when expressed in oocytes

Figure 3.23 shows representative recordings of wild type and GluN2A^{N615K}-containing NMDARs expressed in oocytes. These are held at the same holding potential and plotted to the same scale, and it is immediately apparent that the current flowing during openings of GluN2A^{N615K} NMDARs is of much smaller amplitude than that flowing during wild type GluN2A openings. This four-fold reduction in conductance is quantified in Figure 3.23C and Table 3.4.

Table 3.4: Summary values for outside-out single channel recordings in oocytes

	GluN2A	GluN2A^{N615K}	GluN2A^{R586K}
Conductance (pS)	58 ± 3	15 ± 1	61 ± 2
Mean open time (ms)	4.1 ± 0.3	11.4 ± 2.6	3.2 ± 0.3
τ1 (ms)	4.0 ± 0.3	12.1 ± 3.1	3.5 ± 0.2
Number of openings	2555	774	1139
n (oocytes)	4	3	3

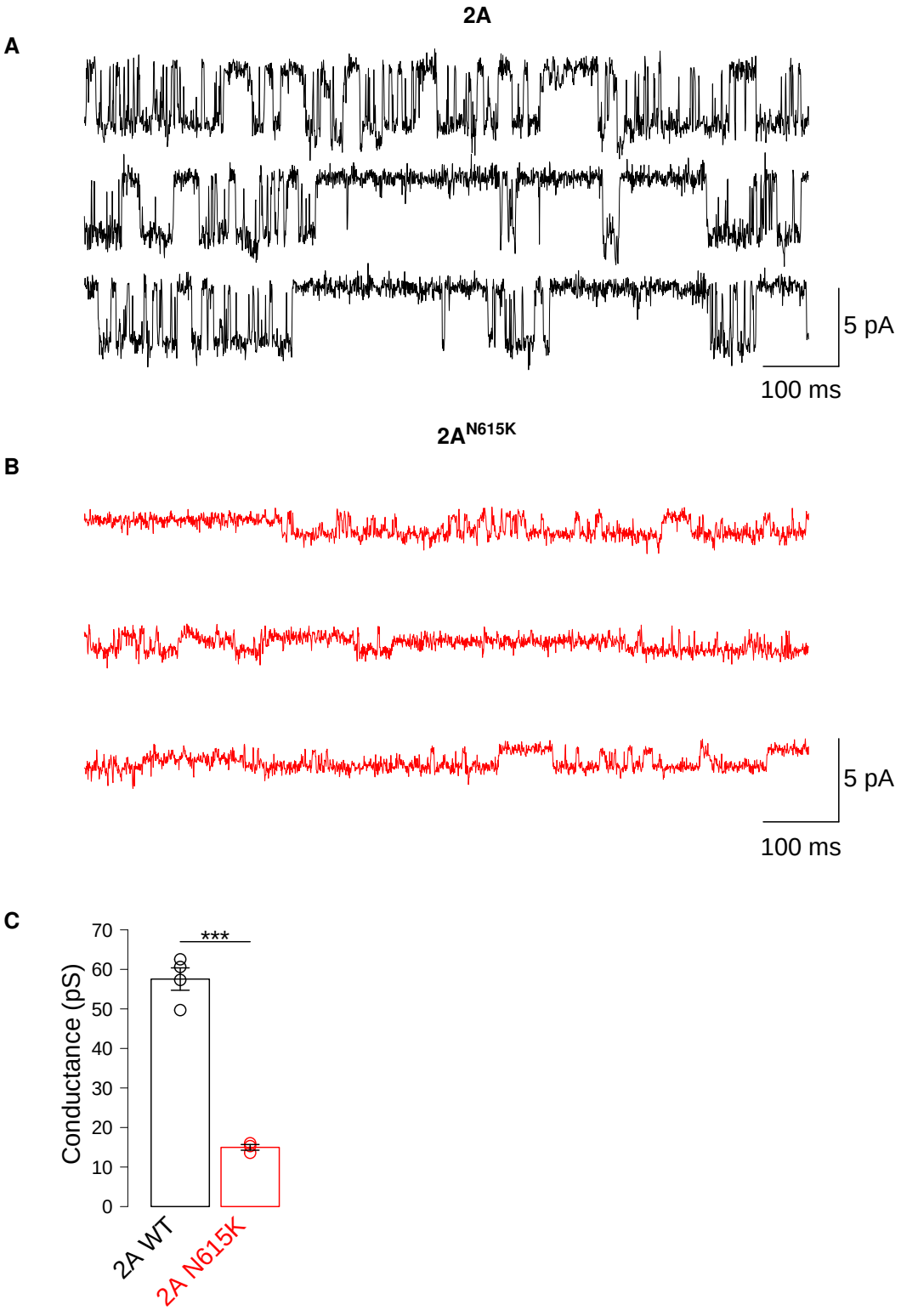

Figure 3.23: **GluN2A^{N615K} reduces single channel conductance in oocytes**
(A) Representative voltage-clamp recordings from outside-out patched pulled from oocytes expressing 2A wild type containing NMDARs. Holding potential –60 mV.
(B) As for **(A)** but oocytes expressing 2A^{N615K} containing NMDARs.
(C) The bar chart shows conductance. A t–test showed that conductance in NMDARs containing 2A^{N615K} was signficantly lower than in NMDARs containing wild type 2A subunits ($t(3.4) = 14.6$, $p = 0.00036$). See Table 3.4 for samples sizes and summary values.

Figure 3.24 shows the dwell time analysis performed. As some of the patches had multiple channels present, analysis of closed time and open probability was difficult. Analysis was therefore restricted to open times only, with any events consisting of multiple channel openings discarded. There was a trend towards longer openings in GluN2A^{N615K} containing NMDARs, but this did not achieve significance. The small number of recordings made in oocytes limited the power to detect differences between groups.

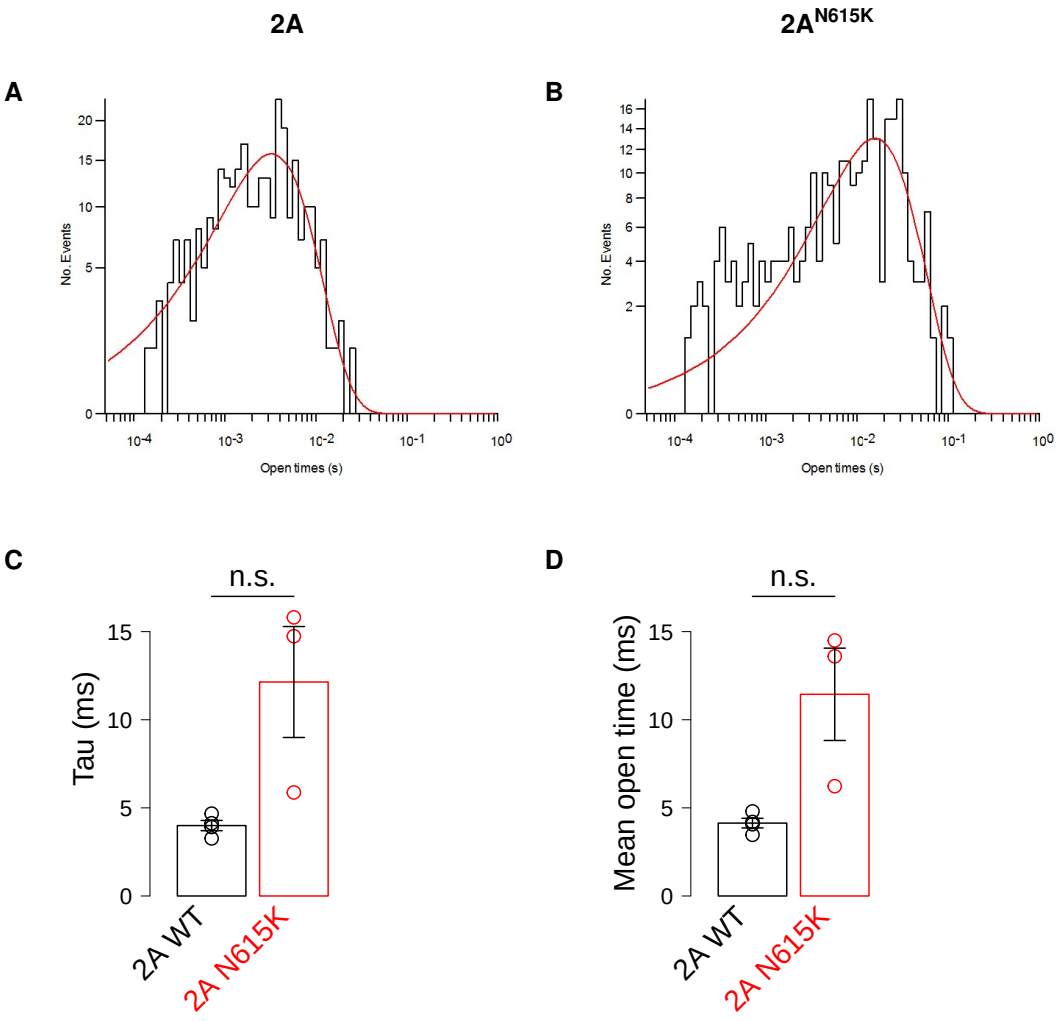

Figure 3.24: **GluN2A^{N615K} does not influence NMDAR open times in oocytes**
(A) Representative histogram showing frequency of wild type 2A single channel open times, fitted with an exponential decay curve.
(B) As for **(A)** but oocytes expressing 2A^{N615K} containing NMDARs.
(C) The bar chart shows the time constants (tau) fitted to single channel open time frequency distributions. A single exponential was fitted in each case. A t–test showed no significant difference between wild type 2A and 2A^{N615K} containing NMDARs.
(D) The bar chart shows mean single channel open times. A t–test showed no significant difference between wild type 2A and 2A^{N615K} containing NMDARs.
See Table 3.4 for samples sizes, event numbers, and summary values.

3.5.2 The GluN2A^{R586K} mutation does not affect single channel properties when expressed in oocytes

Figure 3.25 shows representative recordings of wild type and GluN2A^{R586K} containing NMDARs expressed in outside-out patches pulled from oocytes. These traces give an impression of similar amplitudes and open durations, and indeed there were no differences identified in conductance or open times when comparing GluN2A^{R586K} and wild type GluN2A (Figure 3.25C, 3.26 and Table 3.4).

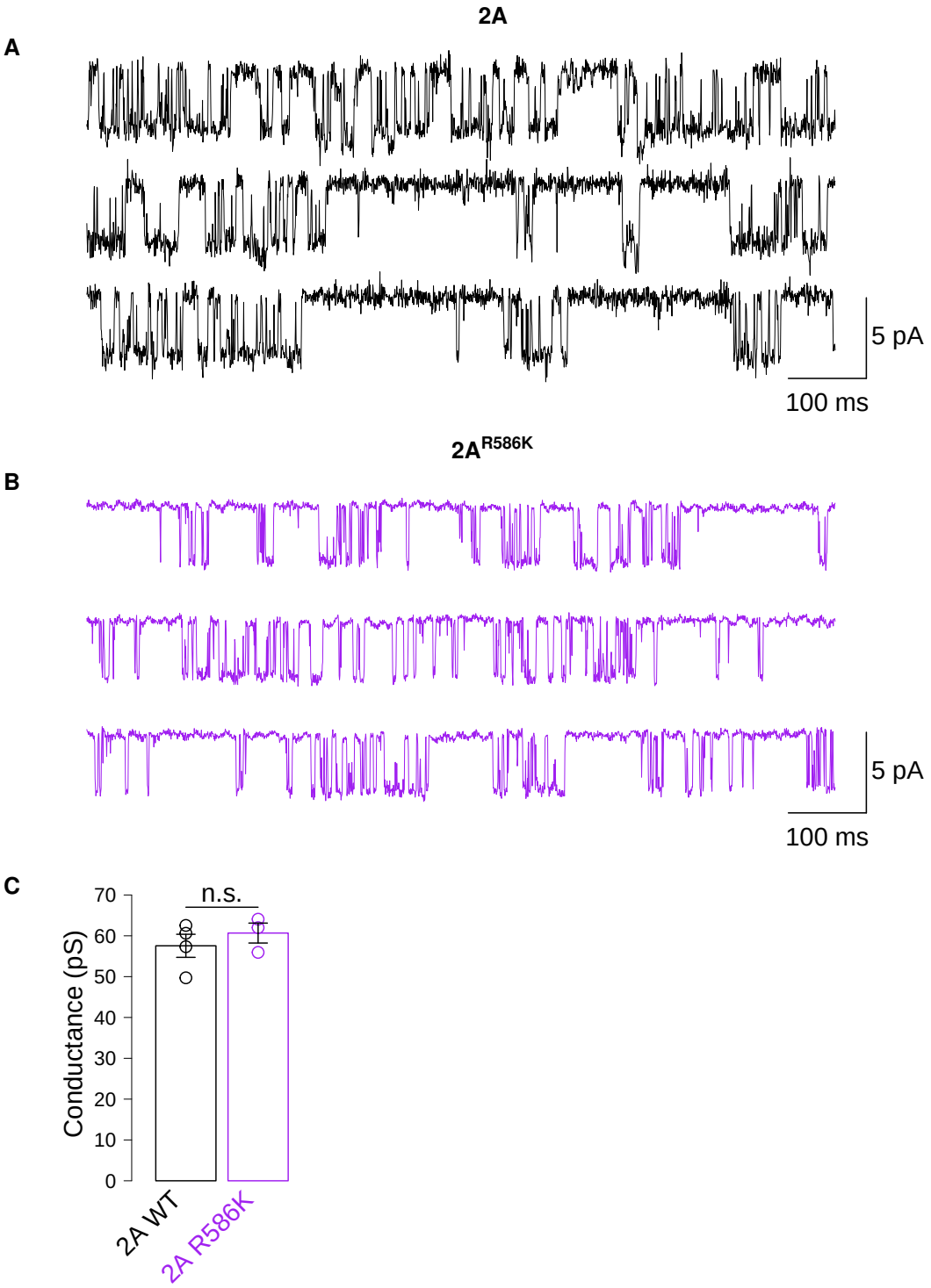

Figure 3.25: **GluN2A^{R586K} does not influence single channel conductance in oocytes**
(A) Representative voltage-clamp recordings from outside-out patches pulled from oocytes expressing 2A wild type NMDARs. Holding potential –60 mV.
(B) As for **(A)** but oocytes expressing 2A^{R586K} containing NMDARs.
(C) The bar charts show conductance. A t–test showed no significant difference between wild type 2A and 2A^{R586K} containing NMDARs.
See Table 3.4 for samples sizes and summary values.

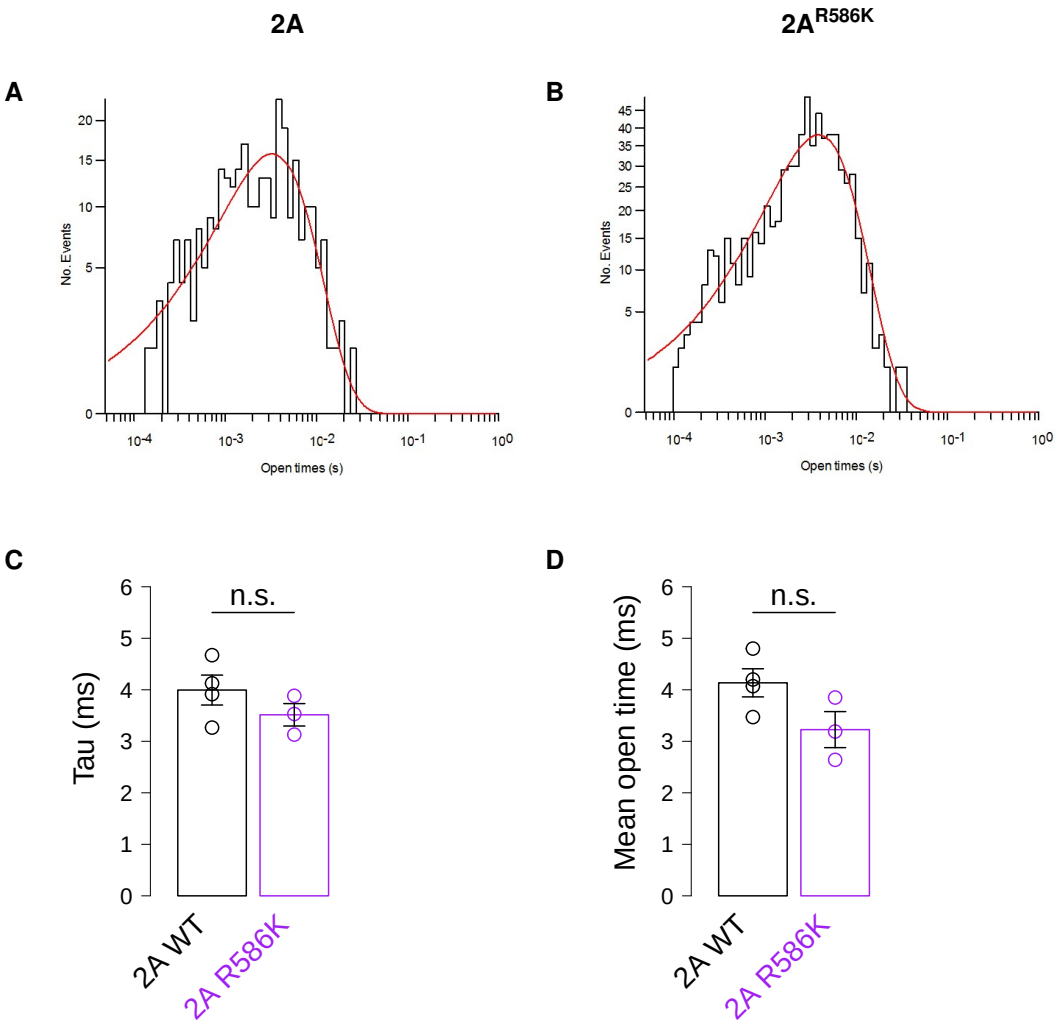

Figure 3.26: **GluN2A^{R586K} does not influence NMDAR open times in oocytes**
(A) Representative histogram showing frequency of wild type 2A single channel open times, fitted with an exponential decay curve.
(B) As for **(A)** but oocytes expressing 2A^{R586K} containing NMDARs.
(C) The bar chart shows the time constants (tau) fitted to single channel open time frequency distributions. A single exponential was fitted in each case. A t–test showed no significant difference between wild type 2A and 2A^{R586K} containing NMDARs.
(D) The bar chart shows mean single channel open times. A t–test showed no significant difference between wild type 2A and 2A^{R586K} containing NMDARs.
See Table 3.4 for samples sizes, event numbers, and summary values.

3.5.3 The GluN2A^{N615K} mutation reduces conductance and increases open times when expressed in HEK293 cells

GluN2A^{R586K} subunits were not explored further as the data in oocytes excluded any major efffect upon single channel properties. However, GluN2A^{N615K} subunits were expressed in HEK293 cells and again found to have a marked impact on single channel properties.

Figure 3.27 shows representative traces from cell-attached patches formed with HEK293 cells expressing wild type and mutant NMDARs. The channel openings now appear as positive deflections from baseline because the NMDAR-mediated cation current is flowing away from the patch electrode, rather than towards it (as with outside-out patches or whole-cell configurations). The traces are plotted to the same scale and patches held at the same holding potential, although as the membrane potential of the HEK293 cells was unknown, the patch potential (holding potential minus membrane potential) and hence the driving force for current flow may be different. There are also two channels present in the GluN2A^{N615K} trace, with a few double amplitude openings evident. Even with these complications, a marked difference in current amplitude can be seen between the two subunit types. The conductance was quantified by measuring the current amplitude at a range of holding potentials, and calculating the slope of the line: this gives the conductance (Figure 3.27C). The lower conductance seen in GluN2A^{WT} diheteromers expressed in HEK293 cells (43 pS) compared to oocytes (58 pS) is likely to reflect the higher Ca^{2+} concentration used for external solutions in recordings in HEK293 cells (2 mM) than in oocytes (0.85 mM) as higher Ca^{2+} decreases NMDAR conductance (Gibb and Colquhoun, 1992). The slopes of the GluN2A^{N615K} containing NMDARs are about a third that of the wild type NMDARs (Figure 3.27E, Table 3.5). Figure 3.27D shows the same data with lines constrained to pass through the origin (as no driving force results in no current) to allow an approximation of patch potential to be obtained and the groups more clearly compared.

Table 3.5: Summary values for cell-attached single channel recordings in HEK293 cells

	GluN2A	GluN2A^{N615K}	GluN2B	GluN2B^{N615I}
Conductance (pS)	43 ± 3	16 ± 1	54 ± 2	14 ± 2
Mean open time (ms)	0.85 ± 0.05	1.28 ± 0.09	0.69 ± 0.07	0.51 ± 0.04
τ_1 (ms)	0.74 ± 0.05	0.51 ± 0.07	0.59 ± 0.08	0.45 ± 0.05
τ_2 (ms)	not fitted	1.87 ± 0.11	not fitted	not fitted
$\%\tau_1$	–	51 ± 5	–	–
$\tau_{weighted}$ (ms)	0.74 ± 0.05	1.13 ± 0.09	0.59 ± 0.08	0.45 ± 0.05
Number of openings	6748	3635	3106	7371
n (cells)	8	12	3	6

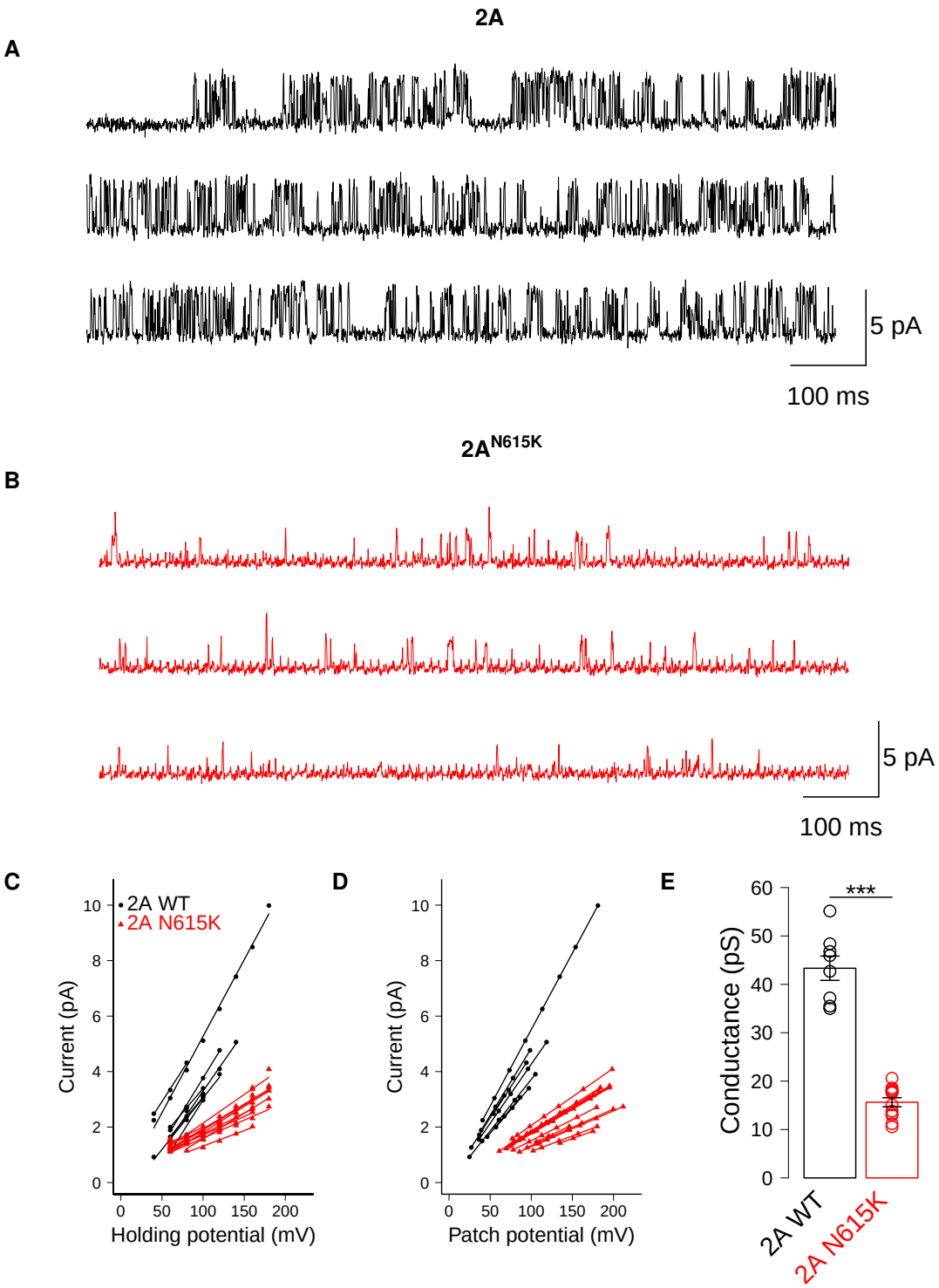

Figure 3.27: **GluN2A^{N615K} reduces single channel conductance in HEK293 cells**

Figure 3.27: **GluN2A^{N615K} reduces single channel conductance in HEK293 cells**
(A) Representative voltage-clamp recordings from cell-attached patches in HEK293 cells expressing 2A wild type NMDARs. Holding potential –100 mV.
(B) As for **(A)** but HEK293 cells expressing 2A^{N615K} containing NMDARs. There are two channels in this patch.
(C) Single-channel unitary amplitude plotted against holding potential (membrane potential unknown) and fitted with linear regression. The slope of the regression line is the conductance. The estimated membrane potentials may be higher than expected (approximately –40 mV) as the cells are depolarised in the presence of glutamate released from nearby dying cells.
(D) Single-channel unitary amplitude plotted against patch potential by setting intercept to zero.
(E) The bar chart shows conductance. A t–test showed that conductance in NMDARs containing 2A^{N615K} was signficantly lower than in NMDARs containing 2A subunits (t(9.0) = 10.3, $p < 3e{-}6$). See Table 3.5 for samples sizes and summary values.

Figure 3.28 shows the dwell time analysis performed. As the majority of the patches had multiple channels present, dwell time analysis was again restricted to open times only, with any events consisting of multiple channel openings discarded. The mean open times in GluN2A^{N615K} containing NMDARs were found to be longer than those in wild type NMDARs, and required a second, longer, time constant to provide a good fit to the open time distribution (see Table 3.5 for values), giving a longer weighted time constant. These findings are similar to what was found in the smaller data set in oocytes (section 3.5.1). Open probabilities could not be compared because a range of agonist concentrations were used.

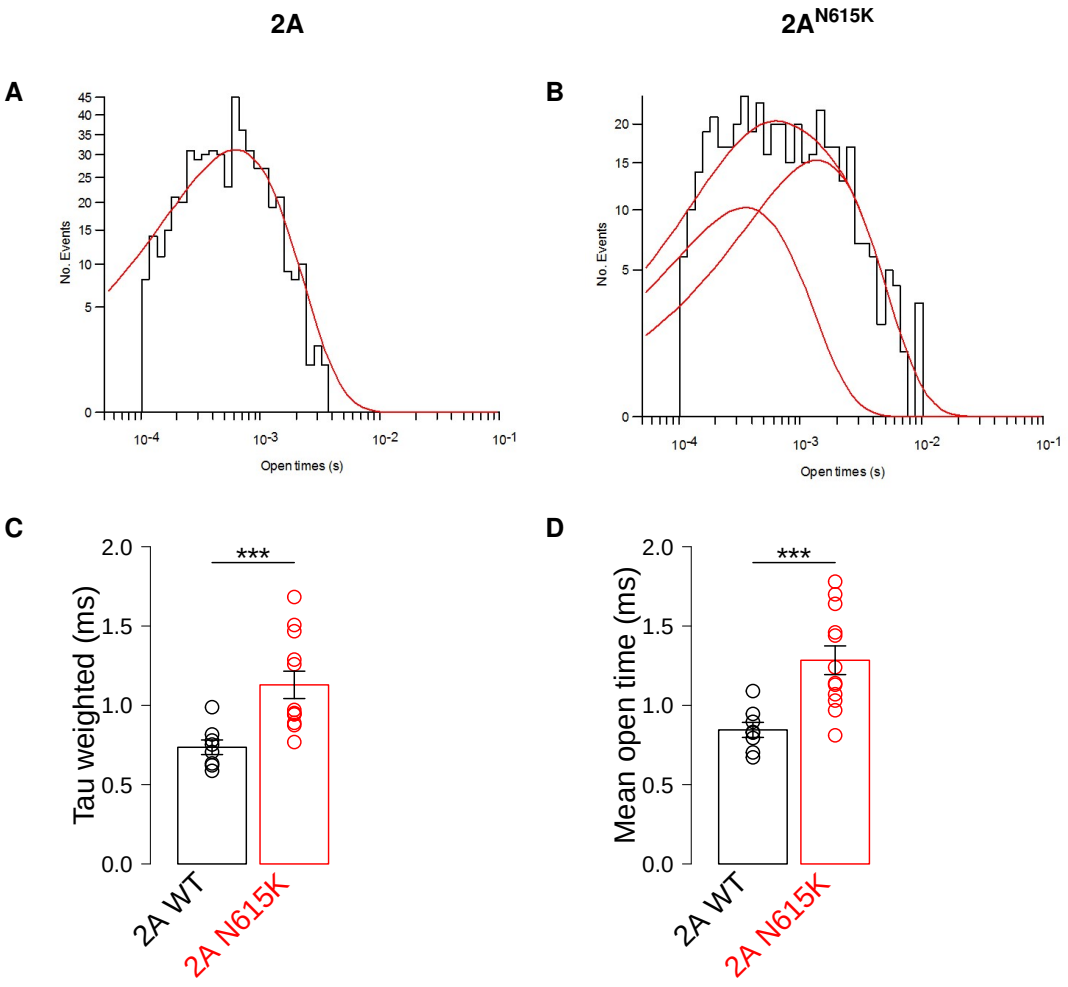

Figure 3.28: **GluN2A^{N615K} increases NMDAR open times in HEK293 cells**
(A) Representative histogram showing frequency of wild type 2A single channel open times, fitted with an exponential decay curve.
(B) As for **(A)** but cells expressing 2A^{N615K} containing NMDARs.
(C) The bar chart shows the weighted time constants fitted to single channel open time frequency distributions. A t–test showed that NMDARs containing 2A^{N615K} had significantly longer time constants than wild type 2A NMDARs ($t(16.1) = 4.0$, $p = 0.00097$).
(D) The bar chart shows mean single channel open times. A t–test showed that NMDARs containing 2A^{N615K} had significantly longer time constants than wild type 2A NMDARs ($t(16.0) = 4.3$, $p = 0.00055$).
See Table 3.5 for samples sizes, event numbers, and summary values.

3.5.4 The GluN2B^{N615I} mutation reduces conductance

One of the GluN2B pore mutants was investigated next: GluN2B^{N615I}. Figure 3.29 shows representative traces from cell-attached patches formed with HEK293 cells expressing wild type and mutant NMDAR. As with GluN2A^{N615K}, the conductance slopes for the mutant subunit are well separated from the wild type NMDAR, whether plotted against holding potential (Figure 3.29C) or patch potential (Figure 3.29D). This was quantified to show a four-fold reduction in conductance (Figure 3.29E and Table 3.5).

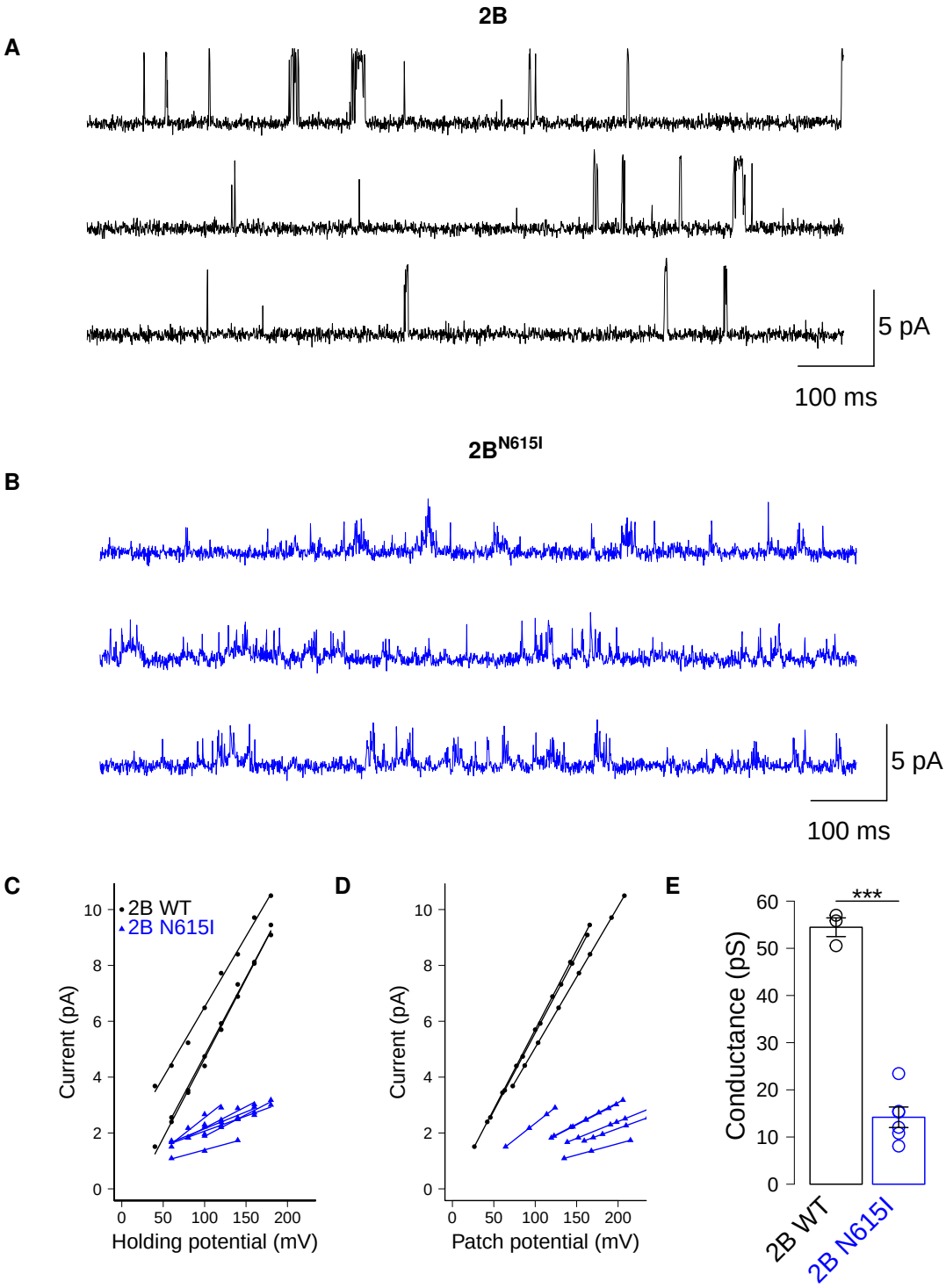

Figure 3.29: **GluN2B^{N615I} reduces single channel conductance in HEK293 cells**

Figure 3.29: **GluN2A^{N615K} reduces single channel conductance in HEK293 cells**
(A) Representative voltage-clamp recordings from cell-attached patches in HEK293 cells expressing 2B wild type NMDARs. Holding potential –100 mV.
(B) As for **(A)** but HEK293 cells expressing 2B^{N615I} containing NMDARs. There are two channels in this patch.
(C) Single-channel unitary amplitude plotted against holding potential (membrane potential unknown) and fitted with linear regression. The slope of the regression line is the conductance.
(D) Single-channel unitary amplitude plotted against patch potential by setting intercept to zero.
(E) The bar chart shows conductance. A t–test showed that conductance in NMDARs containing 2B^{N615I} was signficantly lower than in NMDARs containing 2B subunits ($t(6.1) = 13.7$, $p < 8e{-}6$). See Table 3.5 for samples sizes and summary values.

Figure 3.30 shows the open times of wild type GluN2B and GluN2B^{N615I} containing NMDARs, which were similar to each other and to those of wild type GluN2A.

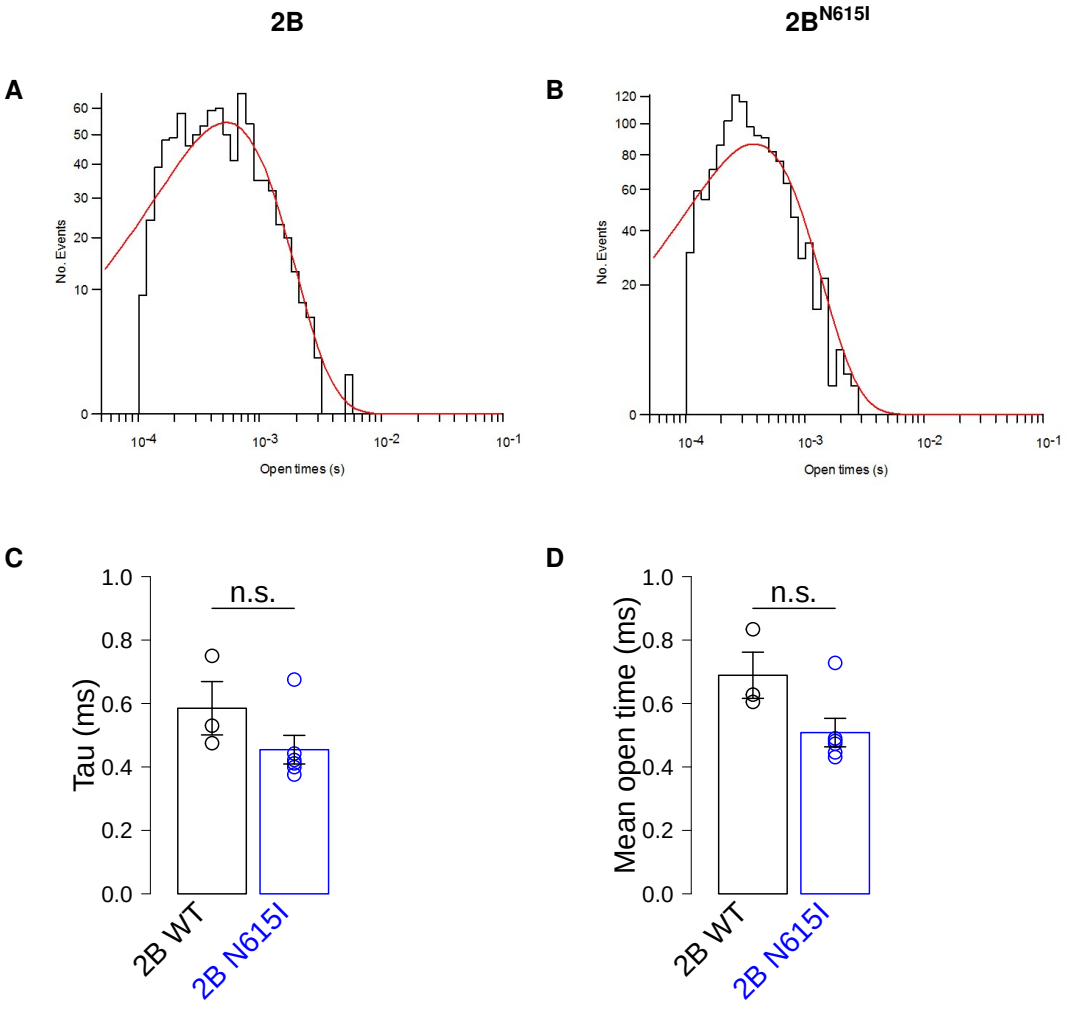

Figure 3.30: **GluN2B^{N615I} does not influence NMDAR open times in HEK293 cells**
(A) Representative histogram showing frequency of wild type 2B single channel open times, fitted with an exponential decay curve.
(B) As for **(A)** but HEK293 cells expressing 2B^{N615I} containing NMDARs.
(C) The bar chart shows the time constants fitted to single channel open time frequency distributions. A single exponential was fitted in each case. A t–test showed no significant difference between wild type 2B and 2B^{N615I} containing NMDARs.
(D) The bar chart shows mean single channel open times. A t–test showed no significant difference between wild type 2B and 2B^{N615I} NMDARs.
See Table 3.5 for samples sizes, event numbers, and summary values.

3.6 Discussion

3.6.1 Summary of findings

This chapter assessed the impact of four NMDAR subunit disease-associated mutations on a range of basic receptor properties in three heterologous systems. The principal finding is that three of the four mutations studied result in substantial alterations in key receptor properties: GluN2A^{N615K} , GluN2B^{N615I} and GluN2B^{V618G} all cause reduced Mg^{2+} block and current density, GluN2A^{N615K} and GluN2B^{N615I} cause reduced single channel conductance and GluN2A^{N615K} also increases channel open times. These effects support the mutations' role in disease causation. The GluN2A^{R586K} mutation was not found to have any effect on any of the parameters assessed, suggesting this mutation may not be relevant to the carrier's disorder.

3.6.2 GluN2A and GluN2B pore mutations reduce Mg^{2+} block

The GluN2A^{N615K} mutation was found to cause negligible Mg^{2+} block when expressed as diheteromers in oocytes, replicating previous work (Endele et al., 2010). This mutation and the two GluN2B pore mutations were also found to significantly reduce Mg^{2+} block when expressed in cultured neurons (although the evidence is weaker for GluN2B^{V618G}, as the ifenprodil insensitive versions did not show a significant difference). GluN2A^{N615K} caused the biggest reduction (approximately halving Mg^{2+} block on average), with a lesser reduction seen with GluN2B^{N615I} (an average drop of around a quarter) and GluN2B^{V618G} (an average drop of around 10%).

The difference in effect between the mutations will relate both to the different residues they encode and to their slightly different positions in the pore. The GluN2A^{N615K} mutation is likely to have the largest effect because it modifies the residue previously found to be the strongest determinant of Mg^{2+} block (the "N+1" site asparagine) (Wollmuth et al., 1998), whereas the GluN2B^{N615I} mutation modifies the next most important site (the "N" site asparagine) and the GluN2B^{V618G} mutation influences a nearby residue which has not previously been identified as important in Mg^{2+} block.

The properties of the replacement residues are also likely to impact on Mg^{2+} block and ion permeation. Figure 3.31 shows amino acids clustered by their biochemical properties in a Venn diagram. Asparagine is a hydrophilic (polar), uncharged amino acid. In the case of GluN2A^{N615K}, asparagine is replaced with lysine, which is positively charged. This positive charge would be expected to repel rather than interact with Mg^{2+} ions and other cations. In the case of GluN2B^{N615I}, asparagine is replaced with isoleucine, which is also uncharged but hydrophobic. As transmembrane ion pores require a lining of hydrophilic residues, the presence of a hydrophobic residue is likely to be quite structurally disruptive, even if the residue does not directly repel positively charged ions. In the case of GluN2B^{V618G}, a relatively large, hydrophobic valine is replaced by a very small glycine. As glycine is so small, this alteration may be easier to accommodate than the other mutations.

The reduction in Mg^{2+} block seen with the three mutations in neurons was much more variable and of lower magnitude than that seen in oocytes, within this study and by others (Endele et al., 2010; Lemke et al., 2014). This is due to the presence of endogenous GluN2B subunits within neurons, and

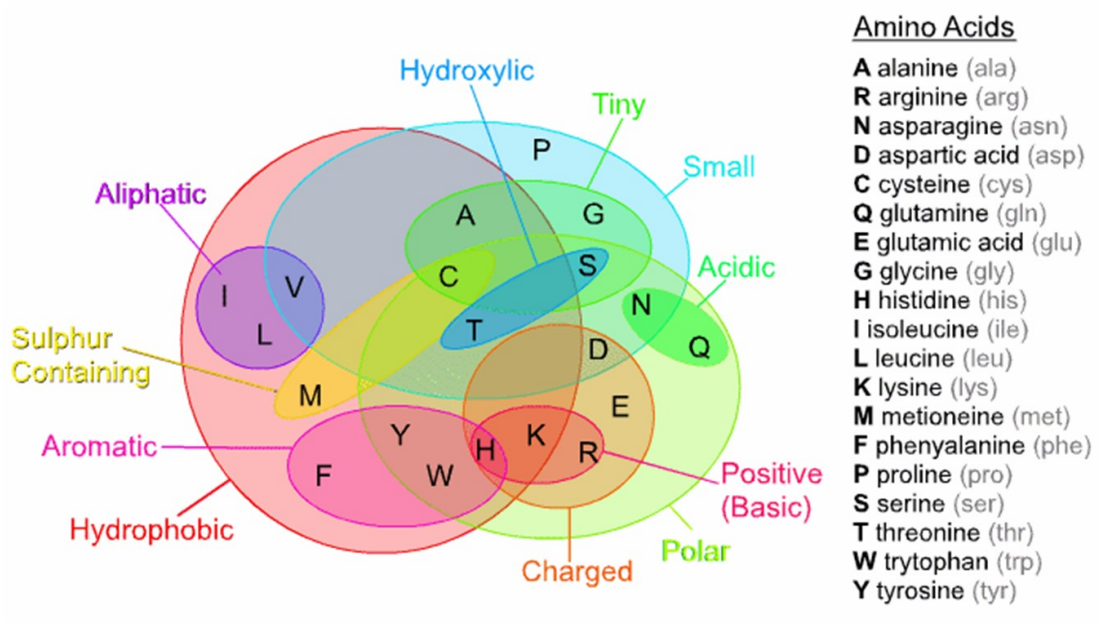

Figure 3.31: **Biochemical properties of amino acids**
This figure shows the 20 naturally arising amino acids plotted on a Venn diagram to emphasise shared and contrasting properties. Taken from Esquivel et al. (2013).

arises from either cell to cell variability in the proportion of wild type versus mutant NMDAR diheteromers, and/or incorporation of mutant subunits into triheteromers with wild type GluN2B. The fact that reductions in Mg^{2+} block are seen despite the presence of wild type NMDAR subunits demonstrates that the mutant subunits are being expressed at the cell surface. It also supports the idea that these heterozygously carried mutations could have an impact in an individual who also has wild type receptors.

Any reduction in Mg^{2+} block is of high physiological relevance as voltage dependent block by Mg^{2+} is crucial to the NMDAR's role as a molecular coincidence detector (Bliss and Collingridge, 1993), whereby opening of NMDARs requires both the presence of glutamate and depolarisation of the postsynaptic membrane (Mayer et al., 1984; Nowak et al., 1984). If block by Mg^{2+} is removed or reduced, it is possible that synaptic plasticity would become partially uncoupled from the inputs received at the synapse, leading to dysregulation of learning and memory, and potentially leading to the associated phenotype of intellectual disability.

3.6.3 GluN2A^{N615K} alters potency of channel blockers

GluN2A^{N615K} was also found to alter the potency of small molecule channel blockers, with the potency of memantine and amantadine markedly reduced, ketamine somewhat reduced and dextromethorphan enhanced. These findings are consistent with subsequently published work (Pierson et al., 2014). The variation in the mutation's effect on different channel blockers likely relates to the variation in residues that are of primary importance for interaction with the blockers.

Considering memantine and amantadine (which is structurally very similar to memantine), studies employing site directed mutagenesis have shown that memantine interacts with the same residues as

Mg^{2+}, with the "N" and "N+1" site contributing in the case of GluN2B (Kashiwagi et al., 2002) and GluN2A (Chen and Lipton, 2005). However, the GluN1 "N" site is the dominant site for interaction with memantine, and other residues also impact on memantine binding (reviewed in (Johnson and Kotermanski, 2006) and see Figure 3.32. This is probably why the effect of the $GluN2A^{N615K}$ mutation on memantine and amantadine block is less marked than its effect on Mg^{2+} block.

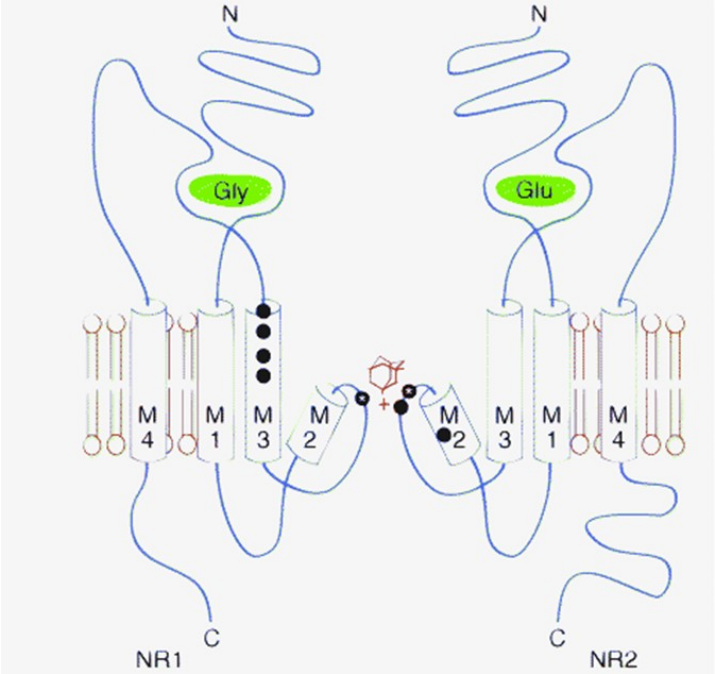

Figure 3.32: **Sites important for binding of memantine**
This figure shows the location of residues identified as important in binding of memantine as black circles. The "N" sites in GluN1 ("NR1") and GluN2A/B ("NR2") are marked with white asterisks within black circles. The "N+1" site in GluN2A/B is the neighbouring black circle. Figure taken from Johnson and Kotermanski (2006).

Ketamine also interacts with residues involved in Mg^{2+} block, with the GluN1 "N" site identified as key, and the GluN2B "N" site as also important (Yamakura et al., 1993). The role of the "N+1" site in either subunit, or the GluN2A "N" site, does not appear to have been directly tested. The data presented here suggest that the GluN2A "N+1" site is less important for interacting with ketamine than for memantine or amantadine.

In contrast to the channel blockers discussed so far, dextromethorphan's primary metabolite dextrorphan interacts with residues in the more extracellular portion of the pore vestibule (LePage et al., 2005). Dextrorphan's binding is not influenced by mutations in the GluN1 "N" site (LePage et al., 2005) but no previous work has assessed the impact of mutating the GluN2A "N+1" site. The results of this study and others (Pierson et al., 2014) suggest that the GluN2A "N+1" site does somehow modulate the binding of dextromethorphan, potentially via a conformational change in the more extracellular region of the pore.

The increased potency conferred by the $GluN2A^{N615K}$ mutation suggests that dextromethorphan (a common ingredient in cough medicines) may be of therapeutic benefit to the carrier of the $GluN2A^{N615K}$

mutation or similar pore mutations. However, if the primary problem is insufficient current flow, rather than inappropriate current flow (see next section), dextromethorphan could potentially exacerbate symptoms.

3.6.4 GluN2A and GluN2B pore mutations reduce current density and GluN2A^{N615K} and GluN2B^{N615I} reduce conductance

All three pore mutations were found to significantly reduce NMDAR current density when expressed in neurons, with GluN2B^{N615I} associated with a reduction to about half, and GluN2A^{N615K} and GluN2B^{V618G} a reduction of about a third (although the evidence is weaker for GluN2B^{V618G}, as the ifenprodil insensitive versions did not show a significant difference). Although this could reflect reduced expression of the mutant subunits, the fact that the change in current density was associated with a reduction in Mg^{2+} block argues that the mutant subunits are being expressed and are reducing conductance. When conductance was directly evaluated via single channel recordings, a substantial three to four-fold reduction in conductance was indeed found with GluN2A^{N615K} and GluN2B^{N615I}.

Because the residues that interact with Mg^{2+} also comprise one of the narrowest parts of the ion permeation pathway, it makes sense that mutations that affect Mg^{2+} block also affect conductance. Mutations of the "N" site have been found to influence conductance previously in GluN1 (Behe et al., 1995; Schneggenburger and Ascher, 1997) and GluN2B (Premkumar et al., 1997). As with Mg^{2+} block, different amino acid class alterations at slightly different parts of the pore could explain the differences in extent of reduction in current density seen with the different mutations.

A reduction in conductance could be detrimental to normal neuronal function as a given NMDAR activation would allow smaller currents through, contributing less to overall charge transfer and potentially altering Ca^{2+} signalling. The impact on Ca^{2+} signalling is hard to predict, as previous work has found the mutations to also influence Ca^{2+} permeability: GluN2A^{N615K} reduces it (Endele et al., 2010) and the two GluN2B mutations increase it (Lemke et al., 2014). Thus a diheteromeric GluN2A^{N615K} NMDAR would allow smaller currents of all cations to pass when activated, but a diheteromeric GluN2B^{N615I} might allow smaller sodium currents but equal or even elevated Ca^{2+} currents.

In contrast to the "gain of function" reduction in Mg^{2+} block observed, the reduction in conductance is a "loss of function". This makes it hard to predict whether blocking or potentiating mutant subunit function would be of benefit.

3.6.5 GluN2A^{N615K} increases channel open time duration

An interesting and unpredicted finding was that the GluN2A^{N615K} mutation increases channel open times by about 50%. This may be a false result, as the lower conductance of the mutant makes brief closures harder to detect than in wild type NMDARs. Indeed, the finding in the next chapter that deactivation rates are unaffected by the GluN2A^{N615K} mutation (see Section 4.3.2) is not consistent with a prolonged channel opening time, unless the burst pattern is also altered.

However, if the finding of prolonged openings is true, this implies the mutation is having some impact on channel gating. Gating is classically thought of as dependent primarily on agonist binding and dissociation, coupled to a conformational change in the channel: opening of the "activation gate". In

NMDARs, the activation gate is known to be formed by the SYTANLAAF motif in the M3 region (reviewed in Traynelis et al. (2010)). However, gating can also be affected by the permeation pathway if the channel is unable to shut while a permeant ion is within. Previous work mutating the GluN1 "N" site supports this idea (Schneggenburger and Ascher, 1997). Thus, mutations affecting conductance, perhaps by slowing the speed of ion travel through the pore, could potentially increase open times. An increase in mean open time is of physiological relevance as this could increase the charge transfer during a given exposure to agonist, influencing excitability and Ca^{2+} entry. However, the consequences are hard to predict in the case of the GluN2A^{N615K} mutation, which has the opposing effects of both reducing conductance and prolonging opening.

3.6.6 GluN2A^{R586K} has no effect on Mg^{2+} block or conductance

The GluN2A^{R586K} mutation was not found to influence Mg^{2+} block, current density or conductance despite its relatively close proximity to the location of the other mutations studied here (the pore mutations are in the membrane re-entrant loop (M2) and the GluN2A^{R586K} mutation is in in the M1-M2 linker region, a cytosolic loop between the first transmembrane domain (M1) and M2). It is hard to hypothesise about the likely impact of the GluN2A^{R586K} mutation as little work has been done on the functional role of the M1-M2 linker region, and it was not possible to resolve it in a recent crystal structure of the NMDAR transmembrane regions (Lee et al., 2014). It is possible the GluN2A^{R586K} mutation leads to alterations in function that have not been investigated in this study. It is also possible that the mutation does not alter NMDAR function, and that its presence in an individual with a neurodevelopmental disorder was coincidental. This is particularly likely as the mutation was inherited. Unfortunately no information was provided on the phenotype of the parent who also carried the mutation.

3.6.7 Limitations

The major limitation of work done in this chapter is that the mutant NMDAR expressed in oocytes and HEK293 cells were all diheteromeric, whereas a substantial proportion of NMDAR expressed physiologically are triheteromeric (see Chapter 4). It is very hard to predict what impact, if any, a mutant subunit would have in partnership with a wild type GluN2 subunit. Some of the NMDAR expressed in cultured neurons may well have been triheteromers containing mutant subunits but this would have been as part of a mixed population and there was no way of isolating out their properties. A further limitation is the poor approximation of heterozygosity in neurons: the mutant subunits were overexpressed and may conceivably not be incorporated into functional receptors to the same extent *in vivo*. Further, the developmental impact of the mutations could not be assessed as they were only transiently transfected in neurons, in the case of GluN2B mutants much later than their expression would normally begin, and in the case of GluN2A mutants, much earlier.

3.6.8 Conclusion

This chapter has provided evidence that the GluN2A^{N615K}, GluN2B^{N615I} and GluN2B^{V618G} mutations are able to influence important receptor properties in ways which could potentially alter synaptic plasticity

and influence risk for the neurodevelopmental disorders experienced by their carriers. It has not found any evidence to support GluN2A^{R586K} as a disease causing mutation.

CHAPTER 4

One missense mutation has a dominant negative effect in triheteromeric NMDARs

4.1 Chapter summary and key findings

1. Triheteromeric NMDARs containing one wild type subunit and one GluN2A^{N615K} subunit were generated. This was confirmed using glutatamate deactivation rates.

2. Glutamate deactivation rates are not influenced by any of the pore mutations (GluN2A^{N615K}, GluN2B^{N615I} or GluN2B^{V618G}).

3. Triheteromers consisting of a wild type subunit and GluN2A^{N615K} subunit show a reduction in Mg^{2+} block and a slowing in Mg^{2+} on and off rates.

4. The identity of the wild type partnering subunit matters: Mg^{2+} block in triheteromers containing wild type GluN2A subunits is less influenced by the presence of the mutant GluN2A^{N615K} subunit than in triheteromers containing wild type GluN2B.

5. Diheteromers consisting of two GluN2B^{N615I} or two GluN2B^{V618G} subunits show a potentiation of current in the presence of Mg^{2+}.

6. The dominant negative influence of the GluN2A^{N615K} subunit when partnered with wild type subunits supports a role in disease causation.

4.2 Introduction

NMDARs are heterotetramers comprised of four subunits, two type one and two others, of which GluN2A and GluN2B are the commonest in the rodent forebrain (Monyer et al., 1994). The identity of the subunits partnering GluN1 impacts on NMDAR properties important in synaptic plasticity (reviewed in (Wyllie et al., 2013)). For example, GluN2B has a slower deactivation timecourse than GluN2A (Vicini et al., 1998), prolonging the duration of activity following a brief exposure to glutamate and thus influencing charge transfer and potentially synaptic plasticity (Erreger et al., 2005).

When both partnering subunits are the same, NMDARs are termed *diheteromers*. However, when two different subunits are paired with GluN1, NMDARs are termed *triheteromers*. Evidence from co-immunoprecipitation studies (Al-Hallaq et al., 2007; Dunah and Standaert, 2003; Luo et al., 1997; Sheng et al., 1994) and electrophysiology (Gray et al., 2011; Rauner and Kohr, 2011; Tovar et al., 2013) suggest that a substantial proportion of NMDARs in the forebrain of adult rodents are GluN2A/GluN2B triheteromers, although one co-immunoprecipitation studies found the proportion to be low, at 6% (Chazot and Stephenson, 1997).

The work in Chapter 3 referred to the impact of NMDAR pore mutations in diheteromers. However, these mutations have only been found heterozygously, and it is probable that they will predominantly be expressed alongside wild type subunits in triheteromers. In order to better model the impact of a mutation on NMDAR properties in humans it is therefore necessary to express the mutant subunit as part of a triheteromer.

Expressing triheteromeric NMDARs is a significant technical challenge. It was first achieved by Hatton and Paoletti, who demonstrated that sensitivity to subunit-specific allosteric modulators (zinc and ifenprodil) was intermediate in triheteromers (Hatton and Paoletti, 2005). However, this approach was limited by the requirement for one subunit within each triheteromer to carry mutations removing Mg^{2+} block and greatly reducing glutamate potency. Recently, two groups independently developed related methodologies to dictate NMDAR subunit composition by modifying NMDAR subunit C termini to include ectopic endoplasmic reticulum retention signals (Hansen et al., 2014; Stroebel et al., 2014). Both rely on fusing peptide tags to NMDAR C termini which will only allow escape from the endoplasmic reticulum when partnered with the appropriate tag. Table 4.1 compares the two approaches and Figure 4.1 shows a schematic of the method used by Hansen et al.

Table 4.1: Comparison of two related methodologies for generating triheteromeric NMDARs

	Hansen 2014	Stroebel 2014
Control of expression	Fusion of peptide tags to C termini	
C termini	Largely intact but 2B replaced by 2A	Almost absent
GluN1	Wild type GluN1-1a	Mutated GluN1-1a
Expression	Well expressed, care needed to avoid leak	Less expression, minimal leak
Cell types	Oocytes and HEK293 cells	Oocytes only

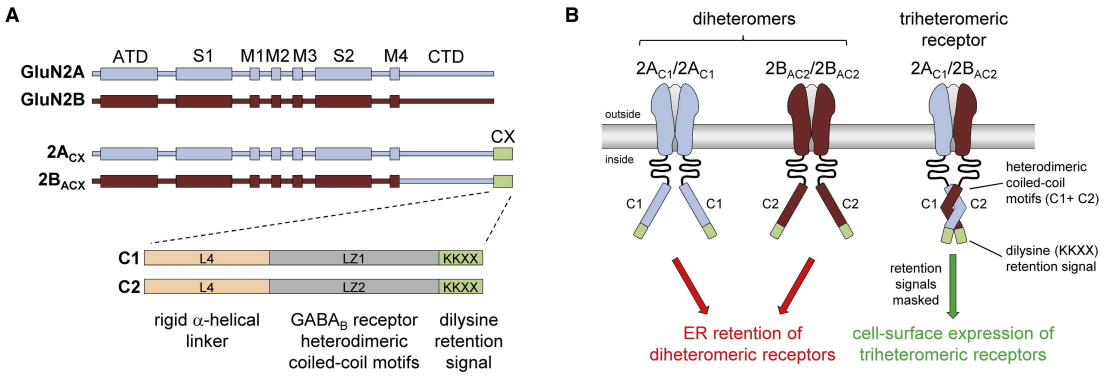

Figure 4.1: **Generation of obligate triheteromeric NMDAR.**
Taken from Hansen et al. (2014). **(A)** Schematic of wild type and modified GluN2 subunits. "CX" denotes the C1 or C2 peptide tags modifying endoplasmic reticulum retention, fused to the end of the GluN2A C terminus. In the case of GluN2B modified subunits, the C terminus has been replaced with that of GluN2A. **(B)** Depicts the outcome of different pairings of subunits with modified C termini: subunit pairings which both have C1 or both have C2 will have exposed retention signals and be retained in the endoplasmic reticulum. Subunits which have partnering modifications will have their retention signals masked and achieve surface expression.

Both approaches suffer to some extent from leak currents, whereby non-desired subunit combinations are able to escape retention and achieve surface expression. As this seems to result from the endoplasmic reticulum retention pathways being overwhelmed, leak currrents can be minimised by limiting GluN1 expression and avoiding cells with large magnitude currents (Hansen et al., 2014).

Despite their differences, the two approaches made very similar observations about GluN2A/GluN2B triheteromeric properties. Firstly, where properties differ between GluN2A and GluN2B, the majority of triheteromer properties are intermediate, but dominated by GluN2A. The open probability, glutamate potency, glutamate deactivation rate, zinc sensitivity and ifenprodil sensitivity of GluN2A/GluN2B triheteromers are closer to that of GluN2A diheteromers than GluN2B diheteromers (Hansen et al., 2014; Stroebel et al., 2014). The exceptions are triheteromeric glycine potency, which is closer to that seen in GluN2B diheteromers (Stroebel et al., 2014), and spermine potentiation, which is almost identical to that seen in GluN2A diheteromers (Stroebel et al., 2014). This means spermine potentiation could potentially be more sensitive in detecting the onset of GluN2A expression than the more commonly used ifenprodil inhibition, because the expression of triheteromers will shift the spermine response to that of GluN2A, rather than to an intermediate value as in the case of ifenprodil. This observation is used in Chapter 5.

This chapter describes the application of the technique developed by Hansen et al. to express triheteromeric receptors containing one wild type subunit and one mutant subunit in HEK293T cells. HEK293T cells were chosen over oocytes because of their year-round availability and relative ease of making electrophysiological recordings, in particular the ability to assess glutamate deactivation rates. The expression of mutant subunits as triheteromers with wild type partner subunits allows better modelling of the impact of the mutant subunit in its heterozygous human carrier, who is likely to have a mixed population of wild type and mutant diheteromers and triheteromers.

The overarching finding of this chapter is that the GluN2A^{N615K} mutation has a dominant negative effect on NMDARs containing wild type subunits. This strengthens the evidence in support of the hypothesis that this mutation is responsible for the severe neurodevelopmental disorder experienced by

its carrier. The key property investigated was Mg^{2+} block, which was found to be reduced in $GluN2A^{N615K}$ containing triheteromeric NMDARs.

4.3 Glutamate deactivation rates

4.3.1 Glutamate deactivation rates allow triheteromers to be distinguished from diheteromers

Previous work identified that the glutamate deactivation rates of GluN2A/GluN2B triheteromers were intermediate to those of GluN2A and GluN2B diheteromers (Hansen et al., 2014; Stroebel et al., 2014). To replicate this finding, HEK293T cells were transfected to express either diheteromers with unmodified C termini (e.g. wild type 2A/2A), diheteromers with modified C termini (e.g. $2A_{C1}/2A_{C2}$) or triheteromers with modified C termini (e.g. $2A_{C1}/2B_{C2}$). Whole-cell voltage-clamp recordings were then made while cells underwent precisely controlled glutamate exposure (5 ms or 2 s). This allowed the assessment of glutamate deactivation rates: the rate of decline of current following the removal of glutamate. Example traces showing glutamate deactivation currents following a 5 ms exposure are in Figure 4.2A and following a 2 s exposure in Figure 4.3A. These currents can be well approximated by one or two component exponential decay functions. The weighted time constants fitted to the deactivation curves after a 5 ms exposure are shown in Figure 4.2B and C and after a 2 s exposure in Figure 4.3B and C. Summary values for fast, slow, and weighted time constants are provided in Table 4.3 and 4.4. The nomenclature used in this chapter is quite complex, so please see Table 4.2 for a guide.

Table 4.2: Nomenclature used to describe wild type and mutant triheteromeric constructs

Full name	Short name (used in tables and figures)	Group name (for pooled data)
Wild type constructs		
GluN2A wild type	2A	2A WT
$GluN2A_{C1}$/ $GluN2A_{C2}$	$2A_{C1C2}$	
GluN2B wild type	2B	2B WT
$GluN2B_{AC1}$/ $GluN2B_{AC2}$	$2B_{C1C2}$	
$GluN2A_{C1}$/ $GluN2B_{AC2}$	2A/2B	2A/2B WT
$GluN2B_{AC1}$/ $GluN2A_{C2}$	2B/2A	
Mutant constructs: $GluN2A^{N615K}$ as example		
$GluN2A^{N615K}$	$2A^{N615K}$	2A N615K
$GluN2A_{C1}{}^{N615K}/GluN2A_{C2}{}^{N615K}$	$2A^{N615K}{}_{C1C2}$	
$GluN2A_{C1}{}^{N615K}/GluN2A_{C2}{}^{WT}$	$2A^{N615K}/2A$	2A N615K / 2A WT
$GluN2A_{C1}{}^{WT}/GluN2A_{C2}{}^{N615K}$	$2A/2A^{N615K}$	
$GluN2A_{C1}{}^{N615K}/GluN2B_{AC2}{}^{WT}$	$2A^{N615K}/2B$	2A N615K / 2B WT
$GluN2B_{AC1}{}^{WT}/GluN2A_{C2}{}^{N615K}$	$2B/2A^{N615K}$	

The data in Figures 4.2, 4.3, and Tables 4.3, 4.4 demonstrate three important points. Firstly, the modified C termini do not influence glutamate deactivation rate: the time constants for diheteromers with wild type and modified C termini are the same, following either a 5 ms or 2 s agonist exposure. Wild type and modified C termini data were therefore pooled for subsequent analyses. Secondly, the pairing of a given subunit with a given modified C terminus does not influence the likelihood of assembly: 2A/2B triheteromers have the same glutamate deactivation rates as 2B/2A triheteromers. (If a particular modified subunit was more likely to assemble with itself ("escape") this would have led to diheteromeric outliers.) These data were therefore pooled for subsequent analyses. Finally, and importantly, the glutamate deactivation rates for triheteromers are significantly different to those for either diheteromer, showing an intermediate value closest to that of GluN2A diheteromers.

Table 4.3: Glutamate deactivation time constants (1 mM, 5 ms exposure) for wild type NMDARs

GluN2 subunits	τ_{fast} (ms)	τ_{slow} (ms)	% fast	$\tau_{weighted}$ (ms)	n
2A	47 ± 4	227 ± 60	94 ± 3	55 ± 2	6
$2A_{C1C2}$	41 ± 3	113 ± 14	93 ± 4	45 ± 4	7
2A WT	$\mathbf{44 \pm 3}$	$\mathbf{178 \pm 40}$	$\mathbf{93 \pm 3}$	$\mathbf{50 \pm 3}$	**13**
2B	255 ± 16	959 ± 54	57 ± 2	555 ± 35	7
$2B_{C1C2}$	256 ± 36	1000 ± 188	68 ± 4	454 ± 42	8
2B WT	$\mathbf{255 \pm 20}$	$\mathbf{981 \pm 100}$	$\mathbf{63 \pm 3}$	$\mathbf{501 \pm 30}$	**15**
2A/2B	68 ± 6	218 ± 40	92 ± 4	79 ± 3	8
2B/2A	53 ± 4	336 ± 97	89 ± 3	75 ± 7	7
2A/2B WT	$\mathbf{61 \pm 4}$	$\mathbf{289 \pm 61}$	$\mathbf{91 \pm 2}$	$\mathbf{77 \pm 4}$	**15**

Table 4.4: Glutamate deactivation time constants (1 mM, 2 s exposure) for wild type NMDARs

GluN2 subunits	τ_{fast} (ms)	τ_{slow} (ms)	% fast	$\tau_{weighted}$ (ms)	n
2A	64 ± 8	233 ± 21	95 ± 2	73 ± 5	6
$2A_{C1C2}$	62 ± 5	not fitted	100 4	62 ± 5	7
2A WT	$\mathbf{63 \pm 4}$	$\mathbf{233 \pm 21}$	$\mathbf{98 \pm 1}$	$\mathbf{67 \pm 4}$	**13**
2B	356 ± 58	923 ± 157	60 ± 8.5	676 ± 40	7
$2B_{C1C2}$	385 ± 60	1134 ± 111	78 ± 5	558 ± 45	8
2B WT	$\mathbf{372 \pm 41}$	$\mathbf{1020 \pm 100}$	$\mathbf{70 \pm 5}$	$\mathbf{613 \pm 33}$	**15**
2A/2B	93 ± 9	248	98 ± 2	96 ± 8	8
2B/2A	75 ± 5	529 ± 83	95 ± 1	95 ± 9	7
2A/2B WT	$\mathbf{84 \pm 6}$	$\mathbf{484 \pm 82}$	$\mathbf{97 \pm 1}$	$\mathbf{96 \pm 6}$	**15**

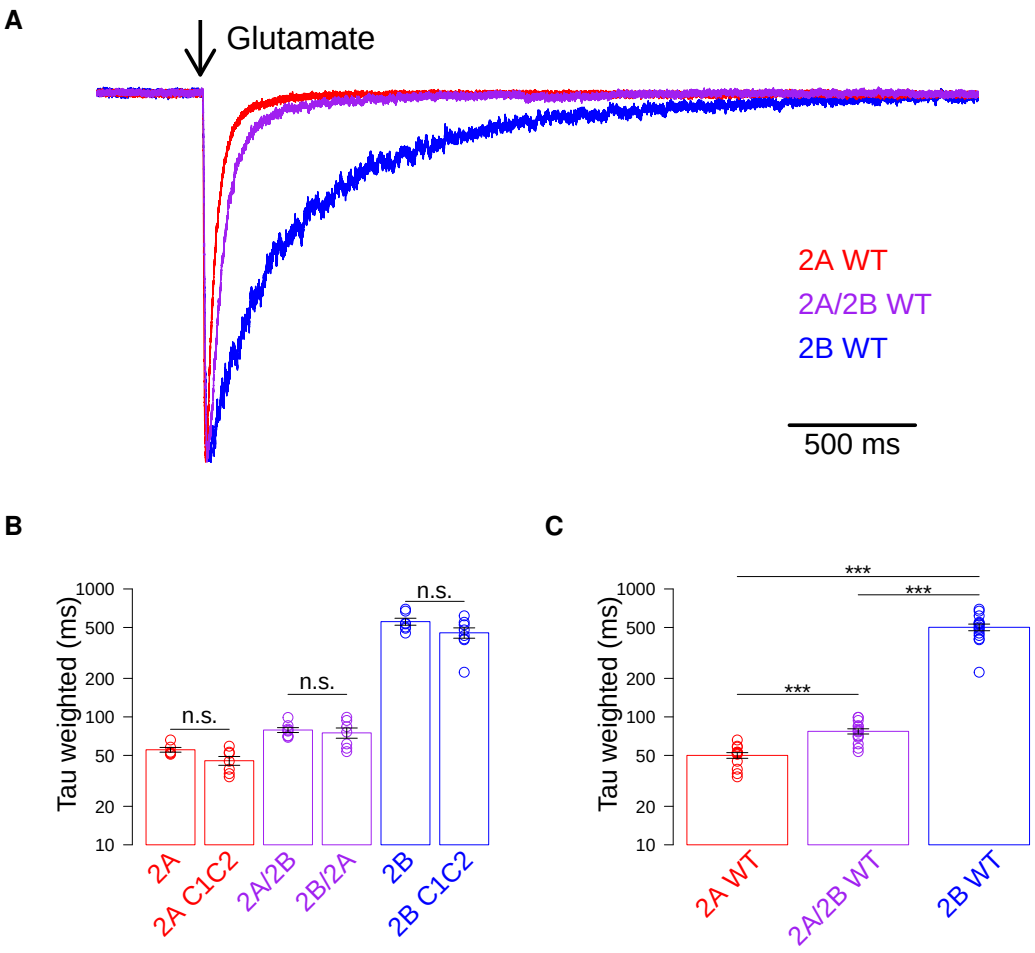

Figure 4.2: **Glutamate deactivation rates following 5 ms exposure are unaffected by modification of C termini**

(A) Representative whole-cell voltage-clamp recordings from HEK293T cells expressing wild type 2A and 2B diheteromers, and 2A/2B triheteromers, activated by brief exposure to glutamate (1 mM, 5 ms). Responses are normalised to the peak amplitude.

(B) The bar graph shows glutamate deactivation weighted time constants for wild type construct pairs with and without modified C termini. t–tests (Bonferroni corrected) showed no significant differences between construct pairs.

(C) The bar graph shows glutamate deactivation weighted time constants with construct pairs pooled. A one-way ANOVA showed a significant effect of subunit ($F(2,40)= 194$, $p < 2e{-}16$), with post hoc t–tests (Bonferroni corrected) demonstrating significant differences between 2A and 2B ($t(14.2) = 15.0$, $p_{corr} = 1.2e{-}09$), and with triheteromers exhibiting an intermediate value significantly different to both 2A ($t(24.5) = 6.0$, $p_{corr} = 6.9e{-}06$) and 2B ($t(14.4) = 14.1$, $p_{corr} = 2.5e{-}09$).

See Table 4.2 for how pairs were pooled and see Table 4.3 for summary values and sample sizes.

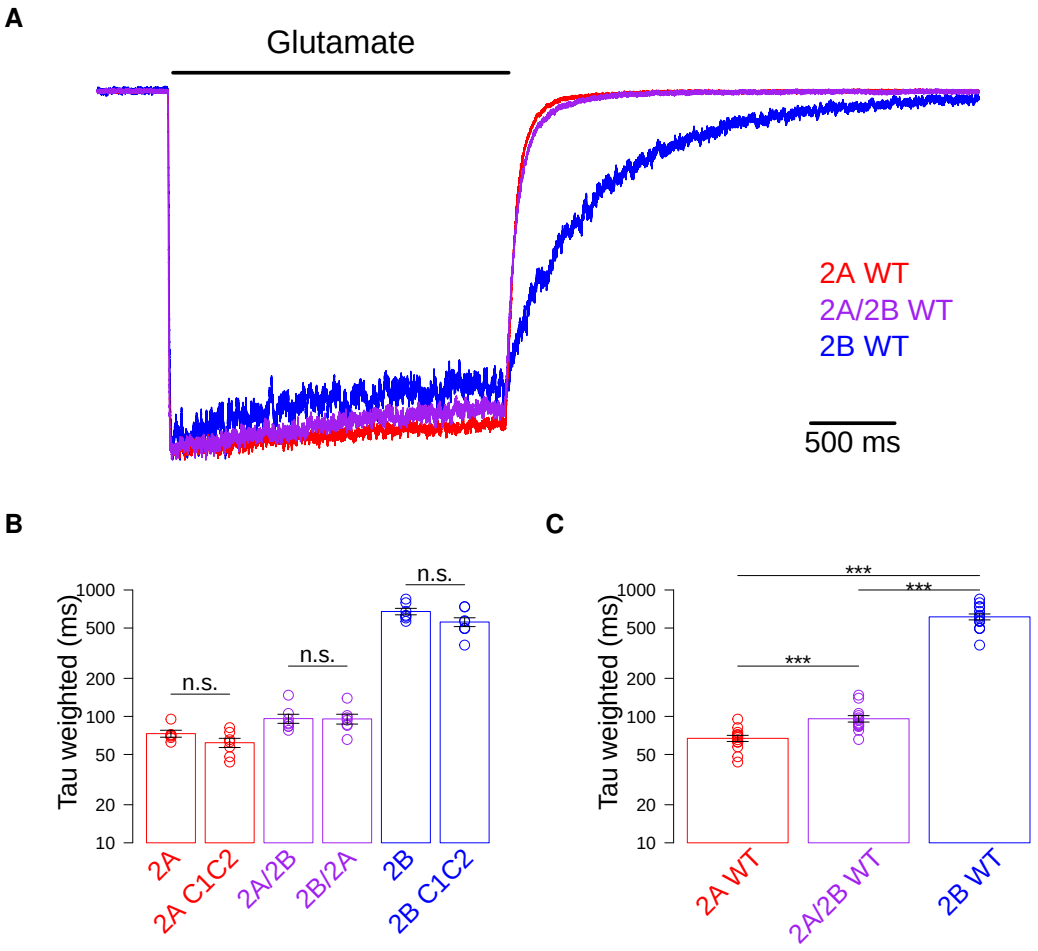

Figure 4.3: **Glutamate deactivation rates following 2 s exposure are unaffected by modification of C termini**

(A) Representative whole-cell voltage-clamp recordings from HEK293T cells expressing wild type 2A and 2B diheteromers, and 2A/2B triheteromers, activated by prolonged exposure to glutamate (1 mM, 2 s). Responses are normalised to the peak amplitude.

(B) The bar graph shows glutamate deactivation weighted time constants for wild type construct pairs with and without modified C termini. t–tests (Bonferroni corrected) showed no significant differences between construct pairs.

(C) The bar graph shows glutamate deactivation weighted time constants with construct pairs pooled. A one-way ANOVA showed a significant effect of subunit ($F(2,40)= 231$, $p < 2e{-}16$), with post hoc t–tests (Bonferroni corrected) demonstrating significant differences between 2A and 2B ($t(14.4) = 16.4$, p_{corr} =3.2e-10), and with trihetomers exhibiting an intermediate value significantly different to both 2A ($t(23.7) = 4.3$, p_{corr} = 0.0008) and 2B ($t(14.8) = 15.4$, p_{corr} = 4.8e-10).

See Table 4.2 for how pairs were pooled and see Table 4.4 for summary values and sample sizes.

4.3.2 The GluN2A^{N615K} mutation does not influence glutamate deactivation rates

Glutamate deactivation rates for diheteromers containing the GluN2A^{N615K} pore mutation were examined next (Figure 4.4 and Tables 4.5 and 4.6). The first finding is that, as for the wild type subunits, the modified C termini do not influence glutamate deactivation rates in GluN2A^{N615K} subunits. These data were pooled for subsequent analyses. The second finding is that the glutatamate deactivation rates for GluN2A^{N615K} are the same as those for GluN2A wild type.

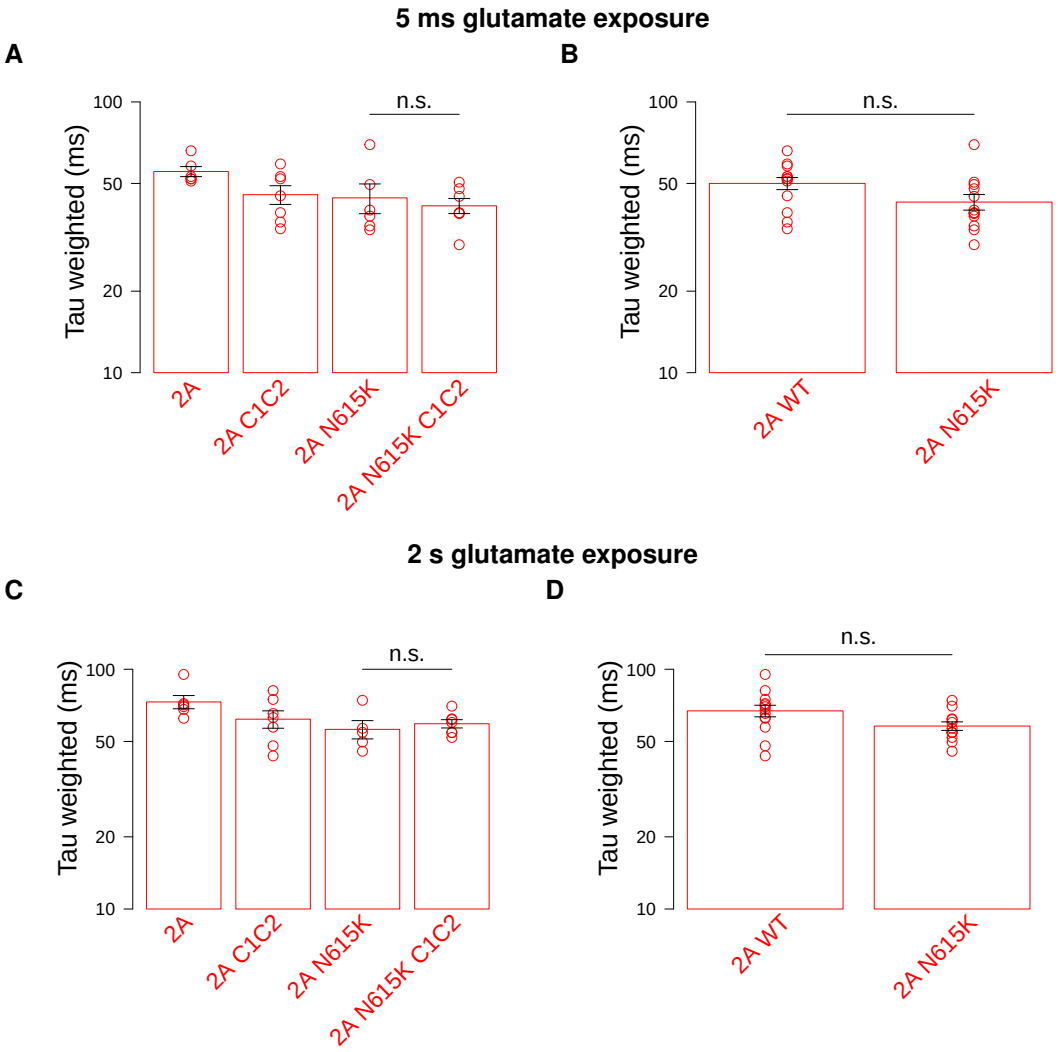

Figure 4.4: **GluN2A^{N615K} does not alter glutamate deactivation rates**
(A) The bar graph shows glutamate deactivation (1 mM, 5 ms exposure) weighted time constants for 2A^{N615K} construct pairs with and without modified C termini. A t–test showed no significant difference between the construct pairs.
(B) The bar graph shows glutamate deactivation (1 mM, 5 ms exposure) weighted time constants with construct pairs pooled. A t–test showed no significant difference between 2A and 2A^{N615K} glutamate deactivation rates.
(C) The bar graph shows glutamate deactivation (1 mM, 2 s exposure) weighted time constants for 2A^{N615K} construct pairs with and without modified C termini. A t–test showed no significant difference between the construct pairs.
(D) The bar graph shows glutamate deactivation (1 mM, 2 s exposure) weighted time constants for 2A^{N615K} construct pairs with construct pairs pooled. A t–test showed no significant difference between 2A and 2A^{N615K} glutamate deactivation rates.
See Table 4.2 for how pairs were pooled and see Tables 4.5 and 4.6 for summary values and sample sizes.

Next, subunit pairings designed to produce triheteromers containing one mutant GluN2A^{N615K} subunit were investigated (Figure 4.5 and Tables 4.5 and 4.6). As seen with wild type subunits, the partnering of a particular C termini modification with a particular subunit did not influence glutamate deactivation rates. These data were therefore pooled for subsequent analyses. As would be expected, triheteromers containing two GluN2A subunits (one mutant, one wild type) exhibited deactivation rates indistinguishable from wild type or mutant GluN2A diheteromers. Similarly, triheteromers containing one GluN2B subunit and one GluN2A^{N615K} mutant subunit displayed deactivation rates indistinguishable from those seen in wild type triheteromers. This is an important finding as it confirmed that subunit pairings containing GluN2A^{N615K} mutant subunits were able to assemble as triheteromers.

Table 4.5: Glutamate deactivation time constants (1 mM, 5 ms exposure) for GluN2A^{N615K} containing NMDARs

GluN2 subunits	τ_{fast} (ms)	τ_{slow} (ms)	% fast	$\tau_{weighted}$ (ms)	n
2A^{N615K}	35 ± 1	223 ± 55	96 ± 2	44 ± 6	6
2A$^{N615K}_{C1C2}$	40 ± 3	186	99 ± 1	41 ± 3	7
2A N615K	**38 ± 2**	**214 ± 40**	**98 ± 1**	**43 ± 3**	**13**
2A^{N615K}/2A	43 ± 3	175 ± 24	97 ± 1	47 ± 2	10
2A/2A^{N615K}	51 ± 2	470	100 ± 0	52 ± 2	10
2A N615K / 2A WT	**47 ± 2**	**234 ± 62**	**98 ± 1**	**49 ± 2**	**20**
2A^{N615K}/2B	54 ± 5	318 ± 80	89 ± 3	73 ± 5	10
2B/2A^{N615K}	63 ± 5	343 ± 73	93 ± 3	85 ± 11	10
2A N615K / 2B WT	**59 ± 4**	**328 ± 55**	**91 ± 2**	**79 ± 6**	**20**

Table 4.6: Glutamate deactivation time constants (1 mM, 2 s exposure) for GluN2A^{N615K} containing NMDARs

GluN2 subunits	τ_{fast} (ms)	τ_{slow} (ms)	% fast	$\tau_{weighted}$ (ms)	n
2A^{N615K}	56 ± 5	not fitted	100	56 ± 5	5
2A$^{N615K}_{C1C2}$	57 ± 4	289	99 ± 1	59 ± 2	7
2A N615K	**57 ± 3**	**289**	**100 ± 0**	**58 ± 2**	**12**
2A^{N615K}/2A	64 ± 5	237	99 ± 1	66 ± 5	10
2A/2A^{N615K}	77 ± 6	not fitted	100 ± 0	77 ± 6	10
2A N615K / 2A WT	**70 ± 4**	**237**	**100 ± 0**	**71 ± 4**	**20**
2A^{N615K}/2B	81 ± 7	412 ± 145	96 ± 2	91 ± 4	10
2B/2A^{N615K}	121 ± 29	253 ± 104	81 ± 11	103 ± 7	10
2A N615K / 2B WT	**101 ± 15**	**321 ± 85**	**89 ± 6**	**97 ± 4**	**20**

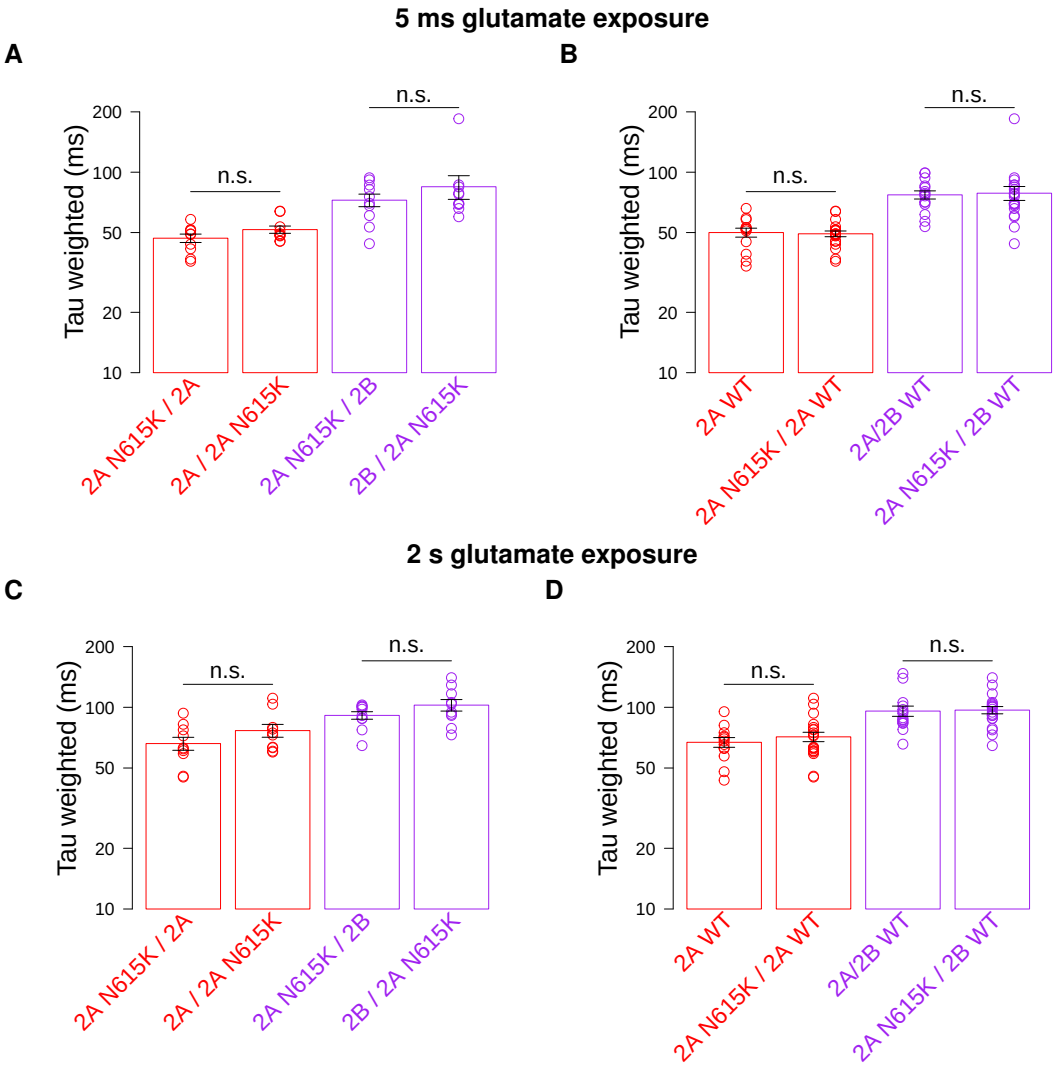

Figure 4.5: **GluN2A^{N615K} subunits can form triheteromers with wild type GluN2 subunits**
(A) The bar graph shows glutamate deactivation (1 mM, 5 ms exposure) weighted time constants for 2A^{N615K} triheteromeric subunit pairs with alternate pairings of subunit and modified C terminus. t–tests showed no significant differences between the construct pairs.
(B) The bar graph shows glutamate deactivation (1 mM, 5 ms exposure) weighted time constants for 2A^{N615K} triheteromeric subunit pairs with construct pairs pooled. t–tests showed no significant differences between the subunit pairs.
(C) The bar graph shows glutamate deactivation (1 mM, 2 s exposure) weighted time constants for 2A^{N615K} triheteromeric subunit pairs with alternate pairings of subunit and modified C terminus. t–tests showed no significant differences between the subunit pairs.
(D) The bar graph shows glutamate deactivation (1 mM, 2 s exposure) weighted time constants for wild type and 2A^{N615K} triheteromeric subunit pairs with construct pairs pooled. t–tests showed no significant difference between wild type and 2A^{N615K} containing triheteromers' glutamate deactivation rates.
See Table 4.2 for how pairs were pooled and see Tables 4.5 and 4.6 for summary values and sample sizes.

4.3.3 The GluN2B^{N615I} and GluN2B^{V618G} mutations do not influence glutamate deactivation rates

The effect of pore mutations in the GluN2B subunit on glutamate deactivation rates were assessed next (Figure 4.6 and Tables 4.7 and 4.8). The modified C termini were associated with a faster deactivation rate in GluN2B^{N615I} diheteromers. Therefore, only GluN2B pore mutant subunits with wild type C termini were used for comparison with wild type GluN2B. This demonstrated that the GluN2B^{N615I} and GluN2B^{V618G} mutations do not influence glutamate deactivation rates.

Table 4.7: Glutamate deactivation time constants (1 mM, 5 ms exposure) for GluN2B^{N615I} and GluN2B^{V618G} containing NMDARs

GluN2 subunits	τ_{fast} (ms)	τ_{slow} (ms)	% fast	$\tau_{weighted}$ (ms)	n
2B^{N615I}	248 ± 10	856 ± 35	58 ± 3	502 ± 17	6
2B$^{N615I}_{C1C2}$	230 ± 22	754 ± 64	70 ± 6	384 ± 15	7
2B^{N615I}/2A	55 ± 4	159 ± 88	85 ± 13	60 ± 3	5
2B^{N615I}/2B	220 ± 13	744 ± 61	57 ± 7	397 ± 23	6
2B^{V618G}	157 ± 19	1006 ± 93	40 ± 1	666 ± 57	4
2B$^{V618G}_{C1C2}$	79	976	52	509	1
2B^{V618G}/2A	40 ± 4	127 ± 64	87 ± 12	46 ± 4	5
2B^{V618G}/2B	249 ± 14	833 ± 80	57 ± 5	497 ± 19	3

Table 4.8: Glutamate deactivation time constants (1 mM, 2 s exposure) for GluN2B^{N615I} and GluN2B^{V618G} containing NMDARs

GluN2 subunits	τ_{fast} (ms)	τ_{slow} (ms)	% fast	$\tau_{weighted}$ (ms)	n
2B^{N615I}	345 ± 15	1055 ± 53	59 ± 2	632 ± 30	6
2B$^{N615I}_{C1C2}$	314 ± 12	1110	72 ± 4	502 ± 14	7
2B^{N615I}/2A	76 ± 5	not fitted	100 ± 0	77 ± 5	5
2B^{N615I}/2B	303 ± 10	1358 ± 368	65 ± 8	559 ± 47	6
2B^{V618G}	461 ± 70	2053 ± 800	53 ± 9	1064 ± 216	4
2B$^{V618G}_{C1C2}$	108	1102	43	673	1
2B^{V618G}/2A	55 ± 8	290	98 ± 2	59 ± 5	5
2B^{V618G}/2B	343 ± 24	1214 ± 134	64 ± 5	649 ± 17	3

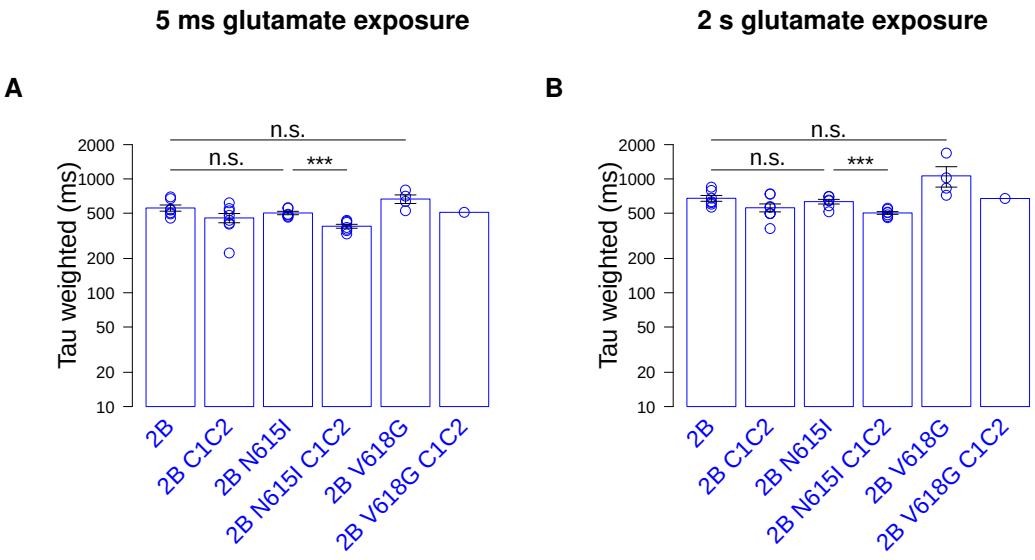

Figure 4.6: **GluN2B pore mutations do not alter glutamate deactivation rates**
(A) The bar graph shows glutamate deactivation (1 mM, 5 ms exposure) weighted time constants for 2B, $2B^{N615I}$ and $2B^{V618G}$ diiheteromeric construct pairs with and without modified C termini. A t-test showed a signifcant difference between $2B^{N615I}$ with and without modified C termini ($t(10.5) = 5.1$, $p = 0.0004$). Statistical comparisons were not possible with $2B^{V618G}{}_{C1C2}$ as only one cell with modified C termini was obtained. Subunit pairs were therefore not pooled. Instead, wild type and mutant subunits without modified C termini were compared. t–tests showed no significant differences.
(B) The bar graph shows glutamate deactivation (1 mM, 2 s exposure) weighted time constants for 2B, $2B^{N615I}$ and $2B^{V618G}$ diiheteromeric subunit pairs with and without modified C termini. A t–test showed a signifcant difference between $2B^{N615I}$ with and without modified C termini ($t(7.1) = 34.0$, $p = 0.0053$). Statistical comparisons were not possible with $2B^{V618G}{}_{C1C2}$ as only one cell with modified C termini was obtained. Subunit pairs were therefore not pooled. Instead, wild type and mutant subunits without modified C termini were compared. t–tests showed no significant differences.
See Tables 4.7 and 4.8 for summary values and sample sizes.

Subunit pairings designed to produce triheteromers containing one mutant GluN2B subunit produced a complex set of results (Figure 4.7 and Tables 4.7 and 4.8). These data show that cells transfected with subunits designed to produce triheteromers containing two GluN2B subunits, one mutant and one wild type, mainly show deactivation rates indistinguishable from GluN2B diheteromers containing two wild type or two mutant subunits (with the exception of GluN2B^{N615I} following brief glutamate exposure). However, cells transfected with subunits designed to produce triheteromers containing one GluN2A subunit and one mutant GluN2B subunit showed deactivation rates that were closer to GluN2A than expected, and were in fact faster than those seen in wild type triheteromers. This was seen with both GluN2B pore mutants and at either duration of agonist exposure. This suggests that some GluN2A diheteromers had been able to escape the endoplasmic reticulum retention system, achieve surface expression, and contribute to the glutamate deactivation time course. Because it was not possible to be confident that triheteromers containing one copy of either GluN2B mutant subunit were being generated, the remainder of this chapter discusses only findings related to GluN2B pore mutant diheteromers.

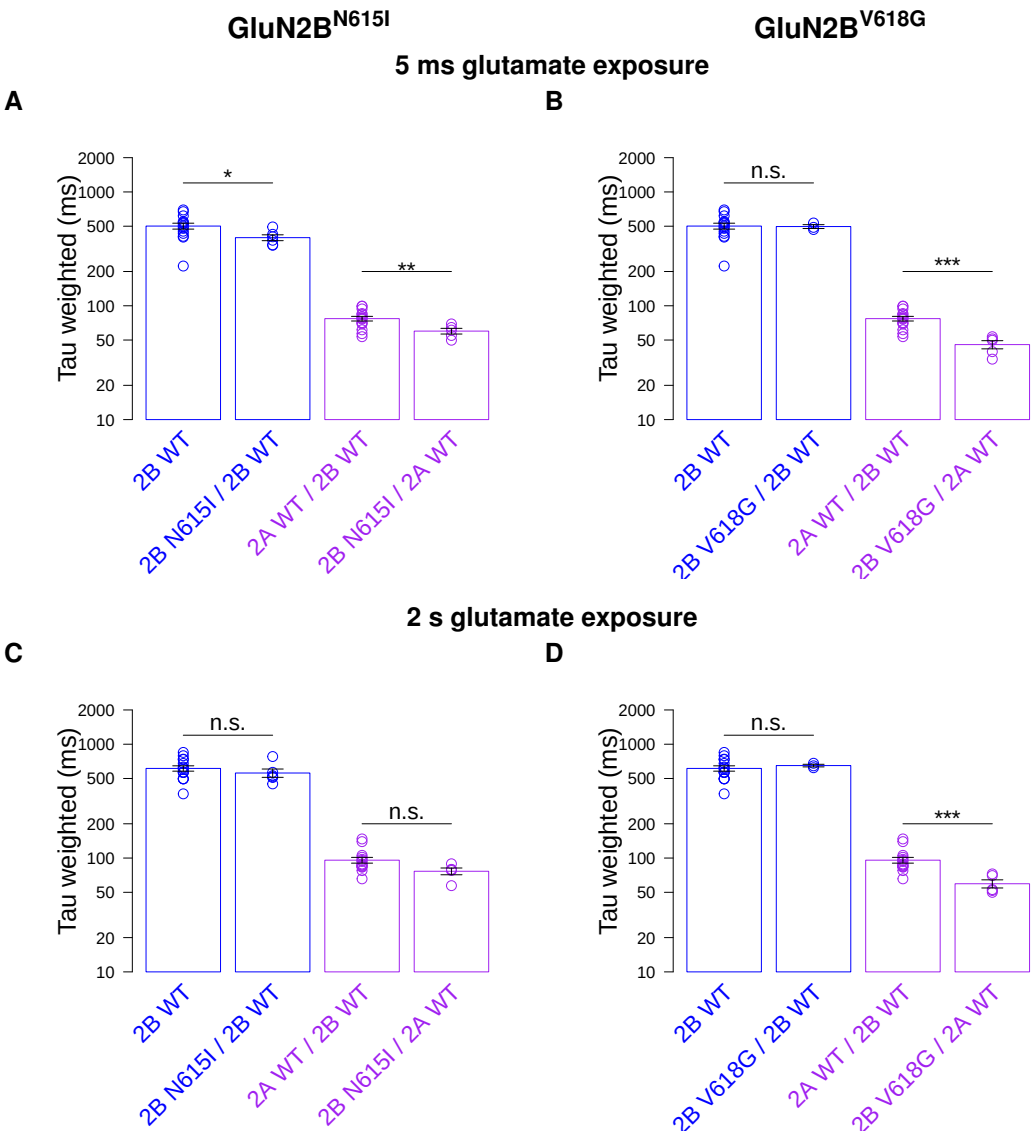

Figure 4.7: **Glutamate deactivation rates in construct pairings designed to produce GluN2B^{N615I} and GluN2B^{V618G} containing triheteromers suggest GluN2A diheteromeric escape current**

(A) Glutamate deactivation (1 mM, 5 ms exposure) weighted time constants for wild type and 2B^{N615I} triheteromeric subunit pairs. t–tests showed significant reductions in deactivation rates in pairs containing 2B^{N615I} with modified C termini compared with 2B diheteromers ($t(17.8) = 2.8$, $p_{corr} = 0.026$) and 2A/2B triheteromers ($t(13.1) = 3.45$, $p_{corr} = 0.008$).

(B) Glutamate deactivation (1 mM, 5 ms exposure) weighted time constants for wild type and 2B^{V618G} triheteromeric subunit pairs. t–tests showed a significant reduction in deactivation rates in pairs containing 2B^{N615I} with modified C termini compared with 2A/2B triheteromers ($t(11.8) = 6.0$, $p_{corr} = 1.2e\text{-}4$) but not with GluN2B diheteromers.

(C) Glutamate deactivation (1 mM, 2 s exposure) weighted time constants for wild type and 2B^{N615I} triheteromeric construct pairs. t–tests showed no significant differences between the construct pairs.

(D) Glutamate deactivation (1 mM, 2 s exposure) weighted time constants for wild type and 2B^{V618G} triheteromeric construct pairs. t–tests showed a significant reduction in deactivation rates in pairs containing 2B^{N615I} with modified C termini compared with 2A/2B triheteromers ($t(14.3) = 4.9$, $p_{corr} = 0.0004$) but not with 2B diheteromers.

See Tables 4.7 and 4.8 for summary values and sample sizes.

4.4 Mg^{2+} block in diheteromeric and triheteromeric NMDARs containing GluN2A^{N615K} subunits

4.4.1 Mg^{2+} percentage inhibition

GluN2A^{N615K} mutant subunits expressed as diheteromers have been previously shown to reduce Mg^{2+} block in this study (Chapter 3) and by others (Endele et al., 2010). However, the mutation's impact on Mg^{2+} block in triheteromers remained unexplored, despite this subunit configuration being more physiologically relevant. Having generated GluN2A^{N615K} containing triheteromers, Mg^{2+} block was therefore a priority for investigation.

First, the extent of Mg^{2+} block was investigated. Transfected cells were first exposed to glutamate, to establish a baseline response, and then underwent precisely timed exposure to glutamate co-applied with Mg^{2+}, before being returned to glutamate alone (in the continuous presence of glycine). This allowed the percentage reduction in glutamate-evoked current in the presence of Mg^{2+} to be calculated, and the precisely controlled timing of exposure also allowed Mg^{2+} block on and off rates to be evaluated (see Section 4.5.2).

Representative traces are shown in Figure 4.8. It was first confirmed that the C terminus modifications did not themselves influence Mg^{2+} block (Figure 4.9). The extent of Mg^{2+} block in subunit pairings with and without modified C termini was not different for either wild type or GluN2A^{N615K} subunits. This meant data from wild type and modified subunits could be pooled for subsequent analyses, and also allowed Mg^{2+} block to be assessed in receptor compositions relying on subunits with modified C termini.

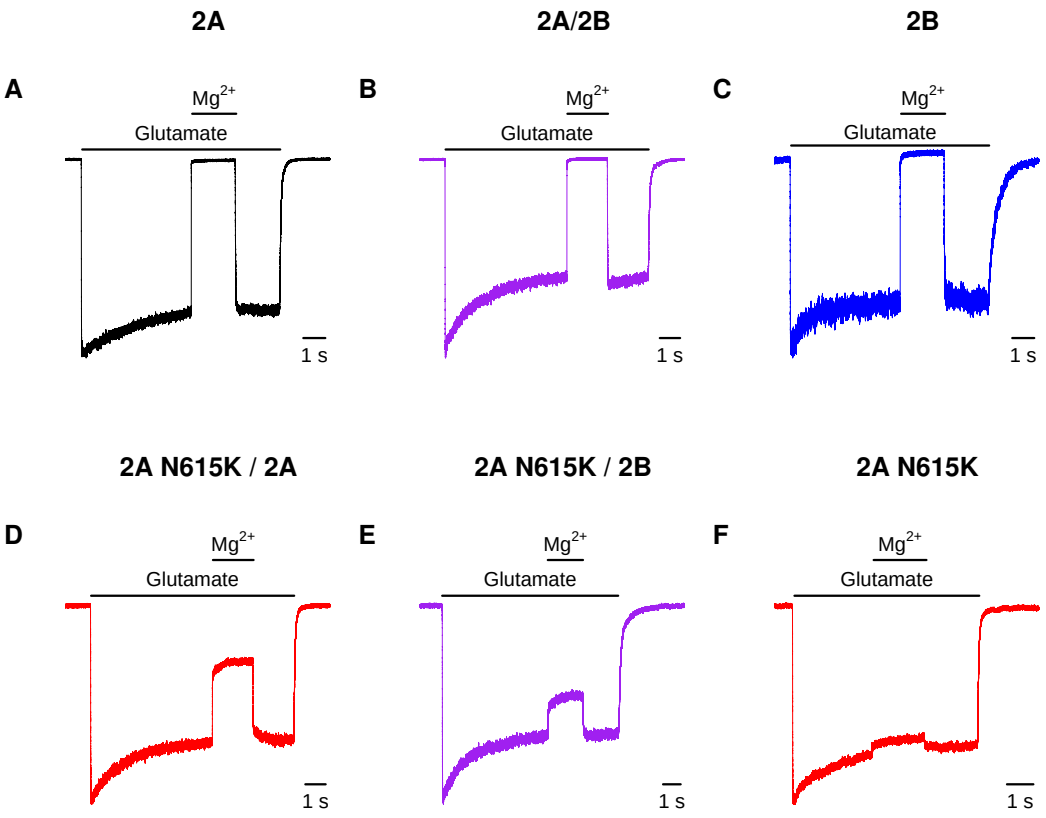

Figure 4.8: **Representative traces showing Mg^{2+} block in wild type and GluN2A^{N615K} mutant diheteromers and triheteromers**
(A–F) Representative whole-cell voltage-clamp recordings from HEK293T cells expressing the subunits indicated during exposure to glutamate (1 mM) and Mg^{2+} (1 mM) while held at –60 mV. Responses normalised to peak amplitude.

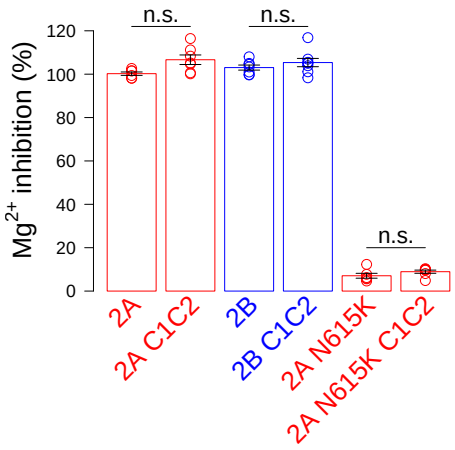

Figure 4.9: **Mg^{2+} block is not altered by modified C termini**
The bar graph shows Mg^{2+} block (1 mM) in NMDARs with and without modified C termini at a holding potential of –60 mV. t–tests (Bonferroni corrected) showed no signficant differences between wild type and modified subunits.

Data comparing percentage Mg^{2+} block in cells expressing wild type, wild type triheteromeric, GluN2A^{N615K} mutant diheteromeric and GluN2A^{N615K} mutant triheteromeric NMDARs are presented in Figures 4.10 and 4.11, and Tables 4.9 and 4.10. These data demonstrate four main findings. Firstly, they show that wild type triheteromers show the same extent of Mg^{2+} inhibition as wild type GluN2A and GluN2B diheteromers: a near complete block at approximately physiological Mg^{2+} concentration (1 mM) and holding potential (–60 mV). Secondly, they replicate previous work showing a highly significant reduction in Mg^{2+} block in GluN2A^{N615K} diheteromers, with block at negligible levels under near physiological conditions. Thirdly, they show that triheteromers containing one mutant GluN2A^{N615K} subunit exhibit Mg^{2+} block intermediate to diheteromers comprised of wild type and GluN2A^{N615K} subunits. This is important because it demonstrates a dominant negative effect of the GluN2A^{N615K} subunit: one alone, paired with a wild type subunit, is sufficient to significantly reduce NMDAR Mg^{2+} block. Finally, they show that the identity of the wild type partner subunit in mutant triheteromers matters: the extent of Mg^{2+} block seen with a wild type GluN2A subunit partner is signficantly higher than that seen with a wild type GluN2B subunit partner.

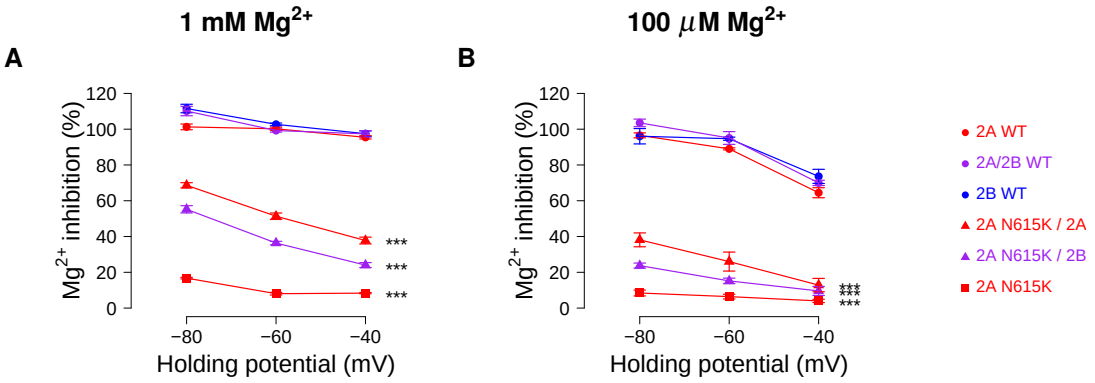

Figure 4.10: **Mg^{2+} block is reduced in GluN2A^{N615K} mutant diheteromers and triheteromers** **(A)** Summary data showing 1 mM Mg^{2+} block at three holding potentials for wild type and 2A^{N615K} containing diheteromers and triheteromers. Stars indicate significance level of comparison of means of mutant NMDARs with relevant wild type control (see text below). A two-way repeated measures ANOVA showed a significant main effect of subunit ($F(5, 80) = 538$, $p < 2e{-}16$) and of holding potential ($F(2, 160) = 701$, $p < 2e{-}16$). There was also a significant interaction ($F(10,160) = 44$, $p < 2e{-}16$), however, as the key contrasts of interest were between subunits, the interaction of subunit with holding potential in determining Mg^{2+} block was not explored. Post hoc t–tests (Bonferroni corrected) showed no significant differences between Mg^{2+} block in wild type subunits. However, Mg^{2+} block was significantly reduced in GluN2A^{N615K} compared to 2A ($t(13.9) = 70.3$, $p_{corr} < 2e{-}15$) and between 2A^{N615K}/2A and 2A ($t(26) = 19.4$, $p_{corr} < 2e{-}15$). 2A/2B and 2A^{N615K}/2B also showed significantly different Mg^{2+} block ($t(29) = 35.1$, $p_{corr} < 2e{-}15$). Further key contrasts (not marked on the figure) showed that 2A^{N615K} diheteromers showed significantly lower Mg^{2+} block than 2A^{N615K}/2A ($t(20) = 19.1$, $p_{corr} < 2e{-}13$) and 2A^{N615K}/2B ($t(21.4) = 18.5$, $p_{corr} < 1e{-}13$). Finally, 2A^{N615K}/2A showed significantly higher Mg^{2+} block than 2A^{N615K}/2B ($t(30.6) = 5.8$, $p_{corr} < 2e{-}5$)). Post hoc paired t–tests comparing holding potentials showed that Mg^{2+} block at –40 mV was significanty less than at –60 mV ($t(85) = 12.2$, $p_{corr} < 3e{-}15$), which was significantly less than at –80 mV ($t(85) = 12.8$, $p_{corr} < 3e{-}15$).

(B) Summary data showing 100 μM Mg^{2+} block at three holding potentials for wild type and GluN2A^{N615K} containing diheteromers and triheteromers. Stars indicate significance level of comparison of means of mutant NMDARs with relevant wild type control (see text below). A two-way repeated measures ANOVA showed a significant main effect of subunit ($F(5, 28) = 255$, $p < 2e{-}16$) and of holding potential ($F(2, 56) = 115$, $p < 2e{-}16$). There was also a significant interaction ($F(10,56) = 5.6$, $p < 1.1e{-}5$), however, as the key contrasts of interest were between subunits, the interaction of subunit with holding potential in determining Mg^{2+} block was not explored. Post hoc t–tests (Bonferroni corrected) showed no significant differences between Mg^{2+} block in wild type subunits. Similarly to the 1 mM Mg^{2+} concentration, there was a significant difference in Mg^{2+} block between 2A and 2A^{N615K} ($t(4.6) = 51$, $p_{corr} < 1.2e{-}6$) and between 2A and 2A^{N615K}/2A ($t(6) = 13.2$, $p_{corr} < 9.5e{-}5$). 2A/2B and 2A^{N615K}/2B also showed significantly different Mg^{2+} block ($t(7) = 30.6$, $p_{corr} < 7.6e{-}8$). Further key contrasts (not marked on the figure) showed that 2A^{N615K} diheteromers showed significantly lower Mg^{2+} block than 2A^{N615K}/2A ($t(5.3) = 4.6$, $p_{corr} < 0.04$) and 2A^{N615K}/2B ($t(10.3) = 6.9$, $p_{corr} < 0.0003$). 2A^{N615K}/2A did not show significantly higher Mg^{2+} block than 2A^{N615K}/2B at this concentration. Post hoc paired t–tests comparing holding potentials showed that Mg^{2+} block at –40 mV was significanty less than at –60 mV ($t(33) = 7.3$, $p_{corr} < 3e{-}7$), which was significantly less than at – 80 mV ($t(33) = 5.6$, $p_{corr} < 4e{-}5$).

See Tables 4.9 and 4.10 for samples sizes and summary values.

Table 4.9: 1 mM Mg^{2+} block in wild type and GluN2A^{N615K} containing diheteromers and triheteromers

	Holding potential			
GluN2 subunits	–80 mV	–60 mV	–40 mV	n
2A WT	105 ± 2	102 ± 1	97 ± 1	11
2A/2B	108 ± 2	102 ± 1	97 ± 1	13
2B WT	111 ± 2	104 ± 1	97 ± 2	13
2A^{N615K}/2A	69 ± 2	53 ± 2	37 ± 3	19
2A^{N615K}/2B	55 ± 2	36 ± 1	23 ± 1	18
2A^{N615K}	14 ± 1	8 ± 1	7 ± 1	12

Table 4.10: 100 μM Mg^{2+} block in wild type and GluN2A^{N615K} containing diheteromers and triheteromers

	Holding potential			
GluN2 subunits	–80 mV	–60 mV	–40 mV	n
2A WT	97 ± 1	89 ± 1	64 ± 3	4
2A/2B	104 ± 2	95 ± 4	70 ± 1	5
2B WT	97 ± 4	89 ± 5	71 ± 4	6
2A^{N615K}/2A	38 ± 4	26 ± 5	13 ± 4	6
2A^{N615K}/2B	24 ± 1	15 ± 2	10 ± 3	8
2A^{N615K}	8 ± 2	6 ± 1	4 ± 1	5

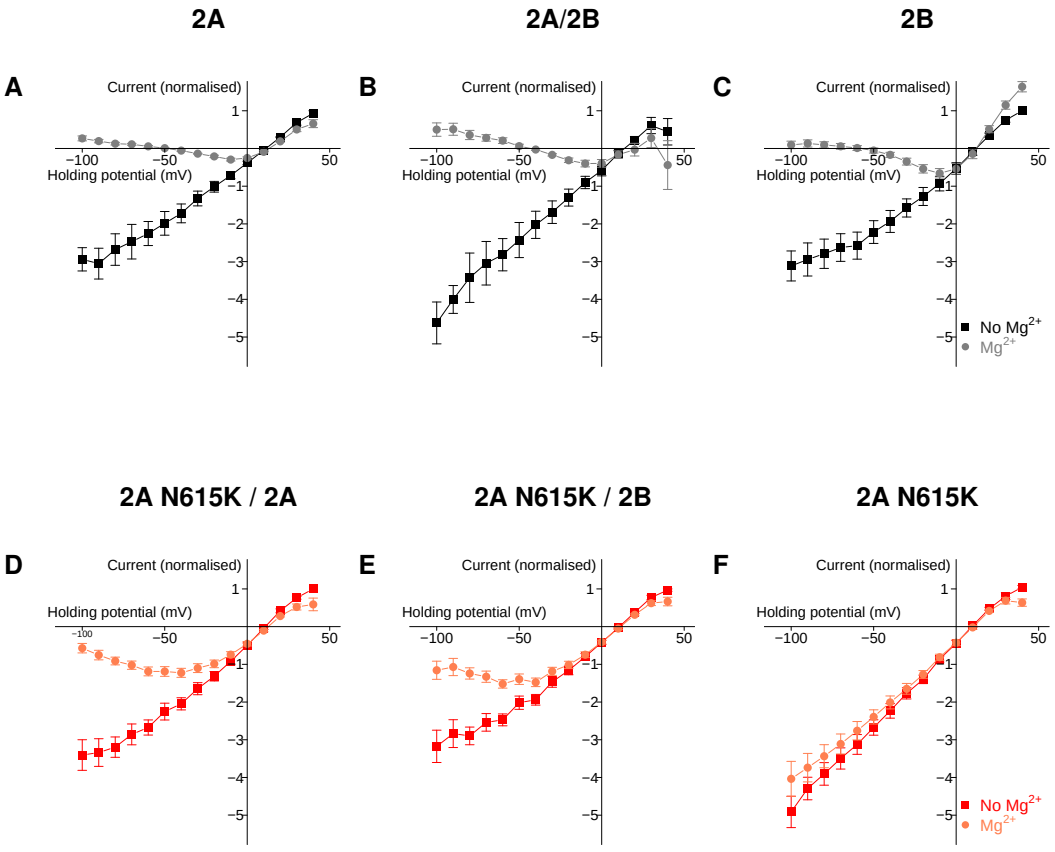

Figure 4.11: **Mg^{2+} block is reduced in GluN2A^{N615K} mutant diheteromers and triheteromers: current–voltage curves**

(A-F) Current-voltage plots showing a similar extent of Mg^{2+} block for diheteromeric and triheteromeric wild type subunits (2A (n = 6), 2A/2B (n = 6), 2B (n = 4)), but a reduction in block for 2A^{N615K}/2A triheteromers (n = 15), a further reduction with 2A^{N615K}/2B triheteromers (n = 13) and almost negligible block with 2A^{N615K} diheteromers (n = 6).

4.4.2 Mg^{2+} block kinetics

The kinetics of Mg^{2+} block were measured using the experimental set up described in Section 4.5.1 and analysed as described in the Methods chapter (Section 2.3.3). Only recordings made in the presence of 1 mM Mg^{2+} at –80 mV were analysed, as larger amplitude responses can be fitted most accurately.

4.4.2.1 Mg^{2+} block on rates

Data showing Mg^{2+} block on rates are presented in Figure 4.12 and Table 4.11. These data are highly variable, reflecting the technical difficulty of achieving exactly timed solution exchange across cells of different size and slightly different position relative to the solution interface. Variability may also be introduced by the difficulty in fitting the low amplitude, slow onset of Mg^{2+} block in GluN2A^{N615K} diheteromers. These issues mattered less for the glutamate deactivation rates reported earlier in the chapter as their time courses are much longer, and amplitudes larger. However, the detection of between group differences for the rapid on/off rates of Mg^{2+} ideally requires a larger number of cells, and this experiment lacked power to identify all possible differences. With the awareness that there may be some type II errors, some conclusions can be drawn from these data. The first finding is that there is no difference in Mg^{2+} block on rates between wild type subunits: all block rapidly. Secondly, there is no difference between GluN2A^{N615K} mutant triheteromers containing a GluN2A or GluN2B wild type partner. Data for receptors with “0” mutant subunits (wild type) was therefore pooled, as was that for NMDARs with one mutant subunit, presented in Figure 4.12C. This led to the third finding: triheteromers containing one mutant GluN2A^{N615K} subunit show a slower Mg^{2+} on rate than wild type diheteromers. This is an interesting finding both because it provides further evidence of the dominant negative effect of the GluN2A^{N615K} mutation, and also because it strengthens the evidence that mutant triheteromers are being generated rather than a mixed population of wild type and mutant diheteromers. If a mixed population was present, nearly all of the Mg^{2+} block seen would be due to wild type diheteromers, and their larger amplitude, more rapid component would be expected to dominate the fit parameters.

Table 4.11: Mg^{2+} (1 mM) on rates in wild type and GluN2A^{N615K} containing diheteromers and triheteromers in the continuous presence of glutamate (1 mM)

GluN2 subunits	Tau fast (ms)	Tau slow (ms)	% fast	Tau weighted (ms)	n
2A WT	1.9 ± 0.1	314 ± 32	96 ± 1	12.5 ± 3.6	11
2A/2B	2.1 ± 0.2	325 ± 62	96 ± 1	17.3 ± 5.6	13
2B WT	2.4 ± 0.3	211 ± 34	95 ± 1	12.0 ± 2.3	14
No mutant subunits	$\mathbf{2.2 \pm 0.1}$	$\mathbf{280 \pm 27}$	$\mathbf{96 \pm 1}$	$\mathbf{14.0 \pm 2.3}$	**38**
2A^{N615K}/2A	3.7 ± 0.3	273 ± 23	75 ± 3	69.2 ± 10.5	19
2A^{N615K}/2B	3.4 ± 0.3	265 ± 26	77 ± 4	62.6 ± 11.3	17
1 mutant subunit	$\mathbf{3.6 \pm 0.2}$	$\mathbf{269 \pm 17}$	$\mathbf{76 \pm 3}$	$\mathbf{66.1 \pm 7.6}$	**36**
2A^{N615K} 2 mutant subunits	$\mathbf{5.2 \pm 0.8}$	$\mathbf{341 \pm 87}$	$\mathbf{65 \pm 9}$	$\mathbf{140.7 \pm 54.8}$	**13**

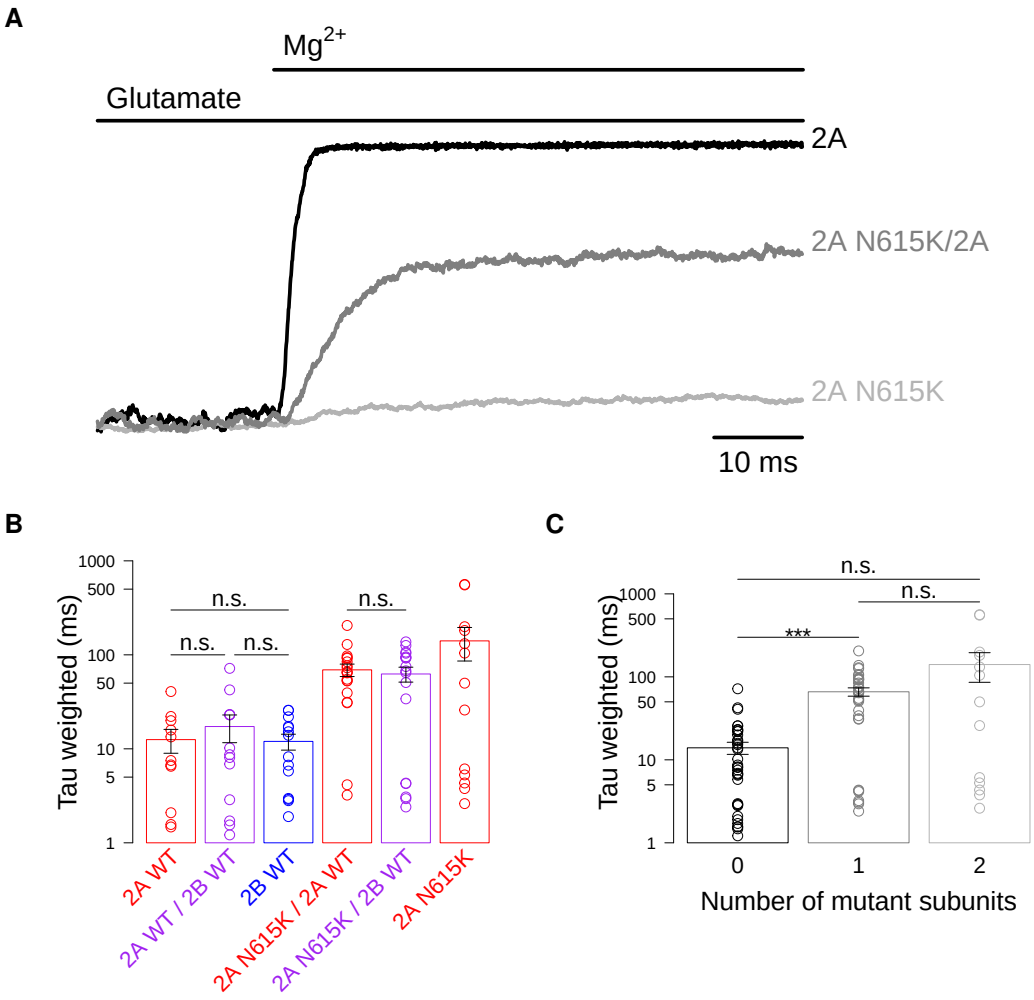

Figure 4.12: **Triheteromers containing GluN2A^{N615K} have slower Mg^{2+} on rates**
(A) Representative whole-cell voltage-clamp recordings from HEK293T cells expressing wild type 2A diheteromers, 2A^{N615K}/2A triheteromers and 2A^{N615K} diheteromers, showing inhibition by Mg^{2+}. Responses are normalised to the peak amplitude.
(B) The bar graph shows Mg^{2+} on rate weighted time constants for wild type and 2A^{N615K} containing NMDARs. t–tests showed no significant differences between wild type subunits, or between triheteromers containing one 2A^{N615K} subunit. These NMDARs were therefore pooled for subsequent analysis.
(C) The bar graph shows glutamate deactivation weighted time constants with pooling of NMDARs carrying zero, one or two mutant subunits. A one-way ANOVA showed a significant effect of mutation number ($F(2,84) = 12.6$, $p < 2e{-}5$), with post hoc t–tests (Bonferroni corrected) demonstrating a significant difference between NMDARs containing no mutations and triheteromers containing one mutation ($t(41.5) = 6.6$, $p_{corr} = 2e{-}7$).
See Table 4.11 for summary values and sample sizes.

4.4.2.2 Mg^{2+} block off rates

Data showing Mg^{2+} block off rates are presented in Figure 4.13 and Table 4.12. Comparing off rates between subunits shows a very similar pattern to what was found for on rates. All the wild type subunits show the same off rate. Triheteromers with one mutant GluN2A^{N615K} show the same off rate whether partnered with wild type GluN2A or GluN2B. When data is pooled by number of mutant subunits, it can be seen that triheteromers containing only one mutant GluN2A^{N615K} subunit show an off rate which is intermediate between wild type and mutant diheteromers, and significantly slower than that seen in wild type diheteromers.

Table 4.12: Mg^{2+} (1 mM) off rates in wild type and GluN2A^{N615K} containing diheteromers and triheteromers in the continuous presence of glutamate (1 mM)

GluN2 subunits	Tau fast (ms)	Tau slow (ms)	% fast	Tau weighted (ms)	n
2A WT	24 ± 2	183 ± 58	92 ± 5	30 ± 3	11
2A/2B	22 ± 3	180 ± 42	89 ± 6	34 ± 6	13
2B WT	22 ± 4	213 ± 69	85 ± 3	40 ± 5	14
No mutant subunits	$\mathbf{22 \pm 2}$	$\mathbf{198 \pm 38}$	$\mathbf{89 \pm 3}$	$\mathbf{35 \pm 3}$	**37**
$2A^{N615K}$/2A	23 ± 5	285 ± 31	84 ± 3	62 ± 6	19
$2A^{N615K}$/2B	17 ± 2	204 ± 19	84 ± 2	46 ± 4	17
1 mutant subunit	$\mathbf{20 \pm 3}$	$\mathbf{246 \pm 20}$	$\mathbf{84 \pm 2}$	$\mathbf{54 \pm 4}$	**36**
$2A^{N615K}$ 2 mutant subunits	$\mathbf{18 \pm 5}$	$\mathbf{230 \pm 43}$	$\mathbf{77 \pm 6}$	$\mathbf{76 \pm 18}$	**13**

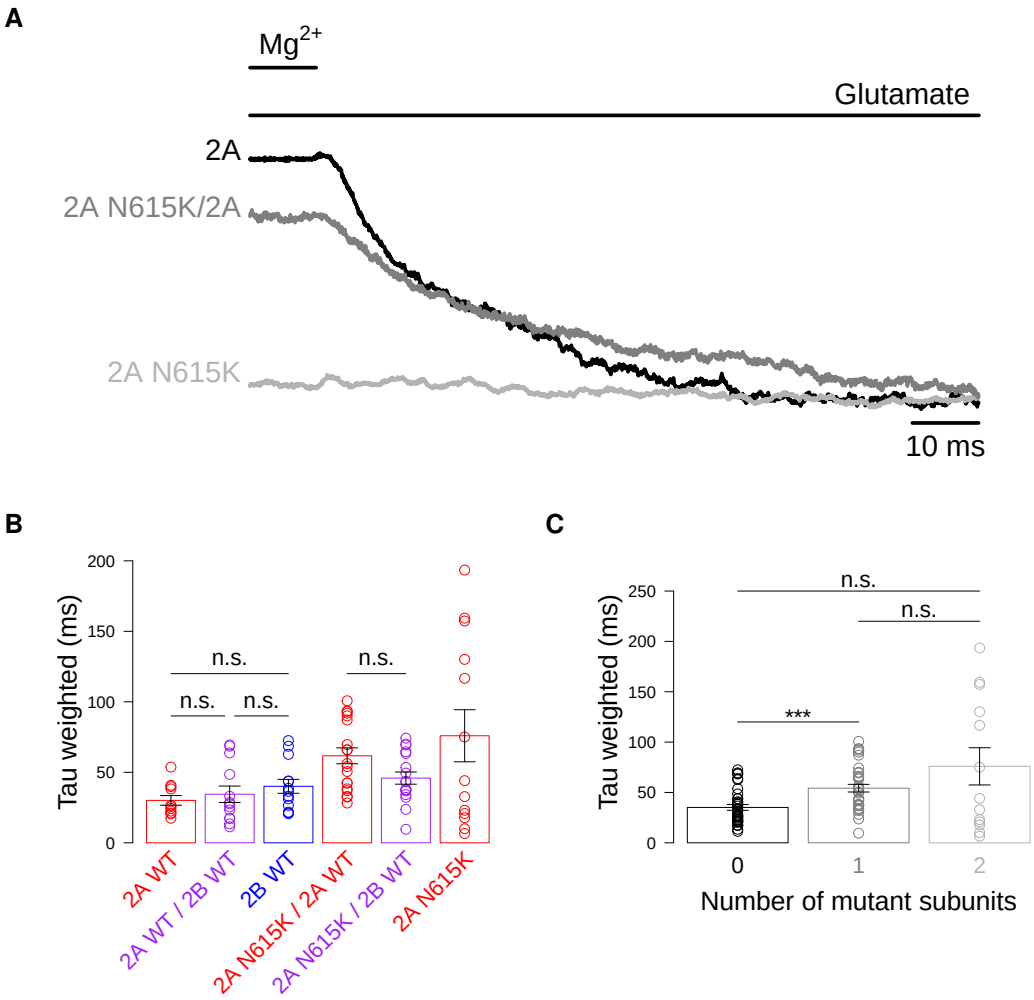

Figure 4.13: **Triheteromers containing GluN2A^{N615K} have slower Mg^{2+} off rates**
(A) Representative whole-cell voltage-clamp recordings from HEK293T cells expressing wild type 2A diheteromers, 2A^{N615K}/2A triheteromers and 2A^{N615K} diheteromers, showing inhibition by Mg^{2+}. Responses are normalised to the peak amplitude.
(B) The bar graph shows Mg^{2+} off rate weighted time constants for wild type and 2A^{N615K} containing NMDARs. t–tests showed no significant differences between wild type subunits, or between triheteromers containing one 2A^{N615K} subunit. These NMDARs were therefore pooled for subsequent analysis.
(C) The bar graph shows glutamate deactivation weighted time constants with pooling of NMDARs carrying zero, one or two mutant subunits. A one way ANOVA showed a significant effect of mutation number ($F(2,83) = 8.8$, $p < 0.0004$), with post hoc t–tests (Bonferroni corrected) demonstrating a significant difference between NMDARs containing no mutations and triheteromers containing one mutation ($t(65.5) = 4.0$, $p_{corr} < 0.0005$).
See Table 4.12 for summary values and sample sizes.

4.5 Mg^{2+} block in diheteromeric NMDARs containing GluN2B^{N615I} or GluN2B^{V618G} subunits

The generation of triheteromers containing one mutant GluN2B subunit (either GluN2B^{N615I} or GluN2B^{V618G}) was more vulnerable to diheteromeric escape current than that of triheteromers containing the mutant GluN2A^{N615K} subunit (see Section 4.3.3). Triheteromers containing either GluN2B mutant are therefore not considered further here. However, there were no difficulties in generating diheteromeric GluN2B mutant NMDARs, whose properties are described further below.

4.5.1 Mg^{2+} percentage inhibition

GluN2B^{N615I} and GluN2B^{V618G} diheteromers have been shown to alter Mg^{2+} block in this study (Chapter 3) and by others (Lemke et al., 2014). However, work done in the previous chapter was in transfected neurons and thus represented a mixed population of wild type and mutant subunit containing NMDARs. The brief functional characterisation performed by Lemke et al., used *Xenopus laevis* oocytes as an expression system, with a small sample size, and did not report kinetics. It was therefore of interest to investigate the properties of the GluN2B pore mutant diheteromers in the alternative expression system of HEK293T cells.

The extent of Mg^{2+} block was investigated as described in Section 4.5.1. Representative traces are shown in Figure 4.14. Data showing percentage Mg^{2+} block in cells expressing wild type, GluN2B^{N615I} and GluN2B^{V618G} diheteromeric NMDARs are presented in Figures 4.15 and 4.16. The most startling aspect of these data is the significant potentiation of current elicited by Mg^{2+} in both mutant subunits. This was an unexpected and surprising finding, repeated across multiple experimental days and transfections.

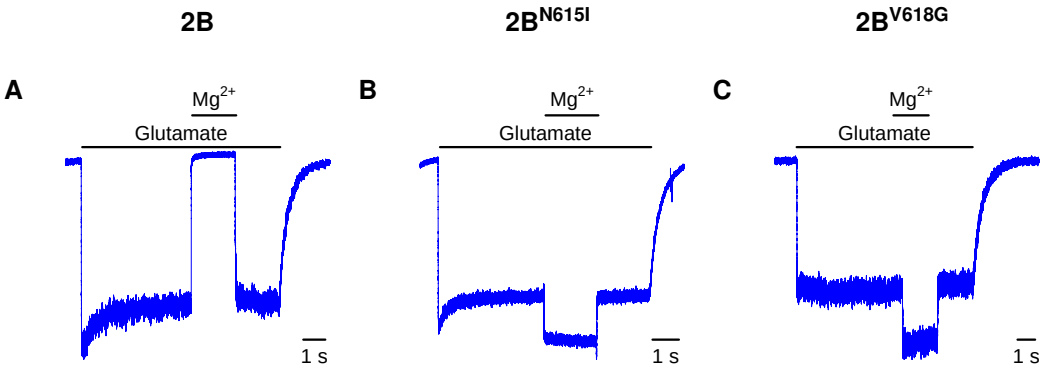

Figure 4.14: **Mg^{2+} potentiates current in 2B mutant diheteromers: representative traces (A–C)** Representative whole-cell voltage-clamp recordings from HEK293T cells expressing the subunits indicated during exposure to glutamate (1 mM) and Mg^{2+} (1 mM) while held at –60 mV. Responses normalised to peak amplitude.

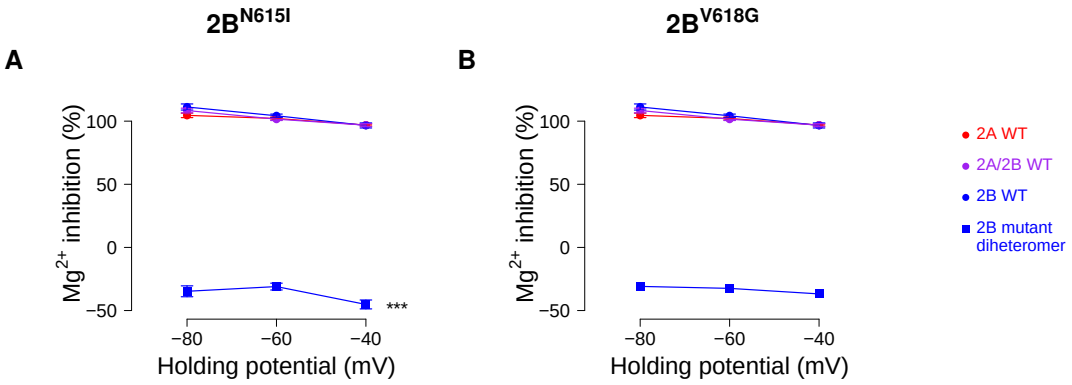

Figure 4.15: **Mg^{2+} potentiates current in 2B mutant diheteromers**
(A) Summary data showing 1 mM Mg^{2+} block at three holding potentials for wild type NMDARs and $2B^{N615I}$ containing diheteromers (with wild type C termini). Stars indicate significance level of comparison of means of $2B^{N615I}$ diheteromers with 2B wild type diheteromers. A two-way repeated measures ANOVA showed a significant main effect of subunit ($F(3, 39) = 538$, $p <$ 2e–16) and of holding potential ($F(2, 78) = 81.8$, $p = 0.001$). There was also a significant interaction ($F(2, 78) = 4$, $p = 0.001$), however, as the key contrasts of interest were between subunits, the interaction of subunit with holding potential in determining Mg^{2+} block was not explored. Post hoc t–tests (Bonferroni corrected) showed no significant differences between Mg^{2+} block in wild type subunits. However, Mg^{2+} block was significantly reduced ($t(6.9) = 47$, $p_{corr} <$ 3e-9) in $2B^{N615I}$ (-37 $\pm$ 4, n = 6) compared to 2B (104 $\pm$ 3, n = 13). Post hoc paired t–tests comparing holding potentials showed that Mg^{2+} block at –40 mV was significanty less than at –60 mV ($t(42) = 8.5$, $p_{corr} <$ 6e–10), which was significantly less than at – 80 mV ($t(42)$ = 3.9, $p_{corr} <$ 0.002).

(B) Summary data showing 1 mM Mg^{2+} block at three holding potentials for wild type NMDARs and $2B^{V618G}$ containing diheteromers (with wild type C termini). A two-way repeated measures ANOVA showed a significant main effect of subunit ($F(3, 34) = 249$, $p <$ 2e–16) and of holding potential ($F(2, 68) = 96.1$, $<$ 2e–16). Post hoc t–tests (Bonferroni corrected) showed no significant differences between Mg^{2+} block in wild type subunits. As only one cell expressing $2B^{V618G}$ was recorded from, statistical tests could not be performed. However, the same potentiation effect was apparent as seen with $2B^{N615I}$ (Mg^{2+} block in $2B^{V618G}$ (-33, n = 1)). Post hoc paired t–tests comparing holding potentials showed that Mg^{2+} block at –40 mV was significanty less than at –60 mV ($t(37) = 8.6$, $p_{corr} <$ 2e–9), which was significantly less than at – 80 mV ($t(37) = 6.0$, $p_{corr} <$ 4e-6).

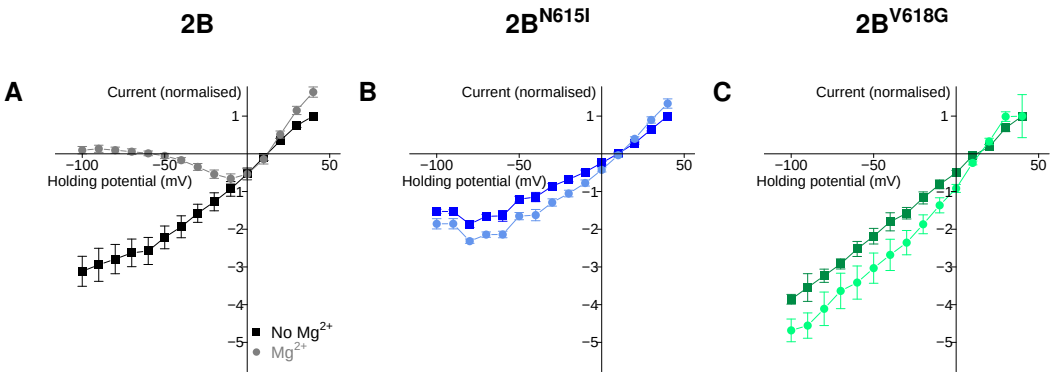

Figure 4.16: **Mg^{2+} potentiates current in 2B mutant diheteromers: current–voltage curves** **(A-C)** Current-voltage plots showing a potentiation of current in the presence of Mg^{2+} at all negative holding potentials with diheteromeric $2B^{N615I}$ (n=6) and $2B^{V618G}$ (n=3) but not wild type 2B (n=4).

Some preliminary experiments were performed to consider some potential mechanisms by which this potentiation may arise. Firstly, current-voltage curves were repeated in a higher concentration of external Ca^{2+} (2 mM vs. 0.5 mM) (see Figure 4.17). If the increased current were due to an increased Ca^{2+} conductance, the current potentiation would be predicted to be higher in the presence of high Ca^{2+} than low Ca^{2+}, and the reversal potential to have shifted more positively (towards that of Ca^{2+}). The data in Figure 4.17 do not show this pattern convincingly, albeit they represent a small number of experiments.

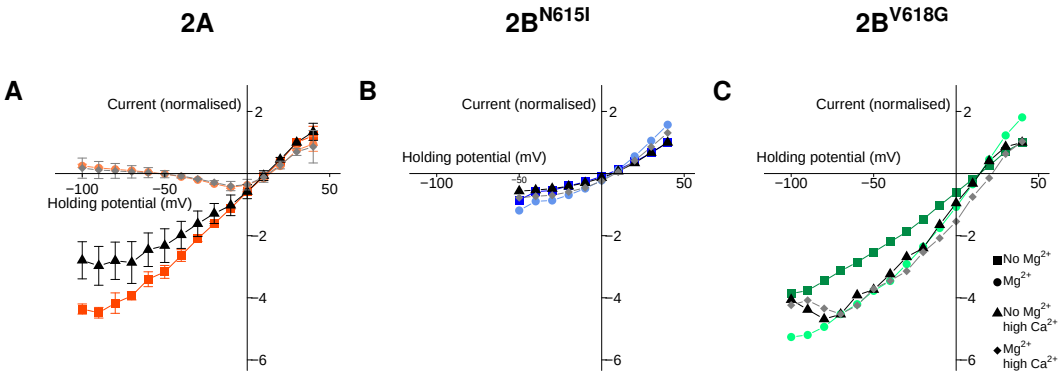

Figure 4.17: **Potentiation of current by Mg^{2+} in 2B mutant diheteromers is unlikely to be due to increased Ca^{2+} conductance**
(A-C) Current-voltage plots showing no influence of increasing Ca^{2+} concentration on potentiation of current by Mg^{2+} in diheteromeric wild type 2A (n=3), $2B^{N615I}$ (cell not recorded from below –50 mV) and $2B^{V618G}$. Low Ca^{2+} = 0.5 mM, high Ca^{2+} = 2 mM.

Secondly, current-voltage curves were repeated with a higher concentration of external Mg^{2+} (10 mM vs 1 mM) (Figure 4.18). If the increased current were due to a new Mg^{2+} conductance, the current potentiation would be predicted to be higher in the presence of high Mg^{2+} than low Mg^{2+}, and the reversal potential to have shifted more positively (towards that of Mg^{2+}). Alternatively, if Mg^{2+} was increasing open probability, or an existing conductance (e.g. Na^{+}), current potentiation would be seen without an alteration in reversal potential. The latter pattern is what the preliminary data in Figure 4.18 suggest. $GluN2B^{V618G}$ diheteromers exhibit an approximately 1.5–fold increase in current in the presence of 1 mM Mg^{2+} and an approximately four-fold increase in current in the presence of 10 mM Mg^{2+}, without

a notable shift in reversal potential. Further, the effect does not appear to be voltage-dependent. In summary, the potentiation of current by Mg^{2+} in GluN2B mutant diheteromers is dose-dependent and voltage-independent, and is unlikely to be due to alterations in Mg^{2+} or Ca^{2+} conductance.

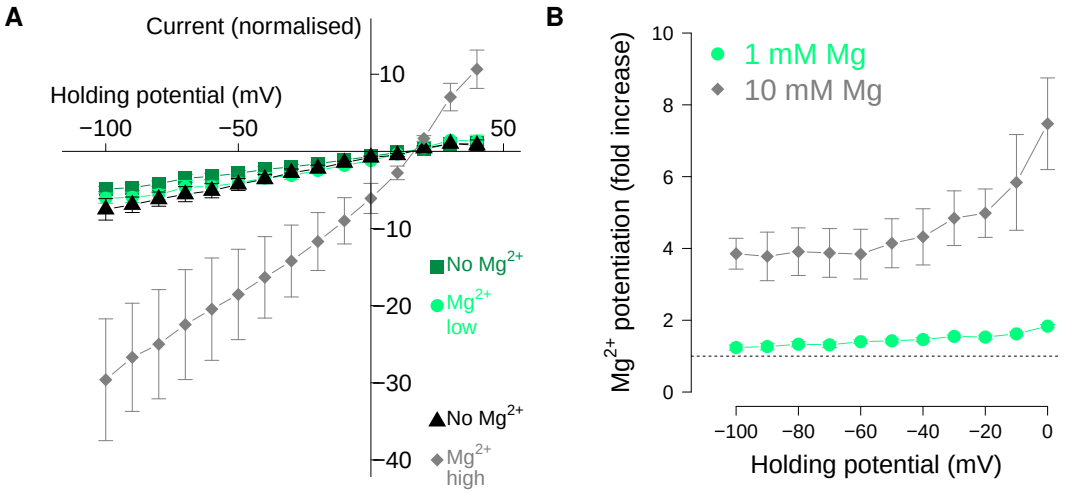

Figure 4.18: **Increasing Mg^{2+} concentration increases Mg^{2+} potentiation in GluN2B^{V618G} mutant diheteromers**

(A) The current-voltage plot shows that increasing Mg^{2+} concentration from low (1 mM) to high (10 mM) is associated with a large increase in potentiation of current in diheteromeric 2B^{V618G} NMDARs (n=3), without alteration in reversal potential.

(B) The plot shows fold potentiation against holding potential for two different Mg^{2+} concentrations (1 mM and 10 mM). The dotted line marks 1, no potentiation. Only negative holding potentials are shown as very small currents at positive holding potentials led to a wide spread of potentiation values. At the holding potentials shown, 1 mM Mg^{2+} is associated with a mean fold potentiation of 1.45 $\pm$ 0.05 and 10 mM Mg^{2+} with a mean fold potentiation of 4.6 $\pm$ 0.34. The degree of potentiation is voltage-independent (the increase in potentiation seen with 10 mM Mg^{2+} approaching a holding potential of zero likely reflects error due to small currents).

4.5.2 Mg^{2+} potentiation kinetics

Mg^{2+} potentiation on and off rates are shown in Table 4.13. As they are quantifying a different process to what is occurring in wild type diheteromers (potentiation rather than block), it is not meaningful to compare them against wild type receptors.

Table 4.13: Kinetics of Mg^{2+} potentiation in GluN2B pore mutant diheteromers.

GluN2 subunits	Tau fast (ms)	n
Mg^{2+} on		
$GluN2B^{N615I}$	14 ± 3	6
$GluN2B^{V618G}$	11	1
Mg^{2+} off		
$GluN2B^{N615I}$	11 ± 1	6
$GluN2B^{V618G}$	9	1

Time courses were fitted well by a single exponential.

4.6 Discussion

4.6.1 Summary of findings

This chapter employed a recently developed technique to dictate the subunit composition of NMDARs. This allowed the generation of NMDARs containing zero, one or two mutant subunits, as required. The key finding is that the disease–associated mutation GluN2A^{N615K} has a dominant negative effect on Mg^{2+} block when incorporated into triheteromers with wild type GluN2 subunits. This supports its role in disease causation. It was also found that the GluN2A^{N615K} mutation slows Mg^{2+} on and off rates, that diheteromeric GluN2B^{N615I} and GluN2B^{V618G} mutant subunits cause potentiation of current by Mg^{2+}, and that none of the pore mutations influence glutamate deactivation rates.

4.6.2 GluN2A^{N615K} reduces Mg^{2+} block in di– and triheteromeric NMDARs

The finding of substantially reduced Mg^{2+} block in GluN2A^{N615K} diheteromers replicates previous work (Endele et al., 2010), and the oocyte work reported in Chapter 3. As described more fully in Chapter 3's discussion, this effect is likely to be due to the substitution of a positively charged lysine residue in place of a neutral asparagine at a residue previously found to be a strong determinant of Mg^{2+} block (Wollmuth et al., 1998).

The finding that one GluN2A^{N615K} subunit is enough to cause significantly reduced Mg^{2+} block in triheteromers extends the work previously done in diheteromers by demonstrating that the GluN2A^{N615K} mutation alters NMDAR properties in the subunit composition most likely to arise physiologically: GluN2A^{N615K}/GluN2B-containing NMDARs. The dominant negative effect in partnership with either wild type subunit demonstrates that the wild type residues are insufficient to fully counteract the repulsion of Mg^{2+} by the introduced lysine residue. The effect of GluN2A^{N615K} on Mg^{2+} block was less marked in partnership with wild type GluN2A, which was an unexpected finding. The residues known to be important for Mg^{2+} binding (the "N" site, "N+1" site, and "S/L" site) are identical in GluN2A and GluN2B. Despite this, differences in Mg^{2+} block exist: GluN2A exhibits slightly faster Mg^{2+} off rates than GluN2B (Clarke et al., 2013; Clarke and Johnson, 2008). The impact of subunit identity may therefore arise via some as yet unidentified difference in sequence between the two subunits which influences Mg^{2+} block.

Interestingly, a recent investigation of the impact of human *GRIN2A* mutations on Zn^{2+} sensitivity in diheteromeric and triheteromeric NMDARs also found that the influence on triheteromers varied with whether the wild type partner was GluN2A or GluN2B, with a GluN2A partner associated with Zn^{2+} sensitivity that was closer to wild type (Serraz et al., 2016). The interpretation of this finding is complicated by the different Zn^{2+} sensitivities of wild type GluN2A and GluN2B subunits. However, it may point to an underlying principle of subtle differences in conformation between assemblies of GluN2 subunits which are the same or different. This possibility could be investigated by introducing a GluN2A mutation at the equivalent site in a GluN2B subunit (for example, GluN2B^{N616K}), and comparing Mg^{2+} block in GluN2B^{N616K}/GluN2B receptors versus GluN2B^{N616K}/GluN2A receptors (if same versus different subunit identity was important in mediating the impact of the mutation, the GluN2B only receptors would show a smaller reduction in Mg^{2+} block than the GluN2B/GluN2A receptors).

4.6.3 GluN2A^{N615K} slows Mg^{2+} block on and off rates

GluN2A^{N615K} was found to slow Mg^{2+} block kinetics when expressed as part of diheteromeric or triheteromeric NMDARs. This slowing likely reflects the alteration in Mg^{2+} binding residues. No previous work has addressed Mg^{2+} block kinetics in the GluN2A^{N615K} mutant subunit, but the off rates of wild type subunits (driven by hyperpolarisation rather than concentration change) have been previously found to be well fitted by two exponentials with τ_{fast} of around 1 ms (Clarke et al., 2013) and a τ_{slow} of 1.2 ms. This study's estimate of a τ_{fast} of 22 ms in wild type NMDARs is substantially higher than that detected by voltage steps, probably because the time for solution exchange (0.7–0.9 ms, from with Mg^{2+} to without Mg^{2+} or vice versa) is much longer than the time taken to change holding potential. Although the time constants identified here are longer than those identified previously by a different method, the comparisons between subunits still stand.

A slowing of Mg^{2+} on and off rates is of physiological relevance as this could influence the coincidence detection properties of the NMDARs required for spike-timing-dependent synaptic plasticity: a longer period of post-synaptic depolarisation would be required to ensure removal of Mg^{2+} block before current could pass through NMDARs containing mutant subunits. Similarly, once a post-synaptic cell was no longer depolarised, the unblocked NMDARs would take longer to reblock, potentially passing current stimulated by uncoordinated activity. It would be interesting to explore this further, potentially by computational modelling.

4.6.4 GluN2B^{N615I} and GluN2B^{V618G} cause Mg^{2+} current potentiation

The finding that the GluN2B pore mutant diheteromers caused potentiation of currents in the presence of Mg^{2+} was very unexpected. The results in Chapter 3 showed an overall reduction in Mg^{2+} block in a mixed population of NMDARs containing wild type and mutant subunits. This was initially interpreted as the majority of receptors showing a reduction in block, but is also consistent with a minority of receptors showing potentiation of current. Previously published work reported a reduction in Mg^{2+} block to 15% (n=3) in GluN2B^{N615I} diheteromers and 49% (n=3) in GluN2B^{V618G} diheteromers, with a wild type block of 96% (Lemke et al., 2014). However, inspection of the representative traces suggests that these data refer to differences in peak responses and the steady state response for GluN2B^{N615I} is in fact larger in the presence of Mg^{2+} (see Figure 4.19).

The mechanism of how the GluN2B pore mutations allow Mg^{2+} to potentiate current has not been confirmed in this study. Preliminary investigations suggested that the effect is dependent on the concentration of Mg^{2+} but is not due to Mg^{2+} itself being conducted, or more Ca^{2+} being conducted. This suggests that Mg^{2+} may be influencing open probability, or the conductance of Na^{+}, or the potency of glutamate. A little discussed finding is that GluN2B diheteromers have previously been shown to demonstrate potentiation by Mg^{2+}, in a manner non-additive with spermine (Paoletti et al., 1995). As the channel is normally blocked by Mg^{2+} at resting membrane potentials, this potentiation normally only emerges at positive membrane potentials. An intriguing possibility is that the GluN2B pore mutations are preventing Mg^{2+} block and thus exposing Mg^{2+} potentiation via the spermine site at all potentials. It is now known that spermine potentiates current through NMDARs by binding to the subunit-interface between GluN2B and GluN1 and stabilising the N termini in a way that increases open probability (Mony et al., 2011; Sirrieh et al., 2015). It is also known that spermine potentiation is not present in NMDARs

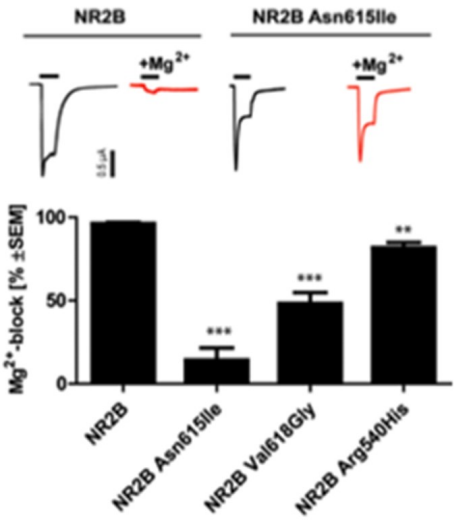

Figure 4.19: **Mg^{2+} block in GluN2B pore mutants: previous work**
Taken from (Lemke et al., 2014). Representative traces showing Mg^{2+} block in wild type 2B and $2B^{N615I}$ diheteromers, with data quantified in the bar chart.

containing the "b" splice variants of GluN1 and is pH-sensitive and voltage-independent. The findings in this study are consistent with these properties, in that the GluN1-1a splice variant was used, and the potentiation is not voltage-dependent. Further, the 4.6-fold mean potentiation seen here with 10 mM Mg^{2+} is very similar to the 3.9 mean potentiation observed by Paoletti et al. (1995) at the same Mg^{2+} concentration. It would therefore be possible to test the hypothesis that the potentiation of current by Mg^{2+} observed in diheteromeric GluN2B pore mutant NMDARs is via Mg^{2+} acting at the spermine site by: testing the pH sensitivity of the potentiation, the influence of GluN1 splice variant a versus b, and by introducing additional mutations into the spermine site.

It proved more difficult to generate triheteromers containing GluN2B pore mutants than triheteromers containing $GluN2A^{N615K}$. This may simply be a chance finding arising due to the small number of cells recorded in the GluN2B mutant groups. Alternatively, the GluN2B pore mutants with modified C termini may have a faster deactivation rate than wild type, as suggested by the finding that $GluN2B^{N615I}{}_{C1C2}$ receptors had a slightly faster deactivation rate than $GluN2B^{N615I}$ receptors. It is also possible that the GluN2B mutations may in some way inhibit the assembly or trafficking of subunits with modified C termini, allowing undesired diheteromers to have an increased escape probability. Further work to explore this would be initially to repeat the experiments with a larger sample size, and potentially to explore the impact of varying the ratios of GluN2 subunits transfected (potentially increasing the ratio of GluN2B pore mutant subunits to wild type subunits would increase the probability of their expression). In any case, findings in GluN2B diheteromers are still of high physiological relevance, as GluN2B diheteromers are the dominant form of forebrain NMDARs during early development (Monyer et al., 1994).

4.6.5 None of the pore mutants affected glutamate deactivation rates

It was found that none of the pore mutations affect glutamate deactivation rates. This is unsurprising, as none of the mutations affect residues previously implicated in NMDAR deactivation (see Section 1.4.3 in

the Introduction). This suggests that alterations in deactivation following glutamate exposure are not part of the mechanism by which these mutations may cause disease, unlike what has been found for another disease-associated NMDAR mutation (Yuan et al., 2014).

4.6.6 Limitations

Although representing a significant advance in the understanding of NMDARs, both the recently published approaches allowing expression of triheteromeric NMDARs have limitations (Hansen et al., 2014; Stroebel et al., 2014). Both methods require substantial modifications of the NMDAR C termini, which means this approach cannot be used to explore triheteromeric properties related to C terminus function. Hansen's approach requires replacement of the GluN2B C termini with that of GluN2A, in order to reduce steric complications created by the substantial differences in sequence between subunits in this domain. Stroebel's approach requires complete removal of both C termini. It is therefore possible that the findings in this chapter are not relevant to the *in vivo* effect of the mutations studied because of the modified C termini employed to generate the receptors for study. However, it is reassuring to note that swapping GluN2A and GluN2B C termini has previously been found not to influence receptor deactivation rates and open probability (Punnakkal et al., 2012), suggesting that the C terminus has more of a permissive than a modulatory role in these receptor properties. The findings in this chapter are also limited in that other NMDAR subunit partnerships have not been investigated. For example, GluN2A^{N615K} with GluN2C or GluN2D, although there is little evidence so far that these subunit combinations arise frequently physiologically.

4.6.7 Conclusion

This chapter has provided further evidence that the GluN2A^{N615K}, GluN2B^{N615I} and GluN2B^{V618G} mutations influence fundamental properties of physiological configurations of NMDARs in a way consistent with causing the neurodevelopmental disorders experienced by their carriers. To achieve further insights into the impact of these mutations on brain function, the obvious next step would be an animal model.

CHAPTER 5

Validation and initial functional assessment of two new rat models: constitutive and conditional knock-out of GluN2A

5.1 Chapter summary and key findings

1. Two genetically modified rats were created: one carrying LoxP sites flanking exon 8 of *Grin2a* (*Grin2a*$^{flox/flox}$) and one carrying a deletion of exon 8 of *Grin2a* (*Grin2a*$^{-/-}$). The genetic alterations were confirmed by sequencing.

2. The *Grin2a*$^{flox/flox}$ rat was functionally validated: the LoxP sites alone do not influence *Grin2a* expression but do allow *Grin2a* knock-out in the presence of Cre recombinase.

3. The *Grin2a*$^{-/-}$ rat was functionally validated: homozygous animals show greatly reduced *Grin2a* mRNA expression, absent GluN2A protein and reduced incorporation of GluN2A into functional NMDARs as assessed electrophysiologically. Heterozygotes show intermediate mRNA, protein and functional levels.

4. A preliminary assessment of the physiological consequences of *Grin2a* knock-out and haploinsufficiency was performed. Neurons cultured from *Grin2a*$^{-/-}$ and *Grin2a*$^{-/+}$ rats showed lower current density and altered coordinated activity compared to *Grin2a*$^{+/+}$ rats. There was no effect on mEPSCs, mIPSCs or excitotoxicity.

5.2 Introduction

5.2.1 Generation of genetically modified rat lines

The findings of previous chapters have demonstrated that GluN2A^{N615K} is a mutation which profoundly influences crucial NMDAR properties in a dominant negative fashion. These findings support the hypothesis that GluN2A^{N615K} causes the epileptic encephalopathy experienced by its carrier. However, they do not prove this. Proof would be provided by a demonstration that removing or negating the consequences of the point mutation prevents or even reverses the neurodevelopmental disorder. No way to prevent the consequences of the point mutation has been identified for use in its human carrier (dextromethorphan could potentially be helpful, but would not fully block the functioning of the mutant subunits without also affecting wild type subunits). However, an animal model genetically engineered to carry the GluN2A^{N615K} mutation offers a way in which the impact of the presence and absence of the mutation can be assessed using genetic techniques. Specifically, the Cre-Lox system can be used, whereby the mutation is placed between two 5'-3' orientated LoxP sites and so can be excised when the DNA is exposed to Cre recombinase. By varying the timing of exposure to Cre recombinase, the impact of the mutation on development could be assessed, as could any critical window for any reversibility seen.

A major benefit to an animal model would be the opportunity to investigate the consequences of the mutation at a whole organism level, allowing in depth investigation of electrophysiological, circuit level and behavioural phenotypes with the aim of identifying pathological mechanisms. Genetically modified animal models also allow the effect of the mutation to be assessed when expressed at genomically driven levels, rather than overexpressed via viral promoters in plasmids or viruses. A rat was chosen as the model organism as they have a relatively complex behavioural repertoire, allowing more accurate assessment of phenotypes such as intellectual disability. In addition, they have brains large enough for structural and functional brain imaging to be performed *in vivo*.

A commercial organisation were employed to perform the genome editing using CRISPR/Cas9 technology. This is a recently developed approach (reviewed by Hsu et al. (2014)) where single cell embryos are injected with single guide RNAs (sgRNA) which bind to the desired genomic DNA site with high specificity, allowing recruitment of the Cas9 endonuclease, which cuts the DNA (in this case creating a double stranded break), which then stimulates the cell's own DNA repair pathways. The cell can repair DNA using either non-homologous end joining, which often results in small insertions or deletions and hence often gene knock-out, or homology directed repair, which, if exogenous template DNA is provided, can allow point mutations to be inserted. Figure 5.1 shows the desired genome modifications and strategy for achieving them.

To achieve the animal model desired here (*Grin2a*$^{T1845A(flox)/+}$), modification of a relatively large region of DNA was required: replacement of all of exon 8 (330 bp) with a donor exon containing the mutation, and insertion of LoxP sites into intronic regions 340 and 500 base pairs away from the exon. This required two double stranded breaks to be made and totalled 1170 bp of replacement. It transpired that this was too ambitious. Although a number of founder mutants were obtained where both LoxP sites were inserted, none of them also had the point mutation. It seemed that the genome editing was occuring in a two step process (see Figure 5.2A). First, one double stranded break would occur and undergo homology directed repair with incoporation of a LoxP site, but the donor DNA would not be

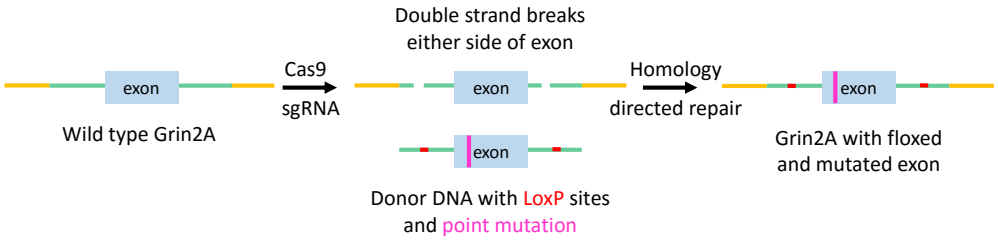

Figure 5.1: **Genome modification approach to generate *Grin2a*$^{T1845A(flox)/+}$**
This schematic shows the genome modification strategy designed to insert a floxed exon carrying the point mutation of interest into the rat genome. *Grin2a*$^{T1845A(flox)/+}$ encodes the mutation required to generate GluN2A^{N615K}. Single cell embryos were injected with two single guide RNAs which bound to 5' and 3' of *Grin2a* exon 8. These recruited the Cas9 endonuclease, which created double stranded breaks, stimulating the cell's own DNA repair pathways. Exogenous donor DNA was provided via a plasmid, containing a replacement exon (with point mutation) and left and right homology arms (green) flanking the double stranded breaks. It was anticipated this would be used to repair the double strand breaks using homology-directed repair. Yellow marks intronic DNA not included within the donor DNA.

required to repair as far as the exon and the point mutation would not be inserted. Second, a double stranded break would occur on the other side of the exon and the same process occur. The outcome was a floxed exon but no point mutation: *Grin2a*$^{flox/+}$.

In some cases two double stranded breaks did occur simultaneously, but were repaired using non-homologous end joining, not homology-directed repair (see Figure 5.2B). This resulted in deletion of exon 8: *Grin2a*$^{-/+}$.

The attempt to generate a *Grin2a*$^{T1845A(flox)/+}$ rat therefore resulted in the generation of two other genetically modified rat models: a *Grin2a*$^{flox/+}$ and a *Grin2a*$^{-/+}$ rat. Although this was not what was intended, these rat models are still potentially useful tools for addressing the overall question of this thesis: what are the functional consequences of mutations in *GRIN2A* and *GRIN2B* associated with mental disorder? This is because a large number of gene disrupting mutations in *GRIN2A* have been identified heterozygously in people with epilepsy-aphasia syndromes (see Section 1.6). Further, a locus near *GRIN2A* was identified as significantly associated with schizophrenia by genome wide association study (Ripke et al., 2014). Although the nature of the impact of this locus on *GRIN2A* (if any) remains to be identified, the most likely impact is that it is modifying the expression of *GRIN2A* in some way, most likely by reducing it (as there is already evidence of NMDAR hypofunction in schizophrenia (Snyder and Gao, 2013)). Thus, the *Grin2a*$^{-/+}$ rat is a useful model for investigating the pathophysiology of epilepsy-aphasia syndromes, with potential relevance also to schizophrenia. The *Grin2a*$^{flox/+}$ rat is useful as it allows the creation of a *Grin2a* knock-out at a range of developmental time points or in a subset of tissues or cell types, allowing potential key times and pathways to be determined.

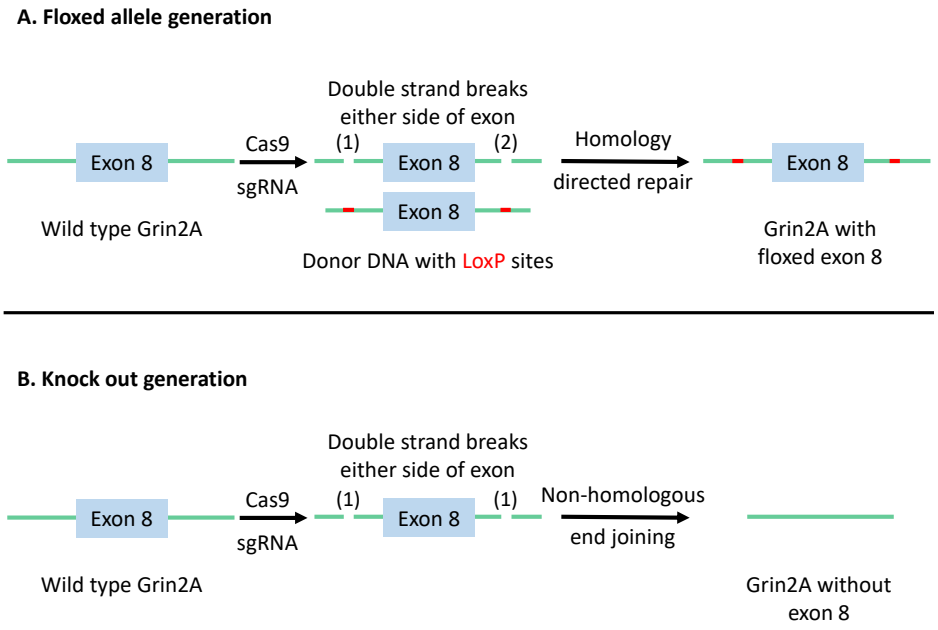

Figure 5.2: **Genome modification events that generated *Grin2a*$^{flox/+}$ and *Grin2a*$^{-/+}$**
This schematic shows the genome modifying events that were presumed to occur when genomes were exposed to the reagents designed to generate the *Grin2a*$^{T1845A(flox)/+}$ rat.
(A) Shows the events underlying generation of the *Grin2a*$^{flox/+}$ rat. Following exposure to sgRNAs, double stranded breaks probably occurred at separate times, allowing recruitment of different sections of the donor DNA for repair, and resulting in insertion of only the sections closest to the double stranded breaks (including the LoxP sites).
(B) Shows the events underlying generation of the *Grin2a*$^{-/+}$ rat. Following exposure to sgRNAs, double stranded breaks probably occurred at the same time, allowing the 5' and 3' ends of the cuts to be joined together using non-homologous end joining. This resulted in a 1065 bp deletion, including exon 8.

5.2.2 Experiments performed with genetically modified rat lines

Before any experiments regarding the role of *Grin2a* in neurodevelopmental disorder could be performed, it was first necessary to validate both models. This was done by sequencing the targeted genomic region, and by quantifying mRNA and protein levels. In the case of the *Grin2a*$^{flox/flox}$ model, a virus was used to confirm Cre-Lox mediated *Grin2a* knock-out.

In the case of the *Grin2a*$^{-/+}$ model, a reduction in GluN2A subunit functional incorporation was confirmed electrophysiologically. In Chapter 3 the GluN2A:GluN2B ratio was assessed using sensitivity to the GluN2B selective negative allosteric modulator, ifenprodil. A different approach was taken in this chapter: potentiation by spermine was used to assay the incorporation of GluN2A into surface NMDARs instead. Spermine is an endogenous polyamine that binds to the subunit interfaces between GluN2B and GluN1 N-terminus domains, increasing open probability of GluN2B diheteromeric NMDARs (Mony et al., 2011; Sirrieh et al., 2015).

A spermine potentiation assay was used here because new evidence suggested it should theoretically be more sensitive than ifenprodil inhibition. The recently developed ability to generate triheteromeric NMDARs (see Chapter 4 Introduction) allowed determination of their sensitivity to compounds modulating NMDARs. It was found that GluN2A/2B triheteromers had a sensitivity to ifenprodil intermediate between GluN2A and GluN2B (but closer to GluN2A) whereas triheteromers showed a potentiation by spermine identical to that of GluN2A (Stroebel et al., 2014). Thus, a given proportion of GluN2A expression should result in a bigger shift in spermine potentiation than in ifenprodil sensitivity, and be easier to detect.

The first part of the chapter addresses the validation of the new rat models. The remaining sections describe a preliminary asessment of functional consequences of GluN2A knock-out. The four functional domains investigated were current density, mEPSCs and mIPSCs, synchronised network activity, and excitotoxicity. A brief rationale for each of these areas is given below.

The magnitude of NMDA-evoked currents in cultured neurons normalised to cell size (current density) was assessed as it is a simple and important property which gives a measure of how many NMDARs a cell is expressing. If a cell is expressing fewer/more NMDARs this may have knock-on effects for all the processes NMDARs can influence. The hypothesis was that GluN2A knock-out would result in lower current density, because other NMDAR subunits would not be sufficiently upregulated to compensate.

mEPSCs are currents caused by activation of glutamate receptors by quantal release of glutamate at individual synapses. They are predominantly mediated by AMPA receptors (AMPARs). Increased amplitude indicates more AMPARs at a given synapse. Increased frequency represents more active synapses per cell, or a higher pre-synaptic vesicle release probability. mEPSCs were assessed because NMDARs can regulate AMPARs membrane trafficking to synapses, with different NMDAR subunits having different effects on AMPAR trafficking. Previous work in acute hippocampal slices found that removal of GluN2A increased mEPSC amplitude, but did not affect frequency (suggesting that GluN2A's normal role would be to inhibit strengthening of synapses) (Gray et al., 2011). However, a study in hippocampal organotypic slices found that overexpression of GluN2A decreased mEPSC frequency, but did not affect amplitude (suggesting that GluN2A's normal role would be to inhibit formation of new synapses) (Gambrill and Barria, 2011). The hypotheses for this study were therefore that cells cultured from *Grin2a*$^{-/+}$ rats would show mEPSC amplitudes that were increased, or unaffected, and mEPSC frequencies that were increased, or unaffected.

mIPSCs are currents caused by activation of GABA receptors by quantal release of GABA at individual synapses. They are predominantly mediated by $GABA_A$ receptors. mIPSCs were assessed because NMDARs can influence many aspects of inhibition in neural networks (see Figure 5.3). Inhibition in the forebrain is a very complex topic, with the combined activities of many different types of interneuron to consider. However, overall, previous work suggests that reduced NMDAR activation in the commonest type of interneuron (parvalbumin-positive) is associated with a reduction in inhibitory output (for review see Moreau and Kullmann (2013)).

There has been little work on the role of individual NMDAR subunits in inhibition. There is some evidence suggesting GluN2A may be particularly important in driving inhibition as parvalbumin-positive interneurons in culture show a five-fold higher GluN2A:GluN2B ratio than neighbouring pyramidal cells (Kinney et al., 2006). Further, in *Grin2a* knock-out mice, NMDA evokes 50% less striatal GABA release than in wild type animals (Miyamoto et al., 2001). The hypothesis for this study was therefore that

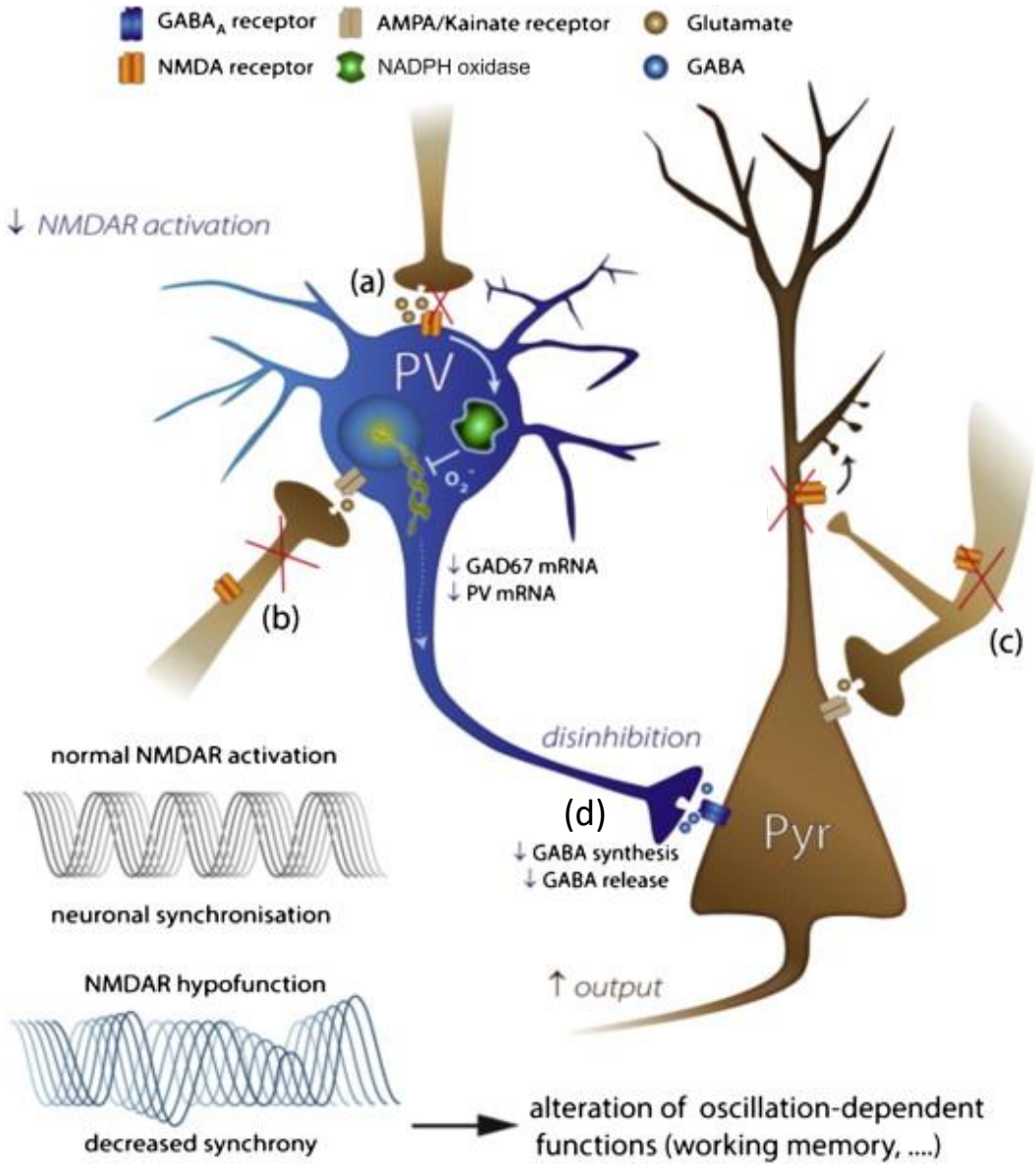

Figure 5.3: **NMDAR hypofunction impairs inhibitory circuits**
This figure shows potential routes NMDAR hypofunction may impact on parvalbumin-positive (PV) interneurons, adapted from Moreau and Kullmann (2013). In summary, less NMDAR activity is associated with less inhibition.
(a) Denotes a pyramidal cell synapsing onto a PV interneuron. Less NMDAR activation has been associated with a reduction in synthesis of PV (a calcium binding protein) and GAD67 (an enzyme which synthesises GABA).
(b) Denotes a pyramidal cell forming a weak synapse onto a PV interneuron because of reduced NMDAR-mediated synaptic potentiation.
(c) Denotes a pyramidal cell forming a weak synapse onto another pyramidal cell because of reduced NMDAR-mediated synaptic potentiation - overall circuit hypoactivity.
(d) Marks a PV interneuron synapsing weakly onto a pyramidal cell because of less pre-synaptic NMDAR activity resulting in reduced GABA synthesis and release.

Grin2a$^{-/+}$ rats would show less inhibitory activity in the form of lower amplitude and lower frequency mIPSCs.

Network activity following disinhibition is another way to assess the impact of GluN2A knock-out on inhibitory networks. Live-cell calcium imaging was used to measure neural activity via calcium transients as scores of cells can be recorded from simultaneously, unlike with standard patch-clamping approaches. Removal of inhibition by blocking $GABA_A$ receptors with bicuculline typically results in rebound activity in the form of large spikes of calcium synchronised across the neurons present. With the hypothesis that GluN2A knock-out would result in less inhibitory input to pyramidal cells, the prediction was that removal of inhibition would result in less disinhibition i.e. lower spike amplitude and frequency.

The final functional assessment performed was of excitotoxicity. There is a large literature linking NMDAR activation to excitotoxic cell death, with the C-terminus of GluN2B identified as more efficient at mediating the pro-death response than that of GluN2A (Martel et al., 2012). The hypothesis for the relative excitotoxic vulnerability for GluN2A knock-out cells therefore depended on whether knock-out cells expressed a compensatory increase in GluN2B subunits, or not (as indicated by current density). If there was no increase in GluN2B expression, the absence of GluN2A should not result in an increased risk of cell death. If, however, there was an increase in GluN2B expression, an increased vulnerability to cell death would be predicted.

The key findings of this chapter are the validation of two new rat models (*Grin2a*$^{flox/+}$ and *Grin2a*$^{-/+}$), and that preliminary functional investigations suggest that GluN2A knock-out reduces current density in culture, and also influences disinhibition.

5.3 Confirmation of targeted genome modification by sequencing

The commercial organisation who created the genetically modified rat lines unfortunately made a number of errors when using sequencing to confirm the modifications had occurred, including falsely attributing an off target insertion of the donor DNA as a targeted insertion. It was therefore necessary to rigorously confirm the nature of the genetic alterations as part of this study.

The approach taken was to amplify a section of genomic DNA which started and ended in intronic regions which were not included in the donor DNA: a "trans donor PCR" (see Figure 5.4). This would avoid false positives generated from off target donor insertions. However, this was difficult to do because it required amplification of a large section of DNA (2.4 kb in the case of floxed exons, 1.3 kb in the case of deleted exons) and so was in competition with several smaller non-specific products. A number of PCR optimisation strategies were trialled, including adding Mg^{2+} to the PCR mix and using GC-rich buffer, but the only modifications of benefit were allowing sufficient elongation time (3 minutes) and using a high processivity enzyme (see Methods Section 2.5.2 for details).

The presence of non-specific products also made it difficult to sequence the segment of interest. Gel extraction and cloning of individual PCR fragments did not help, presumably because of the low abundance of the product of interest relative to other products. The approach which worked best was to perform a nested PCR, whereby the region was initially amplified from genomic DNA with one pair of primers, then DNA oligomers and salts removed from the PCR product and a second PCR run with primers internal to the first pair (see Figure 5.4). Using this approach it was possible to sequence the region of interest and confirm the targeted insertion of LoxP sites and deletion of exon 8.

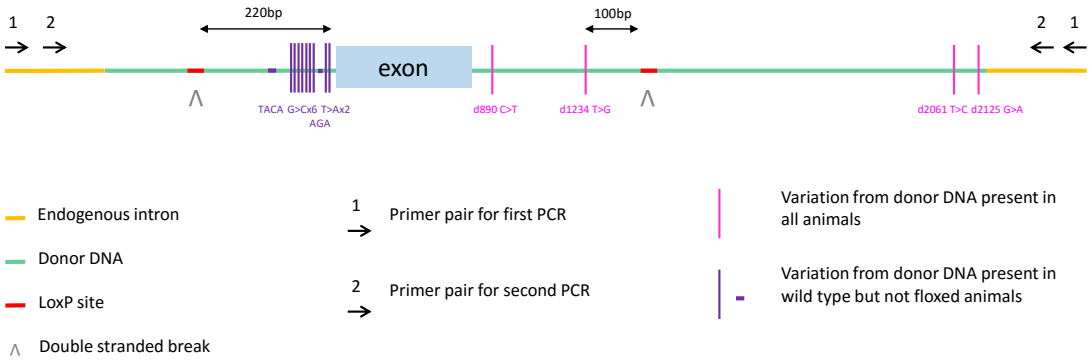

Figure 5.4: **Sequencing strategy and results for genetically modified rat lines**
This schematic shows the sequencing strategy for the genetically modified rat lines: a nested PCR with two pairs of primers starting and ending in endogenous intronic DNA (yellow), spanning the region for which replacement donor DNA provided (green). Pink and purple lines mark the location of variations from the donor DNA found in animals. The pink variations were found in all animals, suggesting the donor DNA was not recruited for repair at those points. The purple lines were found only in wild type animals, suggesting the donor DNA was used for homology-directed repair at least as far as those points. The approximate distance from the double stranded breaks to these points are marked: the donor DNA was used for repair at least 220 bp to 3' of the 5' double stranded break, and for at most 100 bp to 5' of the 3' double stranded break.

Figure 5.4 also highlights a number of differences between the donor DNA and the genomic DNA which give an insight into the DNA repair events which occurred. Four single nucleotide variations were found in all animals sequenced (wild type and mutant), but not in the donor DNA. One was only 100 bp from a double strand break, showing that the donor DNA was no longer being recruited for repair by that point (assuming the donor DNA was correctly synthesised). In contrast, a number of variations were found to 5' of the exon in wild type animals which were not present in the donor DNA or in animals which had the 5' LoxP site integrated, suggesting that the donor DNA was still being used for repair up until that point.

5.4 Validation of *Grin2a*$^{flox/flox}$ rat model

5.4.1 The *Grin2a*$^{flox/flox}$ rat is not a Grin2A hypomorph

Inserting LoxP sites into genes can occasionally be associated with a reduction in gene expression (creation of hypomorphic alleles). GluN2A protein levels in *Grin2a*$^{flox/+}$ and *Grin2a*$^{flox/flox}$ were therefore compared to wild type levels. This was done via immunoblots of cortical extracts from adolescent rats and in extracts from cultured cortical neurons at ages where GluN2A expression is high (see Figure 5.5). No difference in expression was seen.

5.4.2 Exposure to Cre recombinase results in knock-out of GluN2A in *Grin2a*$^{flox/flox}$ rat cultured neurons

The ability of the *Grin2a*$^{flox/flox}$ rat to be conditionally converted to a *Grin2a*$^{-/-}$ rat was tested next. This was done by exposing wild type and *Grin2a*$^{flox/flox}$ cultured cortical neurons to a Cre-expressing virus (an adeno-associated virus (serotype 2) expressing a Cre–eGFP fusion protein driven by the CMV promoter). Excision of *Grin2a* exon 8 was then assessed using PCR (with the same primers as for genotyping (primer pairs 1 in Table 2.6), and GluN2A protein levels assessed by immunoblot (see Figure 5.6). The conditional knock-out was confirmed by the emergence of a *Grin2a* deletion band and reduction in GluN2A protein levels following exposure to Cre in the *Grin2a*$^{flox/flox}$ rats but not in the wild type rats.

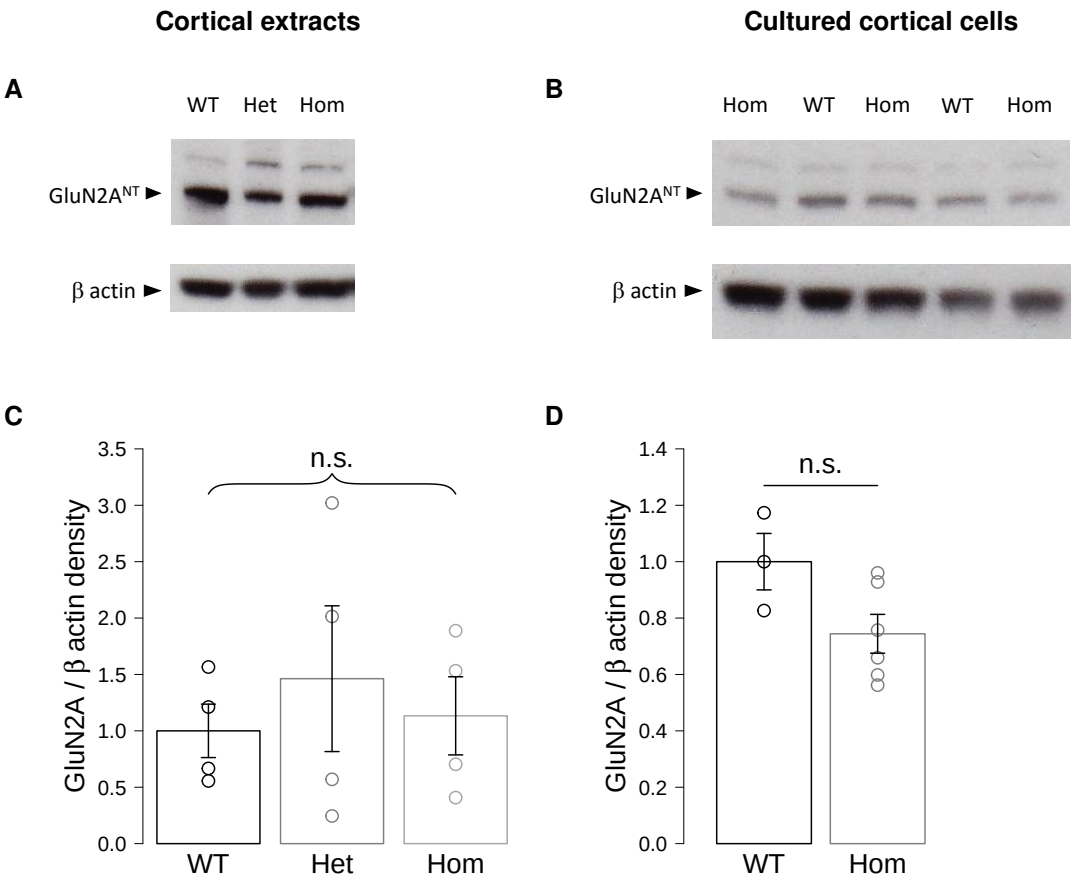

Figure 5.5: **GluN2A protein levels are normal in *Grin2a*$^{flox/flox}$ rat**
(A) Representative immunoblot showing GluN2A levels (N terminus antibody) and loading control (β actin) in neocortical extracts derived from wild-type, *Grin2a*$^{flox/+}$ and *Grin2a*$^{flox/flox}$ littermate rats aged P28.
(B) Representative immunoblot showing GluN2A levels (N terminus antibody) and loading control (β actin) in extracts from DIV 17-18 cortical cells cultured from wild type and *Grin2a*$^{flox/flox}$ embryos.
(C) The bar chart shows GluN2A protein levels normalised to β actin in neocortical extracts from rats aged P28-31. The ratios have also been normalised to wild type ratios from the same blot. Four littermate WT/het/hom trios were assessed. A one-way ANOVA showed no significant effect of genotype ($F(2,9) = 0.287$, $p = 0.76$). Thus GluN2A levels were the same in wild type (1 ± 0.24), *Grin2a*$^{flox/+}$ (1.46 ± 0.65) and *Grin2a*$^{flox/flox}$ rats (1.13 ± 0.35).
(D) The bar chart shows GluN2A protein levels normalised to β actin in extracts from DIV 17-18 cultured cortical cells. The ratios have also been normalised to wild type ratios from the same blot. A t-test showed no significant effect of genotype. Thus GluN2A levels were the same in wild type (1 ± 0.10, $n = 3$) and *Grin2a*$^{flox/flox}$ (0.74 ± 0.07, $n = 6$).

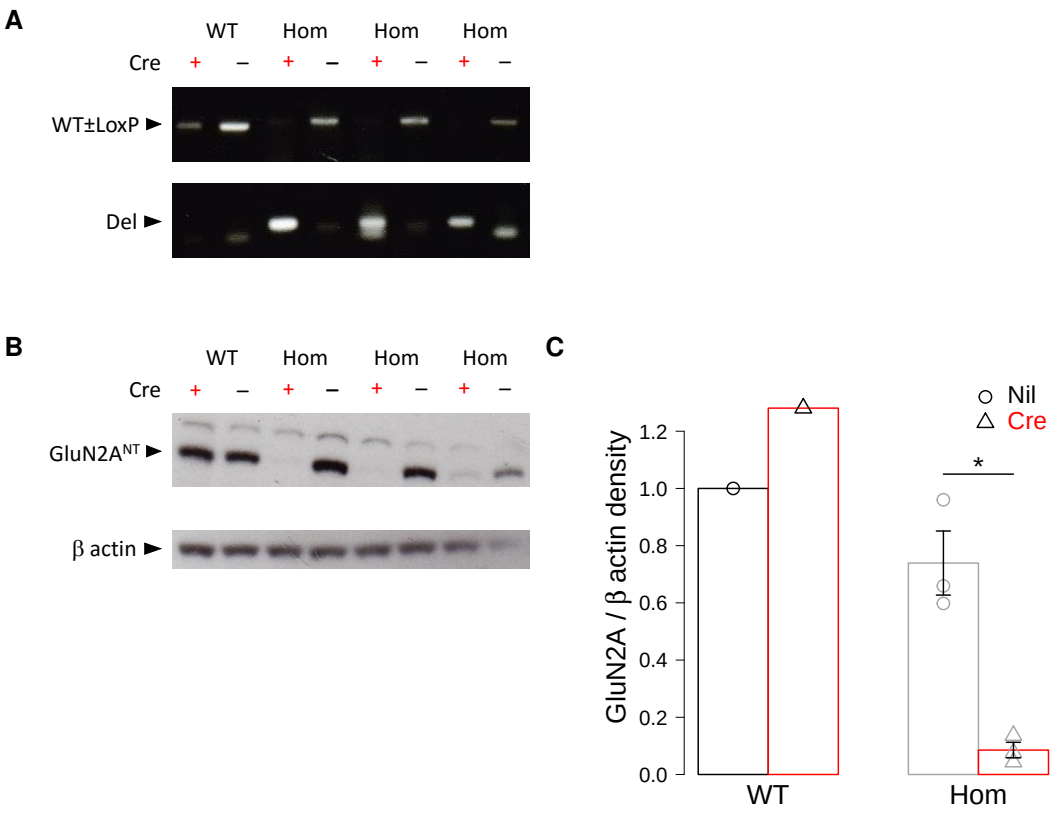

Figure 5.6: **GluN2A is deleted following Cre recombination in *Grin2a*$^{flox/flox}$ rat**
(A) Agarose gel showing PCR products from genomic DNA extracted from DIV 18 cultured cortical cells from wild type and *Grin2a*$^{flox/flox}$ rats, with and without exposure to Cre recombinase on DIV 3. Primers were designed to create "WT bands" (binding either side of the 5' LoxP site) and "del bands" (binding either side of the deleted region). Without Cre exposure, all animals show a WT band product (with the *Grin2a*$^{flox/flox}$ product slightly larger than the wild type, reflecting the presence of LoxP sites) and low abundance non-specific bands with the deletion primers. With Cre exposure, the wild type cells continue to show a WT band and no new deletion band emerges. However, the *Grin2a*$^{flox/flox}$ cells show a marked reduction in WT band intensity, and a prominent new deletion band, demonstrating excision of exon 8.
(B) Immunoblot showing GluN2A levels (N terminus antibody) and loading control (β actin) in extracts from DIV 18 cultured cortical cells from wild type and *Grin2a*$^{flox/flox}$ rats, with and without exposure to Cre recombinase on DIV 3.
(C) The bar chart shows GluN2A protein levels normalised to β actin in extracts from DIV 18 cultured cortical cells from one wild type and three *Grin2a*$^{flox/flox}$ rats, with and without exposure to Cre recombinase on DIV 3. The ratios have been normalised to the wild type level without exposure to Cre. A paired t-test showed a significant reduction ($t(2) = 4.81$, $p = 0.041$) in GluN2A levels in *Grin2a*$^{flox/flox}$ exposed to Cre recombinase (0.09 ± 0.03, $n = 3$) compared to *Grin2a*$^{flox/flox}$ without exposure to Cre (0.74 ± 0.11, $n = 3$).

5.5 Validation of *Grin2a*$^{-/+}$ rat model

The genetic data suggests that humans with gene disrupting mutations in one copy of *GRIN2A* experience GluN2A haploinsufficiency, and that this may contribute towards the pathogenesis of neurodevelopmental disorders. However, most genes can be heterozygously knocked out without phenotypic consequence, as the gene product remaining is sufficient for normal function (haplosufficiency). It was therefore necessary to both confirm that the *Grin2a*$^{-/-}$ rat is a true knock-out, and that the *Grin2a*$^{-/+}$ rat showed intermediate, haploinsufficient, values at both biochemical and functional levels.

First, qPCR was used to quantify mRNA levels in cultured neurons with primers bridging exons prior to the deletion (Figure 5.7). This was done at two ages, to confirm the developmental regulation of *Grin2a* transcription. The qPCR first confirmed an approximately three-fold increase in *Grin2a* transcription from DIV 7 to DIV 15 in cells cultured from wild type rats. The qPCR also demonstrated that mRNA levels were substantially reduced but not completely absent in the *Grin2a*$^{-/-}$ rats, suggesting that the mRNA is transcribed, but is unstable and probably undergoing nonsense mediated decay. At the later time point, it was also possible to confirm that the heterozygous rats showed an intermediate amount of *Grin2a* mRNA.

Next, GluN2A protein levels were assessed, at DIV 7 and DIV 15 in cultured cells and at P27-P28 in necortical extracts (Figure 5.8). Quantification of the GluN2A levels in neocortex confirmed that *Grin2a*$^{-/-}$ rats showed no GluN2A expression, whereas heterozygotes showed intermediate amounts. Quantification of GluN2A levels in cultured cells again identified a several-fold increase in GluN2A expression from DIV 7 to DIV 15 in wild type cells, with absent levels in homozygous animals and intermediate levels in heterozygotes. A N terminus antibody to GluN2A was used in order to allow any truncated products to be identified: there were none.

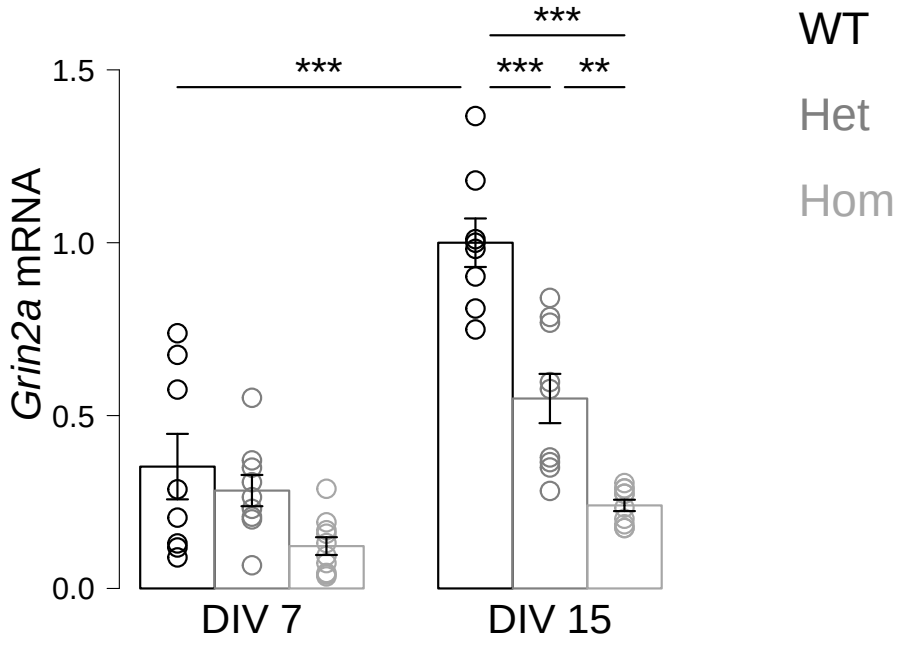

Figure 5.7: ***Grin2a* mRNA levels are reduced in *Grin2a*$^{-/+}$ and *Grin2a*$^{-/-}$ rats**
The bar chart shows *Grin2a* mRNA levels in cultured cortical neurons from wild type, *Grin2a*$^{-/+}$ and *Grin2a*$^{-/-}$ rats at DIV 7 and DIV 15. Levels were normalised to *Gadph*, and then to wild type ratios at DIV 15. A two-way ANOVA showed a significant main effect of genotype ($F(2,48) = 38.1$, $p = 1.25e\text{-}10$), age ($F(1,48) = 49.6$, $p = 6.4e\text{-}9$) and a significant interaction ($F(2,48) = 11.3$, $p = 9.6e\text{-}5$). Planned post-hoc t–tests (Bonferroni corrected) showed that wild type rats showed a significant increase in *Grin2a* mRNA levels from DIV 7 to DIV 15 (DIV 7: 0.35 ± 0.09, DIV 15: 1 ± 0.07 (n=8), $t(12.9) = 5.5$, $p_{corr} = 0.00042$). At DIV 15, there was also a significant reduction in *Grin2a* levels in heterozygotes compared to wild type (het: 0.54 ± 0.07, $t(15.0) = 4.5$, $p_{corr} = 0.0017$) and in homozygotes compared to heterozygotes (hom: 0.24 ± 0.02, $t(8.9) = 4.2$, $p_{corr} = 2.84e\text{-}5$). There was also a significant reduction in homozygotes compared to wild type ($t(7.8) = 10.5$, $p_{corr} = 0.0092$).

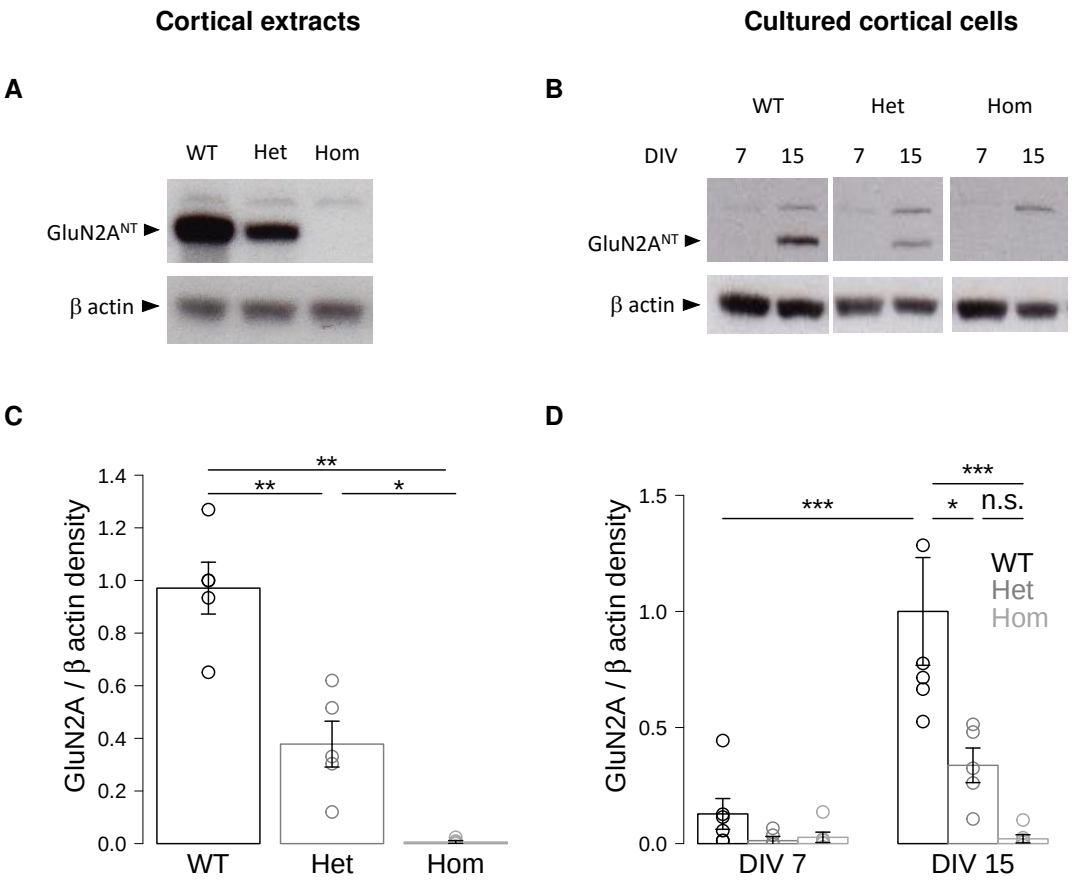

Figure 5.8: **GluN2A protein levels are reduced in *Grin2a*$^{-/+}$ and *Grin2a*$^{-/-}$ rats**
(A) Representative immunoblot showing GluN2A levels (N terminus antibody) and loading control (β actin) in neocortical extracts derived from wild type, *Grin2a*$^{-/+}$ and *Grin2a*$^{-/-}$ littermate rats aged P28.
(B) Representative immunoblot showing GluN2A levels (N terminus antibody) and loading control (β actin) in extracts from DIV 17-18 cortical cells cultured from wild type and *Grin2a*$^{-/-}$ embryos.
(C) The bar chart shows GluN2A protein levels normalised to β actin in neocortical extracts from rats aged P27-28. The ratios have also been normalised to wild type ratios from the same blot. Five littermate WT/het/hom trios were assessed. A one-way ANOVA showed a significant effect of genotype ($F(2,12) = 41$, $p = 4.33e\text{-}6$). Planned post-hoc t–tests (Bonferroni corrected) showed a significant reduction in Grin2A levels in heterozygotes compared to wild type (WT: 1 ± 0.10, het: 0.38 ± 0.09, $t(7.9) = 4.5$, $p_{corr} = 0.0062$) and in homozygotes compared to heterozygotes (hom: 0.01 ± 0.01, $t(4.0) = 4.3$, $p_{corr} = 0.038$). There was also a significant reduction in homozygotes compared to wild type ($t(4.0) = 9.8$, $p_{corr} = 0.0018$).
(D) The bar chart shows GluN2A protein levels normalised to β actin in extracts from DIV 17-18 cultured cortical cells. The ratios have also been normalised to wild type ratios from the same blot. A two-way ANOVA showed a significant main effect of genotype ($F(2,28) = 13.7$, $p = 7e\text{-}5$), age ($F(1,28) = 20.3$, $p = 0.00011$) and a significant interaction ($F(2,28) = 8.7$, $p = 0.0011$). Planned post-hoc t–tests showed that wild type rats showed a significant increase in GluN2A levels from DIV 7 to DIV 15 (DIV 7: 0.13 ± 0.07, DIV 15: 1 ± 0.23 (n=6), $t(5) = 17.1$, $p_{corr} = 5e\text{-}5$). At DIV 15, there was also a significant reduction in GluN2A levels in heterozygotes compared to wild type (het: 0.34 ± 0.07 (n=5), $t(4) = 6.6$, $p_{corr} = 0.011$) and in homozygotes compared to wild type (hom: 0.02 ± 0.02 (n=6), $t(5) = 71.4$, $p_{corr} = 4.1e\text{-}8$).

Functional incorporation of GluN2A subunits into surface expressed NMDARs was then assessed electrophysiologically. This was done by assessing spermine potentiation. GluN2B diheteromers are potentiated by spermine, whereas GluN2A diheteromers and GluN2A/2B triheteromers show no potentiation (Stroebel et al., 2014) (see Section 5.2.2 for the rationale for choosing this assay). Thus, as GluN2A expression increases, spermine potentiation should decrease. This was confirmed using transient transfection to overexpress wild type GluN2A subunits (see Figure 5.9). The impact of GluN2A^{N615K} overexpression on spermine potentiation was also assessed (in case this assay were to be used with a *Grin2a*$^{T1845A(flox)/+}$ rat in due course). The representative traces in Figure 5.9 show the response to 100 μM and 200 μM spermine but only the data from 100 μM spermine are used for analysis (as the currents are smaller they are less prone to loss of voltage-clamp). Figure 5.10 shows that both GluN2A subunits cause a reduction in spermine potentiation.

Next, spermine potentiation was used to track the increase in GluN2A expression with age in wild type rat cultured cortical neurons. Figure 5.11 shows that spermine potentiation drops by the third week in culture, reflecting the onset of GluN2A expression (as also demonstrated by mRNA and protein in the sections above). No further drop in potentiation was seen in the fourth week in culture.

Based on the developmental time course in Figure 5.11, two time points were selected to assess GluN2A incorporation in cells cultured from genetically modified rat embryos: DIV 7-8 (when minimal GluN2A expression is expected) and DIV 15-16 (when wild type cells would be expected to show a clear onset of GluN2A expression). Figure 5.12 shows that spermine potentiation is higher in *Grin2a*$^{-/+}$ and *Grin2a*$^{-/-}$ cells compared to wild type cells. This confirms that the loss of GluN2A is impacting NMDAR function, whether homozygous or heterozygous, thus demonstrating haploinsufficiency.

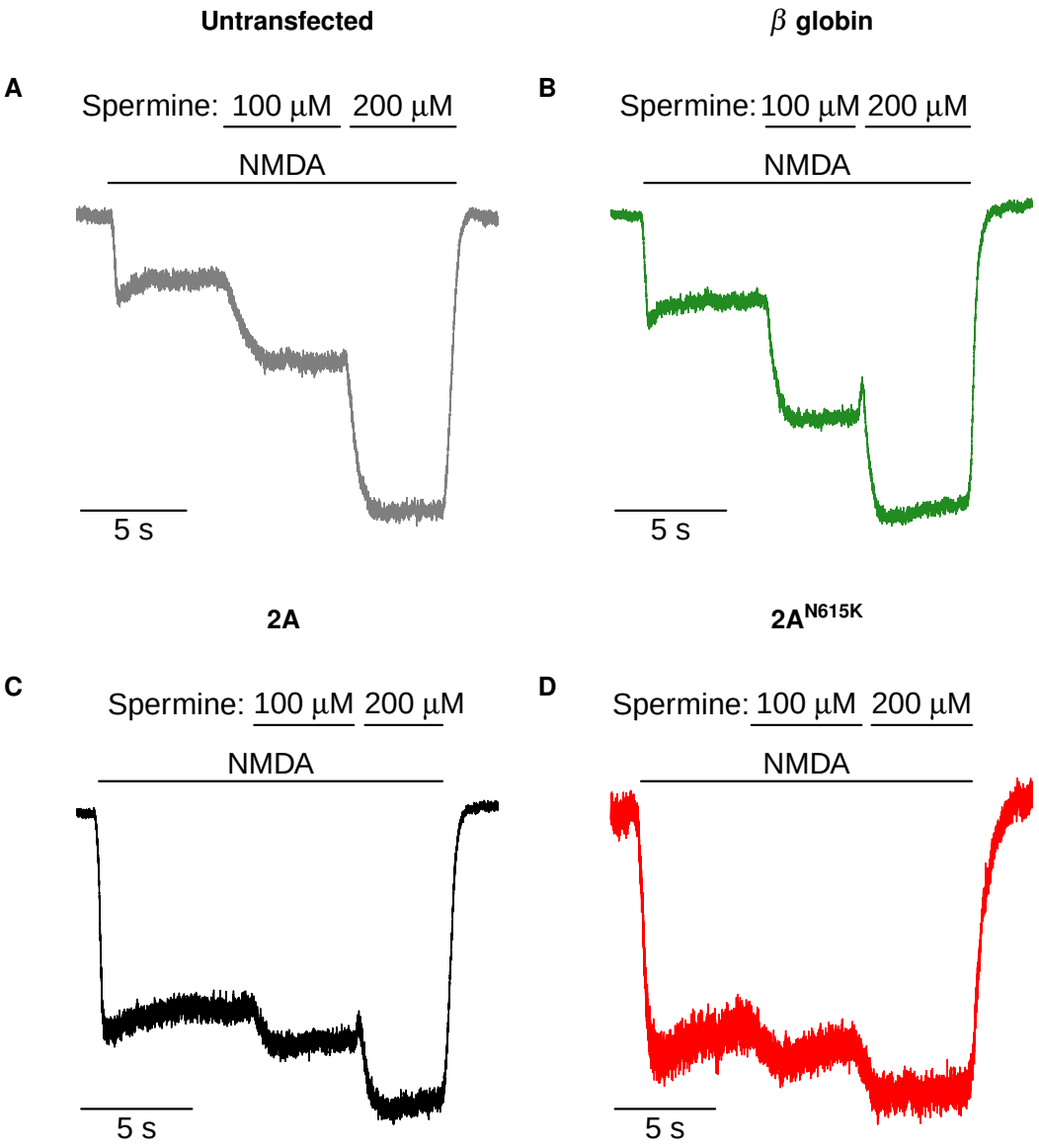

Figure 5.9: **Representative spermine potentiation traces from neurons expressing wild type GluN2A and GluN2A^{N615K} NMDARs**
(A) Representative whole-cell voltage-clamp recording from untransfected DIV 9 neurons, showing potentiation of current evoked by saturating NMDA (150 μM) by spermine (100 μM and 200 μM). Holding potential –30 mV. Responses are normalised to the peak amplitude.
(B-D) As for **(A)** but neurons transfected with an inert control (β globin), 2A or 2A^{N615K} NMDAR subunits respectively.

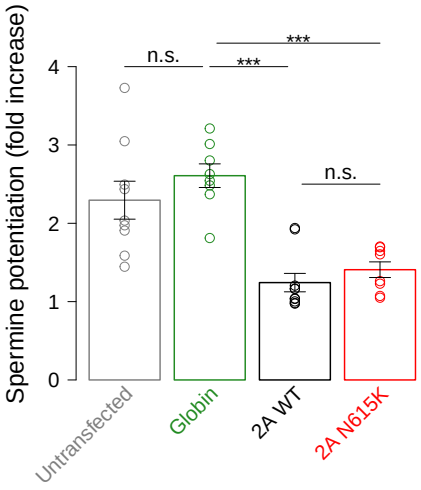

Figure 5.10: **Spermine potentiation is reduced in neurons transfected with wild type GluN2A or GluN2A^{N615K}**

The bar chart shows fold potentiation by spermine (100 μM) for DIV 9 untransfected neurons and neurons transfected with an inert control (β globin), 2A and 2A^{N615K} NMDAR subunits. A one-way ANOVA showed a significant main effect of transfected subunit ($F(3,31) = 16.5$, $p < 1.4e{-}6$). Planned post-hoc independent t–tests showed no significant difference in spermine potentiation between untransfected neurons and neurons transfected with β globin (Untransfected: 2.3 ± 0.2 (n=9), β globin 2.6 ± 0.2 (n=8)). However, there was a highly significant reduction in spermine potentiation in neurons transfected with 2A (($2A : 1.3 \pm 0.1$ (n=10), $t(14.1) = 7.1$, $p_{corr} = 2.0e\text{-}5$) and 2A^{N615K} (2A^{N615K} : 1.4 ± 0.1 (n=8), $t(12.1) = 6.6$, $p_{corr} = 9.1e{-}5$), when compared to a β globin transfection. Finally, there was no significant difference between neurons transfected with 2A and 2A^{N615K} subunits.

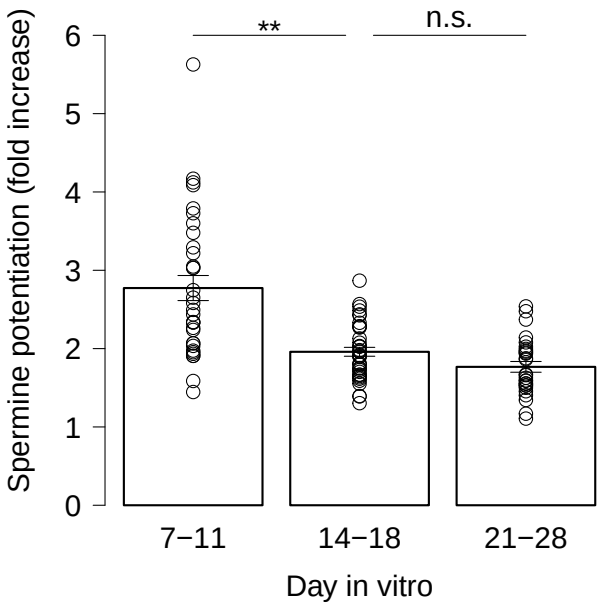

Figure 5.11: **GluN2A expression is demonstrated by a reduction in spermine potentiation by three weeks *in vitro* in cultured neurons**
The bar plot shows fold potentiation by spermine (100 μM) for untransfected wild type neurons at a range of ages. A reduction in spermine potentiation (indicating an increase in GluN2A expression) is evident from the third week in culture onwards. A one-way ANOVA showed a significant main effect of day *in vitro* ($F(2,98) = 9.2$, $p < 1.5e{-}9$). Planned post-hoc independent t–tests showed a significant difference in spermine potentiation between DIV 7-11 and DIV 14-18 neurons (DIV 7-11: 2.8 ± 0.2 (n=33), DIV 14-18: 2.0 ± 0.1 (n=40), $t(40) = 4.8$, $p_{corr} = 0.0019$). However, there was no significant difference between DIV 14-18 and DIV 21-28 neurons (DIV 21-28: 1.8 ± 0.1 (n=28)). n refers to number of cells.

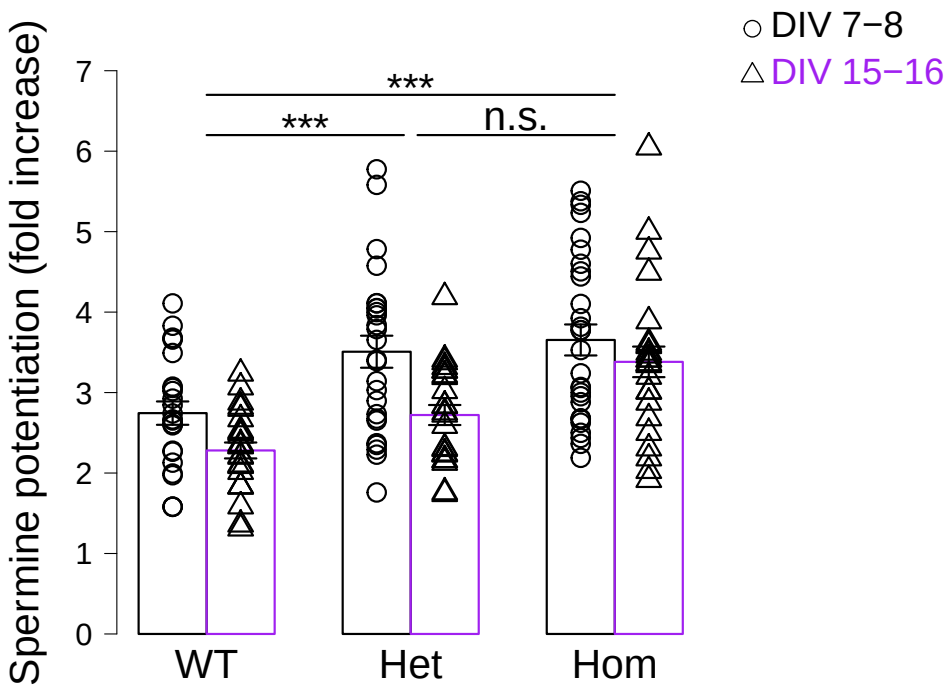

Figure 5.12: **Spermine potentiation is increased in *Grin2a*$^{-/+}$ and *Grin2a*$^{-/-}$ rats**
The bar chart shows spermine potentiation in cultured cortical neurons from wild type, *Grin2a*$^{-/+}$ and *Grin2a*$^{-/-}$ rats at DIV 7-8 and DIV 15-16. A two-way ANOVA showed a significant main effect of genotype ($F(2,148) = 19.1$, $p = 4.1e\text{-}8$) and age ($F(1,148) = 13.7$, $p = 0.0003$) but no significant interaction ($F(2,148) = 1.2$, $p = 0.30$). Planned post-hoc t–tests (Bonferroni corrected) showed that wild type rats showed a significantly lower spermine potentiation than *Grin2a*$^{-/+}$ rats (WT: 2.51 ± 0.09 (n=50), het: 3.13 ± 0.13 (n=50), $t(88.4) = 3.8$, $p_{corr} = 0.00091$) and than *Grin2a*$^{-/-}$ rats (hom: 3.52 ± 0.14 (n=54), $t(92.4) = 6.2$, $p_{corr} = 7.2e\text{-}8$). The difference in spermine potentiation between *Grin2a*$^{-/+}$ and *Grin2a*$^{-/-}$ rats was not significant after correction for multiple comparison. Spermine potentiation at DIV 15-16 was significantly lower than at DIV 7-8 (DIV 15-16: 2.80 ± 0.11 (n=74), DIV 7-8 3.32 ± 0.10 (n=80), $t(150.2) = 3.5$, $p_{corr} = 0.0022$) (pooled across genotypes) (not marked on plot).

Finally, a smaller sample of cells was used to compare the two methods of assessing the degree of GluN2A expression: ifenprodil sensitivity against spermine potentiation. Ifenprodil sensitivity was assessed by comparing NMDA-evoked current density before and after exposure to 1 minute of ifenprodil (3 μM) (as in Section 3.4.1 but without the application of Mg^{2+}). Figure 5.13 shows that both approaches were able to distinguish homozygous from wild type cells, but only spermine potentiation was able to separate heterozygous from wild type cells, and identify the developmental change in GluN2A expression. Thus spermine potentiation is more sensitive than ifenprodil inhibition in detecting reductions in GluN2A surface-expressed NMDARs.

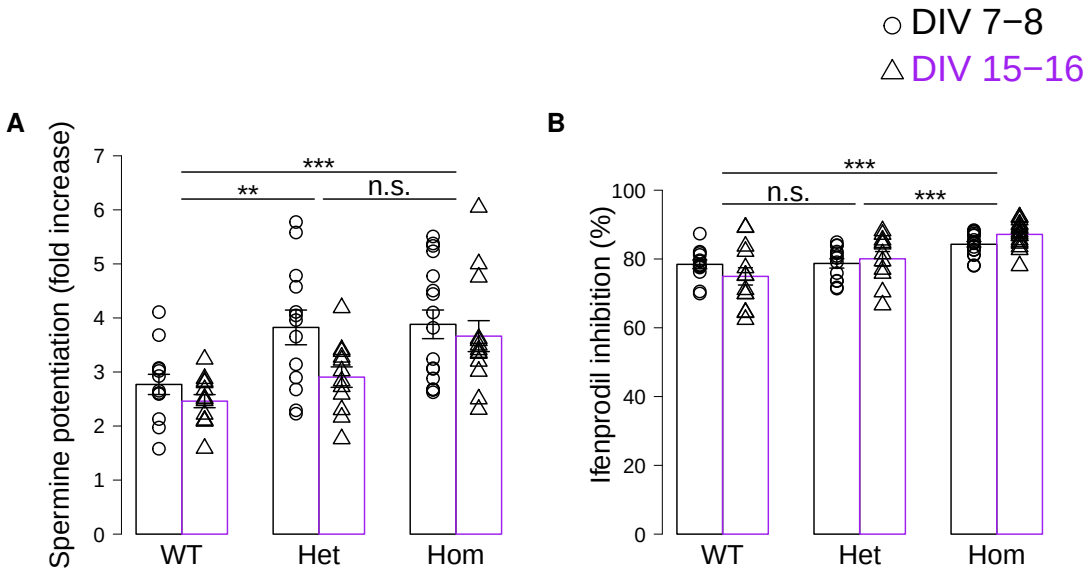

Figure 5.13: **Spermine potentiation is better than ifenprodil sensitivity for detecting *Grin2a*$^{-/+}$ haploinsufficiency**

A The bar chart shows spermine potentiation in cultured cortical neurons from wild type, *Grin2a*$^{-/+}$ and *Grin2a*$^{-/-}$ rats at DIV 7-8 and DIV 15-16. A two-way ANOVA showed a significant main effect of genotype ($F(2,75) = 12.1$, $p = 2.8e\text{-}5$) and age ($F(1,75) = 5.4$, $p = 0.023$) but no significant interaction. Planned post-hoc t–tests (Bonferroni corrected) showed that wild type rats showed a significantly lower spermine potentiation than *Grin2a*$^{-/+}$ rats (WT: 2.62 $\pm$ 0.11 (n=26), het: 3.38 $\pm$ 0.21 (n=25), $t(37.2) = 3.2$, $p_{corr} = 0.01$) and than *Grin2a*$^{-/-}$ rats (hom: 3.79 $\pm$ 0.19 (n=30), $t(46.2) = 5.2$, $p_{corr} = 1.5e\text{-}5$). The difference in spermine potentiation between *Grin2a*$^{-/+}$ and *Grin2a*$^{-/-}$ rats was not significant. Spermine potentiation at DIV 15-16 was not significantly lower than at DIV 7-8 after correction for multiple comparisons.

B The bar chart shows ifenprodil sensitivity in cultured cortical neurons from wild type, *Grin2a*$^{-/+}$ and *Grin2a*$^{-/-}$ rats at DIV 7-8 and DIV 15-16. A two-way ANOVA showed a significant main effect of genotype only ($F(2,78) = 21.2$, $p = 4.5e\text{-}8$). Planned post-hoc t–tests (Bonferroni corrected) showed that wild type rats showed a significantly lower ifenprodil sensitivity than *Grin2a*$^{-/-}$ rats (WT: 77 $\pm$ 1 (n=26), hom: 86 $\pm$ 1 (n=34), $t(88.4) = 3.8$, $p_{corr} = 4.5e\text{-}6$) but were not significantly different to *Grin2a*$^{-/+}$ rats. However, *Grin2a*$^{-/+}$ rats showed a signficantly lower ifenprodil sensitivity than *Grin2a*$^{-/-}$ rats (het: 79 $\pm$ 1 (n=24), $t(92.4) = 6.2$, $p_{corr} = 0.0001$).

5.6 Functional assessment of *Grin2a*$^{-/+}$ rat model

The previous section demonstrated that *Grin2a*$^{-/-}$ rats lack GluN2A, and that *Grin2a*$^{-/+}$ rats are haploinsufficient. Attention was then turned to a preliminary investigation of some potential functional consequences of low or absent levels of GluN2A.

Although the behaviour of the *Grin2a*$^{-/-}$ and *Grin2a*$^{-/+}$ rats was not formally assessed, no differences were observed during general husbandry: the animals were able to eat and drink as normal, breed as normal, and showed no overt neurological phenotype.

The first potential functional consequence to be quantified was current density. This was assessed simply by exposing cultured neurons to saturating NMDA until the current response plateaued, then dividing by the cell's size as estimated by capacitance. Figure 5.14 shows that there is no difference between genotypes at young ages, when there is minimal GluN2A expression, but lower current density in *Grin2a*$^{-/+}$ and *Grin2a*$^{-/-}$ cells at older ages, when wild type cells have started expressing higher levels of GluN2A. This shows that any compensatory increase in expression of other GluN subunits is not sufficient to match the current normally mediated by GluN2A-containing NMDARs.

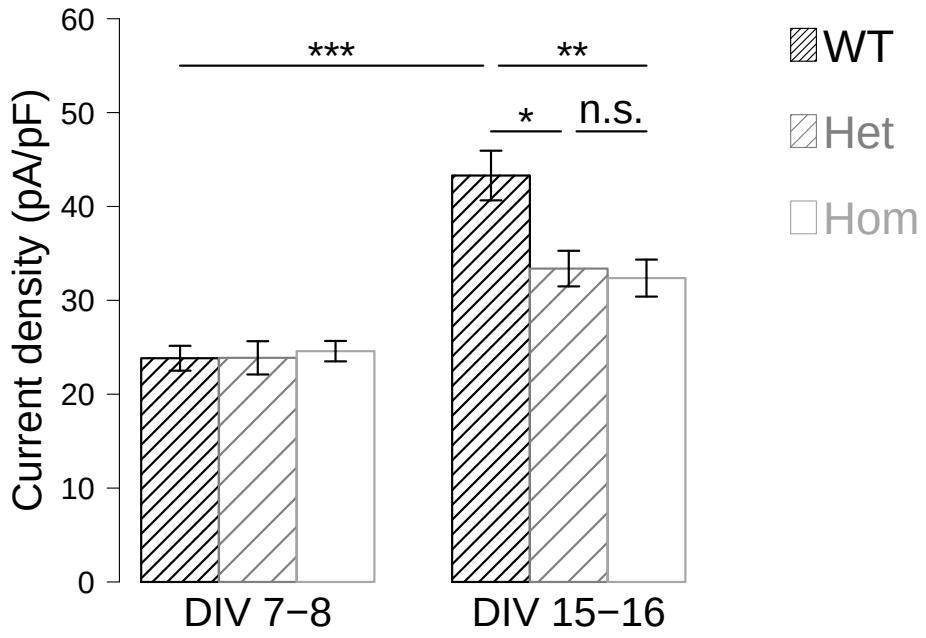

Figure 5.14: **Current density is reduced in *Grin2a*$^{-/+}$ and *Grin2a*$^{-/-}$ rat neurons after two weeks in culture**
The bar chart shows current density in cultured cortical neurons from wild type, *Grin2a*$^{-/+}$ and *Grin2a*$^{-/-}$ rats at DIV 7-8 and DIV 15-16. A two-way ANOVA showed a significant main effect of genotype ($F(2,235) = 5.6$, $p = 0.0043$), age ($F(1,235) = 66.1$, $p = 2.5e\text{-}14$) and a significant interaction ($F(2,235) = 6.0$, $p = 0.0029$). Planned post-hoc t–tests (Bonferroni corrected) showed that wild type rats showed a significant increase in current density from DIV 7 to DIV 15 (DIV 7: 24 ± 1 (n=38), DIV 15: 43 ± 3 (n=38), $t(54.5) = 6.6$, $p_{corr} = 7.6e\text{-}8$). At DIV 15, there a significant reduction in current density in heterozygotes compared to wild type (het: 33 ± 2 (n=35), $t(65.9) = 3.0$, $p_{corr} = 0.013$) and in homozygotes compared to wild type (hom: 32 ± 2 (n=42), $t(70.1) = 3.3$, $p_{corr} = 0.0059$). There was no significant difference in current density at DIV15 between *Grin2a*$^{-/+}$ and *Grin2a*$^{-/-}$ cells. Points for individual cells not shown due to large n.

The next properties to be assessed were the frequencies and amplitudes of mEPSCs and mIPSCs, and the excitation:inhibition ratio. Figure 5.15 shows a representative recording of mEPSCs made in a cortical neuron cultured from a wild type rat. Complete inhibition by the AMPAR antagonist CNQX confirmed these events to be AMPAR mediated. Figure 5.16 shows the amplitudes and frequencies of mEPSCs in wild-type, *Grin2a*$^{-/+}$ and *Grin2a*$^{-/-}$ rats. There is no difference in either parameter between genotypes.

mIPSC are presented next. Figure 5.17 shows a representative recording of a mIPSC made in a cortical neuron cultured from a wild type rat. Complete inhibition by the $GABA_AR$ antagonist bicuculline confirmed these events to be GABAR mediated. Figure 5.18 shows the amplitudes and frequencies of the mIPSCs in wild-type, *Grin2a*$^{-/+}$ and *Grin2a*$^{-/-}$ rats. There is no difference in either parameter between genotypes.

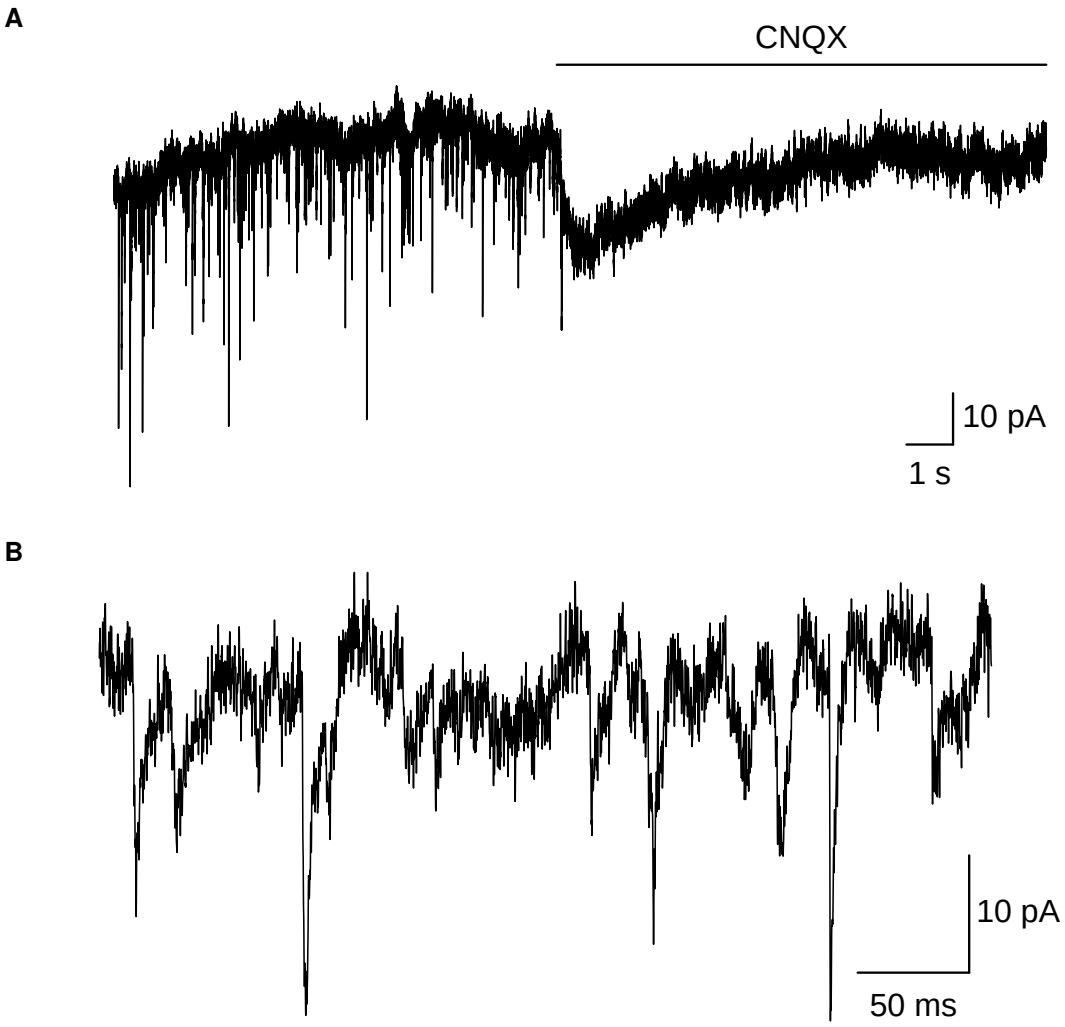

Figure 5.15: **Representative trace showing AMPAR mediated mEPSCs**
(A) Representative whole-cell voltage-clamp recording from DIV 18 cortical neuron cultured from a wild type rat. The application of the AMPA receptor antagonist CNQX (20 μM) abolishes the mEPSCs. Holding potential –65 mV.
(B) As for **(A)** but shorter time scale.

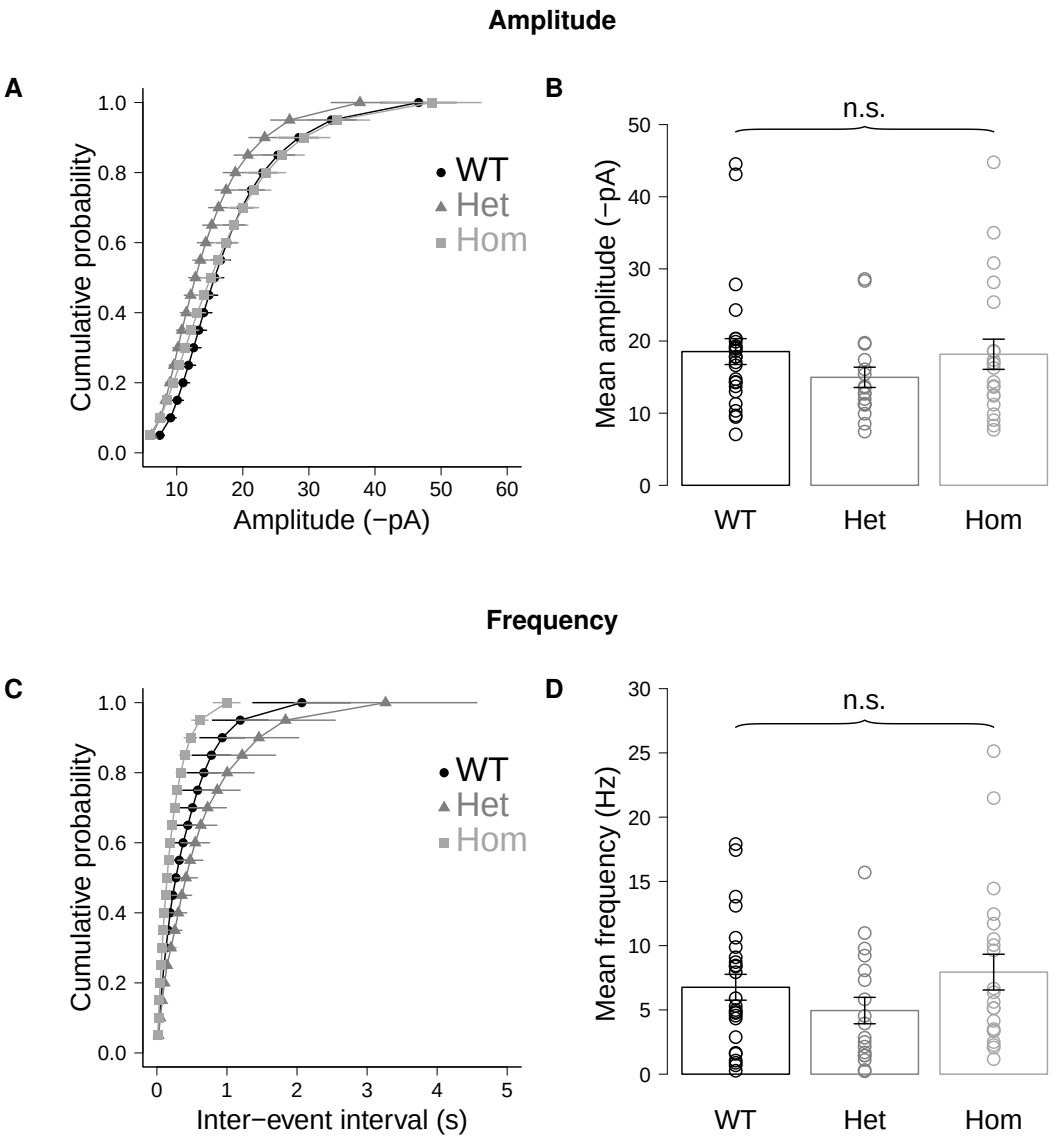

Figure 5.16: **mEPSC amplitudes and frequencies in cultured neurons are unaffected by *Grin2a* knock-out**

(A) Cumulative probability plot of mEPSC amplitudes measured in DIV 18-20 neurons cultured from wild type, *Grin2a*$^{-/+}$ and *Grin2a*$^{-/-}$ rats.

(B) The bar chart shows mean mEPSC amplitudes. A one-way ANOVA showed no significant effect of genotype on mEPSC amplitude (WT: 19 $\pm$ 2 (n=25 cells from 8 animals), het: 15 $\pm$ 1 (n=18 cells from 8 animals), hom: 18 $\pm$ 2 (n=21 cells from 8 animals)).

(C) Cumulative probability plot of mEPSC inter event intervals measured in DIV 18-20 neurons cultured from wild-type, *Grin2a*$^{-/+}$ and *Grin2a*$^{-/-}$ rats.

(D) The bar chart shows mean mEPSC frequencies. A one-way ANOVA showed no significant effect of genotype on mEPSC frequency (WT: 7 $\pm$ 1 , het: 5 $\pm$ 1, hom: 8 $\pm$ 1). Sample sizes as for amplitudes (see **(B)**).

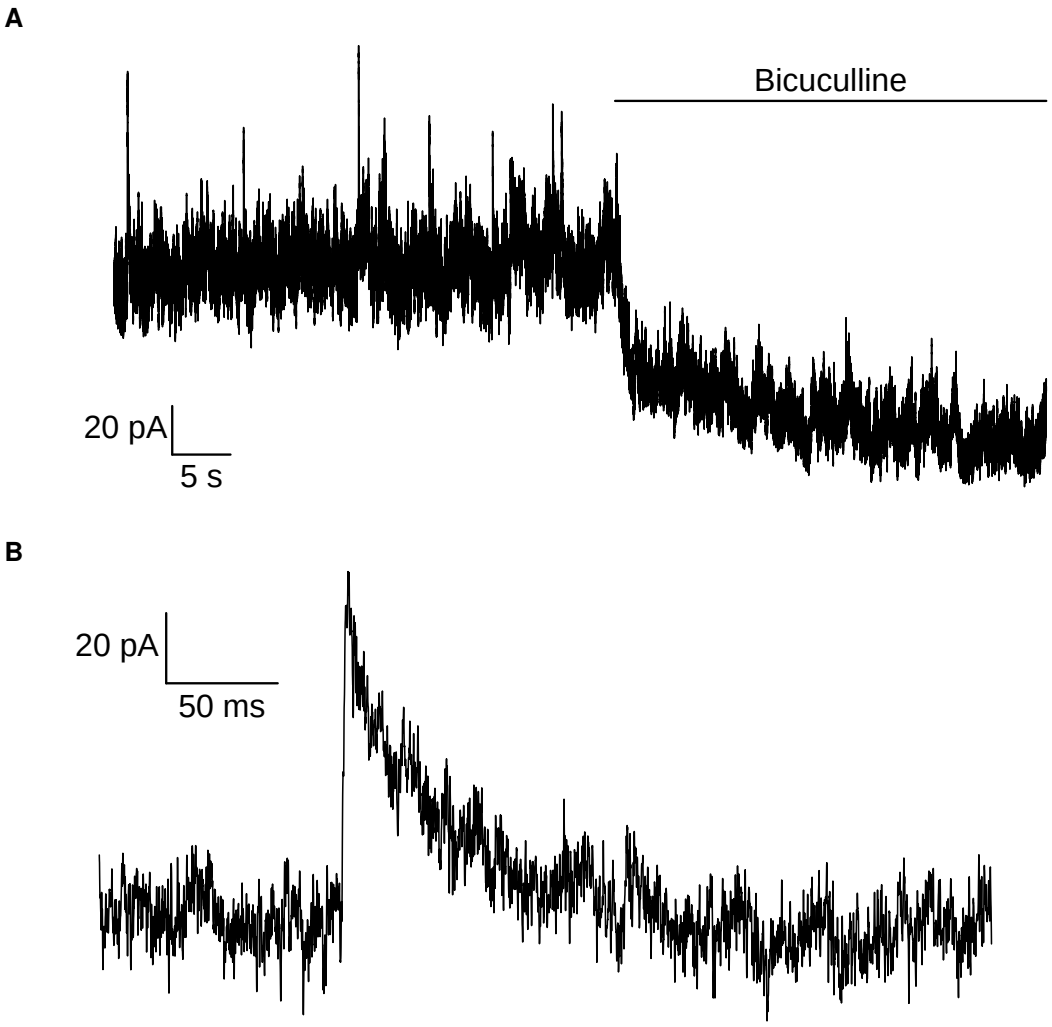

Figure 5.17: **Representative trace showing GABAR mediated mIPSCs**
(A) Representative whole-cell voltage-clamp recording from DIV 18 cortical neuron cultured from a wild type rat. The application of the GABA receptor antagonist bicuculline (50 μM) abolishes the mIPSCs. Holding potential –65 mV.
(B) As for **(A)** but shorter time scale.

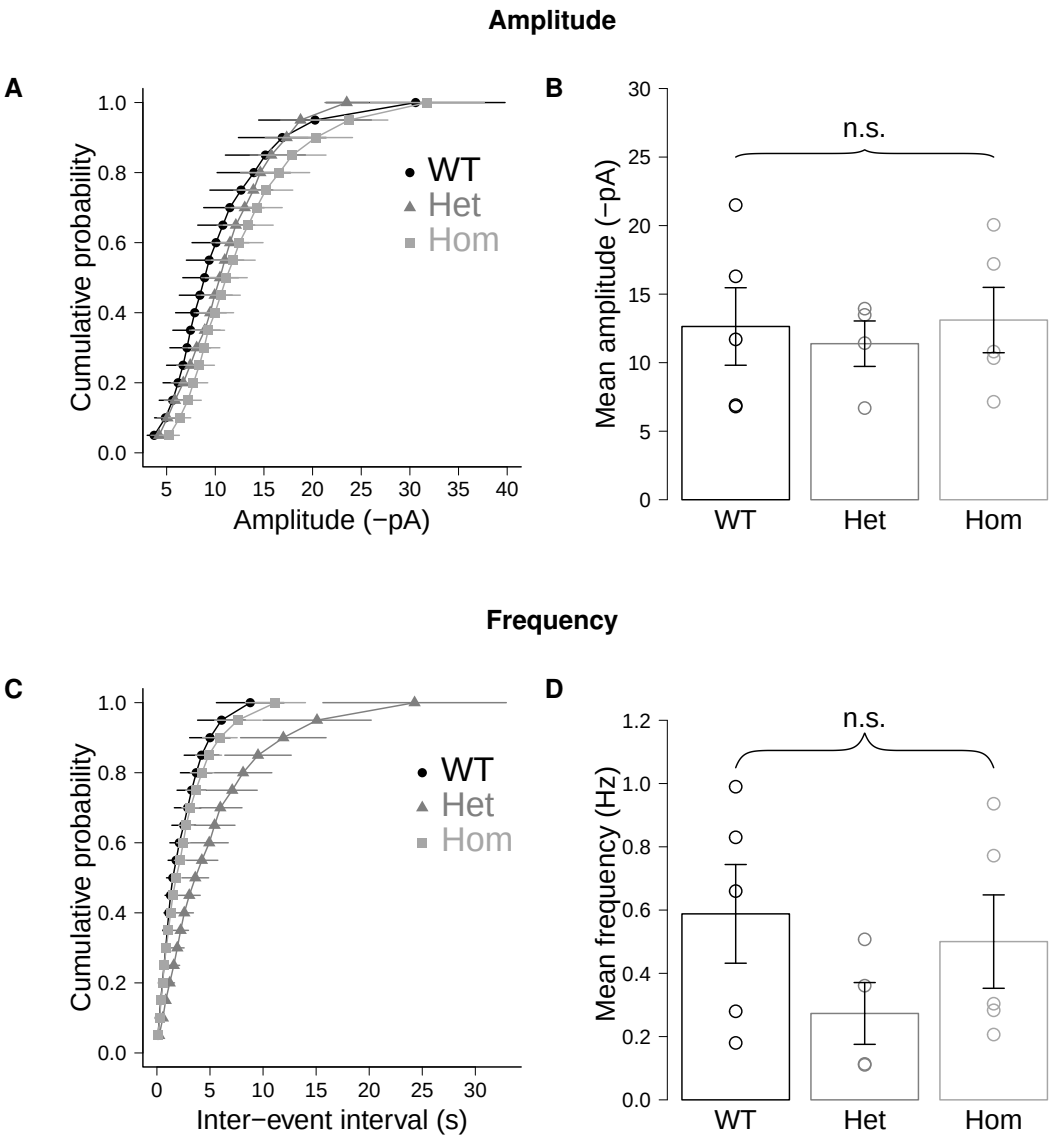

Figure 5.18: **mIPSC amplitudes and frequencies in cultured neurons are unaffected by *Grin2a* knock-out**

(A) Cumulative probability plot of mIPSC amplitudes measured in DIV 18 neurons cultured from wild type, *Grin2a*$^{-/+}$ and *Grin2a*$^{-/-}$ rats.

(B) The bar chart shows mean mIPSC amplitudes. A one-way ANOVA showed no significant effect of genotype on mIPSC amplitude (WT: 13 $\pm$ 3 (n=5 cells from 1 animal), het: 11 $\pm$ 2 (n=4 cells from 3 animals), hom: 13 $\pm$ 2 (n=5 cells from 3 animals)).

(C) Cumulative probability plot of mIPSC inter event intervals measured in DIV 18 neurons cultured from wild-type, *Grin2a*$^{-/+}$ and *Grin2a*$^{-/-}$ rats.

(D) The bar chart shows mean mIPSC frequencies. A one-way ANOVA showed no significant effect of genotype on mIPSC frequency (WT: 0.59 $\pm$ 0.16 , het: 0.27 $\pm$ 0.10, hom: 0.50 $\pm$ 0.15). Sample sizes as for amplitudes (see **(B)**).

Finally, excitation:inhibition ratios for miniature synaptic events are presented. These were calculated from cells in which both mEPSCs and mIPSCs were recorded. Figure 5.19 shows the ratios of amplitudes and frequencies in in wild-type, *Grin2a*$^{-/+}$ and *Grin2a*$^{-/-}$ rats. There is no difference in either parameter between genotypes.

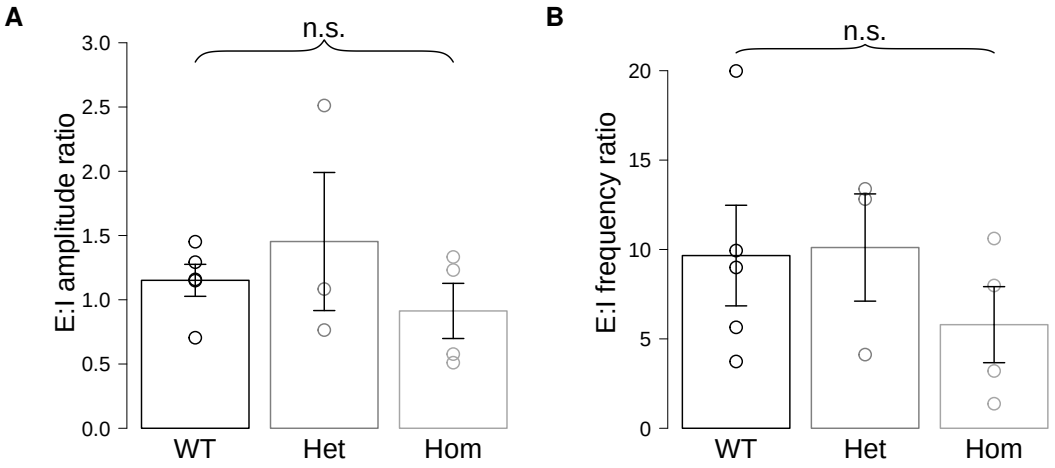

Figure 5.19: **Ratio of mEPSC:mIPSC amplitudes and frequencies in cultured neurons are unaffected by *Grin2a* knock-out**
(A) The bar chart shows the ratio of mean mEPSC:mIPSC amplitudes, recorded in the same cell. A one-way ANOVA showed no significant effect of genotype on the ratio (WT: 1.2 $\pm$ 0.1 (n=5 cells from 1 animal), het: 1.5 $\pm$ 0.5 (n=3 cells from 3 animals), hom: 0.9 $\pm$ 0.2 (n=4 cells from 3 animals)).
(B) The bar chart shows the ratio of mean mEPSC:mIPSC frequencies, recorded in the same cell. A one-way ANOVA showed no significant effect of genotype on the ratio (WT: 10 $\pm$ 3, het: 10 $\pm$ 3, hom: 6 $\pm$ 2). Sample sizes as for amplitudes (see **(A)**).

The degree of inhibition can also be indirectly measured by the degree of disinhibition. This was the approach taken next. Live-cell calcium imaging with a fluorescent dye was used to concurrently measure the calcium levels in 50 cells, before and after disinhibition via application of bicuculline. Figure 5.20 shows representative traces. Calcium imaging traces are normally presented as multiples of Ca^{2+}'s dissociation constant from the dye (K_d), with the fluorescence levels calibrated individually for each cover slip. This allows comparisons of Ca^{2+} concentrations between cover slips. However, the calcium transients generated in the presence of bicuculline matched the saturating response the indicator dye could generate, preventing their accurate quantification. Thus, only the raw fluoresence levels are presented as traces here. The basal calcium levels are reported as multiples of K_d, but the amplitude of the bicuculline induced Ca^{2+} transients cannot be calculated and so have not been analysed. The analysis of frequency and duration of transients is unaffected by the difficulty in assessing high Ca^{2+} concentrations.

Figures 5.21 and 5.22 show the quantification of key calcium imaging parameters for neurons cultured from wild type, *Grin2a*$^{-/+}$ and *Grin2a*$^{-/-}$ rats. Figure 5.21 shows firstly that there is no difference in culture density between the genotypes. This is important to exclude as cell density can affect network activity (Pacico and Mingorance-Le Meur, 2014). Secondly, there is no difference in basal Ca^{2+} levels between genotypes, and none of the genotypes exhibited any spontaneous Ca^{2+} transients during the wash period.

Figure 5.22 shows that nearly all cover slips showed coordinated spikes of elevated Ca^{2+} levels in the presence of bicuculline. However, *Grin2a*$^{-/-}$ cover slips on average showed a lower frequency of spikes than wild type. Heterozygous neurons showed an intermediate frequency of spikes, but this was not significantly different to the other genotypes. Finally, some of the homozygous cover slips showed an altered spike morphology, with a quick succession of spikes preventing return to baseline (see traces in Figure 5.20). This was quantified by measuring spike duration, defined as consecutive fluorescence intensities greater than 5% above baseline. However, this did not show any differences between genotypes.

Wild-type

A

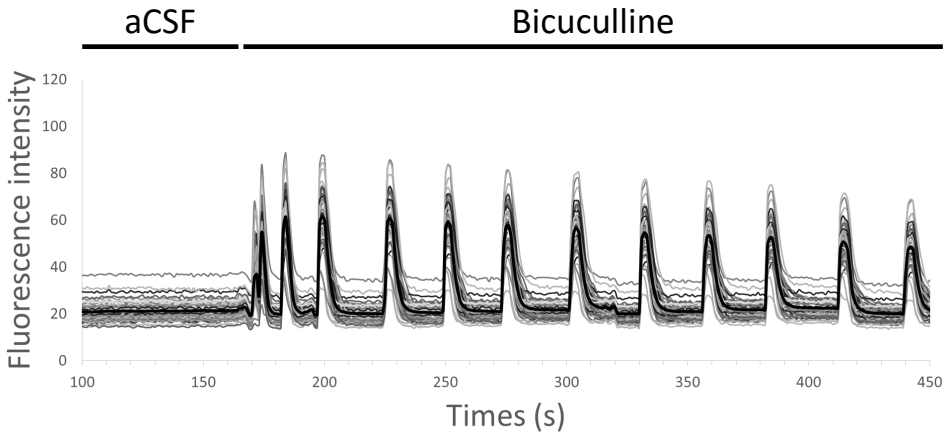

Heterozygous

B

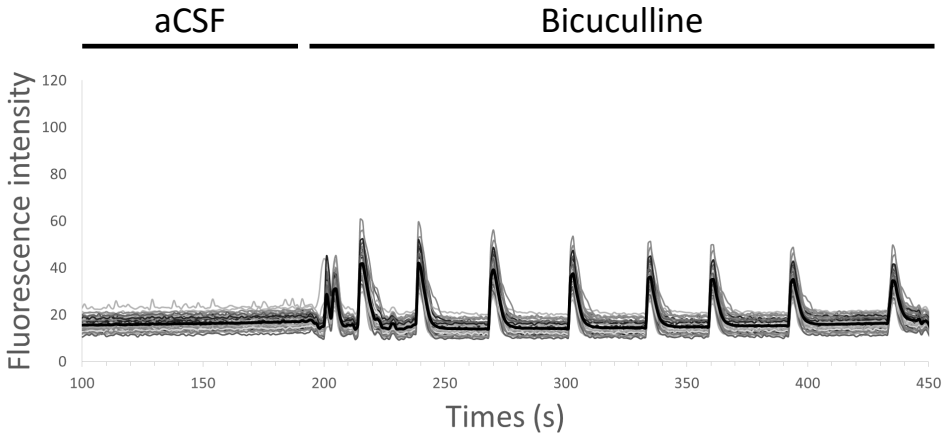

Homozygous

C

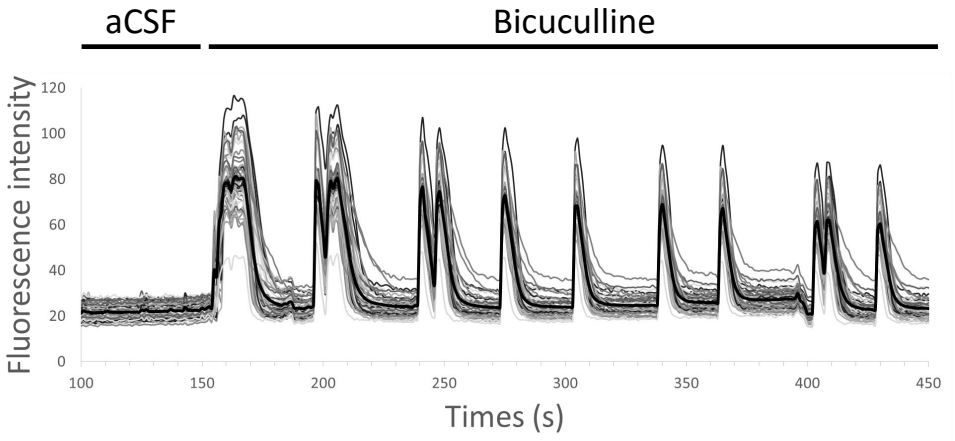

Figure 5.20: **Representative traces showing Ca^{2+} levels in response to bicuculline in neurons cultured from wild type, *Grin2a*$^{-/+}$ and *Grin2a*$^{-/-}$ rats**

(A) Representative trace showing fluorescence intensity of Ca^{2+} sensitive dye (Fluo-3) recorded from DIV 17 cultured cortical neurons during washing with aCSF (artificial cerebrospinal fluid) then bicuculline (50 μM). The thick black line is the average for the cover slip. The thin grey lines show responses of individual cells.

(B) As for **(A)** but cells cultured from *Grin2a*$^{-/+}$ rat.

(C) As for **(A)** but cells cultured from *Grin2a*$^{-/-}$ rat.

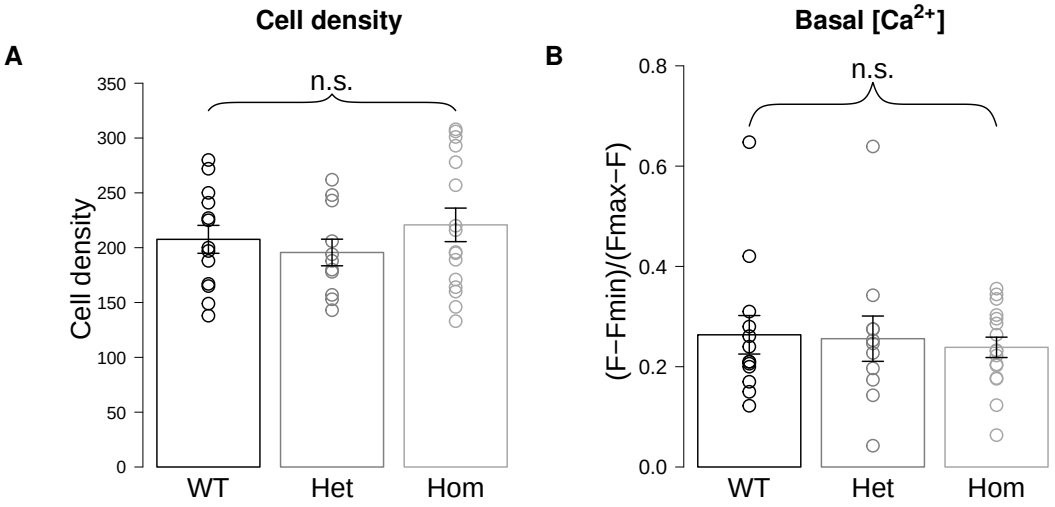

Figure 5.21: **Basal Ca^{2+} levels and cell density in cultured neurons are unaffected by *Grin2a* knock-out**

(A) The bar chart shows cell counts from the cover slips above, counting all cells in a field of view of set area (307 μm^2). A one-way ANOVA showed no significant effect of genotype on cell density (WT: 108 $\pm$ 13, het: 196 $\pm$ 12, hom: 221 $\pm$ 15).

(B) The bar chart shows basal Ca^{2+} levels in DIV 17 neurons cultured from wild type, *Grin2a*$^{-/+}$ and *Grin2a*$^{-/-}$ rats. The Ca^{2+} levels shown are means of 50 cells per cover slip, and were averaged over 50 seconds during washing with aCSF. A one-way ANOVA showed no significant effect of genotype on basal Ca^{2+} levels (WT: 0.26 $\pm$ 0.04 (n=13 cover slips from 4 animals), het: 0.26 $\pm$ 0.05 (n=11 cover slips from 5 animals), hom: 0.24 $\pm$ 0.02 (n=16 cover slips from 6 animals)).

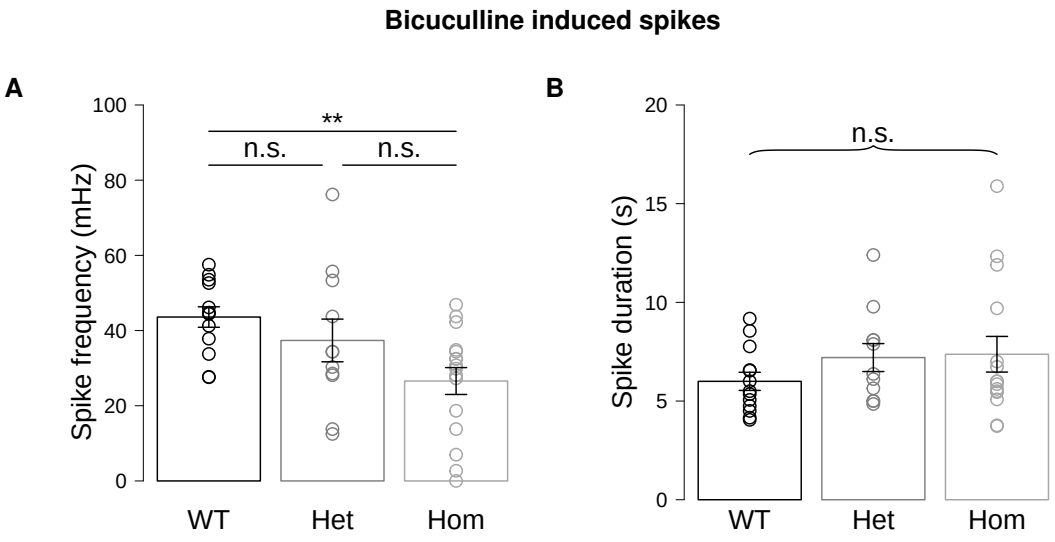

Figure 5.22: **Bicuculline-evoked coordinated Ca^{2+} spikes are less frequent in neurons cultured from *Grin2a*$^{-/-}$ rats**

(A) The bar chart shows frequency of bicuculline evoked spikes in cover slips cultured from wild type, *Grin2a*$^{-/+}$ and *Grin2a*$^{-/-}$ rats. A one-way ANOVA showed a significant effect of genotype on spiking frequency ($F(2,37) = 5.1$, $p = 0.0107$). Post-hoc t–tests (Bonferroni corrected) showed that cells cultured from wild type animals spiked together more frequently than those cultured from *Grin2a*$^{-/-}$ animals (WT: 44 ± 3 (n=13 cover slips from 4 animals), hom: 27 ± 4 (n=16 cover slips from 6 animals), $t(26.4) = 3.8$, $p_{corr} = 0.0024$)). Cells cultured from *Grin2a*$^{-/+}$ rats did not show spike frequency significantly different to either wild type or *Grin2a*$^{-/-}$ rats (het: 37 ± 6, (n=11 cover slips from 5 animals)).

(B) The bar chart shows durations of bicuculline evoked spikes in cover slips cultured from wild type, *Grin2a*$^{-/+}$ and *Grin2a*$^{-/-}$ rats. A one-way ANOVA showed no effect of genotype on spike duration (WT: 6.0 ± 0.5, het: 7.2 ± 0.7, hom: 7.4 ± 0.9). Sample sizes as in **(A)** except one fewer *Grin2a*$^{-/-}$ cover slip, as it demonstrated no spikes.

The final potential functional consequence of low or absent levels of GluN2A to be assessed was excitotoxicity. This was measured by exposing cells to a range of NMDA concentrations for one hour, then fixing and staining with a DNA binding dye (DAPI) the next day. Cells which were alive at the time of staining show diffuse, even, nuclear DNA, whereas cells which were dead at the time of staining show condensed, pyknotic nuclei. Figure 5.23 shows representative images and quantification of the percentage of dead cells at each NMDA concentration for neurons cultured from wild-type, *Grin2a*$^{-/+}$ and *Grin2a*$^{-/-}$ rats. There was no difference in vulnerability to excitotoxicity between genotypes.

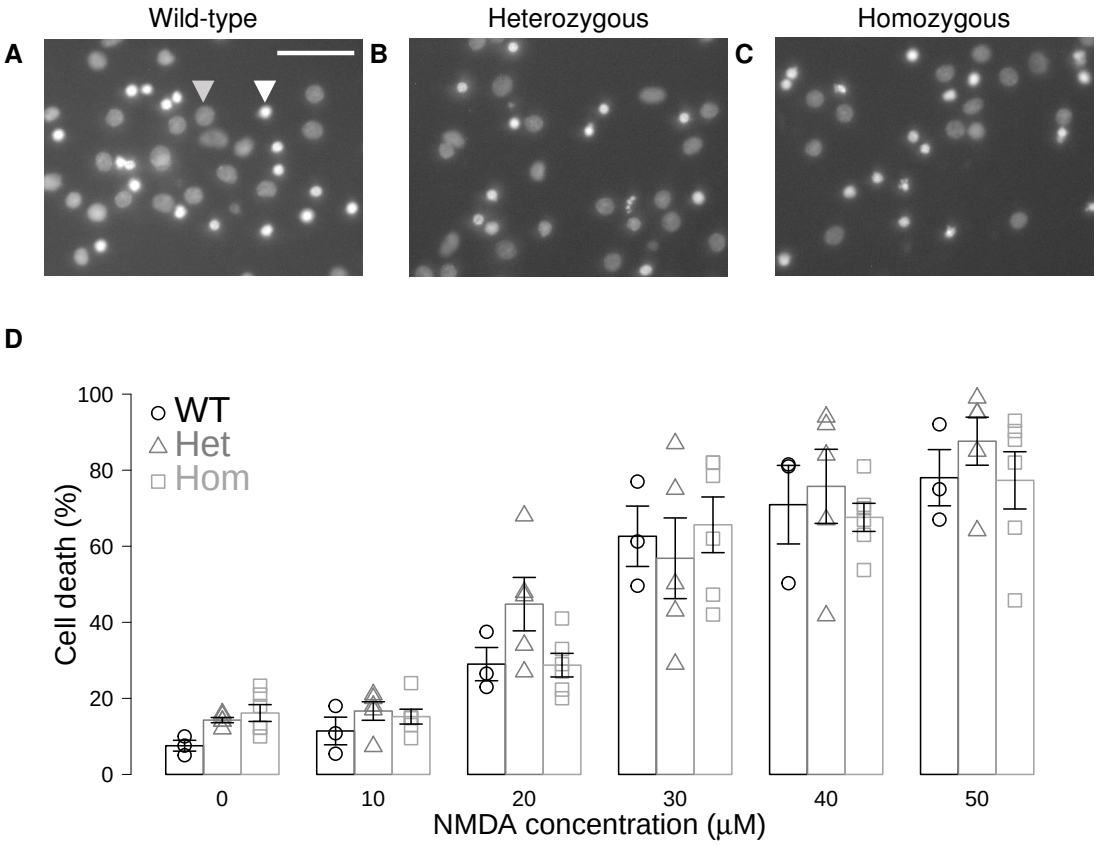

Figure 5.23: **Cell death in cultured neurons is unaffected by *Grin2a* knock-out**
(A) The image shows a representative x20 field of view from a cover slip of wild type DIV 17 cultured cortical neurons fixed and stained with DAPI 23 hours after exposure to NMDA 30 μM. The white triangle marks a dead cell, the grey triangle a cell that was living at the time of staining. The white bar marks 50 μm. All images have had brightness of faint objects enhanced by using ImageJ's (Schneider et al., 2012) non-linear intensity adjustment function with gamma set to 0.5.
(B) As **(A)** but neurons cultured from *Grin2a*$^{-/+}$ rat.
(C) As **(A)** but neurons cultured from *Grin2a*$^{-/-}$ rat.
(D) The bar chart shows % cell death in DIV 17 neurons cultured from wild-type, *Grin2a*$^{-/+}$ and *Grin2a*$^{-/-}$ rats. A two-way ANOVA showed no significant effect of genotype on cell death but a significant effect of NMDA concentration ($F(5,66) = 66$, $p < 2e\text{-}16$).

5.7 Discussion

5.7.1 Summary of findings

This chapter first described the validation of two new rat models allowing the constitutive and conditional knock-out of *Grin2a*. It then described some initial functional investigations into the consequences of *Grin2a* knock-out, identifying a reduction in current density and altered inhibition in cultured neurons. *Grin2a* knock-out was not found to affect frequency or amplitude of miniature synaptic events, or excitotoxicity. Heterozygous *Grin2a* knock-out resulted in functional haploinsufficiency, including reduced current density, but did not impact on any other functional property assessed.

5.7.2 Validation of *Grin2a*$^{flox/flox}$ and *Grin2a*$^{-/-}$ model

Investigation of the *Grin2a*$^{flox/flox}$ rat confirmed the appropriate exon is floxed and that exposure to Cre results in excision of the exon. It also confirmed that the LoxP sites do not influence GluN2A expression in the absence of exposure to Cre. It is useful to confirm that *Grin2a* can be conditionally knocked out in these rats when cultured. However, the knock-out would need to be revalidated in any further experimental conditions, for example, if a virus for *in vivo* injection was used, or if the line were crossed with a Cre line.

Similarly, it is useful to have confirmed that *Grin2a* is constitutively knocked out in the cortices and cultured cortical neurons of the *Grin2a*$^{-/-}$ rats. However, conceivably different tissue types could process the modified *Grin2a* transcript differently, so it would be important to confirm knock-out in the particular region of interest for future experiments, for example, the hippocampus.

To my knowledge, these are the first rat models of *Grin2a* knock-out. However, a mouse *Grin2a* knock-out was generated in the 1990s. Table 5.1 summarises findings in the mouse model. Overall, *Grin2a* knock-out is associated with a relatively mild phenotype. A range of reductions in synaptic plasticity have been identified, as have some specific mild learning impairments. Three studies observed increased motor activity in unfamiliar environments, and the initial publication reporting the line described them as “jumpy” (Sakimura et al., 1995). No studies have reported spontaneous seizures (and none have been observed in the *Grin2a*$^{-/-}$ rats maintained during this study).

5.7.3 *Grin2a*$^{-/+}$ and *Grin2a*$^{-/-}$ neurons have reduced current density

A reduction in NMDA-evoked current density in cultured neurons aged older than two weeks was identified in heterozygous and homozygous knock-out rats. This is of interest for two reaons. Firstly, it shows that cultured neurons do not wholly compensate for the absence of GluN2A by increasing expression of other GluN2 or GluN3 subunits. It is possible that there is some increase in other GluN subunits but any increase is insufficient to match the loss of GluN2A. A more complete picture of changes in other GluN subunits could be provided by performing immunoblots for the other GluN subunits in *Grin2a*$^{-/+}$ and *Grin2a*$^{-/-}$ rats.

Table 5.1: Phenotypes observed in *Grin2a*$^{-/-}$ mice

Phenotype	Study
Basic phenotypic assessment	
Normal skeletal structure, eye structure, haematology, biochemistry, startle response, tremor, open field behaviour, time on rotarod	International Mouse Phenotyping Consortium (www.mousephenotype.org)
Altered synaptic plasticity	
Reduced in hippocampus	Kiyama et al. (1998); Sakimura et al. (1995) Ito et al. (1996); Longordo et al. (2009) Kannangara et al. (2015)
Reduced in visual pathways	Cho et al. (2009); Philpot et al. (2007) Zhao and Constantine-Paton (2007)
Reduced in cerebellum	Andreescu et al. (2011)
Altered behaviour	
Impaired spatial reference memory	Miyamoto et al. (2001); Sakimura et al. (1995) Kannangara et al. (2015)
Impairments in other types of memory	
Reduced spatial working memory	Bannerman et al. (2008)
Reduced context dependent fear conditioning, particularly when short exposure to context	Kiyama et al. (1998)
Reduced motor learning (phase reversal adaptation of vestibulo-ocular reflex)	Andreescu et al. (2011)
Reduced eye blink conditioning	Kishimoto et al. (1997)
Reduced visual discrimination learning	Brigman et al. (2008)
Impaired set shifting	Marquardt et al. (2014)
Altered motor activity	
Increased motor activity in new environment	Miyamoto et al. (2001); Tomiyama et al. (2013) Boyce-Rustay and Holmes (2006b)
Reduced motor coordination (time on rotarod)	Boyce-Rustay and Holmes (2006a)
Other phenotypes	
Dendritic alterations in immature cells in dentate gyrus	Kannangara et al. (2014)
Smaller injury size following transient (but not prolonged) ischaemia	Morikawa et al. (1998)
Increased NMDA-evoked release of dopamine in striatum	Miyamoto et al. (2001)
Decreased NMDA-evoked release of GABA in striatum	Miyamoto et al. (2001)
Less sensitivity to seizure following electrical stimulation of inferior colliculus	Sakamoto et al. (2002)

All phenotypes reported as *Grin2a*$^{-/-}$ mice relative to wild type

A reduction in current density is also of interest because this will impact on NMDAR signalling. A given stimulus will evoke less response in the heterozygotes or homozygotes than in wild type. This would be expected to influence excitability via smaller changes in membrane potential due to NMDAR activation, and potentially to impact on synaptic plasticity via less Ca^{2+} entry. These possibilities could be explored by making recordings from acute slices *in vitro* in regions such as the hippocampus and assessing NMDAR-mediated EPSP and response to paradigms designed to evoke NMDAR-mediated synaptic plasticity, such as long term potentiation and depression. Indeed, previous work with *Grin2a*$^{-/-}$ mice has shown a range of reductions in synaptic plasticity (see Table 5.1).

5.7.4 *Grin2a* knock-out does not influence properties of miniature synaptic events

No effect of *Grin2a* knock-out was found on the amplitude or frequency of mEPSCs or mIPSCs, or their ratio, in mature cultured cortical neurons. This is in contrast to what has been found previously, albeit those findings have opposed each other. One group conditionally knocked out GluN2A in mice using viral injections on P0/P1 and recording from CA1 pyramidal neurons in acute slices on P17. They identified a reduction in mEPSC amplitude in the absence of GluN2A, but no effect on frequency (Gray et al., 2011). The other group made recordings in hippocampal organotypic slices, overexpressing GluN2A after biolistic transfection 60-72 hours prior to recording. They identified a reduction in mEPSC frequency with overexpression of GluN2A but no effect on amplitude (Gambrill and Barria, 2011). A few differences between the current study and the previous work stand out. Firstly, both the previous studies were done in hippocampal preparations, whereas this study was performed in cortical neurons. Secondly, neither previous study caused GluN2A alterations in all the cells in the preparation, whereas this study generated cells where the entire network experienced a complete absence of GluN2A. Finally, this study was performed in dissociated cultures, meaning that normal regional architecture was abolished, in contrast to slices. Regional differences, network level compensation, or altered networks following dissociation, could all therefore explain the lack of differences found in this study compared to previous work.

To investigate the impact of *Grin2a* knock-out in a more physiological manner, it would be useful to assess mEPSCs and mIPSCs in acute slices from *Grin2a*$^{-/-}$ rats. It would also be interesting to investigate the possibility of network compensation further, as “synaptic scaling” is known to operate widely in cultured neocortical neurons - modulating network activity induces compensatory changes in mEPSC or mIPSC amplitude via bidirectional changes in AMPAR or $GABA_AR$ density respectively (reviewed in Turrigiano (2011)). If homeostatic plasticity has occurred in *Grin2a*$^{-/-}$ cultures to maintain mEPSC frequency and amplitude similar to wild type, it could be hypothesised that the system will have less reserve to deal with a second pertubation to synaptic activity, such as the overnight application of TTX, and differences between genotypes could potentially be revealed in this way.

5.7.5 *Grin2a* knock-out reduces disinhibition

Knock-out of *Grin2a* was found to reduce the frequency of coordinated calcium transients following blockade of inhibitory neurotransmission by bicuculline in mature cultured cortical neurons. This could be due to a reduction in inhibitory inputs to *Grin2a*$^{-/-}$ cells resulting in less disinhibition when inhibition is removed. Although some previous work supports the idea that NMDARs are important for inhibitory function (Moreau and Kullmann, 2013), no evidence to directly support this was provided here. A

reduction in coordinated activity following bicuculline could also arise from an overall reduction in network coordination. Further work to explore the causes of the altered network coordination would include assessing the number of interneurons in *Grin2a*$^{-/-}$ rats, with parvalbumin-positive interneurons being of most interest, and using multi-electrode arrays to make field recordings from cultures or acute slices at rest and following stimulation. The multi-electrode array recordings could allow coordinated network activity to be assessed in a more precise manner than is possible with Ca^{2+} imaging, where the need to avoid photo bleaching limits the sampling frequency (in this study, to once per second).

Coordinated neural activity, particularly gamma oscillations, have been linked to a range of cognitive functions, and reductions in coordination identified in a range of neurodevelopmental disorders (reviewed by Uhlhaas and Singer (2012)). If *Grin2a* knock-out does indeed cause a reduction in coordinated network activity, this may be of great relevance to the pathophysiology of epilepsy-aphasia syndromes. It would be interesting to make EEG recordings from *Grin2a*$^{-/+}$ rats and see if there is any evidence of alterations in coordination, particularly in the gamma band. It would also be interesting to look for EEG findings typical of those found in epilepsy-aphasia syndrome: paroxysmal centrotemporal spikes, particularly during sleep (Berroya et al., 2005; Smith and Hoeppner, 2003). Unexpectedly, the only study which has addressed seizures in *Grin2a* knock-out mice found that they showed a higher resistance to seizures evoked by direct electrical stimulation of the inferior colliculus (stimulating the same pathway as audiogenic seizures) (Sakamoto et al., 2002).

5.7.6 *Grin2a* knock-out does not influence excitotoxicity

Knock-out of *Grin2a* was found not to influence the vulnerability of cells to death induced by prolonged elevated ambient levels of NMDA. This is consistent with previous work highlighting the C terminus of GluN2B as critical in mediating cell death under these conditions (Martel et al., 2012). The finding that the current density in *Grin2a*$^{-/-}$ was significantly lower than in wild type cells suggests that minimal, if any, compensatory increase in GluN2B expression occurred in *Grin2a*$^{-/-}$ cells. If their GluN2B expression levels were similar to those of wild type cells, it would be expected that their vulnerability to NMDA evoked cell death would be similar also. Although some previous work using pharmacological blockage concludes GluN2A is neuroprotective (for example, (Terasaki et al., 2010; von Engelhardt et al., 2007)), the findings of this study suggest it is neutral with regard to excitotoxicity.

5.7.7 Limitations

The major limitations of this chapter are with regard to the relevance of the findings in *Grin2a*$^{-/+}$ rats to *GRIN2A* disrupting mutations in humans with epilepsy-aphasia syndromes. Firstly, the only assessment of functional consquences performed here has been in dissociated cultured cortical neurons. This system was chosen as it was a relatively simple way to quickly assess a range of parameters. However, assessment of functional impact at the whole organism or regional level would be much preferable, and offers a rich vein of future work in this area. The second limitation is that not all the functional consequences detected in homozygous knock-outs have been detected in heterozygotes. Although functional consequences in homozygotes are of physiological interest, to be relevant to disease they should also be detectable in heterozygous knock-outs.

5.7.8 Conclusion

This chapter has validated two new rat models: a constitutive and conditional knock-out of *Grin2a*. It established that *Grin2a*$^{-/+}$ rats experience haploinsufficiency, and that this is associated with a reduction in NMDA-evoked current density. This chapter has therefore taken some preliminary steps towards using *Grin2a*$^{-/+}$ rats as a model for epilepsy-aphasia syndromes in humans.

CHAPTER 6

General discussion

6.1.1 Summary of key findings

This thesis assessed the functional consequences of four missense mutations in the type 2A and 2B subunits of the NMDA receptor, and performed a validation and preliminary functional investigation of rat models where the 2A subunit was knocked-out heterozygously or homozygously. The key findings of this thesis are: three of the four missense mutations were found to significantly alter physiologically fundamental properties of the NMDAR: compared to wild type, GluN2A^{N615K} was found to reduce Mg^{2+} block, GluN2B^{N615I} and GluN2B^{V618G} to cause potentiation by Mg^{2+}, and GluN2A^{N615K} and GluN2B^{N615I} showed reduced conductance. GluN2A^{R586K} was not found to influence the parameters assessed. When GluN2A^{N615K} was expressed alongside wild type subunits in the same NMDA receptor, it was found to have a dominant negative effect. In the rat *Grin2a* knock-out model, heterozygous neurons had lower GluN2A protein expression and current density, and homozygous neurons showed reduced coordinated neural activity.

6.1.2 How might these mutations contribute to neurodevelopmental disorders?

The overall aim of this thesis was to use the knowledge generated from functional investigations of mutations in NMDARs found in humans with neurodevelopmental disorders to better understand the pathogenesis of neurodevelopmental disorders. What progress has been made towards this aim?

Firstly, three of the four missense mutations were found to cause marked disruption to a NMDAR property which is already known to be integral to important brain functions: Mg^{2+} block. In the case of GluN2A^{N615K}, this effect was found to be dominant negative. Mg^{2+} block is essential to the NMDAR's role as a molecular coincidence detector and hence its roles in synaptogenesis and synaptic plasticity (see Section 1.4.7 and 1.4.8). As these processes are thought to represent the cellular basis of learning and memory, a mutation which altered them could plausibly lead to neurodevelopmental disorder, particularly intellectual disability.

Secondly, two of the four missense mutations were found to reduce single channel conductance: the rate of flow of ions through the channel. As most, if not all, of the NMDAR's signalling is ionotropic, reductions in this would influence many NMDAR functions. For example, less excitatory drive could disrupt the rhythm of neural oscillations. Less Ca^{2+} entry during an activation could result in inappropriate intracellular signals for regulation of AMPA receptor density or gene expression.

Thirdly, the heterozygous *Grin2a*$^{-/+}$ rat was found to show reduced current density. As with the point mutations, this could result in alterations in excitatory drive and Ca^{2+} dependent signalling. The alteration in coordinated neural activity seen in the homozygous *Grin2a*$^{-/-}$ rat suggests changes in excitatory drive may be important.

The identification of altered functional consequences associated with these mutations is thus consistent with them having a role in causing neurodevelopmental disorders. However, this thesis has not been able to prove this. No reversal of the altered property with subequent reversal of phenotype has been attempted. It remains possible that the altered properties identified are not important in causing disease, or that additional altered properties that have not been assessed are also important. The hypothesised impact on circuit level functions such as plasticity has not been assessed. Any compensation which could occur during development of a whole organism has also not been assessed.

Finally, the impact of the mutations in NMDARs expressed in human cells, rather than heterologously in rodent cells, has not been evaluated.

Despite these limitations I believe the severity of the alteration in NMDAR properties observed makes it highly likely that these mutations do influence risk for neurodevelopmental disorder in their carriers. Overall, the functional consequences of these mutations highlight synaptic plasticity, neural oscillations and possibly synaptogenesis as candidate mechanisms which are disrupted in epileptic encephalopathies and epilepsy-aphasia syndromes.

6.1.3 Do functional consequences of mutations in NMDARs indicate a shared aetiology for NMDAR-synaptopathies?

The NMDAR mutations studied in this thesis are not the only ones to have been functionally investigated. Is there a pattern of functional alteration common to all NMDAR mutations found in people with neurodevelopmental disorders? Table 6.1 presents a summary of the functional consequences of the 19 other mutations for which functional investigations have been published so far. As in this thesis, these investigations have all been peformed in heterologous systems and extrapolation to humans brains needs to be done cautiously. The table shows that the functional consequences of the mutations influence a range of receptor properties, and in opposing overall directions (activating/"gain of function" or inhibiting/"loss of function"). There is no one consequence of mutations in either gene, unsurprisingly given their diverse locations. In the small number of mutations assessed so far in *GRIN2B*, there is a pattern of activating mutations being associated with epilepsy, and inhibitory mutations being associated with intellectual disability, but more mutations would need to be tested before this pattern could be viewed as definite. However, there is clearly no one overall consequence for *GRIN2A* mutations associated with epilepsy-aphasia syndromes, as these disorders are associated with mutations which both increase and decrease overall channel activation.

The different directions of effect for *GRIN2A* mutation functional consequences may reflect the fact that most of the mutations have undergone targeted rather than consistent functional evaluation, and may affect more than one property without this being known. For example, opposing effects on different properties have been identified in this thesis for GluN2A^{N615K} and GluN2B^{N615I}. A thorough evaluation of each mutation and synthesis of effects may lead to the identification of an overall pattern of increased or decreased function. Alternatively, there may be some specific shared consequence of all the mutations which remains to be identified, for example, an interaction with a particular intracellular protein. However, it remains possible that similar symptoms can be caused by a disruption of neural homeostasis in opposite directions. This has already been proposed in the aberrant protein synthesis theory of intellectual disability and autism, where too much or too little protein synthesis give a similar phenotype (Auerbach et al., 2011). Similarly to *GRIN2A*, the same type of epilepsy has been observed in people carrying mutations of opposing effect in the case of the nicotinic acetylcholine receptor (causing autosomal dominant nocturnal frontal lobe epilepsy) and the type 1.1 voltage gated sodium channel (causing Dravet syndrome) (Avanzini et al., 2007).

Table 6.1: Functional consequences of mutations identified in *GRIN2A* and *GRIN2B*

Study	Disorder	Protein domain	Mutation	Consequence
		GluN2A		
Activating				
Lemke et al. (2013)	Epilepsy-aphasia syndrome	N terminus	GluN2A^{A243V}	Zn^{2+} inhibition reduced
Lesca et al. (2013)	Epilepsy-aphasia syndrome	Ligand binding domain (S1)	GluN2A^{R518H}	Channel opening time increased four fold
Carvill et al. (2013)	Epilepsy-aphasia syndrome	Ligand binding domain (S1)	GluN2A^{T531M}	Channel opening time increased four fold
Endele et al. (2010)	Epileptic encephalopathy	Pore (M2)	GluN2A^{N615K}	Ca^{2+} permeability reduced three fold
Lesca et al. (2013)	Epilepsy-aphasia syndrome	Pore (M3)	GluN2A^{F652V}	Channel opening time increased two fold
Yuan et al. (2014)	Epileptic encephalopathy	Ligand binding domain (S2-M4 linker)	GluN2A^{L812M} (di- and tri-het)	Glutamate and glycine potency increased, Zn^{2+} H^{+} and Mg^{2+} sensitivity reduced, open probability increased.
Inhibitory				
Serraz et al. (2016)	Epilepsy-aphasia syndrome	N terminus	GluN2A^{P79R} (di- and tri-het)	Protein expression reduced. Zn^{2+} inhibition reduced four fold but H^{+} inhibition increased.
Serraz et al. (2016)	Epilepsy-aphasia syndrome	N terminus	GluN2A^{C231Y}	Protein expression markedly reduced
Serraz et al. (2016)	Epilepsy-aphasia syndrome	N terminus	GluN2A^{R370W} (di- and tri-het)	Zn^{2+} inhibition increased $>$ ten fold
Serraz et al. (2016)	Epilepsy-aphasia syndrome	Ligand binding domain	GluN2A^{C436R}	Protein expression markedly reduced
No effect				
Serraz et al. (2016)	Epilepsy-aphasia syndrome	N terminus	GluN2A^{F183I} GluN2A^{I184S} GluN2A^{C243V} GluN2A^{C290V} GluN2A^{G295S}	No effect on expression, glutamate affinity, glycine affinity, open probability, Zn^{2+} or H^{+} inhibition
		GluN2B		
Activating				
Lemke et al. (2014)	Epileptic encephalopathy	Pore (M2)	GluN2B^{N615I}	Ca^{2+} permeability increased three fold
Lemke et al. (2014)	Epileptic encephalopathy	Pore (M2)	GluN2B^{V618G}	Ca^{2+} permeability increased three fold
Inhibitory				
Endele et al. (2010)	Intellectual disability (moderate)	N terminus	GluN2B^{R682C}	Glycine affinity two fold reduction
Adams et al. (2014)	Intellectual disability (severe)	Ligand binding domain (S1)	GluN2B^{E413G}	Glutamate affinity reduced 50-fold

Di- and tri-het refers to diheteromers and triheteromers. Where not specified, only diheteromers were investigated. Findings which have been replicated in this thesis are not included in the table.

6.1.4 Do functional consequences of mutations in other genes indicate a shared aetiology for epileptic encephalopathies?

How do the findings of this thesis relate to other causes of the same disorders? The three missense mutations studied here are all associated with epileptic encephalopathy. Do other causes of epileptic encephalopathy demonstrate alterations at the circuit level similar to those proposed for these mutations? For example, do they show alterations in synaptic plasticity or neural oscillations? The answer to this question is uncertain. As the majority of genetic causes of epileptic encephalopathies have only been identified within the last five years, the major animal models in this field represent acquired epilepsy, seeking to model the impact of early life infection, hypoxia or stress, on the brain and assessing predominantly seizure phenomenology and behavioural outcomes rather than neural circuit effects (reviewed in Galanopoulou and Moshe (2015), Shao and Stafstrom (2016) and Auvin et al. (2016)).

One of the main animal models of epileptic encephalopathy is intra-peritoneal injection of NMDA, which in addition to causing truncal flexion seizures is acutely associated with impairments in learning and coordination (Shao and Stafstrom, 2016). Interestingly, maternal exposure to prenatal stress or stress hormones shortens the latency of time to seizure following injection (Shao and Stafstrom, 2016). Using this model, it was recently found that rats which had undergone NMDA injection as juveniles showed enhanced hippocampal LTP as adults (Tsuji et al., 2016). Thus, exposure to excess NMDAR activation during development is associated with seizures, cognitive impairment and later alterations in synaptic plasticity. This supports the theory that activating NMDAR mutations could also cause these effects, but does not speak to any convergence across multiple causes of epileptic encephalopathy.

The animal models of genes found to be mutated in epileptic encephalopathies available so far provide some evidence of convergence on interneuron dysfunction. Mutations in the transcription factor *ARX* (West syndrome) are associated with interneuron migration abnormalities (Marsh et al., 2009), and mutations in the sodium channel gene *SCN1A* (Dravet syndrome) are associated with impaired firing of fast-spiking interneurons (Yu et al., 2006). This resonates with the proposed importance of NMDAR subunits for interneuron function (see Section 5.2.2 in Chapter 5's Introduction) and with the abnormalities in disinhibition observed in homozygous *Grin2a*$^{-/-}$ rats in Chapter 5. However, further investigation with different genes is needed to clarify the importance of interneuron dysfunction more generally in epileptic encephalopathies.

6.1.5 How can the findings of this thesis be used clinically?

Is there any clinical utility to the findings of this thesis? Firstly, are there any pharmacological treatments available which could reverse the functional alterations seen? Unfortunately, in the case of the missense mutations, existing pharmacological treatments are unlikely to be of benefit. This is partly because the nature of the direction of useful modification is unclear - if a channel is open too much (i.e. has loss of Mg^{2+} block), blocking it could be helpful. However, if it is allowing too little current to pass (i.e. a reduction in single channel conductance), potentiating it could be helpful. Which, if any, of these interventions is of benefit could potentially be established in an animal model, but not in heterologous systems without robust validation of a "cellular phenotype" which relates to clinical symptoms. Further, because the mutations are carried heterozygously, the impact of any drug on the wild type subunit needs to be considered. Improving the function of the mutant while disrupting the function of the wild type subunit is unlikely to be of overall benefit. This would likely be a problem if dextromethorphan were used to block receptors containing GluN2A^{N615K} subunits as the difference in potency between GluN2A^{N615K} and wild type subunits is not large.

Despite these difficulties, a treatment based on correcting the consequence of a missense point mutation in a NMDAR subunit has been trialled and found to be of benefit (Pierson et al., 2014). In this case, a child with epileptic encephalopathy was found to heterozygously carry the GluN2A^{L812M} mutation. Electrophysiological assessment showed this mutation to result in overactivation of NMDARs with all the parameters assessed. Memantine potency was reduced about three fold by the mutation compared to wild type, but maximal effective block was the same. Aged nine years old, the child was therefore given a trial of memantine with the aim of reducing activity of receptors containing his mutated subunits. The trial reduced the frequency of his seizures to a third of what they had been, and abolished his myoclonic jerks, but did not influence his cognition. Thus, in this case knowledge of the functional consequences of a point mutation did allow useful, personalised treatment. This allows optimism that were a drug to be identified which reduced the effects of the missense mutations studied here, it could still be of benefit in someone with established symptoms.

Considering the mutations which probably result in an absent protein, modelled by the *Grin2a*$^{-/+}$ rat, the picture is a little simpler. Here, the problem is not enough GluN2A activity, and this could potentially be improved by positive allosteric modulators which are selective for GluN2A over GluN2B, for example, GNE-6901 or GNE-8324, members of a recently identified new class of modulator which stabilise the GluN1/GluN2A ligand binding domain subunit interface in an open conformation (Hackos et al., 2016). Alternatives would include UBP512, although at the required concentrations this also inhibits GluN2C and GluN2D (Costa et al., 2010). Positive allosteric modulators which enhance both GluN2A and GluN2B activity, for example pregnenolone sulphate (Malayev et al., 2002) or UBP710 (Costa et al., 2010), could potentially also be useful, although may increase the risk of GluN2B-mediated excitotoxicity. It would be important to establish the efficacy of these drugs on GluN2A/GluN2B triheteromeric receptors before using them in animals, and indeed the GNE compounds have already been shown to potentiate GluN2A/GluN2B triheteromers, although to a lesser extent than their potentiation of GluN2A diheteromers (Hackos et al., 2016).

A new field of treatment possibilities for genetic disorders is provided by gene therapy: editing, replacing or blocking the expression of a mutated gene (Naldini, 2015). Major obstacles remain to its implementation *in vivo*, and there are concerns about the ethics of irreversible treatments. However, there are some relatively simple, reversible forms of targeted gene therapy which have already shown benefit

in vitro in disorders caused by ion channel mutations. For example, allele-specific RNA interference was used to specifically downregulate a heterozygous mutant allele encoding a potassium channel which causes heart arrhythmias (Matsa et al., 2014). This approach could potentially benefit carriers of dominant negative mutations such as GluN2A^{N615K}. Those with *GRIN2A* nonsense mutations could potentially benefit from trialling an antibiotic such as gentamicin. This has been used to induce read through of a premature stop codon in a $GABA_A$ receptor subunit associated with the epileptic encephalopathy Dravet's syndrome, showing partial rescue *in vitro* (Huang et al., 2012).

The second domain of clinical utility of these results is in diagnosis, prognosis, and reproductive planning. Knowing that the GluN2A^{N615K}, GluN2B^{N615I} and GluN2B^{V618G} mutations are associated with marked functional consequences, but GluN2A^{R586K} is not, is useful to clinical geneticists and families who are either trying to understand the cause of a disorder in a child or plan regarding future pregnancies. This information may also be relevant to similar but non-identical mutations, as it highlights which residues can tolerate a change, and which cannot without altering important properties.

6.1.6 What future work would be useful?

The results of this thesis suggest a range of future experiments. Continuing to work with heterologous expression systems, it would be interesting to assess single channel conductance in NMDARs containing GluN2B^{V618G} mutant subunits, and in triheteromeric versions of all three of the mutant subunits. Ca^{2+} permeabiility of diheteromeric mutant subunits has been assessed by others, but this would also be interesting to examine in triheteromers. These experiments would improve mechanistic understanding of the consequences of the mutations.

To allow assessment of circuit level dysfunction and behaviour, the GluN2A^{N615K}, GluN2B^{N615I} and GluN2B^{V618G} could all be usefully explored in animal models. Circuit level function could be assessed by making multi-electrode array recordings from acute slice preparations, amongst other approaches. Animal models would also allow pharmacological agents to be trialled, and the effect of removing the mutation could be tested if genetic reversibility were included within the model design.

The *Grin2a*$^{-/+}$ rat has been validated and stands ready for a range of future experiments. Of particular interest would be to assess the impact of GluN2A haploinsufficiency on EPSCs in principal cells and interneurons in the hippocampus. This could help to clarify which cell type is more affected, with the hypothesis that excitatory drive to interneurons would show a greater reduction. It would also be interesting to assess synaptic plasticity in hippocampal slices, with the hypothesis that GluN2A heterozygotes would show a reduction in LTP, as seen in mice (see Table 5.1 in Chapter 5's discussion). Network dynamics could also be investigated in hippocampal slices via multi-electrode array recordings. Spontaneous and evoked activity could be assessed for frequency, power and burst profiles, with the hypothesis that the GluN2A heterozgotes would show lower gamma power but greater propensity to epileptiform activity in the presence of pro-convulsant agents.

Considering experiments at the whole organism level, seizure susceptibility would be important to assess by monitoring response to a seizure inducing stimulus (e.g. noise), with the hypothesis that GluN2A heterozygotes would show a lower seizure threshold. Analysing the EEG of alert, spontaneously behaving animals during sleep and awake periods would be potentially very useful translationally - with the hypothesis that GluN2A heterozygote rats would show spike and wave activity during the slow wave

stages of their sleep cycle, and potentially some spikes over the motor cortex when awake (based on what has been observed in humans). Cognitive dysfunction would also be important to assess. *Grin2a*$^{-/-}$ mice show some mild impairments in spatial memory, fear conditioning and set shifting (see Table 5.1). *Grin2a*$^{-/-}$ rats would be expected to share these deficits, but in addition allow a more complex repertoire of cognitive testing than is easy to achieve in mice. For example, object-place recognition, which tests the rat's ability to distinguish objects based on a memory combining their familiary and their location when first presented, and which has been shown to be NMDAR-dependent (Barker and Warburton, 2008). Use of these more complex tests may be required to identify potentially subtle deficits in heterozygous animals, given that many *GRIN2A*$^{+/-}$ humans do not show intellectual disability.

The *Grin2a*$^{flox/flox}$ rat has also been validated. When combined with exposure to Cre recombinase this rat allows assessment of the importance of GluN2A in development and in particular cell types or brain regions. Cre expression could be achieved by crossing the *Grin2a*$^{flox/flox}$ line with a Cre-expressing genetically modified line, although there are not many of these available in rats yet. Alternatively, Cre expression could be achieved using viruses injected *in vivo* or into organotypic slices. The use of cell type specific promoters would allow the importance of GluN2A in interneurons to be addressed, with the hypothesis that selective knock-out of GluN2A in interneurons alone would result in an epilepsy-related phenotype. Injection of virus at different ages would allow the identification of any "critical period" after which GluN2A removal does not result in impairment. The presence or absence of such a period would have implications for the timing of any future treatments for GluN2A haploinsufficiency.

6.1.7 Conclusion

In conclusion, this thesis addressed the hypothesis that mutations in NMDAR subunits cause neurodevelopmental disorders in humans. I found that three of the four missense mutations studied caused substantial changes in physiologically pivotal NMDAR properties. I also found that a rat model of gene disrupting mutations in the GluN2A subunit experienced haploinsufficiency with a reduction in NMDAR currents. Overall, these findings strengthen the evidence that these NMDAR subunit mutations cause neurodevelopmental disorders, and further emphasise NMDAR-related functions such as synaptic plasticity as likely candidates for disruption during the pathogenesis of mental disorder.

Bibliography

Adams, D. R., Yuan, H., Holyoak, T., Arajs, K. H., Hakimi, P., Markello, T. C., Wolfe, L. A., Vilboux, T., Burton, B. K., Fajardo, K. F., Grahame, G., Holloman, C., Sincan, M., Smith, A. C., Wells, G. A., Huang, Y., Vega, H., Snyder, J. P., Golas, G. A., Tifft, C. J., Boerkoel, C. F., Hanson, R. W., Traynelis, S. F., Kerr, D. S., and Gahl, W. A. (2014). Three rare diseases in one Sib pair: RAI1, PCK1, GRIN2B mutations associated with Smith-Magenis Syndrome, cytosolic PEPCK deficiency and NMDA receptor glutamate insensitivity. *Mol. Genet. Metab.*, 113(3):161–170.

Al-Hallaq, R. A., Conrads, T. P., Veenstra, T. D., and Wenthold, R. J. (2007). NMDA di-heteromeric receptor populations and associated proteins in rat hippocampus. *J. Neurosci.*, 27(31):8334–8343.

Allen, A. S., Berkovic, S. F., Cossette, P., Delanty, N., Dlugos, D., Eichler, E. E., Epstein, M. P., Glauser, T., Goldstein, D. B., Han, Y., Heinzen, E. L., Hitomi, Y., Howell, K. B., Johnson, M. R., Kuzniecky, R., Lowenstein, D. H., Lu, Y. F., Madou, M. R., Marson, A. G., Mefford, H. C., Esmaeeli Nieh, S., O'Brien, T. J., Ottman, R., Petrovski, S., Poduri, A., Ruzzo, E. K., Scheffer, I. E., Sherr, E. H., Yuskaitis, C. J., Abou-Khalil, B., Alldredge, B. K., Bautista, J. F., Berkovic, S. F., Boro, A., Cascino, G. D., Consalvo, D., Crumrine, P., Devinsky, O., Dlugos, D., Epstein, M. P., Fiol, M., Fountain, N. B., French, J., Friedman, D., Geller, E. B., Glauser, T., Glynn, S., Haut, S. R., Hayward, J., Helmers, S. L., Joshi, S., Kanner, A., Kirsch, H. E., Knowlton, R. C., Kossoff, E. H., Kuperman, R., Kuzniecky, R., Lowenstein, D. H., McGuire, S. M., Motika, P. V., Novotny, E. J., Ottman, R., Paolicchi, J. M., Parent, J. M., Park, K., Poduri, A., Scheffer, I. E., Shellhaas, R. A., Sherr, E. H., Shih, J. J., Singh, R., Sirven, J., Smith, M. C., Sullivan, J., Lin Thio, L., Venkat, A., Vining, E. P., Von Allmen, G. K., Weisenberg, J. L., Widdess-Walsh, P., and Winawer, M. R. (2013). De novo mutations in epileptic encephalopathies. *Nature*, 501(7466):217–221.

Andreescu, C. E., Prestori, F., Brandalise, F., D'Errico, A., De Jeu, M. T., Rossi, P., Botta, L., Kohr, G., Perin, P., D'Angelo, E., and De Zeeuw, C. I. (2011). NR2A subunit of the N-methyl D-aspartate receptors are required for potentiation at the mossy fiber to granule cell synapse and vestibulo-cerebellar motor learning. *Neuroscience*, 176:274–283.

Auerbach, B. D., Osterweil, E. K., and Bear, M. F. (2011). Mutations causing syndromic autism define an axis of synaptic pathophysiology. *Nature*, 480(7375):63–68.

Auvin, S., Cilio, M. R., and Vezzani, A. (2016). Current understanding and neurobiology of epileptic encephalopathies. *Neurobiol. Dis.*, 92(Pt A):72–89.

Avanzini, G., Franceschetti, S., and Mantegazza, M. (2007). Epileptogenic channelopathies: experimental models of human pathologies. *Epilepsia*, 48 Suppl 2:51–64.

Bannerman, D. M., Niewoehner, B., Lyon, L., Romberg, C., Schmitt, W. B., Taylor, A., Sanderson, D. J., Cottam, J., Sprengel, R., Seeburg, P. H., Kohr, G., and Rawlins, J. N. (2008). NMDA receptor subunit NR2A is required for rapidly acquired spatial working memory but not incremental spatial reference memory. *J. Neurosci.*, 28(14):3623–3630.

Barker, G. R. and Warburton, E. C. (2008). NMDA receptor plasticity in the perirhinal and prefrontal cortices is crucial for the acquisition of long-term object-in-place associative memory. *J. Neurosci.*, 28(11):2837–2844.

Barnby, G., Abbott, A., Sykes, N., Morris, A., Weeks, D. E., Mott, R., Lamb, J., Bailey, A. J., and Monaco, A. P. (2005). Candidate-gene screening and association analysis at the autism-susceptibility locus on chromosome 16p: evidence of association at GRIN2A and ABAT. *Am. J. Hum. Genet.*, 76(6):950–966.

Behe, P., Stern, P., Wyllie, D. J., Nassar, M., Schoepfer, R., and Colquhoun, D. (1995). Determination of NMDA NR1 subunit copy number in recombinant NMDA receptors. *Proc. Biol. Sci.*, 262(1364):205–213.

Belforte, J. E., Zsiros, V., Sklar, E. R., Jiang, Z., Yu, G., Li, Y., Quinlan, E. M., and Nakazawa, K. (2010). Postnatal NMDA receptor ablation in corticolimbic interneurons confers schizophrenia-like phenotypes. *Nat. Neurosci.*, 13(1):76–83.

Berg, A. T., Berkovic, S. F., Brodie, M. J., Buchhalter, J., Cross, J. H., van Emde Boas, W., Engel, J., French, J., Glauser, T. A., Mathern, G. W., Moshe, S. L., Nordli, D., Plouin, P., and Scheffer, I. E. (2010). Revised terminology and concepts for organization of seizures and epilepsies: report of the ILAE Commission on Classification and Terminology, 2005-2009. *Epilepsia*, 51(4):676–685.

Berl, S. and Waelsch, H. (1958). Determination of glutamic acid, glutamine, glutathione and gamma-aminobutyric acid and their distribution in brain tissue. *J. Neurochem.*, 3(2):161–169.

Berroya, A. M., Bleasel, A. F., Stevermuer, T. L., Lawson, J., and Bye, A. M. (2005). Spike morphology, location, and frequency in benign epilepsy with centrotemporal spikes. *J. Child Neurol.*, 20(3):188–194.

Bitanihirwe, B. K., Lim, M. P., Kelley, J. F., Kaneko, T., and Woo, T. U. (2009). Glutamatergic deficits and parvalbumin-containing inhibitory neurons in the prefrontal cortex in schizophrenia. *BMC Psychiatry*, 9:71.

Bliss, T. V. and Collingridge, G. L. (1993). A synaptic model of memory: long-term potentiation in the hippocampus. *Nature*, 361(6407):31–39.

Bliss, T. V. and Lomo, T. (1973). Long-lasting potentiation of synaptic transmission in the dentate area of the anaesthetized rabbit following stimulation of the perforant path. *J. Physiol. (Lond.)*, 232(2):331–356.

Boyce-Rustay, J. M. and Holmes, A. (2006a). Ethanol-related behaviors in mice lacking the NMDA receptor NR2A subunit. *Psychopharmacology (Berl.)*, 187(4):455–466.

Boyce-Rustay, J. M. and Holmes, A. (2006b). Genetic inactivation of the NMDA receptor NR2A subunit has anxiolytic- and antidepressant-like effects in mice. *Neuropsychopharmacology*, 31(11):2405–2414.

Bramswig, N. C., Ludecke, H. J., Alanay, Y., Albrecht, B., Barthelmie, A., Boduroglu, K., Braunholz, D., Caliebe, A., Chrzanowska, K. H., Czeschik, J. C., Endele, S., Graf, E., Guillen-Navarro, E., Kiper, P. O., Lopez-Gonzalez, V., Parenti, I., Pozojevic, J., Utine, G. E., Wieland, T., Kaiser, F. J., Wollnik, B., Strom, T. M., and Wieczorek, D. (2015). Exome sequencing unravels unexpected differential diagnoses in individuals with the tentative diagnosis of Coffin-Siris and Nicolaides-Baraitser syndromes. *Hum. Genet.*, 134(6):553–568.

Brigman, J. L., Feyder, M., Saksida, L. M., Bussey, T. J., Mishina, M., and Holmes, A. (2008). Impaired discrimination learning in mice lacking the NMDA receptor NR2A subunit. *Learn. Mem.*, 15(2):50–54.

Burnashev, N., Schoepfer, R., Monyer, H., Ruppersberg, J. P., Gunther, W., Seeburg, P. H., and Sakmann, B. (1992). Control by asparagine residues of calcium permeability and magnesium blockade in the NMDA receptor. *Science*, 257(5075):1415–1419.

Burnashev, N. and Szepetowski, P. (2015). NMDA receptor subunit mutations in neurodevelopmental disorders. *Curr Opin Pharmacol*, 20:73–82.

Carvill, G. L., Regan, B. M., Yendle, S. C., O'Roak, B. J., Lozovaya, N., Bruneau, N., Burnashev, N., Khan, A., Cook, J., Geraghty, E., Sadleir, L. G., Turner, S. J., Tsai, M. H., Webster, R., Ouvrier, R., Damiano, J. A., Berkovic, S. F., Shendure, J., Hildebrand, M. S., Szepetowski,

P., Scheffer, I. E., and Mefford, H. C. (2013). GRIN2A mutations cause epilepsy-aphasia spectrum disorders. *Nat. Genet.*, 45(9):1073–1076.

Chatterton, J. E., Awobuluyi, M., Premkumar, L. S., Takahashi, H., Talantova, M., Shin, Y., Cui, J., Tu, S., Sevarino, K. A., Nakanishi, N., Tong, G., Lipton, S. A., and Zhang, D. (2002). Excitatory glycine receptors containing the NR3 family of NMDA receptor subunits. *Nature*, 415(6873):793–798.

Chazot, P. L. and Stephenson, F. A. (1997). Molecular dissection of native mammalian forebrain NMDA receptors containing the NR1 C2 exon: direct demonstration of NMDA receptors comprising NR1, NR2A, and NR2B subunits within the same complex. *J. Neurochem.*, 69(5):2138–2144.

Chen, H. S. and Lipton, S. A. (2005). Pharmacological implications of two distinct mechanisms of interaction of memantine with N-methyl-D-aspartate-gated channels. *J. Pharmacol. Exp. Ther.*, 314(3):961–971.

Cho, K. K., Khibnik, L., Philpot, B. D., and Bear, M. F. (2009). The ratio of NR2A/B NMDA receptor subunits determines the qualities of ocular dominance plasticity in visual cortex. *Proc. Natl. Acad. Sci. U.S.A.*, 106(13):5377–5382.

Clarke, R. J., Glasgow, N. G., and Johnson, J. W. (2013). Mechanistic and structural determinants of NMDA receptor voltage-dependent gating and slow Mg2+ unblock. *J. Neurosci.*, 33(9):4140–4150.

Clarke, R. J. and Johnson, J. W. (2008). Voltage-dependent gating of NR1/2B NMDA receptors. *J. Physiol. (Lond.)*, 586(23):5727–5741.

Cline, H. and Haas, K. (2008). The regulation of dendritic arbor development and plasticity by glutamatergic synaptic input: a review of the synaptotrophic hypothesis. *J. Physiol. (Lond.)*, 586(6):1509–1517.

Collingridge, G. L., Herron, C. E., and Lester, R. A. (1988). Frequency-dependent N-methyl-D-aspartate receptor-mediated synaptic transmission in rat hippocampus. *J. Physiol. (Lond.)*, 399:301–312.

Conroy, J., McGettigan, P. A., McCreary, D., Shah, N., Collins, K., Parry-Fielder, B., Moran, M., Hanrahan, D., Deonna, T. W., Korff, C. M., Webb, D., Ennis, S., Lynch, S. A., and King, M. D. (2014). Towards the identification of a genetic basis for Landau-Kleffner syndrome. *Epilepsia*, 55(6):858–865.

Costa, B. M., Irvine, M. W., Fang, G., Eaves, R. J., Mayo-Martin, M. B., Skifter, D. A., Jane, D. E., and Monaghan, D. T. (2010). A novel family of negative and positive allosteric modulators of NMDA receptors. *J. Pharmacol. Exp. Ther.*, 335(3):614–621.

Cowan, L. D. (2002). The epidemiology of the epilepsies in children. *Ment Retard Dev Disabil Res Rev*, 8(3):171–181.

Cull-Candy, S., Brickley, S., and Farrant, M. (2001). NMDA receptor subunits: diversity, development and disease. *Curr. Opin. Neurobiol.*, 11(3):327–335.

Curtis, D. R., Phillis, J. W., and Watkins, J. C. (1960). The chemical excitation of spinal neurones by certain acidic amino acids. *J. Physiol. (Lond.)*, 150:656–682.

Dale, N. and Roberts, A. (1985). Dual-component amino-acid-mediated synaptic potentials: excitatory drive for swimming in Xenopus embryos. *J. Physiol. (Lond.)*, 363:35–59.

Dalmau, J., Tuzun, E., Wu, H. Y., Masjuan, J., Rossi, J. E., Voloschin, A., Baehring, J. M., Shimazaki, H., Koide, R., King, D., Mason, W., Sansing, L. H., Dichter, M. A., Rosenfeld, M. R., and Lynch, D. R. (2007). Paraneoplastic anti-N-methyl-D-aspartate receptor encephalitis associated with ovarian teratoma. *Ann. Neurol.*, 61(1):25–36.

de Ligt, J., Willemsen, M. H., van Bon, B. W., Kleefstra, T., Yntema, H. G., Kroes, T., Vulto-van Silfhout, A. T., Koolen, D. A., de Vries, P., Gilissen, C., del Rosario, M., Hoischen, A., Scheffer, H., de Vries, B. B., Brunner, H. G., Veltman, J. A., and Vissers, L. E. (2012). Diagnostic exome sequencing in persons with severe intellectual disability. *N. Engl. J. Med.*, 367(20):1921–1929.

Deb, S., Thomas, M., and Bright, C. (2001). Mental disorder in adults with intellectual disability. 1: Prevalence of functional psychiatric illness among a community-based population aged between 16 and 64 years. *J Intellect Disabil Res*, 45(Pt 6):495–505.

DeVries, S. P. and Patel, A. D. (2013). Two patients with a GRIN2A mutation and childhood-onset epilepsy. *Pediatr. Neurol.*, 49(6):482–485.

Dimassi, S., Andrieux, J., Labalme, A., Lesca, G., Cordier, M. P., Boute, O., Neut, D., Edery, P., Sanlaville, D., and Schluth-Bolard, C. (2013). Interstitial 12p13.1 deletion involving GRIN2B in three patients with intellectual disability. *Am. J. Med. Genet. A*, 161A(10):2564–2569.

Dimassi, S., Labalme, A., Lesca, G., Rudolf, G., Bruneau, N., Hirsch, E., Arzimanoglou, A., Motte, J., de Saint Martin, A., Boutry-Kryza, N., Cloarec, R., Benitto, A., Ameil, A., Edery, P., Ryvlin, P., De Bellescize, J., Szepetowski, P., and Sanlaville, D. (2014). A subset of genomic alterations detected in rolandic epilepsies contains candidate or known epilepsy genes including GRIN2A and PRRT2. *Epilepsia*, 55(2):370–378.

Dravid, S. M., Prakash, A., and Traynelis, S. F. (2008). Activation of recombinant NR1/NR2C NMDA receptors. *J. Physiol. (Lond.)*, 586(18):4425–4439.

Dudek, S. M. and Bear, M. F. (1992). Homosynaptic long-term depression in area CA1 of hippocampus and effects of N-methyl-D-aspartate receptor blockade. *Proc. Natl. Acad. Sci. U.S.A.*, 89(10):4363–4367.

Dunah, A. W. and Standaert, D. G. (2003). Subcellular segregation of distinct heteromeric NMDA glutamate receptors in the striatum. *J. Neurochem.*, 85(4):935–943.

Dyment, D. A., Tetreault, M., Beaulieu, C. L., Hartley, T., Ferreira, P., Chardon, J. W., Marcadier, J., Sawyer, S. L., Mosca, S. J., Innes, A. M., Parboosingh, J. S., Bulman, D. E., Schwartzentruber, J., Majewski, J., Tarnopolsky, M., Boycott, K. M., Boycott, K., Friedman, J., Michaud, J., Bernier, F., Brudno, M., Fernandez, B., Knoppers, B., Samuels, M., Scherer, S., Boycott, K., MacKenzie, A., Majewski, J., Brudno, M., Bulman, D., and Dyment, D. (2015). Whole-exome sequencing broadens the phenotypic spectrum of rare pediatric epilepsy: a retrospective study. *Clin. Genet.*, 88(1):34–40.

Elsabbagh, M., Divan, G., Koh, Y. J., Kim, Y. S., Kauchali, S., Marcin, C., Montiel-Nava, C., Patel, V., Paula, C. S., Wang, C., Yasamy, M. T., and Fombonne, E. (2012). Global prevalence of autism and other pervasive developmental disorders. *Autism Res*, 5(3):160–179.

Endele, S., Rosenberger, G., Geider, K., Popp, B., Tamer, C., Stefanova, I., Milh, M., Kortum, F., Fritsch, A., Pientka, F. K., Hellenbroich, Y., Kalscheuer, V. M., Kohlhase, J., Moog, U., Rappold, G., Rauch, A., Ropers, H. H., von Spiczak, S., Tonnies, H., Villeneuve, N., Villard, L., Zabel, B., Zenker, M., Laube, B., Reis, A., Wieczorek, D., Van Maldergem, L., and Kutsche, K. (2010). Mutations in GRIN2A and GRIN2B encoding regulatory subunits of NMDA receptors cause variable neurodevelopmental phenotypes. *Nat. Genet.*, 42(11):1021–1026.

Erreger, K., Dravid, S. M., Banke, T. G., Wyllie, D. J., and Traynelis, S. F. (2005). Subunit-specific gating controls rat NR1/NR2A and NR1/NR2B NMDA channel kinetics and synaptic signalling profiles. *J. Physiol. (Lond.)*, 563(Pt 2):345–358.

Esquivel, R., Molina-Espiritu, M., Salas, F., Soriano, C., Barrientos, C., Dehesa, J., and Dobado, J. (2013). Decoding the Building Blocks of Life from the Perspective of Quantum Information. *Advances in Quantum Mechanics, Paul Bracken (Ed.). InTech*, Chapter 27,(ISBN 978-953-51-1089-7).

Evans, R. C. and Blackwell, K. T. (2015). Calcium: amplitude, duration, or location? *Biol. Bull.*, 228(1):75–83.

Fainberg, N., Harper, A., Tchapyjnikov, D., and Mikati, M. A. (2016). Response to immunotherapy in a patient with Landau-Kleffner syndrome and GRIN2A mutation. *Epileptic Disord*, 18(1):97–100.

Farley, M. A., McMahon, W. M., Fombonne, E., Jenson, W. R., Miller, J., Gardner, M., Block, H., Pingree, C. B., Ritvo, E. R., Ritvo, R. A., and Coon, H. (2009). Twenty-year outcome for individuals with autism and average or near-average cognitive abilities. *Autism Res*, 2(2):109–118.

Fejerman, N. and Caraballo, R. H. (2007). *Benign Focal Epilepsies in Infancy, Childhood, and Adolescence*, volume 21. John Libbey Eurotext, 1 edition. An optional note.

Fisher, R. S., Acevedo, C., Arzimanoglou, A., Bogacz, A., Cross, J. H., Elger, C. E., Engel, J., Forsgren, L., French, J. A., Glynn, M., Hesdorffer, D. C., Lee, B. I., Mathern, G. W., Moshe, S. L., Perucca, E., Scheffer, I. E., Tomson, T., Watanabe, M., and Wiebe, S. (2014). ILAE official report: a practical clinical definition of epilepsy. *Epilepsia*, 55(4):475–482.

Fletcher, E. J., Martin, D., Aram, J. A., Lodge, D., and Honore, T. (1988). Quinoxalinediones selectively block quisqualate and kainate receptors and synaptic events in rat neocortex and hippocampus and frog spinal cord in vitro. *Br. J. Pharmacol.*, 95(2):585–597.

Forrest, D., Yuzaki, M., Soares, H. D., Ng, L., Luk, D. C., Sheng, M., Stewart, C. L., Morgan, J. I., Connor, J. A., and Curran, T. (1994). Targeted disruption of NMDA receptor 1 gene abolishes NMDA response and results in neonatal death. *Neuron*, 13(2):325–338.

Forsgren, L., Beghi, E., Oun, A., and Sillanpaa, M. (2005). The epidemiology of epilepsy in Europe - a systematic review. *Eur. J. Neurol.*, 12(4):245–253.

Freunscht, I., Popp, B., Blank, R., Endele, S., Moog, U., Petri, H., Prott, E. C., Reis, A., Rubo, J., Zabel, B., Zenker, M., Hebebrand, J., and Wieczorek, D. (2013). Behavioral phenotype in five individuals with de novo mutations within the GRIN2B gene. *Behav Brain Funct*, 9:20.

Frizelle, P. A., Chen, P. E., and Wyllie, D. J. (2006). Equilibrium constants for (R)-[(S)-1-(4-bromo-phenyl)-ethylamino]-(2,3-dioxo-1,2,3,4-tetrahydroquinoxalin-5-yl)-methyl]-phosphonic acid (NVP-AAM077) acting at recombinant NR1/NR2A and NR1/NR2B N-methyl-D-aspartate receptors: Implications for studies of synaptic transmission. *Mol. Pharmacol.*, 70(3):1022–1032.

Furshpan, E. J. and Potter, D. D. (1989). Seizure-like activity and cellular damage in rat hippocampal neurons in cell culture. *Neuron*, 3(2):199–207.

Galanopoulou, A. S. and Moshe, S. L. (2015). Pathogenesis and new candidate treatments for infantile spasms and early life epileptic encephalopathies: A view from preclinical studies. *Neurobiol. Dis.*, 79:135–149.

Gambrill, A. C. and Barria, A. (2011). NMDA receptor subunit composition controls synaptogenesis and synapse stabilization. *Proc. Natl. Acad. Sci. U.S.A.*, 108(14):5855–5860.

Geschwind, D. H. and State, M. W. (2015). Gene hunting in autism spectrum disorder: on the path to precision medicine. *Lancet Neurol*, 14(11):1109–1120.

Gibb, A. J. and Colquhoun, D. (1992). Activation of N-methyl-D-aspartate receptors by L-glutamate in cells dissociated from adult rat hippocampus. *J. Physiol. (Lond.)*, 456:143–179.

Gilissen, C., Hehir-Kwa, J. Y., Thung, D. T., van de Vorst, M., van Bon, B. W., Willemsen, M. H., Kwint, M., Janssen, I. M., Hoischen, A., Schenck, A., Leach, R., Klein, R., Tearle, R., Bo, T., Pfundt, R., Yntema, H. G., de Vries, B. B., Kleefstra, T., Brunner, H. G., Vissers, L. E., and Veltman, J. A. (2014). Genome sequencing identifies major causes of severe intellectual disability. *Nature*, 511(7509):344–347.

Gonzalez-Burgos, G. and Lewis, D. A. (2012). NMDA receptor hypofunction, parvalbumin-positive neurons, and cortical gamma oscillations in schizophrenia. *Schizophr Bull*, 38(5):950–957.

Gray, J. A., Shi, Y., Usui, H., During, M. J., Sakimura, K., and Nicoll, R. A. (2011). Distinct modes of AMPA receptor suppression at developing synapses by GluN2A and GluN2B: single-cell NMDA receptor subunit deletion in vivo. *Neuron*, 71(6):1085–1101.

Gray, J. A., Zito, K., and Hell, J. W. (2016). Non-ionotropic signaling by the NMDA receptor: controversy and opportunity. *F1000Res*, 5.

Guzman, S. J., Schlogl, A., and Schmidt-Hieber, C. (2014). Stimfit: quantifying electrophysiological data with Python. *Front Neuroinform*, 8:16.

Hackos, D. H., Lupardus, P. J., Grand, T., Chen, Y., Wang, T. M., Reynen, P., Gustafson, A., Wallweber, H. J., Volgraf, M., Sellers, B. D., Schwarz, J. B., Paoletti, P., Sheng, M., Zhou, Q., and Hanson, J. E. (2016). Positive Allosteric Modulators of GluN2A-Containing NMDARs with Distinct Modes of Action and Impacts on Circuit Function. *Neuron*, 89(5):983–999.

Hamdan, F. F., Gauthier, J., Araki, Y., Lin, D. T., Yoshizawa, Y., Higashi, K., Park, A. R., Spiegelman, D., Dobrzeniecka, S., Piton, A., Tomitori, H., Daoud, H., Massicotte, C., Henrion, E., Diallo, O., Shekarabi, M., Marineau, C., Shevell, M., Maranda, B., Mitchell, G., Nadeau, A., D'Anjou, G., Vanasse, M., Srour, M., Lafreniere, R. G., Drapeau, P., Lacaille, J. C., Kim, E., Lee, J. R., Igarashi, K., Huganir, R. L., Rouleau, G. A., Michaud, J. L., Yang, Y., Noreau, A., Raymond, A., Levert, A., Thibodeau, P., Cote, M., Kuku, F., Laurent, S., Jolivet, P., Duguay, J., Lachapelle, K., and Bachand, I. (2011). Excess of de novo deleterious mutations in genes associated with glutamatergic systems in nonsyndromic intellectual disability. *Am. J. Hum. Genet.*, 88(3):306–316.

Hamdan, F. F., Srour, M., Capo-Chichi, J. M., Daoud, H., Nassif, C., Patry, L., Massicotte, C., Ambalavanan, A., Spiegelman, D., Diallo, O., Henrion, E., Dionne-Laporte, A., Fougerat, A., Pshezhetsky, A. V., Venkateswaran, S., Rouleau, G. A., and Michaud, J. L. (2014). De novo mutations in moderate or severe intellectual disability. *PLoS Genet.*, 10(10):e1004772.

Hansen, K. B., Ogden, K. K., Yuan, H., and Traynelis, S. F. (2014). Distinct functional and pharmacological properties of Triheteromeric GluN1/GluN2A/GluN2B NMDA receptors. *Neuron*, 81(5):1084–1096.

Hardingham, G. E. and Bading, H. (2010). Synaptic versus extrasynaptic NMDA receptor signalling: implications for neurodegenerative disorders. *Nat. Rev. Neurosci.*, 11(10):682–696.

Hardingham, G. E. and Do, K. Q. (2016). Linking early-life NMDAR hypofunction and oxidative stress in schizophrenia pathogenesis. *Nat. Rev. Neurosci.*, 17(2):125–134.

Harris, E. W. and Cotman, C. W. (1986). Long-term potentiation of guinea pig mossy fiber responses is not blocked by N-methyl D-aspartate antagonists. *Neurosci. Lett.*, 70(1):132–137.

Hashimoto, K., Malchow, B., Falkai, P., and Schmitt, A. (2013). Glutamate modulators as potential therapeutic drugs in schizophrenia and affective disorders. *Eur Arch Psychiatry Clin Neurosci*, 263(5):367–377.

Hatton, C. J. and Paoletti, P. (2005). Modulation of triheteromeric NMDA receptors by N-terminal domain ligands. *Neuron*, 46(2):261–274.

Hayashi, T. (1952). A physiological study of epileptic seizures following cortical stimulation in animals and its application to human clinics. *Jpn. J. Physiol.*, 3(1):46–64.

Hegarty, J. D., Baldessarini, R. J., Tohen, M., Waternaux, C., and Oepen, G. (1994). One hundred years of schizophrenia: a meta-analysis of the outcome literature. *Am J Psychiatry*, 151(10):1409–1416.

Henson, M. A., Roberts, A. C., Salimi, K., Vadlamudi, S., Hamer, R. M., Gilmore, J. H., Jarskog, L. F., and Philpot, B. D. (2008). Developmental regulation of the NMDA receptor subunits, NR3A and NR1, in human prefrontal cortex. *Cereb. Cortex*, 18(11):2560–2573.

Holbrook, J. A., Neu-Yilik, G., Hentze, M. W., and Kulozik, A. E. (2004). Nonsense-mediated decay approaches the clinic. *Nat. Genet.*, 36(8):801–808.

Hollmann, M., O'Shea-Greenfield, A., Rogers, S. W., and Heinemann, S. (1989). Cloning by functional expression of a member of the glutamate receptor family. *Nature*, 342(6250):643–648.

Honore, T., Davies, S. N., Drejer, J., Fletcher, E. J., Jacobsen, P., Lodge, D., and Nielsen, F. E. (1988). Quinoxalinediones: potent competitive non-NMDA glutamate receptor antagonists. *Science*, 241(4866):701–703.

Horak, M. and Wenthold, R. J. (2009). Different roles of C-terminal cassettes in the trafficking of full-length NR1 subunits to the cell surface. *J. Biol. Chem.*, 284(15):9683–9691.

Hsu, P. D., Lander, E. S., and Zhang, F. (2014). Development and applications of CRISPR-Cas9 for genome engineering. *Cell*, 157(6):1262–1278.

Huang, X., Tian, M., Hernandez, C. C., Hu, N., and Macdonald, R. L. (2012). The GABRG2 nonsense mutation, Q40X, associated with Dravet syndrome activated NMD and generated a truncated subunit that was partially rescued by aminoglycoside-induced stop codon read-through. *Neurobiol. Dis.*, 48(1):115–123.

Huganir, R. L. and Nicoll, R. A. (2013). AMPARs and synaptic plasticity: the last 25 years. *Neuron*, 80(3):704–717.

Husi, H., Ward, M. A., Choudhary, J. S., Blackstock, W. P., and Grant, S. G. (2000). Proteomic analysis of NMDA receptor-adhesion protein signaling complexes. *Nat. Neurosci.*, 3(7):661–669.

Hyde, T. M. and Weinberger, D. R. (1997). Seizures and schizophrenia. *Schizophr Bull*, 23(4):611–622.

Ito, I., Sakimura, K., Mishina, M., and Sugiyama, H. (1996). Age-dependent reduction of hippocampal LTP in mice lacking N-methyl-D-aspartate receptor epsilon 1 subunit. *Neurosci. Lett.*, 203(1):69–71.

Ito, M., Sakurai, M., and Tongroach, P. (1982). Climbing fibre induced depression of both mossy fibre responsiveness and glutamate sensitivity of cerebellar Purkinje cells. *J. Physiol. (Lond.)*, 324:113–134.

Jantzie, L. L., Talos, D. M., Jackson, M. C., Park, H. K., Graham, D. A., Lechpammer, M., Folkerth, R. D., Volpe, J. J., and Jensen, F. E. (2015). Developmental expression of N-methyl-D-aspartate (NMDA) receptor subunits in human white and gray matter: potential mechanism of increased vulnerability in the immature brain. *Cereb. Cortex*, 25(2):482–495.

Johnson, J. W. and Ascher, P. (1987). Glycine potentiates the NMDA response in cultured mouse brain neurons. *Nature*, 325(6104):529–531.

Johnson, J. W. and Kotermanski, S. E. (2006). Mechanism of action of memantine. *Curr Opin Pharmacol*, 6(1):61–67.

Kandel, E. R., Dudai, Y., and Mayford, M. R. (2014). The molecular and systems biology of memory. *Cell*, 157(1):163–186.

Kannangara, T. S., Bostrom, C. A., Ratzlaff, A., Thompson, L., Cater, R. M., Gil-Mohapel, J., and Christie, B. R. (2014). Deletion of the NMDA receptor GluN2A subunit significantly decreases dendritic growth in maturing dentate granule neurons. *PLoS ONE*, 9(8):e103155.

Kannangara, T. S., Eadie, B. D., Bostrom, C. A., Morch, K., Brocardo, P. S., and Christie, B. R. (2015). GluN2A-/- Mice Lack Bidirectional Synaptic Plasticity in the Dentate Gyrus and Perform Poorly on Spatial Pattern Separation Tasks. *Cereb. Cortex*, 25(8):2102–2113.

Karakas, E. and Furukawa, H. (2014). Crystal structure of a heterotetrameric NMDA receptor ion channel. *Science*, 344(6187):992–997.

Kashiwagi, K., Masuko, T., Nguyen, C. D., Kuno, T., Tanaka, I., Igarashi, K., and Williams, K. (2002). Channel blockers acting at N-methyl-D-aspartate receptors: differential effects of mutations in the vestibule and ion channel pore. *Mol. Pharmacol.*, 61(3):533–545.

Kehoe, L. A., Bellone, C., De Roo, M., Zandueta, A., Dey, P. N., Perez-Otano, I., and Muller, D. (2014). GluN3A promotes dendritic spine pruning and destabilization during postnatal development. *J. Neurosci.*, 34(28):9213–9221.

Kelsch, W., Li, Z., Eliava, M., Goengrich, C., and Monyer, H. (2012). GluN2B-containing NMDA receptors promote wiring of adult-born neurons into olfactory bulb circuits. *J. Neurosci.*, 32(36):12603–12611.

Kenny, E. M., Cormican, P., Furlong, S., Heron, E., Kenny, G., Fahey, C., Kelleher, E., Ennis, S., Tropea, D., Anney, R., Corvin, A. P., Donohoe, G., Gallagher, L., Gill, M., and Morris, D. W. (2014). Excess of rare novel loss-of-function variants in synaptic genes in schizophrenia and autism spectrum disorders. *Mol. Psychiatry*, 19(8):872–879.

Kielinen, M., Rantala, H., Timonen, E., Linna, S. L., and Moilanen, I. (2004). Associated medical disorders and disabilities in children with autistic disorder: a population-based study. *Autism*, 8(1):49–60.

Kinney, J. W., Davis, C. N., Tabarean, I., Conti, B., Bartfai, T., and Behrens, M. M. (2006). A specific role for NR2A-containing NMDA receptors in the maintenance of parvalbumin and GAD67 immunoreactivity in cultured interneurons. *J. Neurosci.*, 26(5):1604–1615.

Kishimoto, Y., Kawahara, S., Kirino, Y., Kadotani, H., Nakamura, Y., Ikeda, M., and Yoshioka, T. (1997). Conditioned eyeblink response is impaired in mutant mice lacking NMDA receptor subunit NR2A. *Neuroreport*, 8(17):3717–3721.

Kiyama, Y., Manabe, T., Sakimura, K., Kawakami, F., Mori, H., and Mishina, M. (1998). Increased thresholds for long-term potentiation and contextual learning in mice lacking the NMDA-type glutamate receptor epsilon1 subunit. *J. Neurosci.*, 18(17):6704–6712.

Kramer, U., Nevo, Y., Neufeld, M. Y., Fatal, A., Leitner, Y., and Harel, S. (1998). Epidemiology of epilepsy in childhood: a cohort of 440 consecutive patients. *Pediatr. Neurol.*, 18(1):46–50.

Krukowski, A. E. and Miller, K. D. (2001). Thalamocortical NMDA conductances and intracortical inhibition can explain cortical temporal tuning. *Nat. Neurosci.*, 4(4):424–430.

Kumar, S. S. and Huguenard, J. R. (2003). Pathway-specific differences in subunit composition of synaptic NMDA receptors on pyramidal neurons in neocortex. *J. Neurosci.*, 23(31):10074–10083.

Large, M., Sharma, S., Compton, M. T., Slade, T., and Nielssen, O. (2011). Cannabis use and earlier onset of psychosis: a systematic meta-analysis. *Arch. Gen. Psychiatry*, 68(6):555–561.

Larsson, K. and Eeg-Olofsson, O. (2006). A population based study of epilepsy in children from a Swedish county. *Eur. J. Paediatr. Neurol.*, 10(3):107–113.

Laurie, D. J. and Seeburg, P. H. (1994). Regional and developmental heterogeneity in splicing of the rat brain NMDAR1 mRNA. *J. Neurosci.*, 14(5 Pt 2):3180–3194.

Laursen, T. M. (2011). Life expectancy among persons with schizophrenia or bipolar affective disorder. *Schizophr. Res.*, 131(1-3):101–104.

Law, A. J., Weickert, C. S., Webster, M. J., Herman, M. M., Kleinman, J. E., and Harrison, P. J. (2003). Expression of NMDA receptor NR1, NR2A and NR2B subunit mRNAs during development of the human hippocampal formation. *Eur. J. Neurosci.*, 18(5):1197–1205.

Lee, C. H., Lu, W., Michel, J. C., Goehring, A., Du, J., Song, X., and Gouaux, E. (2014). NMDA receptor structures reveal subunit arrangement and pore architecture. *Nature*, 511(7508):191–197.

Lemke, J. R., Hendrickx, R., Geider, K., Laube, B., Schwake, M., Harvey, R. J., James, V. M., Pepler, A., Steiner, I., Hortnagel, K., Neidhardt, J., Ruf, S., Wolff, M., Bartholdi, D., Caraballo, R., Platzer, K., Suls, A., De Jonghe, P., Biskup, S., and Weckhuysen, S. (2014). GRIN2B mutations in West syndrome and intellectual disability with focal epilepsy. *Ann. Neurol.*, 75(1):147–154.

Lemke, J. R., Lal, D., Reinthaler, E. M., Steiner, I., Nothnagel, M., Alber, M., Geider, K., Laube, B., Schwake, M., Finsterwalder, K., Franke, A., Schilhabel, M., Jahn, J. A., Muhle, H., Boor, R., Van Paesschen, W., Caraballo, R., Fejerman, N., Weckhuysen, S., De Jonghe, P., Larsen, J., M?ller, R. S., Hjalgrim, H., Addis, L., Tang, S., Hughes, E., Pal, D. K., Veri, K., Vaher, U., Talvik, T., Dimova, P., Guerrero Lopez, R., Serratosa, J. M., Linnankivi, T., Lehesjoki, A. E., Ruf, S., Wolff, M., Buerki, S., Wohlrab, G., Kroell, J., Datta, A. N., Fiedler, B., Kurlemann, G., Kluger, G., Hahn, A., Haberlandt, D. E., Kutzer, C., Sperner, J., Becker, F., Weber, Y. G., Feucht, M., Steinbock, H., Neophythou, B., Ronen, G. M., Gruber-Sedlmayr, U., Geldner, J., Harvey, R. J., Hoffmann, P., Herms, S., Altmuller, J., Toliat, M. R., Thiele, H., Nurnberg, P., Wilhelm, C., Stephani, U., Helbig, I., Lerche, H., Zimprich, F., Neubauer, B. A., Biskup, S., and von Spiczak, S. (2013). Mutations in GRIN2A cause idiopathic focal epilepsy with rolandic spikes. *Nat. Genet.*, 45(9):1067–1072.

LePage, K. T., Ishmael, J. E., Low, C. M., Traynelis, S. F., and Murray, T. F. (2005). Differential binding properties of [3H]dextrorphan and [3H]MK-801 in heterologously expressed NMDA receptors. *Neuropharmacology*, 49(1):1–16.

Lesca, G., Rudolf, G., Bruneau, N., Lozovaya, N., Labalme, A., Boutry-Kryza, N., Salmi, M., Tsintsadze, T., Addis, L., Motte, J., Wright, S., Tsintsadze, V., Michel, A., Doummar, D., Lascelles, K., Strug, L., Waters, P., de Bellescize, J., Vrielynck, P., de Saint Martin, A., Ville, D., Ryvlin, P., Arzimanoglou, A., Hirsch, E., Vincent, A., Pal, D., Burnashev, N., Sanlaville, D., and Szepetowski, P. (2013). GRIN2A mutations in acquired epileptic aphasia and related childhood focal epilepsies and encephalopathies with speech and language dysfunction. *Nat. Genet.*, 45(9):1061–1066.

Lesca, G., Rudolf, G., Labalme, A., Hirsch, E., Arzimanoglou, A., Genton, P., Motte, J., de Saint Martin, A., Valenti, M. P., Boulay, C., De Bellescize, J., Keo-Kosal, P., Boutry-Kryza, N., Edery, P., Sanlaville, D., and Szepetowski, P. (2012). Epileptic encephalopathies of the Landau-Kleffner and continuous spike and waves during slow-wave sleep types: genomic dissection makes the link with autism. *Epilepsia*, 53(9):1526–1538.

Lhatoo, S. D. and Sander, J. W. (2001). The epidemiology of epilepsy and learning disability. *Epilepsia*, 42 Suppl 1:6–9.

Li, Y., Erzurumlu, R. S., Chen, C., Jhaveri, S., and Tonegawa, S. (1994). Whisker-related neuronal patterns fail to develop in the trigeminal brainstem nuclei of NMDAR1 knockout mice. *Cell*, 76(3):427–437.

Loddenkemper, T., Fernandez, I. S., and Peters, J. M. (2011). Continuous spike and waves during sleep and electrical status epilepticus in sleep. *J Clin Neurophysiol*, 28(2):154–164.

Lodge, D. (2009). The history of the pharmacology and cloning of ionotropic glutamate receptors and the development of idiosyncratic nomenclature. *Neuropharmacology*, 56(1):6–21.

Longordo, F., Kopp, C., Mishina, M., Lujan, R., and Luthi, A. (2009). NR2A at CA1 synapses is obligatory for the susceptibility of hippocampal plasticity to sleep loss. *J. Neurosci.*, 29(28):9026–9041.

Luo, J., Wang, Y., Yasuda, R. P., Dunah, A. W., and Wolfe, B. B. (1997). The majority of N-methyl-D-aspartate receptor complexes in adult rat cerebral cortex contain at least three different subunits (NR1/NR2A/NR2B). *Mol. Pharmacol.*, 51(1):79–86.

MacDermott, A. B., Mayer, M. L., Westbrook, G. L., Smith, S. J., and Barker, J. L. (1986). NMDA-receptor activation increases cytoplasmic calcium concentration in cultured spinal cord neurones. *Nature*, 321(6069):519–522.

Malayev, A., Gibbs, T. T., and Farb, D. H. (2002). Inhibition of the NMDA response by pregnenolone sulphate reveals subtype selective modulation of NMDA receptors by sulphated steroids. *Br. J. Pharmacol.*, 135(4):901–909.

Marino, M., Misuri, L., and Brogioli, D. (2014). A new open source software for the calculation of the liquid junction potential between two solutions according to the stationary Nernst-Planck equation. *arXiv[physics.chem-ph]*, 1403.3640v2.

Marquardt, K., Saha, M., Mishina, M., Young, J. W., and Brigman, J. L. (2014). Loss of GluN2A-containing NMDA receptors impairs extra-dimensional set-shifting. *Genes Brain Behav.*, 13(7):611–617.

Marsh, E., Fulp, C., Gomez, E., Nasrallah, I., Minarcik, J., Sudi, J., Christian, S. L., Mancini, G., Labosky, P., Dobyns, W., Brooks-Kayal, A., and Golden, J. A. (2009). Targeted loss of Arx results in a developmental epilepsy mouse model and recapitulates the human phenotype in heterozygous females. *Brain*, 132(Pt 6):1563–1576.

Martel, M. A., Ryan, T. J., Bell, K. F., Fowler, J. H., McMahon, A., Al-Mubarak, B., Komiyama, N. H., Horsburgh, K., Kind, P. C., Grant, S. G., Wyllie, D. J., and Hardingham, G. E. (2012). The subtype of GluN2 C-terminal domain determines the response to excitotoxic insults. *Neuron*, 74(3):543–556.

Masdeu, J. C., Dalmau, J., and Berman, K. F. (2016). NMDA Receptor Internalization by Autoantibodies: A Reversible Mechanism Underlying Psychosis? *Trends Neurosci.*

Matsa, E., Dixon, J. E., Medway, C., Georgiou, O., Patel, M. J., Morgan, K., Kemp, P. J., Staniforth, A., Mellor, I., and Denning, C. (2014). Allele-specific RNA interference rescues the long-QT syndrome phenotype in human-induced pluripotency stem cell cardiomyocytes. *Eur. Heart J.*, 35(16):1078–1087.

Maulik, P. K., Mascarenhas, M. N., Mathers, C. D., Dua, T., and Saxena, S. (2011). Prevalence of intellectual disability: a meta-analysis of population-based studies. *Res Dev Disabil*, 32(2):419–436.

Mayer, M. L., Westbrook, G. L., and Guthrie, P. B. (1984). Voltage-dependent block by Mg2+ of NMDA responses in spinal cord neurones. *Nature*, 309(5965):261–263.

McCulloch, R. M., Johnston, G. A., Game, C. J., and Curtis, D. R. (1974). The differential sensitivity of spinal interneurones and Renshaw cells to Kainate and N-methyl-D-aspartate. *Exp Brain Res*, 21(5):515–518.

McGrath, J., Saha, S., Chant, D., and Welham, J. (2008). Schizophrenia: a concise overview of incidence, prevalence, and mortality. *Epidemiol Rev*, 30:67–76.

McKay, S., Griffiths, N. H., Butters, P. A., Thubron, E. B., Hardingham, G. E., and Wyllie, D. J. (2012). Direct pharmacological monitoring of the developmental switch in NMDA receptor subunit composition using TCN 213, a GluN2A-selective, glycine-dependent antagonist. *Br. J. Pharmacol.*, 166(3):924–937.

McLennan, H. and Lodge, D. (1979). The antagonism of amino acid-induced excitation of spinal neurones in the cat. *Brain Res.*, 169(1):83–90.

McTague, A., Howell, K. B., Cross, J. H., Kurian, M. A., and Scheffer, I. E. (2016). The genetic landscape of the epileptic encephalopathies of infancy and childhood. *Lancet Neurol*, 15(3):304–316.

Merritt, K., Egerton, A., Kempton, M. J., Taylor, M. J., and McGuire, P. K. (2016). Nature of Glutamate Alterations in Schizophrenia: A Meta-analysis of Proton Magnetic Resonance Spectroscopy Studies. *JAMA Psychiatry*.

Minta, A., Kao, J. P., and Tsien, R. Y. (1989). Fluorescent indicators for cytosolic calcium based on rhodamine and fluorescein chromophores. *J. Biol. Chem.*, 264(14):8171–8178.

Miyamoto, Y., Yamada, K., Noda, Y., Mori, H., Mishina, M., and Nabeshima, T. (2001). Hyperfunction of dopaminergic and serotonergic neuronal systems in mice lacking the NMDA receptor epsilon1 subunit. *J. Neurosci.*, 21(2):750–757.

Moghaddam, B. and Krystal, J. H. (2012). Capturing the angel in "angel dust": twenty years of translational neuroscience studies of NMDA receptor antagonists in animals and humans. *Schizophr Bull*, 38(5):942–949.

Mony, L., Zhu, S., Carvalho, S., and Paoletti, P. (2011). Molecular basis of positive allosteric modulation of GluN2B NMDA receptors by polyamines. *EMBO J.*, 30(15):3134–3146.

Monyer, H., Burnashev, N., Laurie, D. J., Sakmann, B., and Seeburg, P. H. (1994). Developmental and regional expression in the rat brain and functional properties of four NMDA receptors. *Neuron*, 12(3):529–540.

Moreau, A. W. and Kullmann, D. M. (2013). NMDA receptor-dependent function and plasticity in inhibitory circuits. *Neuropharmacology*, 74:23–31.

Mori, H., Masaki, H., Yamakura, T., and Mishina, M. (1992). Identification by mutagenesis of a Mg(2+)-block site of the NMDA receptor channel. *Nature*, 358(6388):673–675.

Morikawa, E., Mori, H., Kiyama, Y., Mishina, M., Asano, T., and Kirino, T. (1998). Attenuation of focal ischemic brain injury in mice deficient in the epsilon1 (NR2A) subunit of NMDA receptor. *J. Neurosci.*, 18(23):9727–9732.

Moriyoshi, K., Masu, M., Ishii, T., Shigemoto, R., Mizuno, N., and Nakanishi, S. (1991). Molecular cloning and characterization of the rat NMDA receptor. *Nature*, 354(6348):31–37.

Mothet, J. P., Parent, A. T., Wolosker, H., Brady, R. O., Linden, D. J., Ferris, C. D., Rogawski, M. A., and Snyder, S. H. (2000). D-serine is an endogenous ligand for the glycine site of the N-methyl-D-aspartate receptor. *Proc. Natl. Acad. Sci. U.S.A.*, 97(9):4926–4931.

Mulkey, R. M. and Malenka, R. C. (1992). Mechanisms underlying induction of homosynaptic long-term depression in area CA1 of the hippocampus. *Neuron*, 9(5):967–975.

Murray, C. J., Barber, R. M., Foreman, K. J., Abbasoglu Ozgoren, A., Abd-Allah, F., Abera, S. F., and Aboyans, V. e. a. (2015). Global, regional, and national disability-adjusted life years (DALYs) for 306 diseases and injuries and healthy life expectancy (HALE) for 188 countries, 1990-2013: quantifying the epidemiological transition. *Lancet*, 386(10009):2145–2191.

Myers, C. T. and Mefford, H. C. (2015). Advancing epilepsy genetics in the genomic era. *Genome Med*, 7:91.

Myers, R. A., Casals, F., Gauthier, J., Hamdan, F. F., Keebler, J., Boyko, A. R., Bustamante, C. D., Piton, A. M., Spiegelman, D., Henrion, E., Zilversmit, M., Hussin, J., Quinlan, J., Yang, Y., Lafreniere, R. G., Griffing, A. R., Stone, E. A., Rouleau, G. A., and Awadalla, P. (2011). A population genetic approach to mapping neurological disorder genes using deep resequencing. *PLoS Genet.*, 7(2):e1001318.

Naldini, L. (2015). Gene therapy returns to centre stage. *Nature*, 526(7573):351–360.

Nowak, L., Bregestovski, P., Ascher, P., Herbet, A., and Prochiantz, A. (1984). Magnesium gates glutamate-activated channels in mouse central neurones. *Nature*, 307(5950):462–465.

O'Dushlaine, C., Rossin, L., Lee, P. H., Duncan, L., Parikshak, N. N., Newhouse, S., and Ripke, S. e. a. (2015). Psychiatric genome-wide association study analyses implicate neuronal, immune and histone pathways. *Nat. Neurosci.*, 18(2):199–209.

Ohba, C., Shiina, M., Tohyama, J., Haginoya, K., Lerman-Sagie, T., Okamoto, N., Blumkin, L., Lev, D., Mukaida, S., Nozaki, F., Uematsu, M., Onuma, A., Kodera, H., Nakashima, M., Tsurusaki, Y., Miyake, N., Tanaka, F., Kato, M., Ogata, K., Saitsu, H., and Matsumoto, N. (2015). GRIN1 mutations cause encephalopathy with infantile-onset epilepsy, and hyperkinetic and stereotyped movement disorders. *Epilepsia*, 56(6):841–848.

Oliet, S. H., Malenka, R. C., and Nicoll, R. A. (1997). Two distinct forms of long-term depression coexist in CA1 hippocampal pyramidal cells. *Neuron*, 18(6):969–982.

Olverman, H. J., Jones, A. W., and Watkins, J. C. (1984). L-glutamate has higher affinity than other amino acids for [3H]-D-AP5 binding sites in rat brain membranes. *Nature*, 307(5950):460–462.

O'Roak, B. J., Deriziotis, P., Lee, C., Vives, L., Schwartz, J. J., Girirajan, S., Karakoc, E., Mackenzie, A. P., Ng, S. B., Baker, C., Rieder, M. J., Nickerson, D. A., Bernier, R., Fisher, S. E., Shendure, J., and Eichler, E. E. (2011). Exome sequencing in sporadic autism spectrum disorders identifies severe de novo mutations. *Nat. Genet.*, 43(6):585–589.

O'Roak, B. J., Vives, L., Fu, W., Egertson, J. D., Stanaway, I. B., Phelps, I. G., Carvill, G., Kumar, A., Lee, C., Ankenman, K., Munson, J., Hiatt, J. B., Turner, E. H., Levy, R., O'Day, D. R., Krumm, N., Coe, B. P., Martin, B. K., Borenstein, E., Nickerson, D. A., Mefford, H. C., Doherty, D., Akey, J. M., Bernier, R., Eichler, E. E., and Shendure, J. (2012a). Multiplex targeted sequencing identifies recurrently mutated genes in autism spectrum disorders. *Science*, 338(6114):1619–1622.

O'Roak, B. J., Vives, L., Girirajan, S., Karakoc, E., Krumm, N., Coe, B. P., Levy, R., Ko, A., Lee, C., Smith, J. D., Turner, E. H., Stanaway, I. B., Vernot, B., Malig, M., Baker, C., Reilly, B., Akey, J. M., Borenstein, E., Rieder, M. J., Nickerson, D. A., Bernier, R., Shendure, J., and Eichler, E. E. (2012b). Sporadic autism exomes reveal a highly interconnected protein network of de novo mutations. *Nature*, 485(7397):246–250.

Pachernegg, S., Strutz-Seebohm, N., and Hollmann, M. (2012). GluN3 subunit-containing NMDA receptors: not just one-trick ponies. *Trends Neurosci.*, 35(4):240–249.

Pacico, N. and Mingorance-Le Meur, A. (2014). New in vitro phenotypic assay for epilepsy: fluorescent measurement of synchronized neuronal calcium oscillations. *PLoS ONE*, 9(1):e84755.

Pan, Y., Chen, J., Guo, H., Ou, J., Peng, Y., Liu, Q., Shen, Y., Shi, L., Liu, Y., Xiong, Z., Zhu, T., Luo, S., Hu, Z., Zhao, J., and Xia, K. (2015). Association of genetic variants of GRIN2B with autism. *Sci Rep*, 5:8296.

Panayiotopoulos, C. P. (2005). *The Epilepsies: Seizures, Syndromes and Managements*. Chapter 7. Bladon Medical Publishing, Oxfordshire, 1 edition. An optional note.

Paoletti, P., Bellone, C., and Zhou, Q. (2013). NMDA receptor subunit diversity: impact on receptor properties, synaptic plasticity and disease. *Nat. Rev. Neurosci.*, 14(6):383–400.

Paoletti, P., Neyton, J., and Ascher, P. (1995). Glycine-independent and subunit-specific potentiation of NMDA responses by extracellular Mg2+. *Neuron*, 15(5):1109–1120.

Parsons, M. P. and Raymond, L. A. (2014). Extrasynaptic NMDA receptor involvement in central nervous system disorders. *Neuron*, 82(2):279–293.

Perin-Dureau, F., Rachline, J., Neyton, J., and Paoletti, P. (2002). Mapping the binding site of the neuroprotectant ifenprodil on NMDA receptors. *J. Neurosci.*, 22(14):5955–5965.

Philpot, B. D., Cho, K. K., and Bear, M. F. (2007). Obligatory role of NR2A for metaplasticity in visual cortex. *Neuron*, 53(4):495–502.

Pierson, T. M., Yuan, H., Marsh, E. D., Fuentes-Fajardo, K., Adams, D. R., Markello, T., Golas, G., Simeonov, D. R., Holloman, C., Tankovic, A., Karamchandani, M. M., Schreiber, J. M., Mullikin, J. C., Tifft, C. J., Toro, C., Boerkoel, C. F., Traynelis, S. F., and Gahl, W. A. (2014). GRIN2A mutation and early-onset epileptic encephalopathy: personalized therapy with memantine. *Ann Clin Transl Neurol*, 1(3):190–198.

Pina-Crespo, J. C., Talantova, M., Micu, I., States, B., Chen, H. S., Tu, S., Nakanishi, N., Tong, G., Zhang, D., Heinemann, S. F., Zamponi, G. W., Stys, P. K., and Lipton, S. A. (2010). Excitatory glycine responses of CNS myelin mediated by NR1/NR3 "NMDA" receptor subunits. *J. Neurosci.*, 30(34):11501–11505.

Poirsier, C., Landais, E., Bednarek, N., Nobecourt, J. M., Khoury, M., Schmidt, P., Morville, P., Gruson, N., Clomes, S., Michel, N., Riot, A., Manjeongean, C., Gaillard, D., and Doco-Fenzy, M. (2014). Report on 3 patients with 12p duplication including GRIN2B. *Eur J Med Genet*, 57(5):185–194.

Premkumar, L. S., Qin, F., and Auerbach, A. (1997). Subconductance states of a mutant NMDA receptor channel kinetics, calcium, and voltage dependence. *J. Gen. Physiol.*, 109(2):181–189.

Punnakkal, P., Jendritza, P., and Kohr, G. (2012). Influence of the intracellular GluN2 C-terminal domain on NMDA receptor function. *Neuropharmacology*, 62(5-6):1985–1992.

R Core Team (2014). *R: A Language and Environment for Statistical Computing*. R Foundation for Statistical Computing, Vienna, Austria.

Rangan, A. V., Cai, D., and McLaughlin, D. W. (2005). Modeling the spatiotemporal cortical activity associated with the line-motion illusion in primary visual cortex. *Proc. Natl. Acad. Sci. U.S.A.*, 102(52):18793–18800.

Rauner, C. and Kohr, G. (2011). Triheteromeric NR1/NR2A/NR2B receptors constitute the major N-methyl-D-aspartate receptor population in adult hippocampal synapses. *J. Biol. Chem.*, 286(9):7558–7566.

Reutlinger, C., Helbig, I., Gawelczyk, B., Subero, J. I., Tonnies, H., Muhle, H., Finsterwalder, K., Vermeer, S., Pfundt, R., Sperner, J., Stefanova, I., Gillessen-Kaesbach, G., von Spiczak, S., van Baalen, A., Boor, R., Siebert, R., Stephani, U., and Caliebe, A. (2010). Deletions in 16p13 including GRIN2A in patients with intellectual disability, various dysmorphic features, and seizure disorders of the rolandic region. *Epilepsia*, 51(9):1870–1873.

Reynolds, I. J. and Palmer, A. M. (1991). Regional variations in [3H]MK801 binding to rat brain N-methyl-D-aspartate receptors. *J. Neurochem.*, 56(5):1731–1740.

Ripke, S., Neale, B. M., Corvin, A., Walters, J. T., Farh, K. H., Holmans, P. A., and Lee, P. e. a. (2014). Biological insights from 108 schizophrenia-associated genetic loci. *Nature*, 511(7510):421–427.

Ritter, L. M., Unis, A. S., and Meador-Woodruff, J. H. (2001). Ontogeny of ionotropic glutamate receptor expression in human fetal brain. *Brain Res. Dev. Brain Res.*, 127(2):123–133.

Ronald, A. and Hoekstra, R. A. (2011). Autism spectrum disorders and autistic traits: a decade of new twin studies. *Am. J. Med. Genet. B Neuropsychiatr. Genet.*, 156B(3):255–274.

Rossi, P., Sola, E., Taglietti, V., Borchardt, T., Steigerwald, F., Utvik, J. K., Ottersen, O. P., Kohr, G., and D'Angelo, E. (2002). NMDA receptor 2 (NR2) C-terminal control of NR open probability regulates synaptic transmission and plasticity at a cerebellar synapse. *J. Neurosci.*, 22(22):9687–9697.

Rozeboom, A. M., Queenan, B. N., Partridge, J. G., Farnham, C., Wu, J. Y., Vicini, S., and Pak, D. T. (2015). Evidence for glycinergic GluN1/GluN3 NMDA receptors in hippocampal metaplasticity. *Neurobiol Learn Mem*, 125:265–273.

Rumbaugh, G., Prybylowski, K., Wang, J. F., and Vicini, S. (2000). Exon 5 and spermine regulate deactivation of NMDA receptor subtypes. *J. Neurophysiol.*, 83(3):1300–1306.

Sakamoto, T., Mishina, M., and Niki, H. (2002). Mutation of NMDA receptor subunit epsilon 1: effects on audiogenic-like seizures induced by electrical stimulation of the inferior colliculus in mice. *Brain Res. Mol. Brain Res.*, 102(1-2):113–117.

Sakimura, K., Kutsuwada, T., Ito, I., Manabe, T., Takayama, C., Kushiya, E., Yagi, T., Aizawa, S., Inoue, Y., and Sugiyama, H. (1995). Reduced hippocampal LTP and spatial learning in mice lacking NMDA receptor epsilon 1 subunit. *Nature*, 373(6510):151–155.

Sakurada, K., Masu, M., and Nakanishi, S. (1993). Alteration of Ca2+ permeability and sensitivity to Mg2+ and channel blockers by a single amino acid substitution in the N-methyl-D-aspartate receptor. *J. Biol. Chem.*, 268(1):410–415.

Sandbichler, A. M., Aschberger, T., and Pelster, B. (2013). A method to evaluate the efficiency of transfection reagents in an adherent zebrafish cell line. *Biores Open Access*, 2(1):20–27.

Sawtell, N. B., Frenkel, M. Y., Philpot, B. D., Nakazawa, K., Tonegawa, S., and Bear, M. F. (2003). NMDA receptor-dependent ocular dominance plasticity in adult visual cortex. *Neuron*, 38(6):977–985.

Schneggenburger, R. and Ascher, P. (1997). Coupling of permeation and gating in an NMDA-channel pore mutant. *Neuron*, 18(1):167–177.

Schneider, C. A., Rasband, W. S., and Eliceiri, K. W. (2012). NIH Image to ImageJ: 25 years of image analysis. *Nat. Methods*, 9(7):671–675.

Serraz, B., Grand, T., and Paoletti, P. (2016). Altered zinc sensitivity of NMDA receptors harboring clinically-relevant mutations. *Neuropharmacology*, 109:196–204.

Shao, L. and Stafstrom, C. E. (2016). Pediatric epileptic encephalopathies: pathophysiology and animal models. *Seminars in Pediatric Neurology*.

Sheng, M., Cummings, J., Roldan, L. A., Jan, Y. N., and Jan, L. Y. (1994). Changing subunit composition of heteromeric NMDA receptors during development of rat cortex. *Nature*, 368(6467):144–147.

Shinnar, S., O'Dell, C., and Berg, A. T. (1999). Distribution of epilepsy syndromes in a cohort of children prospectively monitored from the time of their first unprovoked seizure. *Epilepsia*, 40(10):1378–1383.

Singh, D., Lau, M., Ayers, T., Singh, Y., Akingbola, O., Barbiero, L., and Nelson, S. (2015). De Novo Heterogeneous Mutations in SCN2A and GRIN2A Genes and Seizures With Ictal Vocalizations. *Clin Pediatr (Phila)*.

Sirrieh, R. E., MacLean, D. M., and Jayaraman, V. (2015). Subtype-dependent N-methyl-D-aspartate receptor amino-terminal domain conformations and modulation by spermine. *J. Biol. Chem.*, 290(20):12812–12820.

Sladeczek, F., Pin, J. P., Recasens, M., Bockaert, J., and Weiss, S. (1985). Glutamate stimulates inositol phosphate formation in striatal neurones. *Nature*, 317(6039):717–719.

Smith, M. C. and Hoeppner, T. J. (2003). Epileptic encephalopathy of late childhood: Landau-Kleffner syndrome and the syndrome of continuous spikes and waves during slow-wave sleep. *J Clin Neurophysiol*, 20(6):462–472.

Snyder, M. A. and Gao, W. J. (2013). NMDA hypofunction as a convergence point for progression and symptoms of schizophrenia. *Front Cell Neurosci*, 7:31.

Stroebel, D., Carvalho, S., Grand, T., Zhu, S., and Paoletti, P. (2014). Controlling NMDA receptor subunit composition using ectopic retention signals. *J. Neurosci.*, 34(50):16630–16636.

Sullivan, P. F., Daly, M. J., and O'Donovan, M. (2012). Genetic architectures of psychiatric disorders: the emerging picture and its implications. *Nat. Rev. Genet.*, 13(8):537–551.

Sullivan, P. F., Kendler, K. S., and Neale, M. C. (2003). Schizophrenia as a complex trait: evidence from a meta-analysis of twin studies. *Arch. Gen. Psychiatry*, 60(12):1187–1192.

Talkowski, M. E., Rosenfeld, J. A., Blumenthal, I., Pillalamarri, V., Chiang, C., Heilbut, A., Ernst, C., Hanscom, C., Rossin, E., Lindgren, A. M., Pereira, S., Ruderfer, D., Kirby, A., Ripke, S., Harris, D. J., Lee, J. H., Ha, K., Kim, H. G., Solomon, B. D., Gropman, A. L., Lucente, D., Sims, K., Ohsumi, T. K., Borowsky, M. L., Loranger, S., Quade, B., Lage, K., Miles, J., Wu, B. L., Shen, Y., Neale, B., Shaffer, L. G., Daly, M. J., Morton, C. C., and Gusella, J. F. (2012). Sequencing chromosomal abnormalities reveals neurodevelopmental loci that confer risk across diagnostic boundaries. *Cell*, 149(3):525–537.

Tarabeux, J., Kebir, O., Gauthier, J., Hamdan, F. F., Xiong, L., Piton, A., Spiegelman, D., Henrion, E., Millet, B., Fathalli, F., Joober, R., Rapoport, J. L., DeLisi, L. E., Fombonne, E., Mottron, L., Forget-Dubois, N., Boivin, M., Michaud, J. L., Drapeau, P., Lafreniere, R. G., Rouleau, G. A., Krebs, M. O., Bachand, I., Chicoine, M., Cote, M., Daignault, K., Desjarlais, A., Diallo, O., Dobrzeniecka, S., Duguay, J., Drits, M., Jolivet, P., Karamera, L., Kuku, F., Lachapelle, K., Laliberte, G., Laurent, S., Levert, A., Liao, M., Marineau, C., Marino, C., Noreau, A., Peng, H., Raymond, A., Reynolds, A., Rochefort, D., St-Onge, J., Thibodeau, P., Tsurudome, K., Yang, Y., Leroy, S., Bendjemaa, N., Ossian, K., Chayet, M., and Mouaffak, F. (2011). Rare mutations in N-methyl-D-aspartate glutamate receptors in autism spectrum disorders and schizophrenia. *Transl Psychiatry*, 1:e55.

Terasaki, Y., Sasaki, T., Yagita, Y., Okazaki, S., Sugiyama, Y., Oyama, N., Omura-Matsuoka, E., Sakoda, S., and Kitagawa, K. (2010). Activation of NR2A receptors induces ischemic tolerance through CREB signaling. *J. Cereb. Blood Flow Metab.*, 30(8):1441–1449.

Titulaer, M. J., McCracken, L., Gabilondo, I., Armangue, T., Glaser, C., Iizuka, T., Honig, L. S., Benseler, S. M., Kawachi, I., Martinez-Hernandez, E., Aguilar, E., Gresa-Arribas, N., Ryan-Florance, N., Torrents, A., Saiz, A., Rosenfeld, M. R., Balice-Gordon, R., Graus, F., and Dalmau, J. (2013). Treatment and prognostic factors for long-term outcome in patients with anti-NMDA receptor encephalitis: an observational cohort study. *Lancet Neurol*, 12(2):157–165.

Tomiyama, K., Kato, R., Hara, Y., Kobayashi, M., Mishina, M., Yanagawa, Y., Kinsella, A., Koshikawa, N., and Waddington, J. L. (2013). Phenotypic characterization of orofacial movement topography in mutants with disruption of amino acid mechanisms: glutamate N2A/B/D [GluR1/2/4] subtypes and the GABA synthesizing enzyme GAD65. *Neuroscience*, 250:743–754.

Tovar, K. R., McGinley, M. J., and Westbrook, G. L. (2013). Triheteromeric NMDA receptors at hippocampal synapses. *J. Neurosci.*, 33(21):9150–9160.

Traynelis, S. F., Hartley, M., and Heinemann, S. F. (1995). Control of proton sensitivity of the NMDA receptor by RNA splicing and polyamines. *Science*, 268(5212):873–876.

Traynelis, S. F., Wollmuth, L. P., McBain, C. J., Menniti, F. S., Vance, K. M., Ogden, K. K., Hansen, K. B., Yuan, H., Myers, S. J., and Dingledine, R. (2010). Glutamate receptor ion channels: structure, regulation, and function. *Pharmacol. Rev.*, 62(3):405–496.

Tsai, M. H., Vears, D. F., Turner, S. J., Smith, R. L., Berkovic, S. F., Sadleir, L. G., and Scheffer, I. E. (2013). Clinical genetic study of the epilepsy-aphasia spectrum. *Epilepsia*, 54(2):280–287.

Tsuji, M., Takahashi, Y., Watabe, A. M., and Kato, F. (2016). Enhanced long-term potentiation in mature rats in a model of epileptic spasms with betamethasone-priming and postnatal N-methyl-d-aspartate administration. *Epilepsia*, 57(3):495–505.

Turrigiano, G. (2011). Too many cooks? Intrinsic and synaptic homeostatic mechanisms in cortical circuit refinement. *Annu. Rev. Neurosci.*, 34:89–103.

Uhlhaas, P. J. and Singer, W. (2012). Neuronal dynamics and neuropsychiatric disorders: toward a translational paradigm for dysfunctional large-scale networks. *Neuron*, 75(6):963–980.

van Bokhoven, H. (2011). Genetic and epigenetic networks in intellectual disabilities. *Annu. Rev. Genet.*, 45:81–104.

van Harreveld, A. (1959). Compounds in brain extracts causing spreading depression of cerebral cortical activity and contraction of crustacean muscle. *J. Neurochem.*, 3(4):300–315.

Varese, F., Smeets, F., Drukker, M., Lieverse, R., Lataster, T., Viechtbauer, W., Read, J., van Os, J., and Bentall, R. P. (2012). Childhood adversities increase the risk of psychosis: a meta-analysis of patient-control, prospective- and cross-sectional cohort studies. *Schizophr Bull*, 38(4):661–671.

Veltman, J. A. and Brunner, H. G. (2012). De novo mutations in human genetic disease. *Nat. Rev. Genet.*, 13(8):565–575.

Vicini, S., Wang, J. F., Li, J. H., Zhu, W. J., Wang, Y. H., Luo, J. H., Wolfe, B. B., and Grayson, D. R. (1998). Functional and pharmacological differences between recombinant N-methyl-D-aspartate receptors. *J. Neurophysiol.*, 79(2):555–566.

Vissers, L. E., Gilissen, C., and Veltman, J. A. (2016). Genetic studies in intellectual disability and related disorders. *Nat. Rev. Genet.*, 17(1):9–18.

von Engelhardt, J., Coserea, I., Pawlak, V., Fuchs, E. C., Kohr, G., Seeburg, P. H., and Monyer, H. (2007). Excitotoxicity in vitro by NR2A- and NR2B-containing NMDA receptors. *Neuropharmacology*, 53(1):10–17.

von Spiczak, S., Finsterwalder, K., Muhle, H., Franke, A., Schilhabel, M., Stephani, U., and Helbig, I. (2011). Comprehensive analysis of candidate genes for photosensitivity using a complementary bioinformatic and experimental approach. *Epilepsia*, 52(10):e143–147.

Watanabe, M., Inoue, Y., Sakimura, K., and Mishina, M. (1992). Developmental changes in distribution of NMDA receptor channel subunit mRNAs. *Neuroreport*, 3(12):1138–1140.

Wenthold, R. J., Prybylowski, K., Standley, S., Sans, N., and Petralia, R. S. (2003). Trafficking of NMDA receptors. *Annu. Rev. Pharmacol. Toxicol.*, 43:335–358.

West, A. E., Chen, W. G., Dalva, M. B., Dolmetsch, R. E., Kornhauser, J. M., Shaywitz, A. J., Takasu, M. A., Tao, X., and Greenberg, M. E. (2001). Calcium regulation of neuronal gene expression. *Proc. Natl. Acad. Sci. U.S.A.*, 98(20):11024–11031.

WHO (1992). *The ICD-10 classification of mental and behavioural disorders: clinical descriptions and diagnostic guidelines.* World Health Organisation. An optional note.

Williams, H. J., Georgieva, L., Dwyer, S., Kirov, G., Owen, M. J., and O'Donovan, M. C. (2012). Absence of de novo point mutations in exons of GRIN2B in a large schizophrenia trio sample. *Schizophr. Res.*, 141(2-3):274–276.

Williams, K. (1993). Ifenprodil discriminates subtypes of the N-methyl-D-aspartate receptor: selectivity and mechanisms at recombinant heteromeric receptors. *Mol. Pharmacol.*, 44(4):851–859.

Wollmuth, L. P., Kuner, T., and Sakmann, B. (1998). Adjacent asparagines in the NR2-subunit of the NMDA receptor channel control the voltage-dependent block by extracellular Mg2+. *J. Physiol. (Lond.)*, 506 (Pt 1):13–32.

Woodberry, K. A., Giuliano, A. J., and Seidman, L. J. (2008). Premorbid IQ in schizophrenia: a meta-analytic review. *Am J Psychiatry*, 165(5):579–587.

Wyllie, D. J., Livesey, M. R., and Hardingham, G. E. (2013). Influence of GluN2 subunit identity on NMDA receptor function. *Neuropharmacology*, 74:4–17.

Yamakura, T., Mori, H., Masaki, H., Shimoji, K., and Mishina, M. (1993). Different sensitivities of NMDA receptor channel subtypes to non-competitive antagonists. *Neuroreport*, 4(6):687–690.

Yoneda, Y. and Ogita, K. (1991). Heterogeneity of the N-methyl-D-aspartate receptor ionophore complex in rat brain, as revealed by ligand binding techniques. *J. Pharmacol. Exp. Ther.*, 259(1):86–96.

Yu, F. H., Mantegazza, M., Westenbroek, R. E., Robbins, C. A., Kalume, F., Burton, K. A., Spain, W. J., McKnight, G. S., Scheuer, T., and Catterall, W. A. (2006). Reduced sodium current in GABAergic interneurons in a mouse model of severe myoclonic epilepsy in infancy. *Nat. Neurosci.*, 9(9):1142–1149.

Yuan, H., Hansen, K. B., Zhang, J., Pierson, T. M., Markello, T. C., Fajardo, K. V., Holloman, C. M., Golas, G., Adams, D. R., Boerkoel, C. F., Gahl, W. A., and Traynelis, S. F. (2014). Functional analysis of a de novo GRIN2A missense mutation associated with early-onset epileptic encephalopathy. *Nat Commun*, 5:3251.

Zhang, Z. W., Peterson, M., and Liu, H. (2013). Essential role of postsynaptic NMDA receptors in developmental refinement of excitatory synapses. *Proc. Natl. Acad. Sci. U.S.A.*, 110(3):1095–1100.

Zhao, J. P. and Constantine-Paton, M. (2007). NR2A-/- mice lack long-term potentiation but retain NMDA receptor and L-type Ca2+ channel-dependent long-term depression in the juvenile superior colliculus. *J. Neurosci.*, 27(50):13649–13654.

Zuo, J., De Jager, P. L., Takahashi, K. A., Jiang, W., Linden, D. J., and Heintz, N. (1997). Neurodegeneration in Lurcher mice caused by mutation in delta2 glutamate receptor gene. *Nature*, 388(6644):769–773.